Unraveling the impact of subsurface and surface properties of a material on biological adhesion—a multi-scale approach

Dissertation
zur Erlangung des Grades
des Doktors der Naturwissenschaften
der Naturwissenschaftlich-Technischen Fakultät II
- Physik und Mechatronik -
der Universität des Saarlandes

von

Peter Moritz Loskill

Saarbrücken
2012

Tag des Kolloquiums: 29.10.2012

Dekan: Univ.-Prof. Dr. rer. nat. Ch. Wagner

Mitglieder des Prüfungsausschusses:

Vorsitzender:	Univ.-Prof. Dr. rer. nat. L. Santen
Gutachter:	Univ.-Prof. Dr. rer. nat. K. Jacobs Univ.-Prof. Dr. med. M. Herrmann Univ.-Prof. Dr. rer. nat. Ch. Ziegler, TU Kaiserslautern
Akademischer Beisitzer:	Dr. J.-B. Fleury

Kurzzusammenfassung

Das Verständnis der Adhäsion biologischer Objekte an anorganischen Materialien ist ein wichtiges Forschungsziel in der Physik und den Lebenswissenschaften. Um biologische Adhäsion zu beschreiben, berücksichtigen viele Studien lediglich die Eigenschaften der Oberfläche; die Materialzusammensetzung unterhalb der Oberfläche wird häufig übersehen. Langreichweitige Van der Waals (VdW)-Kräfte werden somit vernachlässigt. Die vorliegende Arbeit zeigt, dass Unterschiede im Grenzflächenpotential einen Einfluss auf biologische Objekte (Proteine, Bakterien, Geckos) haben. Mithilfe von Siliziumwafern mit unterschiedlich dicken Oxidschichten wird der VdW-Anteil des Grenzflächenpotentials unabhängig von den Oberflächeneigenschaften variiert. Durch Funktionalisierung der Wafer mit einer Silan-Monolage wird auch die Oberflächenchemie gesondert verändert. Auf diesen Modelloberflächen wurden Adhäsions- und Adsorptionsexperimente durchgeführt. Dabei wurde die Proteinadsorption mittels *in situ* Röntgenreflektometrie, die Bakterienadhäsion mittels AFM-Kraftspektroskopie mit Bakteriensonden und die Geckoadhäsion mittels einer mechanischen Testplattform charakterisiert. Zudem wurde in der vorliegenden Arbeit ermittelt, inwiefern Veränderungen der Oberfläche, wie die Fluorierung von künstlichen Zähnen oder Umordnungen in der bakteriellen Zellwand, die Bakterienadhäsion beeinflussen und inwiefern eine verringerte Quervernetzung der bakteriellen Zellwand deren Elastizität verändert.

Abstract

Understanding the adhesion of biological objects to inorganic surfaces is an important research objective in physics and the life sciences. To characterize biological adhesion, most studies describe a substrate solely by its surface properties; the composition of the material beneath the surface is frequently overlooked. That way, long-range van der Waals (vdW) interactions are disregarded. This work reveals that biological objects of all scales—nanoscopic proteins, microscopic bacteria, and macroscopic geckos—are influenced by nanoscale differences in the interface potential. By using tailored silicon wafers with a variable silicon oxide layer thickness, the vdW part of the interface potential is tuned independently from the surface properties. By modifying the wafers with silane monolayers, the surface chemistry can be varied separately as well. On these model substrates, adsorption and adhesion experiments were performed. Protein adsorption was investigated by *in situ* X-ray reflectometry, bacterial adhesion was explored via AFM force spectroscopy with bacterial probes, and gecko adhesion was characterized using a mechanical testing platform. Moreover, this work investigates whether or not bacterial adhesion is influenced by changes in surface properties such as the fluoridation of artificial teeth or contact-induced rearrangements in the bacterial cell wall and whether or not a reduction of the peptidoglycan crosslinking affects the elasticity of the bacterial cell wall.

Contents

Abbreviations

AFM atomic force microscope

BSA bovine serum albumin

CW cell wall

DLVO Derjaguin-Landau-Verwey-Overbeek

DMT Derjaguin-Muller-Toporov

JKR Johnson-Kendall-Roberts

MD Maugis-Dugdale

MRSA methicillin resistant *Staphylococcus aureus*

OTS octadecyltrichlorosilane

PBP4 penicillin-binding protein 4

PBS phosphate buffered saline

PDA poly(dopamine)

PG peptidoglycan

PLL poly-L-lysine

QCM quartz crystal microbalance

QCM-D quartz crystal microbalance with dissipation

QNM quantitative nanomechanical property mapping

SAM self assembled monolayer

SD surface delay

SERAMs secretable expanded repertoire adhesive molecules

TM tapping mode™

vdW van der Waals

1 Introduction

The adhesion of biological objects to artificial materials, also referred to as bioadhesion, is a process that is of major importance in many different areas: Primarily in medical research, the investigation of bioadhesion is crucial for the performance of implants and catheters or the development of biosensors and biological glues. Yet, many other branches of industry are also affected: In oil or gas pipelines, in the shipping industry, and in the food production, for instance, the adhesion of biofilms (bacteria, proteins) or mussels is a major concern [Kum1998, Zhu2003, Ner2006, Sch2011]. Consequently, it is the objective of various studies to prevent or control the adhesion of biological objects such as proteins, bacteria and eukariotic cells.

Moreover, the capability of organisms, such as mussels, insects, frogs, or geckos, to adhere extremely strong to all kinds of surfaces inspired engineers to mimic the respective responsible structure [Fed2001, Gei2003, Lee2007b, Bar2011]. The hunt for gecko-like adhesives, for instance, enjoys great popularity nowadays, especially because gecko adhesion is self-cleaning and completely reversible [Han2005, Lee2008, Boe2010].

For both purposes, the control and the mimicry of bioadhesion, a comprehensive understanding of the interface between the artificial materials and biological objects is necessary. To gain this understanding, researchers from various fields tackle this topic, situated at the border of physics, chemistry, and biology. Unfortunately, however, bioadhesion is usually an interplay of multiple different interactions. Hence, the only way to gain a comprehensive picture of the involved players is to unravel the various responsible parameters.

The main objective of this thesis is to study single parameters or interactions in terms of their impact on the adhesion of biological objects. Thereto, selected parameters of the surface and the subsurface of substrates are independently examined. To cover a wide range of length scales, different types of biological objects featuring a broad variety of dimensions were studied: nanoscopic proteins, microscopic bacteria, and macroscopic geckos. Proteins and bacteria account for the principal components of most biofilms. Geckos are, as mentioned above, one of the most prominent examples of nature that engineers try to mimic.

The major focus of this thesis lies on van der Waals (vdW) interactions, especially on those arising from a material that is hidden by the topmost surface layer. VdW forces

are the sole type of intermolecular forces that are present in every system and arise—unlike most other interactions—not only from the surface, but from the complete material of which the substrate is constituted. Particularly in the presence of thin surface coatings, the overall vdW interactions can depend strongly on the underlying material, a fact that is frequently overlooked. The main objective of the here presented work is to determine whether a variation in the subsurface characteristics of a substrate affects the adhesion of biological objects and whether an effect is limited to a specific scale.

A further parameter focussed on in this thesis is the impact of the fluoridation of artificial tooth surfaces on bacterial adhesion. It is well known that the application of fluoride compounds has a cariostatic effect. The origin of this effect, however, is usually solely attributed to a decreased demineralization of the teeth. Hence, another objective of the here presented work is to determine whether the fluoridation affects the strength of the force by which oral bacteria adhere to the tooth surfaces. Such an effect would account for an additional source of the cariostatic character of fluoridation.

Besides the modification of substrate properties, the characteristics of the interacting biological objects can be altered. In the case of bacteria, this can be done on different levels of separation of single characteristics: It is either possible to study

- alive and dead examples of the same type of bacteria,
- different species of one specific bacterial genus,
- different strains of one species, or
- genetically modified bacteria together with the respective wild-type strain.

A combination of the first two options is utilized in this thesis to compare the time dependence of alive and dead bacteria of the two *Staphylococcal* species *S. aureus* and *S. carnosus*. The objective, thereby, is to gain insight in the adhesion process and to examine possible differences for pathogenic and non-pathogenic *Staphylococci*.

The other two options are also applied in the here presented work, with the aim to investigate the impact of a reduction in the crosslinking of the cell wall of *S. aureus* on the stiffness of the bacterial cell envelope. To determine if the stiffness or a change in it is correlated with the resistance against antimicrobials, two *S. aureus* strains featuring different degrees of resistance and the respective mutants are investigated.

2 Overview and Connectivity

The work at hand engulfs six publications, three of them already published in and three submitted to peer reviewed journals. Although emerged from multiple projects, the publications are closely connected: In all of them, one parameter of the (sub)surface of materials is separately studied with respect to their impact on biological adhesion. In the publications in Addenda II-IV, the van der Waals forces that arise from interactions with the subsurface material are studied. These studies are preluded by a review of the state of the art in the field of vdW interactions in general and in multilayer systems in particular in Addendum I. The study presented in Addendum V focusses on the effect of a fluoridation of tooth surfaces and the publication in Addendum VI concentrates on the surface properties of bacteria, namely the elasticity of the cell envelope. The biological objects studied cover a wide range of length scales; the publication in Addendum II focusses on nanocopic proteins, the ones in Addenda III, V, VI on microscopic bacteria, and the one in Addendum IV on macroscopic geckos.

Overall, the thesis is organized in five chapters:

- In the 'Context and State of the Art' chapter, the studied objects and applied concepts are introduced and a general literature review is given. A detailed and project-tailored overview of the theoretical concepts and the state of the art is then given in the respective publications.
- The 'Materials and Methods' chapter elucidates the primarily utilized methods and materials that are obligatory for the understanding of the presented unpublished results. Project specific applied methods and used materials are accounted for in the respective publications.
- In the two result chapters 'Influence of Substrate Properties on Surface Processes' and 'Surface Properties of Bacteria', a brief review of each attached publication is given and further unpublished results are presented and discussed.
- The thesis is concluded by the 'Summary and Outlook' chapter, comprising a summary of the presented results and an outlook on possible future and already ongoing follow-up projects.

3 Context and State of the Art

3.1 Surface Forces

In principle, solely the four fundamental forces, namely

- **strong** and **weak interactions**, acting between elementary particles, and
- **gravitational** and **electromagnetic interactions**, acting between atoms and molecules,

are sufficient to describe all processes in nature. Thereby, the first two interactions may be classified as 'sub-atomar' forces and the latter two as 'super-atomar'. The role of the two 'super-atomar' interactions, gravitation and electromagnetism, depends on the scale of the described system. On a macroscopic scale (stellar systems, tides, and falling bodies), gravitation is the major factor. On a microscopic scale, electromagnetism plays a key role and is therefore often referred to as the 'true' intermolecular force.

Although all forces between objects on a microscopic scale are essentially of electromagnetic origin, it is useful to further classify these forces into distinct categories of intermolecular forces. Individually, all of these forces are theoretically described, yet an overall solution for the theoretical description of all electromagnetic interactions in arbitrary systems (from single atoms to multi atom bodies) has not been achieved so far. Due to this classification, an interaction (e. g. adhesion or cohesion) between two objects is the interplay of many different intermolecular forces.

In the following sections, some of the major 'players' in the adhesion process are reviewed. A more comprehensive description of intermolecular forces is given, in general by the textbooks of Israelachvili [Isr1992] and Lyklema [Lyk1991], focused on biology by Leckband & Israelachvili [Lec2001], and on nanotechnology by French *et al.* [Fre2010].

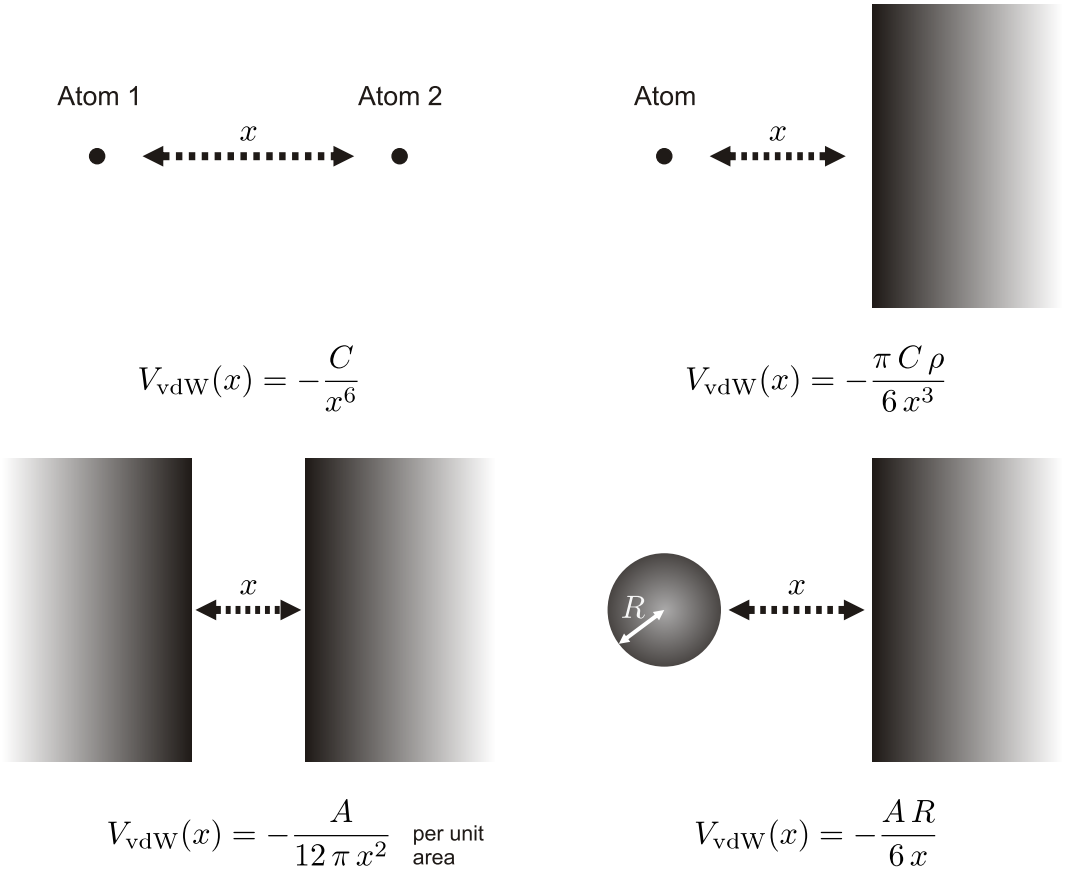

Figure 3.1: Van der Waals potentials for different geometries. Adapted from [Isr1992].

3.1.1 Van der Waals Interactions

Van der Waals (vdW) forces describe the interactions between permanent and induced dipoles. Usually, three types of interactions contribute to the vdW interactions [Isr1992]:

Keesom interactions: Dipol-dipol interactions of freely rotating molecules that carry permanent dipoles.

Debye interactions: Forces between a freely rotating permanent dipole and a nonpolar molecule, wherein a dipole moment is induced by the permanent dipole.

London interactions, also referred to as **dispersion interactions**: Electrodynamic forces between instantaneously induced dipoles. They are of quantum mechanical origin [Lon1937].

The common characteristic of all three types of vdW interactions is the scaling with x^{-6}. Due to this, vdW forces in general are often considered to be of short-range. Yet, this is only true for molecular systems, since the exponent -6 persists only on

Table 3.1: Hamakerconstants $A_{123} = A_{12-32}$ describing various systems that are of relevance in this thesis.

Material 1	Material 2	Material 3	Hamaker constant $[k_\mathrm{B}T]^a$	Source
SiO_2 [b]	vacuum	SiO_2 [b]	17.4	[Tan2005][c]
	water	SiO_2 [b]	1.9	[Tan2005][c]
Si	vacuum	Si	51.7	[Fre1995][c]
		$\alpha-Al_2O_3$	40.4	[Fre1995][c]
Protein[d]	water	Protein[d]	3.1	[Rot1996][c]
		Quartz	1.65	[Rot1996][e]

[a] at room temperature $10^{-20}\,\mathrm{J} = 2.4\,k_\mathrm{B}T$
[b] amorphous
[c] Full spectral method
[d] BSA
[e] Hough and White method [Hou1980]

this scale. On a macroscopic scale, however, vdW forces are of long-range and the exponent of the scaling law increases up to -1 depending on the geometry as depicted in Figure 3.1. Between two semi-infinite half slabs, for instance, the interactions scale with x^{-2} [Isr1992]. The strength of the vdW interactions is determined by the Hamaker constant of the system, which depends on the polarizabilties of the involved materials (cf. Table 3.1).

Van der Waals forces are the only other interactions—besides gravitation—that exist in every system. They can never be completely shielded and are always attractive[1]. Moreover, vdW forces act not only with the surface but with all atoms in the bulk. This is especially of interest for multilayer systems, since in these, layers below the surface can interact with a probe object via vdW forces.

A more comprehensive review of the theory and history of vdW interactions in general and in multilayer systems is given in the **publication in Addendum I**.

3.1.2 Electrostatic Interactions

Two charged atoms, ions, or surfaces interact by 'classical' electrostatic forces. The Coulomb force can be both attractive or repulsive. It is commonly considered as both

[1] A repulsion due to vdW forces is indeed also possible. Yet, this repulsive interaction is a result of a stronger attractive interaction with the medium than between the interacting objects.

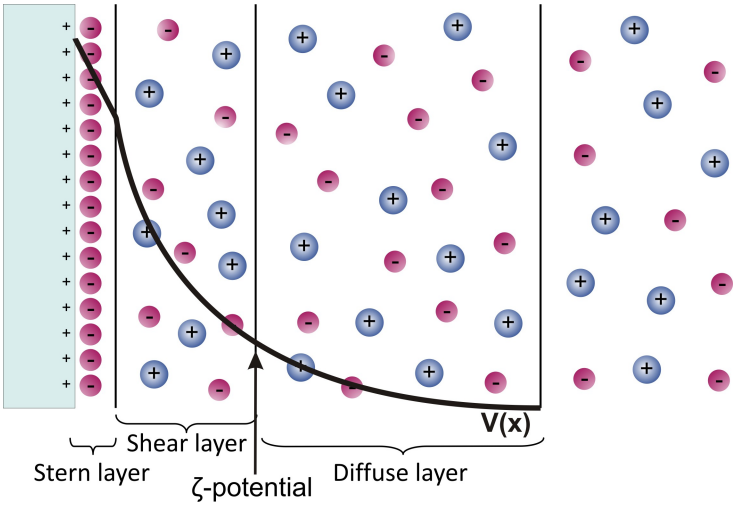

Figure 3.2: Schematic illustration of the electrokinetic double layer overlaid with a typical potential: Adjacent to the surface, a layer of bound counterions forms the Helmholtz or Stern layer, followed by the shear layer and the diffuse layer. The potential is usually described by the ζ-potential. Adapted from [Hof2012].

the strongest and the longest ranging intermolecular force, since, in simple systems, its potential scales with x^{-1}.

In liquids, however, electrolytes strongly affect the electrostatic interactions. Due to the ionization or dissociation of surface groups (e. g. carboxylic or amino groups) and the adsorption of ions, virtually all natural surfaces carry a charge if immersed into water or any liquid of high dielectric constant [Isr1992]. As described by the Gouy-Chapman-Stern model [Gou1910, Cha1913, Ste1924], counterions from the solution—if existent—form an oppositely charged region in the vicinity of the surface to oppose the surface charge. This layer, often referred to as the Helmholtz or Stern layer, is bound to the surface. In addition to the bound ions, a diffuse layer, the so-called Gouy-Chapman layer, is formed by a cloud of further counterions. Both layers together compose the electrokinetic double layer depicted in Figure 3.2 . The transition layer in-between Stern and diffuse layer is often also referred to as the shear layer. The electrokinetic potential at a distance x away from a surface immersed in liquid can be approximated[2] by

$$V_{ED}(x) \approx \psi_0 \, \mathrm{e}^{x\,\kappa} \ , \tag{3.1}$$

with the surface potential ψ_0 and the Debye length $\lambda_\mathrm{D} = \kappa^{-1}$. This characteristic length depends only on the type (monovalent, divalent) and concentration of electrolytes present, and on the temperature via

$$\lambda_\mathrm{D} = \sqrt{\frac{\varepsilon\,\varepsilon_0\,k_\mathrm{B}\,T}{e^2\,I}} \ , \tag{3.2}$$

[2]This approximation is only valid for the case of low potentials.

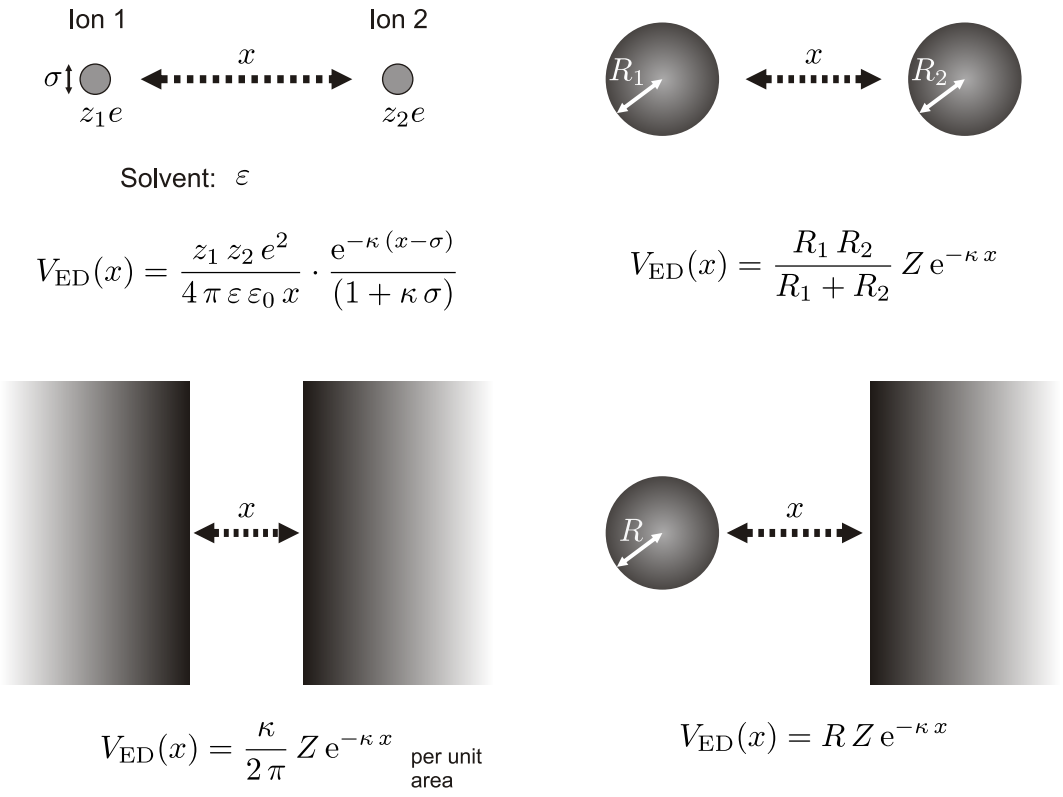

Figure 3.3: The interaction energies of the double layer interaction between two similarly charged objects for different geometries. The interaction constant Z is dependent on the involved materials and $\kappa = \lambda_{\mathrm{D}}^{-1}$ the inverse Debye length. Adapted from [Lec2001].

whereby $I = \sum_i c_i z_i^2$ is the ionic strength, which depends on the concentration c_i and valence z_i of a specific type of ions i. The surface potential ψ_0 can be expressed in terms of the surface charge density σ via

$$\psi_0 = \frac{\lambda_{\mathrm{D}}\,\sigma}{\varepsilon\,\varepsilon_0}\ , \tag{3.3}$$

the simplified Grahame equation for low potentials.

To characterize the electrokinetic potential, the ζ-potential is commonly employed. It describes the potential at the shear (slipping) plane, the plane where hydrodynamic motion becomes possible. It depends on the ion concentration, the pH value, and the temperature [Kir2004].

If two surfaces are close to each other, their electrokinetic double layers start to overlap and they interact via the so-called 'double layer force'. The potential of this interaction depends on the geometry of the system (cf. Figure 3.3)—similar to the vdW potentials in section 3.1.1. The potential between two similarly charged flat

surfaces in an electrolyte of valence z, for instance, is

$$V_{\mathrm{ED}}(x) = \frac{\kappa}{2\,\pi} Z \mathrm{e}^{-\kappa\, x} \tag{3.4}$$

per unit area, with the interaction constant Z and the inverse Debye length $\kappa = \lambda_{\mathrm{D}}^{-1}$. Similar to the Hamaker constant, the constant Z depends on the properties of the surfaces (ψ_0) and the solvent (ε, z) via

$$Z = 64\,\pi\,\varepsilon\,\varepsilon_0\,(k_{\mathrm{b}}\,T)^2\,e^{-2}\,\tanh^2(\frac{z\,e\,\psi_0}{4\,k_{\mathrm{b}}\,T})\ . \tag{3.5}$$

3.1.3 Hydrogen Bonds

The strong electropositive nature of hydrogen atoms is the origin of a very strong[3], short-range interaction, the so-called hydrogen bonds. This bonding occurs if asymmetric molecules—or parts of molecules—such as -OH, -NH, HF, or HCL are involved. Whenever these groups come into contact with a strong electronegative atom in another molecule, such as oxygen, nitrogen, fluorine, or chlorine, the two molecules attract each other. Hydrogen bonds are especially important for the properties of water, since a water molecule possesses two hydrogen as well as an oxygen atom and is thereby capable of forming a total of three hydrogen bonds.

3.1.4 Hydration and Hydrophobic Forces

Between two objects immersed in water, a further type of interactions is induced due to the dipole nature of water molecules and their affinity to build hydrogen bonds. These interactions can be either attractive or repulsive, depending on the hydrophobicity of the surface:

Two hydrophobic (nonpolar) surfaces immersed in water attract each other because of the **hydrophobic effect**. This—purely entropic—effect arises from the lacking ability of the surfaces to develop hydrogen bonds. Consequently, the water molecules have to align themselves so as to maintain the maximal possible amount of hydrogen bonds. Thereby, the mobility of the molecules is constrained, which leads to an increase in entropy. This produces the hydrophobic force, which can be strong at short separations and whose magnitude decreases with decreasing hydrophobicity. The range of the hydrophobic interaction is a controversial subject [Mey2006]. About twenty years ago, Israelachvili and Pashley observed hydrophobic forces reaching far into

[3] The bond enthalpy of a single hydrogen bond is in the range of $10 - 40\,\mathrm{kJ\,mol^{-1}}$ [Lyk1991].

the liquid [Isr1982, Isr1984]. Since then, various possible explanations for this 'long-range' hydrophobic interaction were published, most of them only indirectly related to the hydrophobicity of the surfaces. Among them were, for instance, the interaction between patchy bilayers [Mey2005] or the coalescence of nano bubbles [Ish2000].

Two hydrophilic (polar) surfaces immersed in water repel each other because of the **hydration forces**. Caused by the polarity of the surface, the water molecules in the vicinity of the surface are ordered. Whenever the 'fixed' water layers of two surfaces adjacent to each other start to overlap, a repulsive force is induced. This hydration interaction causes, in the case of perfectly smooth and hard surfaces, an oscillatory force profile and, in the case of soft—biological—surfaces, an exponential decaying force that ranges a few nanometers [Pas1982, Isr1996].

In nonpolar liquids, forces exist that are similar to the hydration forces in water. The so-called repulsive 'structural forces' arise due to the confinement of the liquid molecules at very small separations ($\approx 1\,\mathrm{nm}$).

3.1.5 Steric Repulsion

Two atoms brought into 'close contact' are subject to a strong repulsive force. This steric repulsion—also referred to as hard core or Born repulsion—arises from the overlap of the electron clouds of the two atoms. Due to the Pauli exclusion principle, this overlap is restricted. A—mathematically convenient—theoretical description of this interaction in form of a potential, however, is not intuitive. On a molecular scale, the famous Lennard-Jones-potential [Jon1924] is commonly used. It features a repulsive power-law term in addition to the attractive vdW term:

$$V_{\mathrm{LJ}}(x) = \frac{C_1}{x^{12}} - \frac{C_1}{x^6} \ . \tag{3.6}$$

Between larger bodies, various approximations exist. The hard-sphere potential, for instance, is described by

$$V_{\mathrm{HS}}(x) = \begin{cases} \infty & x \leq \sigma \\ 0 & x > \sigma \end{cases} \ , \tag{3.7}$$

with the hard sphere diameter σ. Along the same line as the molecular Lennard-Jones-potential, a combination of a repulsive power-law potential and the geometry specific vdW term is feasible, leading to a total interaction energy of

$$V_{\mathrm{LJ}}(x) = \frac{C}{x^n} - \frac{A}{x^m} \ , \tag{3.8}$$

whereby n is often adjusted so that $n-m = 6$ preserving the difference in exponents.

3.1.6 A Thermodynamical Approach: Work of Adhesion, Interfacial Energy, and Surface Energy

The typical way—as introduced in the preceding sections—to characterize the adhesion between two objects is to describe the involved interactions by potentials. A different way to describe the adhesion of surfaces is to employ a thermodynamic approach: This approach characterizes the strength of an adhesive contact by the so-called 'work of adhesion'. It is defined as the energy necessary to separate two objects of material 1 and 2 in medium 3 and can be calculated by

$$\Delta G_{\mathrm{Adh}} = \gamma_{1,3,2} = \gamma_{13} + \gamma_{23} - \gamma_{12} \ , \tag{3.9}$$

with the interfacial energies γ_{ij}. The interfacial energy is the free energy change per unit area if two materials increase their interfacial area. It can be calculated, analogous to the work of adhesion, by the Dupré equation

$$\gamma_{12} = \gamma_1 + \gamma_2 - W_{12} \ , \tag{3.10}$$

with the surface energies[4] γ_i. Similar to the interfacial energy, the surface energy is defined as the free energy change per unit area if the surface area of a material is increased—basically, the interfacial energy with vacuum. It can also be understood as half of the work of adhesion $\gamma_{11} = \frac{1}{2}\Delta G_{11}$ needed to separate two alike materials in vacuum (cohesion).

The major challenge in the thermodynamical approach, however, is to determine the involved interfacial energies. Usually, they are derived from measured contact angles of liquids. To do so, multiple different methods exist:

- an equation of state approach [Neu1974];
- a geometric-mean equation that separates the surface energies into a dispersion and a polar component, neglecting spreading pressures [Owe1969];
- a geometric-mean equation that separates the surface energies into a dispersion and a polar component and accounts for spreading pressures but assumes them to be independent of the type of liquid employed [Bus1983];
- an approach[5] that splits surface energies into two parts $\gamma_{\mathrm{Total}} = \gamma_{\mathrm{LW}} + \gamma_{\mathrm{SR}}$, representing Lifshitz-vdW (LW) and short-range (SR)—also referred to as acid-base—interactions, whereby the latter term is further split into hydrogen-accepting and -denoting parts $\gamma_{\mathrm{SR}} = 2\sqrt{\gamma^+\gamma^-}$ [VanOss1986].

Depending on the system, these methods are more or less successful. A further restriction of the thermodynamical approach in general is that it is basically only appropriate

[4] For both surface and interfacial energy, the terms surface and interfacial 'tension' are also frequently used, especially for liquids.

[5] This approach neglects spreading pressures as well.

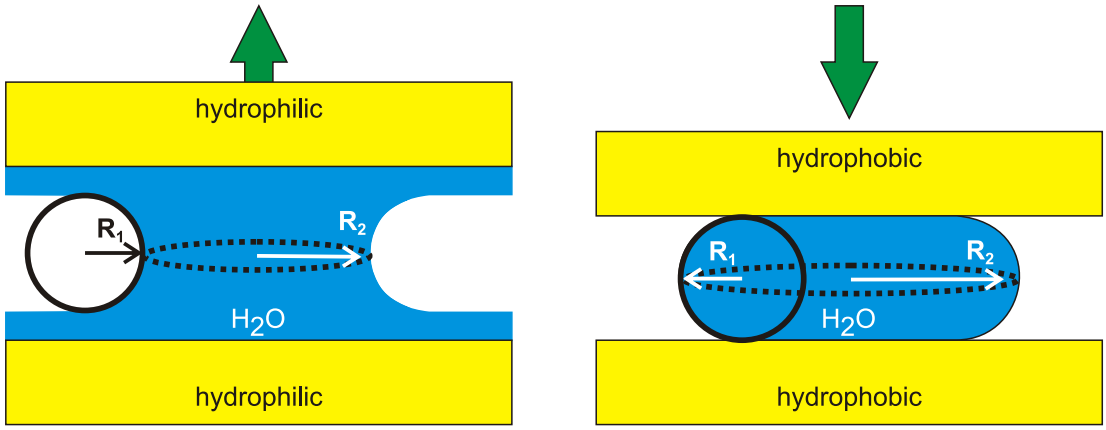

Figure 3.4: Schematic illustration of a liquid bridge between two flat objects—hydrophilic or hydrophobic—with equal contact angles. R_1 and R_2 are the principal radii of a liquid bridge.

for zero separation contact, since the equations lack any kind of separation dependence. Due to these limitations, the thermodynamical approach is strictly speaking only applicable for the interactions of liquids.

3.1.7 Covalent and Chemical bonds

Besides the 'physical' interactions introduced in the sections above, covalent or chemical bonds exist. In principle, these bonds are produced by two or more atoms sharing electrons, an effect that arises from the endeavor of atoms to minimize the energy. Covalent bonds are of very short-range and extremely strong.

3.1.8 Capillary Forces

Systems that are not completely immersed in water can be nevertheless dominated by a water-induced interaction, the capillary force. This force can play a key role, even if the system is seemingly 'dry', owing to the fact that at ambient conditions virtually all surfaces are covered by a layer of water. The thickness of this water layer depends, inter alia, on the wettability of the surface and the humidity; silicon oxide, for instance, is usually covered by 1-2 nm of water [Asa2005]. When two bodies are brought into contact, these water layers can form a capillary bridge, resulting in a capillary force that is directed normally to the planes of the contact lines on the objects. These capillary bridge forces can be either attractive or repulsive, depending on whether the capillary bridge is convex or concave. The strength of a single capillary bridge is

determined by the sum of the forces arising from the surface tension $F_{\text{Tension}}(x)$ and the Laplace pressure $F_{\text{Laplace}}(x)$. In the case of two homogeneous flat objects with equal contact angles Θ separated by a distance x, the capillary bridge force can be calculated by

$$\begin{aligned} F_{\text{Capillary}}(x) &= F_{\text{Tension}}(x) + F_{\text{Laplace}}(x) \\ &= 2\pi R(x)\gamma_{\text{LV}}\sin(\Theta) + \pi R(x)^2 \Delta P_{\text{Laplace}} \ , \end{aligned} \tag{3.11}$$

with the radius $R(x)$ of the interface between solid and liquid, the surface tension γ_{LV} of the liquid-vapor interface, and the Laplace pressure $\Delta P_{\text{Laplace}}$ [For1982]. This pressure is given by

$$\Delta P_{\text{Laplace}} = \gamma_{\text{LV}} \left(\frac{1}{R_1} + \frac{1}{R_2} \right) \ , \tag{3.12}$$

whereby R_1 and R_2 are the two principal radii of a liquid bridge [Lap1806] (cf. Figure 3.4). In the case of two chemically different substrates, the calculation of the capillary bridge force is not possible without further ado [DeSou2008].

Capillary bridge forces play an important role in many biological and nanotechnological systems that are exposed to humid environments[6] [Jan2004, Min2008].

3.2 Proteins

Proteins are macromolecules consisting of one or more polypeptides—linear polymers composed of amino acids. Each amino acid is build up of a central carbon (and a hydrogen atom), an amino group (NH_2), a carboxylic acid group (COOH), and a specific side chain. A total of twenty different amino acids—featuring different side chains—are the building blocks for all naturally found proteins. The amino acids are linked to each other by peptide bonds that form between the carboxyl and amino groups. The sequence of the amino acids is referred to as the primary structure of a protein, which unambiguously identifies it. The secondary structure describes the spatial folding of the polypeptides. Due to hydrogen bonds, the amino acids form characteristic structures, such as α-helices or β-sheets. Finally, the overall shape of a protein that usually defines its function is called the tertiary structure. The shape is mostly stabilized by the hydrophobic effect and can undergo changes if the protein interacts with another object or if the external conditions (e. g. pH or temperature) are changed. These so-called conformational changes can be described as transitions between metastable conformations, visualized by minima in the energy landscape[7].

[6] Obviously, capillary bridge forces do not play a role if the 'humid environment' is a complete immersion into liquid.

[7] Due to the importance of both the entropy and the potential energy, the free energy is a good measure for protein folding. It can be visualized in high dimensional free energy landscapes—similar to geographic landscapes in two dimensions [Abk1994, Din2000].

3.2.1 Protein Adsorption

If a solution that contains proteins is flushed over a surface, the proteins start to adsorb onto it. This adsorption of proteins is often the initial step in the formation of biofilms. Once adsorbed to a surface, the proteins are part of a conditioning layer, which is the foundation for the evolving biofilm [Cha1983, Bry2008, Gar2008]. If strongly bound to the surface, the proteins can provide a link for bacteria to attach. The adsorption can be both physisorption[8] (viz. reversible) or chemisorption[9] (viz. irreversible). Both adsorption processes are driven by an interplay of the interactions described in section 3.1. Which interactions dominate, however, depends on the type of protein, the surface, and the external conditions (e. g. temperature, pH, ionic strength, and buffer composition) [Rab2011]. In general, the adsorption process of a single protein is composed of three steps, namely

1. transport (convective or diffusive) towards the surface,
2. attachment, and
3. spreading,

whereby interrupting desorption events can occur in between the second and third step. Usually, it is not an individual protein that adsorbs, but a collective process of many proteins. Since not all proteins adsorb simultaneously, it is a continuous process. During this process, important parameters such as the surface properties and the concentration change due to already adsorbed proteins, leading to a time-dependent rate of adsorption. Hence, protein adsorption is commonly characterized by the adsorption kinetics—the time-dependent increase of the amount of proteins on the surface.

In the last 40 years, many groups investigated the adsorption of proteins experimentally, theoretically, and via simulations [Rab2011]. The experimental studies applied a wide range of different methods [Ram1994]: Popular choices are ellipsometry [Elw1998], surface plasmon resonance (SPR) [Gre2000], quartz crystal microbalance (QCM) [Laa1988], and reflectometry methods (Neutron [Lu2007] and X-ray [Eve2008]). This way, most studies determined the adsorption kinetics. To follow the adsorption process on a single protein level remains a very difficult task. An indirect way, however, is the use of theoretical models. By assuming rate equations, the macroscopic results of the experimental works can be traced back to events on the molecular scale. Rate equations of various degrees of complexity are used. The most simple and popular model is the Langmuir model, which incorporates only an on-rate and an off-rate [Lam1916, Lan1918]. Other models include various further rates such as

[8] Physisorption is adsorption due to classical physical interactions, whereby the chemical nature of neither the adsorbate nor the surface is changed [Bru1983].

[9] Chemisorption is a class of adsorption, whereby a chemical bond is formed and the chemical nature of both the adsorbate and the surface can change [Nor1990].

exchange or transition rates [Wah1995, Wah1997, Wer2002]. Besides the classical theoretical approaches, computational approaches enjoy great popularity in recent years. Simulations of various complexity are performed to complement experimental studies. The simulation programmers thereby have to trade off structural detail and precision against computational costs and simulated timespans. The options range, for instance, from highly precise quantum mechanical simulations [Cos2008, Rim2008] to molecular dynamics simulations [Kar2002] to Monte Carlo simulations [Bel2008, Rab2010] or combinations of those [Zho2004]. *Ab initio* quantum mechanical simulations allow the access of the adsorbate state, the binding mechanisms, or the energies at the atomic level, but are highly time and scale restricted due to the computational expenses [Eus2004, Lat2008]. Hence, molecular dynamics and Monte Carlo simulations often apply force fields instead of *ab initio* theory. In classical molecular dynamics simulations, all single atoms of the proteins and the solvent are considered. Again, the drawback is that only a limited time frame can be modeled. On the contrary, Monte Carlo simulations model single proteins as—spherical—particles. Thereby they can model processes on large timescales, but have to cut back on detail and precision. Compromises are made by using groups of atoms as the basic unit, so-called coarse-grained models, or by the implicit treatment of solvent molecules.

A more comprehensive introduction of proteins and protein adsorption is given in the thesis and textbook in the references [Mal2003, Häh2011, Bel2012]

3.3 Bacteria

Bacteria exist on pretty much every place on earth. Their total population is estimated to roughly 10^{30} cells. In one cubic centimeter of near-surface soil, approximately 200 million single bacteria can be found [Whi1998] and in the human body, the total number of bacteria is about ten times larger than the number of eukaryotic cells [Tan1992].

Taxonomically, the domain *Bacteria* constitutes one of the three domains[10]—along with *Archaea* and *Eucarya*—in which the life on our planet can be classified [Woe1990]. In principle, the domain *Bacteria*[11] comprises single-celled microorganisms that contain no real cell nucleus. Their genetic material is contained in a specific region in the cytoplasm, the nucleoid [Tha2005]. Moreover, they lack organelles such as mitochondria and the endoplasmic reticulum.

[10] Whether or not the domains *Bacteria* and *Archaea* may be combined to *Procarya* is a controversial topic [May1998, Woe1998].

[11] In microbiology, the term bacterium(-a) is still employed in different contexts. In this work, it stands for representatives of the domain *Bacteria*.

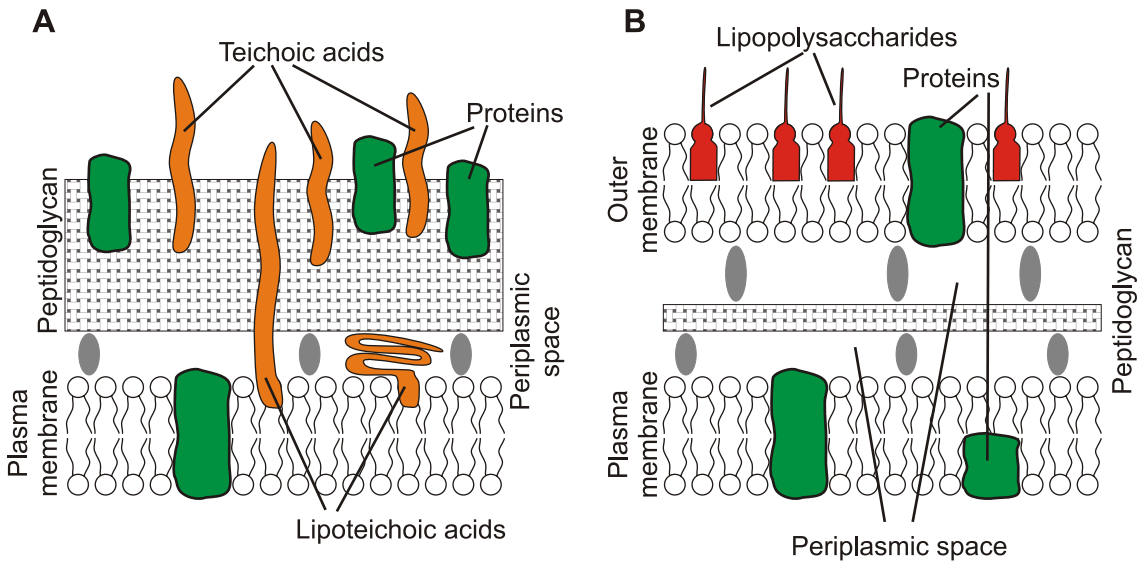

Figure 3.5: Structure of the cell wall of A) Gram-positive and B) Gram-negative bacteria.

The morphology of bacteria is diverse. They vary widely in shape and in size. Their typical diameter is in the range of 0.2 µm to 2 µm [Jos2009]. Morphologically, bacteria can be categorized in three basic shapes: spherical (cocci), rod-shaped (bacilli), and spiral-shaped (spirilla). Yet, a more practical classification, especially in medical microbiology, is given by the Gram method [Gra1884]. The Gram staining reveals two distinct possibilities of the cell wall (CW) structure. Thereby, bacteria can be classified as either Gram-positive or Gram-negative. Gram-negative bacteria feature a CW that is composed of an outer and an inner membrane (cf. Figure 3.5 B). In between the membranes is the periplasmic space that contains a thin oligomolecular layer of peptidoglycan (PG). The outer membrane is typically covered with lipopolysaccharides. On the contrary, the CW of Gram-positive bacteria consists of a much thicker PG layer but lacks an outer membrane (cf. Figure 3.5 A).

Since the bacterial CW is the structure of preeminent importance for all interactions of bacteria with their environment and acts as a mediator for adhesion, a more detailed description of its composition is given in the following section. Moreover, as in this thesis the two Gram-positive genera *Staphylococcus* and *Streptococcus* are investigated, the focus lays on the CW of Gram-positive bacteria[12].

[12]For a more comprehensive overview of the definition and the structure of bacteria, the reader shall be referred to the corresponding chapter in the established textbooks (cf. [Jos2009]).

3.3.1 Cell Wall of Gram-positive Bacteria

The major component of the CW of Gram-positive bacteria is peptidoglycan. This complex polymer is—similar to chitin—composed of long glycan chains of alternating β-1,4-linked N-acetylglucosamine and N-acetylmuramic acid subunits. The glycan chains are further crosslinked via peptide bridges to form a strong, but flexible structure [Sch1972, Vol2008]. The main function of the PG layer is to preserve the cell integrity by withstanding the turgor pressure and to maintain a defined cell shape. Moreover, it serves as a scaffold for anchoring other CW components such as proteins and teichoic acids (cf. Figure 3.5 A).

These CW compounds are responsible for all kind of interactions of the bacterium with the environment. Teichoic acids are strongly negatively charged and thereby define the electromechanical properties of the cell wall [Neu2003]. Moreover, they play a key role in the bacterial adhesion process [Gro2001, Hus2001]. CW proteins feature a wide variety of different functions [Nav1999, Sco2006], including

- the protection of the bacteria from environmental challenges, such as toxic conditions or host immune defense system,
- the maintenance of the CW,
- the contribution to the cell division process (e. g. autolysins), and
- the attachment to different type of environmental components (e. g. adhesins).

The immobilization of the cell wall compounds, however, can vary significantly. Proteins are attached either by covalent binding to the PG or by noncovalent binding to either the PG or secondary wall polymers such as teichoic acids. [Nav1999, Sco2006]. Teichoic acids can be further classified into wall teichoic and lipoteichoic acids [Neu2003, Rei2011], whereby wall teichoic acids are covalently bound to the PG layer and lipoteichoic acids are anchored in the membrane. Whether lipoteichoic acids also always extend into the peptidoglycan layer—strongly affecting their mobility—was recently challenged [Rei2011].

Furthermore, polymeric cell-surface organelles such as flagella and pili (or fimbriae) are also frequently found on and in the CW of Gram-positive bacteria [Tel2006, Des2006].

3.3.2 Bacterial Adhesion

Nowadays, bacterial adhesion is a very active field of research as it is of importance for various topics concerning nature and human life, such as marine science, plant and soil ecology, the food industry, and most importantly, the biomedical field [An1998].

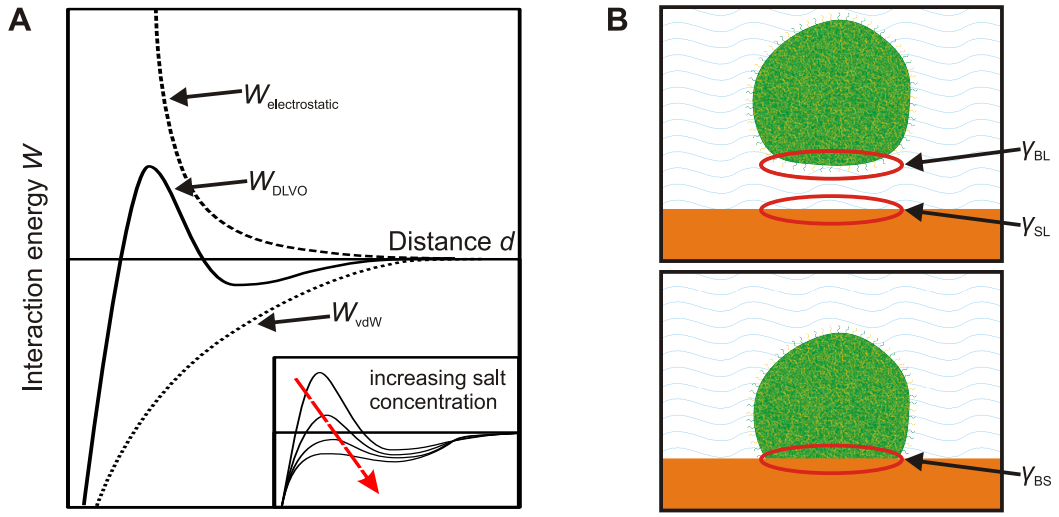

Figure 3.6: Two different theoretical concepts for the description of unspecific bacterial adhesion: A) The classical DLVO theory incorporates the electrostatic interaction $W_{\text{electrostatic}}$ and vdW interactions W_{vdW}. The strength of the electrostatic interaction is strongly dependent on the salt, viz. ion, concentration (cf. inset). The DLVO theory takes only long-range interactions into account. B) Schematic representation of the thermodynamic ansatz, whereby the free energy of the interface is calculated.

The adhesion of bacteria is the initial step in the formation of a biofilm [Cos1987]. If the respective substrate is human tissue or an implanted material, however, it is frequently also the onset of an inflammation [Don2002].

Generally, bacterial adhesion can be classified into specific and unspecific adhesion.

Specific adhesion, also referred to as biological adhesion, combines all kinds of receptor-ligand bonding [Jon1982]. It usually describes adhesion events of very short-range that are based on the lock-and-key principle.

Unspecific adhesion, also referred to as physical adhesion, denotes the global interaction between a bacterial cell and a substrate. It is usually an interplay of the interactions described in section 3.1.

Specific adhesion processes are important for intercellular adhesion, both bacterial cell/bacterial cell and bacterial cell/host interactions [Bea1981, Sha1989]. The responsible adhesion proteins are either anchored in the CW or anchorless and can be classified into adhesins and invasins [Kle2000, Chh2002].

Unspecific adhesion plays a major role in the adhesion to inorganic materials. Furthermore, unspecific adhesion prevalently precedes specific adhesion [Gri1987]: In these cases, the first part—the reversible bacterial attachment— is dominated by unspecific adhesion. The second part—the irreversible bond strengthening—is due to specific

bonding. Since this thesis mainly focuses on unspecific adhesion, a brief review of theoretical concepts and experimental studies is given in the following paragraphs.

To theoretically describe bacterial adhesion, two different physicochemical approaches are available [vanLoo1990, Her1999]:

A popular ansatz is the application of the DLVO theory [Mar1971, Her1999, Dor2009]. This theory—initally introduced by Derjaguin and Landau [Der1941], and Verwey and Overbeek [Ver1948] to describe the interaction between rigid colloids and interfaces—incorporates electrostatic and vdW interactions (cf. Figure 3.6 A). The practicability of the DLVO theory for bacterial adhesion, however, is limited and failed in many studies [Cam2000, Poo2002], as it neglects many essential properties of the system; it basically takes only long-range interactions into account. Hence, to account for the steric repulsion at small separations (cf. section 3.1.5), either cut-off radii or hard sphere potentials are commonly used.

A second, very common ansatz is based on surface thermodynamics [Abs1983, Bus1984]: The strength of the adhesive contact is determined by calculating the free energy of adhesion ΔG_{Adh} introduced in section 3.1.6 using

$$\Delta G_{\mathrm{Adh}} = \gamma_{\mathrm{BS}} - \gamma_{\mathrm{BL}} - \gamma_{\mathrm{SL}} \quad , \tag{3.13}$$

with the involved interfaces bacterium/substrate (BS), bacterium/liquid (BL), and substrate/liquid (SL) (cf. Figure 3.6 B). Although this approach is also frequently applied [Vij2005, Liu2007], it has severe limitations:

- Since it is essentially an equilibrium model, it does not allow any kinetic interpretations [Rij1995].
- It is a stringent contact model. That means, any distance dependence of ΔG_{Adh} is ignored. The question how much of the cell actually makes contact with the substrate is thereby especially critical.
- As discussed in section 3.1.6, multiple different methods exist to calculate interfacial energies[13]. The suitability for bacterial adhesion, however, differs substantially [Bel1990].
- Moreover, contact angles of bacteria are hardly accessible. They depend, inter alia, on drying [Bus1990] and growth conditions [Mam1987].

In other words, supposed all necessary parameters are known, this ansatz is still only valid if the system is in equilibrium and dominated by short-range forces.

A combination of these two approaches is the extended DLVO theory, called XDLVO. Therein, the classical DLVO interactions are supplemented by short-range interac-

[13] All of them commonly rely on contact angles of various liquids that are not involved in the actual adhesion process.

tions, namely electron-acceptor/electron-donor (also referred to as Lewis acid-base) and osmotic interactions [VanOss1989, VanOss1990, vanOss2006]. Although the applications of the XDLVO theory revealed better agreements with experiments as compared to the 'classical' DLVO theory [Mei1995, Bay2009], it is still a limited approach, since it treats bacteria as inert, rigid, and homogeneous solids. In recent years, however, promising theories were introduced such as the model by Gaboriaud *et al.* describing bacteria as soft particles composed of a hard core and a permeable charged gel-like layer [Gab2008].

To experimentally access the adhesion of bacteria, various methods were applied:

Typically, **parallel plate flow chambers** were utilized [vanKoo1992, Har2006]. This macroscopic technique is made up of a flow chamber, which is integrated in a flow system and in which a laminar flow is assured [vanWag1980]. Usually, one side of the chamber is sealed by the material of interest and the other side is transparent to ensure the accessibility by optical means. By flushing bacterial solution through the flow chamber while monitoring the amount of adsorbed bacteria, the adsorption kinetics is revealed. A more technical introduction to parallel plate flow chambers is given in section 4.3.

In recent years, a **quartz crystal microbalance** (QCM) was frequently applied to replace optical microscopy for the determination of the adsorbed amount of bacteria [Olo2005, Ols2009, Str2009, Ols2010]. In principle, a QCM is composed of an oscillating quartz crystal on which the substrate is mounted. By tracking the oscillation frequency, a change in the adsorbed mass can be detected. Unfortunately, it is not possible to access the total number of adsorbed bacteria without further ado, since the frequency depends on multiple parameters, such as viscosity, flow rate, and elasticity. This problem, however, is reduced by more advanced QCMs, which allow for a simultaneous determination of the energy dissipation (QCM-D).

Both flow chambers and QCMs are macroscopic and indirect approaches to characterize bacterial adhesion, since the determined kinetics emerge from an interplay of adsorption and desorption. Experimental methods to directly determine the adhesion forces exerted by bacteria, are, for instance, optical tweezers and atomic force microscopy (AFM).

Optical tweezers are based on the formation of an optical trap by a focused laser beam [Ash1970, Ash1986, Blo1992]. Inside the optical trap, small objects are confined by the radiation pressure, arising from the refractive index mismatch. Optical tweezers enable the manipulation and exertion of forces onto biological objects such as bacteria and viruses [Ash1987, Svo1994, Lia2000, Zha2008, Mof2008]. Yet, since the strength of the applied forces is limited to the pN-range, optical tweezers are better suited to study single molecule interactions than to characterize global bacterial adhesion.

The **AFM** emerged as a very promising tool to study biological interactions in the last decade [Duf2002, Duf2008, Wri2010]. The so-called 'force spectroscopy mode' allows for a direct measurement of forces. By employing suitable AFM-probes, the adhesion of biological objects such as bacteria can be studied [Mer1999, Bow2001, Yon2006, Lee2006, Hel2008]. Since the force ranges of an AFM ($10-10^4$ pN) and optical tweezers ($0.1-100$ pN) are mostly distinct, these two methods are not competing but complementary techniques [Neu2008]. In this work, the AFM is the method of choice. Hence, a detailed technical description is given in section 4.2.

The investigated parameters in the experimental studies are diverse. Many studies examined the impact of the hydrophobicity and surface energy of the substrate [Dij1987, Bru2001, Vij2005, Eme2006, Bok2008b, Liu2011] or the bacteria [vanLoo1987] on the adhesion forces. Other studies concentrated on electrostatic interactions [Cam2000, Poo2002, Kal2010] or surface parameters such as roughness and topography [Tay1998, Eme2006, Whi2006, Ans2010, Sin2011]. Yet, only little work has been performed to investigate the influence of vdW interactions on the adhesion of bacteria [Ste2009]. Moreover, most studies have in common that they did not separate parameters influencing the different interactions independently. For a comprehensive understanding of the bacterial adhesion process, however, it is necessary to seek quantitative information about the single contributions of all involved interactions.

3.3.3 *Staphylococci*

Staphylococci are Gram-positive cocci that are prevalently found in the microflora of mammals. They are catalase-positive and usually $0.8-1$ µm in diameter. The *Staphylococcal* genus enfolds various—pathogenic as well as apathogenic—species. In this work, the species of interest are *Staphylococcus aureus* and *Staphylococcus carnosus*, two of the most commonly found *Staphylococcal* species in human, which will be described in the following paragraphs[14].

Staphylococcus aureus was first described by Rosenbach in 1884 [Ros1884] and named after the golden (latin 'aureus') color of their colonies. They inhibit the nares of nearly 40% of the human population[15] [Klu1997]. Yet, *S. aureus* are opportunistic bacteria: They are non-pathogenic, as long as the host immune system is intact, but highly pathogenic if the immune system is lowered. Hence, infections especially occur in hospitals: *S. aureus* is the most common cause of nosocomial (hospital acquired;

[14] A more comprehensive description of the genus *Staphylococcus* is given in the respective chapters of textbooks [Mad2006, Gat2009].

[15] Yet, only 20% of the human population are persistent carriers, that means almost always carry a *S. aureus* strain.

HA) infections and causes high treatment expenses and economical damages. Moreover, community acquired (CA) infections are increasingly often observed, especially in nursing homes and long-term care facilities [Rub1999].

The biggest threat, however, arises from the resistance against antimicrobial agents. Today, more than 95% of *S. aureus* infections are resistant to first-line antibiotics, e. g. penicillin, ampicillin, and the antipseudomonas penicilins [Neu1992]. Moreover, methicillin-resistance occurs to an increasing extent. Methicillin-resistant *S. aureus* (MRSA) were first reported in 1968 in a hospital in Boston [Bar1968]. In the 1980s, an upsurge of the frequency of occurrence of MRSA took place, which led to the occurrence of a resistance in 30% of all *S. aureus* infections in the beginning of the 1990s [Boy1990, Pan1992]. Nowadays, MRSA is endemic or even epidemic in many hospitals; Methicillin-resistant *S. aureus* infections in some US intensive care units reached nearly 65% [Kle2006].

Yet, even without any resistance, the treatment of *S. aureus* diseases can be complicated, since it is a multifaceted pathogen [Low1998, Arc1998, Fre2006]. Various types of diseases—from minor to life-threatening infections—can be caused by *S. aureus*, such as skin and soft tissue infections [Fra2005], endocarditis [Mil2008], pneumonia [Chi1919], and the toxic shock syndrome [Ber1981].

The high level of pathogenicity of *S. aureus* is due to their abilities to produce multiple toxins, to evade the host immune system, to adhere to—abiotic and biotic—surfaces, and to form biofilms. For the latter three properties, the cell wall plays a key role: As typical for Gram-positive bacteria (cf. section 3.3.1), the cell wall of *S. aureus* is mostly composed of peptidoglycan (50% by weight [Low1998]). The *S. aureus* peptidoglycan is strongly crosslinked ($74\% - 92\%$) and composed of glycan strands, showing a bimodal length distribution of many ($85\% - 90\%$) short ($\approx 6\,\mathrm{nm}$) and fewer ($10\% - 15\%$) long ($\ll 26\,\mathrm{nm}$) strands [deJon1992, Bon2000, Vol2010]. Overall, the *S. aureus* cell wall comprises three layers (cf. Figure 3.5): The typical inner plasma membrane of 5.4 nm thickness, a 15.8(25) nm thick inner wall zone (IWZ) of low density (periplasmic space), and a 19(4) nm thick outer wall zone (OWZ) of high density [Mat2006, Mat2007, Vol2010]. The peptidoglycan in the OWZ is compressed by the high turgor pressure, as revealed by the finding that, if isolated, it is about 1.7-fold thicker (33.8(54) nm) than in intact cells [Vol2010].

Besides peptidoglycan, proteins are another major compound of the cell wall. Wolff *et al.* identified a total of 271 integral membrane proteins in *S. aureus* [Wol2008]. These proteins have various functions, such as immune evasion [Fos2005] and adhesion [Fos1998].

Cell wall proteins can also be classified by the type of anchoring (cf. Figure 3.7), ranging from 'covalently integrated in the peptidoglycan' to 'secreted' [Dre2011], which leads to different degrees of mobility. The proteins of major interest for this

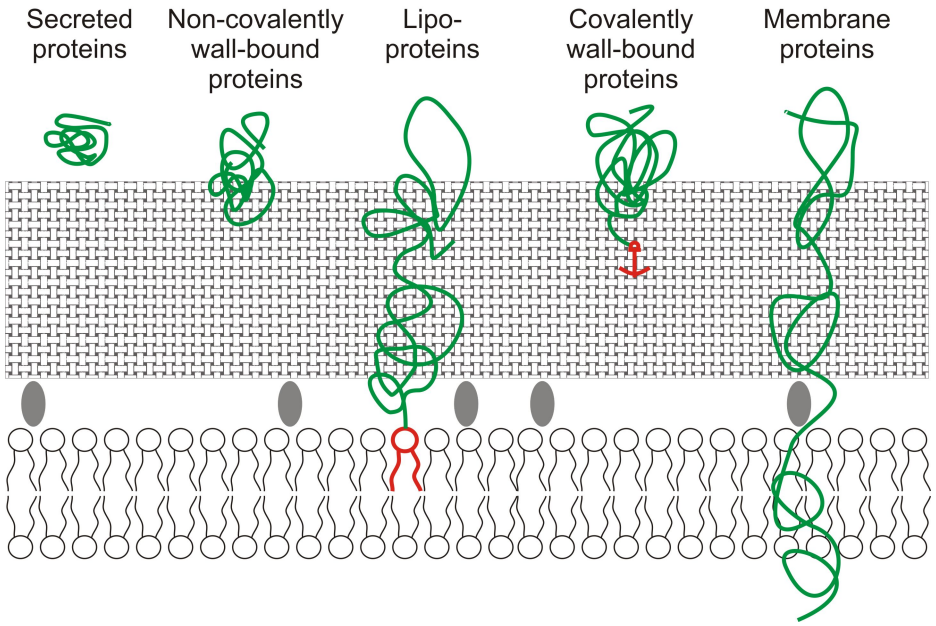

Figure 3.7: Schematic illustration of different classes of proteins integrated on or in the cell wall of *S. aureus*. The grade of anchoring ranges from completely unbound to covalently bound. Adapted from [Dre2011].

study are those which are exposed on the cell surface—also referred to as the 'surfacome' [Dre2011]—and especially those which are involved in the adhesion process (adhesins). *S. aureus* expresses a wide range of surface adhesins. More than twenty different covalently bound adhesins are known. Most of them feature a characteristic Leu-Pro-X-Thr-Gly (LPXTG) motif that anchors them to the cell surface and belong to the MSCRAMM (microbial surface components recognizing adhesive matrix molecules) family, e. g. Cna, Spa, ClfA, ClfB, FnBPA and FnBPB [Fos1998, Maz1999, Cla2006]. These proteins bind to various host factors—such as fibronectin, collagen, von Willebrand factor, or fibrinogen—and thereby enable the bacterium to adhere to the extracellular matrix and foster biofilm formation. Further covalently bound proteins promote the attachment to abiotic surfaces (e. g. Bap [Cuc2001], SasC [Sch2009]).

In addition to the covalently bound adhesins, *S. aureus* produces several non-covalently bound surface adhesins called secretable expanded repertoire adhesive molecules (SERAMs). Important members of this adhesin family are, for instance, Eap (extracellular adhesive protein), Efb (extracellular fibrinogen-binding protein), and Emp (extracellular matrix protein) [Bod1992, Bod1994, Pal1998, Pal1999]. Although SERAMs are secreted and released by the bacterial cell, they are often subsequently rebound to the cell wall surface and thereby serve as a linkage between host factors and *S. aureus*.

Apart from their contribution to the bacterial attachment, many SERAMs have additional functions such as the interference with the host defense and the immune

system [Cha2002, Har2003, Cha2005]. Besides the SERAMS, *S. aureus* features various other mechanisms to evade the host immune system [Fos2005]: The covalently bound protein A is able to bind antibodies and thereby inhibits phagocytic engulfment [Kes1975, Sjö1977]). Further mechanisms to 'hide' from the immune systems are, for instance, the formation of a polysaccharide capsule [Wil1979], the clumping of fibrinogen [Bod1989], and the invasion of host cells [Bay1998]. Additionally to these 'single bacterial defense mechanisms', the formation of biofilms provides a protection from antibiotics and from the immune system [Don2002, Lew2008, Ott2008, Göt2002, And2008].

Staphylococcus carnosus is an apathogenic member of the *Staphylococcus* genus. It is the predominant bacterial species in fermented meat [Sch1982]. Industrially, *S. carnosus* is of importance since they are commonly used in the ripening process of dry sausages and as a starter culture for the fermentation of meat products. For scientific research, *S. carnosus* is also of relevance although it produces no toxins, haemolysins, protein A, coagulase, or clumping factors. Yet, it serves as a host organism for gene cloning and protein production [Göt1990, Bru1997].

3.3.4 *Streptococci*

Another genus of Gram-positive bacteria studied in this work is the *Streptococcus* genus. Streptococci are easily distinguishable from *Staphylococci*, because they form chain-like structures[16]. These characteristic structures are due to their ability to divide only along one axis. A further distinguishing feature is the lacking catalase production of most Streptococci species. As they usually are facultative anaerobes, Streptococci can survive independent of the oxygen concentration. Although most species are nonpathogenic, Streptococci can cause a wide range of diseases, such as meningitis [Sch1996], endocarditis [Rob1979], and pneumonia [Tet2001].

In this work, the species of interest are *Streptococcus mutans* and *Streptococcus oralis*, which are both found in the oral cavity [Kro1999]:

Streptococcus mutans [Cla1924] is one of the major organisms responsible for dental caries [Ham1980, Loe1986]. *S. mutans* adheres strongly to surfaces, due to their capacity to synthesize glucan from sucrose [Gib1975]. Glucan is a sticky extracellular polysaccharide that binds specifically to cell wall proteins of oral *Streptococci* [Ban2003]. Thereby, a slime layer is produced that fosters the formation of

[16]The structures from which the name is derived; Greek '*streptos*'.

biofilms [Gib1973, Lyn2007]. The actual tooth decaying capacity of *S. mutans*, however, arises from the production of lactic acid, which causes the demineralization of the tooth material [Loe1986, Mad2006].

Streptococcus oralis [Bri1982] is an opportunistic pathogen that belongs to the mitis phylogenetic group. It is a commensal of the human oral cavity, but can also be the cause for bacterial endocarditis [Wha2000].

3.4 Geckos

Gekkonoidae, better known under their nontechnical name 'Geckos', are a type of lizards belonging to the *Reptilia* class. Geckos can be found nearly everywhere in the world, mostly in warm climates. Their size varies ranging from 16 mm (*Sphaerodactylus ariasae* and *Sphaerodactylus parthenopion* [Hed2001]) up to 60 cm (*Hoplodactylus delcourti* [Bau1986]). Geckos are best recognized by their lack of an eyelid. Moreover, many Gecko species feature a variety of extraordinary characteristics, such as the ability to make chirping cries[17] and the occurrence of parthenogenesis[18] [Mor1983]. Their most outstanding skill, however, is their climbing capability. Geckos are the largest animal that can walk on the ceiling and are able to stick to almost any surface. This adhesion skill, which raised the interest of researchers of various fields, shall be explored in more detail in the following section.

3.4.1 Gecko Adhesion

Initially, the adhesion skill of the gecko was attributed to the sharp points of its claws taking a hold on slight irregularities of the surface [Mah1941]. Later on, since geckos are able to stick to almost any—rough as well as extremely smooth—surface, the claw theory was contested and a remarkable property of the geckos toe was suggested to be the key adaptation that provides the sticking ability: the hierarchical structure [Mad1964, Rui1965, Ern1966, Hil1968]. The underside of each toe is divided into lamellar structures that terminate in arrays of densely packed hair-like protrusions, called seta (Figure 3.8 A). Individual setae are bundles of β-keratin fibrils several hundred µm long [Riz2005]. These fibrils terminate in triangular, wedge-shaped pads about 150 nm wide at the tip, called spatulae (Figure 3.8 B). As a consequence of this hierarchical structure, the setal arrays have an overall compliance that allows them to

[17] The sound (Malayan imitation *gēkoq*) prompted the term 'gecko'.
[18] Parthenogenesis is a type of asexual reproduction.

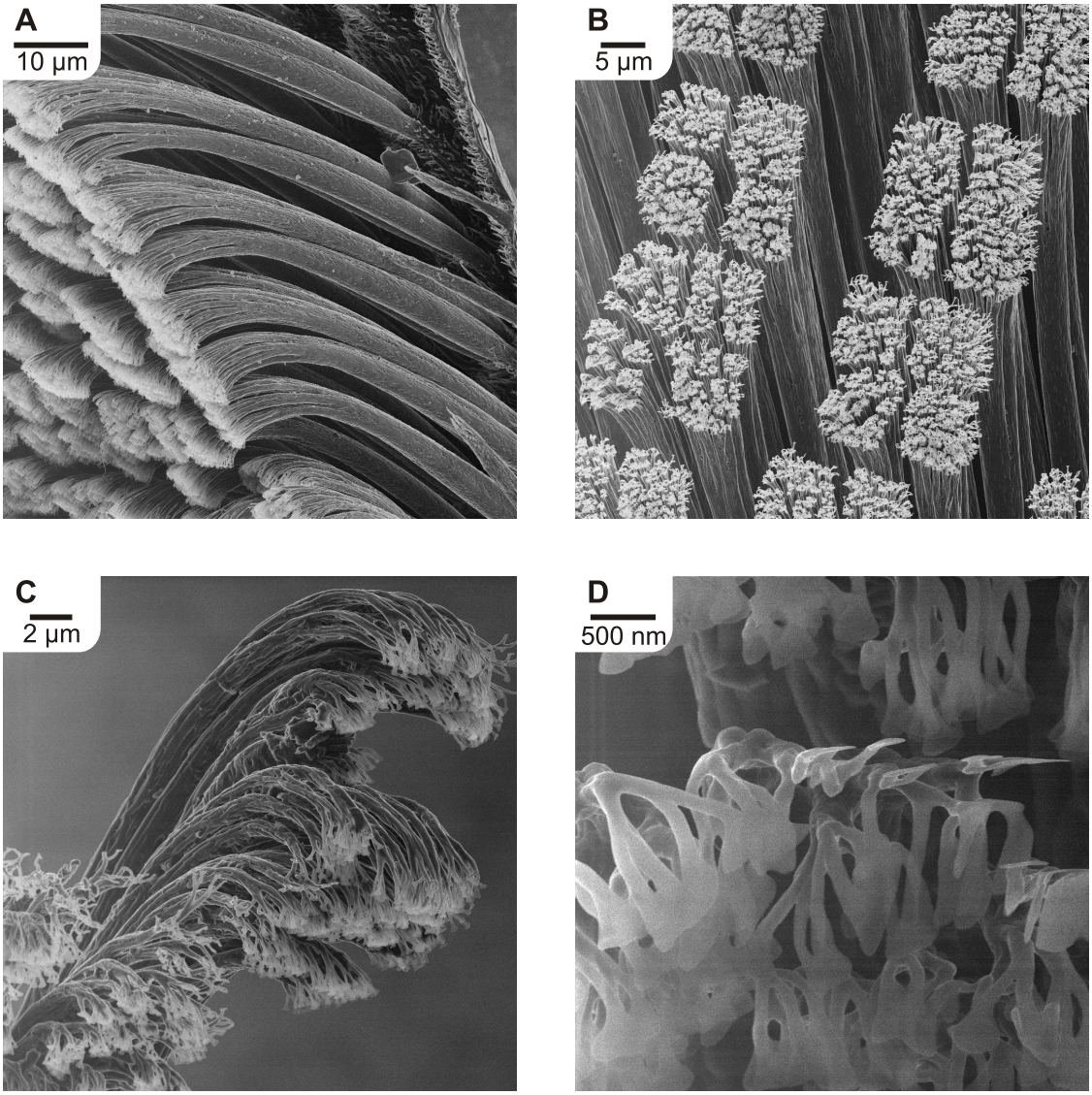

Figure 3.8: Helium ion microscope [Mor2006] images of the adhesive structure of *Gekko gecko*, namely A,B) an array of multiple setae, C) single setae subdividing further into spatulae, and D) the small pads that terminate each spatula. Images taken by Dr. Jijin Yang at Carl Zeiss Microscopy and courtesy of Dr. Jonathan Puthoff. Preparation details are described in Ref. [Yan2011]

closely conform to rough surfaces [Aut2006b]. The large number of nanoscopic contacts that are established at the spatular tips produce considerable overall adhesion on virtually any surface. This adhesion mechanism is also employed by other animals such as bugs, spiders, and flies [Arz2003]. Yet, the gecko—the largest and heaviest of the mentioned examples—possesses the highest-developed system featuring the smallest and most densely packed hairs.

Therefore, the gecko adhesion system provoked not only the interest of researchers in natural science but also of engineers. Since Autumn *et al.* [Aut2002b] published the proof of principle that artificial fibrillar arrays reminiscent of setae can generate high adhesion, multiple promising designs of gecko adhesives have been introduced [Gei2003, Mur2007, Mah2008, Lee2009b].

While the structure of gecko setae is mostly well documented, the mechanisms and interactions leading to the strong adhesive forces are not yet fully understood. As the gecko is able to stick even to atomically smooth surfaces [Aut2002b], a mechanical origin of the adhesion, namely a jamming of the appendages in crevices on the surface, can be ruled out. Due to the very intimate contacts between the terminal end of the spatulae and a surface, intermolecular forces are relevant. First tries to describe the Gecko adhesion were based on water contact angles [Hil1968, Hil1969]. In the last decade, however, van der Waals forces were shown to be a main factor [Aut2002b, Aut2002a, Hub2005]. Furthermore, the impact of humidity on the adhesion forces was discussed extensively. Several studies showed an increase in adhesion force with increasing humidity [Hub2005, Sun2005, Nie2008, Put2010]. Yet, The molecular mechanisms leading to this behavior are explained controversially. Sun *et al.* concluded only capillary forces to be responsible for gecko adhesion [Sun2005]. By measuring the same trends on hydrophilic and hydrophobic substrates, Huber *et al.* and Puthoff *et al.* disproved this assumption and gave explanations based on modified vdW forces [Hub2005] and changes in material properties [Nie2008, Put2010].

3.5 Friction and Contact Mechanics

At the macroscopic scale, the friction force F_{Friction} on an object dragged over a surface is generally regarded to be independent of the contact area and to scale linearly with the applied load L (Amonton's Law)

$$F_{\text{Friction}} = \mu \cdot L \ , \tag{3.14}$$

where μ is the coefficient of friction. Yet, this assumption is only valid owing to the fact that the real contact area is usually unknown due to surface roughness and the influence of other effects, such as wear and tribochemistry. On a microscopic/nanoscopic scale, viz. in the case of only one or a few single asperities, the friction force is proportional to the contact area A and given by

$$F_{\text{Friction}} = \tau \cdot A \ , \tag{3.15}$$

where τ is the interfacial shear strength, which corresponds to the shear force per unit area required to shear the interface [Bow1964, Car1997, Mo2009].

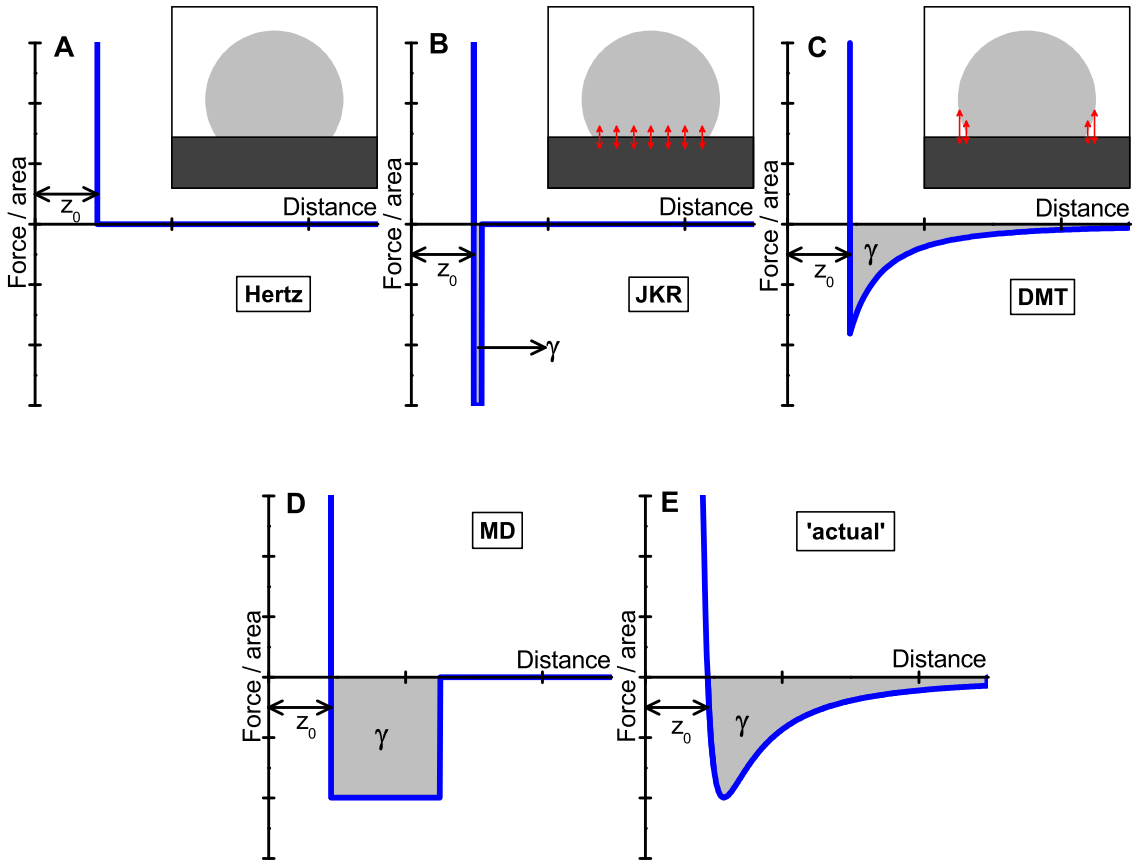

Figure 3.9: Overview of contact mechanic models. Assumed configurations (insets) and the resultant interaction potentials of A) the Hertz model, B) the JKR model, C) the DMT model, and D) the MD model. E) 'Actual' (Lennard-Jones like) interaction potential as a comparison.

Equation 3.15 connects issues of microscale/nanoscale friction with the topic of contact mechanic and the question of the 'actual' contact area of a probe and a surface[19]. This question was addressed by Heinrich Hertz already more than a century ago. In his famous **Hertz theory**[20], the real contact area of a sphere (radius R) pressed against a surface with a load L is calculated [Her1882]. The contact radius a is given by

$$a_{\text{Hertz}} = \left(\frac{R}{K}\right)^{\frac{1}{3}} \cdot L^{\frac{1}{3}} \ , \tag{3.16}$$

with the contact modulus $K = \left(\frac{1-\nu_1^2}{E_1} + \frac{1-\nu_2^2}{E_2}\right)^{-1}$, whereby ν_i and E_i are the Poisson's ratios and the elastic moduli of the involved materials (1,2). The major shortcoming

[19] Equation 3.15 transforms into Equation 3.14 if the 'real contact area' is proportional to the applied load, which is often the case for 'rough', macroscopic surfaces.
[20] J. Boussinesq independently presented the same calculations in 1882 as well.

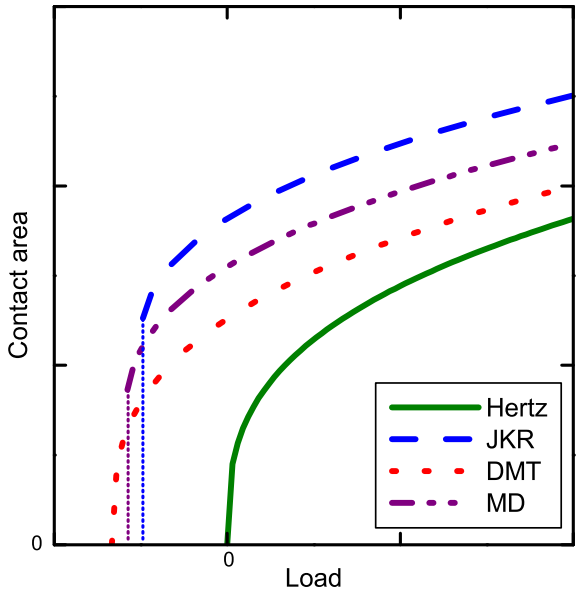

Figure 3.10: The contact area vs. load curves for the Hertz-, JKR-, and DMT-model and an MD intermediate case. Axes are scaled with the MD prefactors β and $\hat{a}$. Figure adapted from [Car1999].

of the Hertzian theory, however, is that all kinds of adhesive forces are disregarded (Figure 3.9 A). Therefore, in the presence of an adhesive interaction, the real contact radius is always larger than the one given by the Hertz theory.

To account for the underestimated contact radius, Johnson *et al.* incorporated the effect of adhesion into the Hertzian theory [Joh1971]. In the **Johnson-Kendall-Roberts (JKR) theory**, elastic energy, potential energy (of the external load), and surface energy are balanced and the contact radius is calculated to

$$a_{\mathrm{JKR}} = \left(\frac{R}{K}\right)^{\frac{1}{3}} \cdot \left[L + 3\pi\gamma_{1,3,2}R + \sqrt{6\pi\gamma RL + (3\pi\gamma_{1,3,2}R)^2}\right]^{\frac{1}{3}}, \tag{3.17}$$

where $\gamma_{1,3,2}$ is the thermodynamic work of adhesion. This is the energy obtained by a change in contact area of the two surfaces (1,2) surrounded by the medium 3 (cf. section 3.1.6). In this way, the JKR theory only includes short-range forces that act at a 'contact distance' $z = z_0$ and can be represented by a delta function $F_{\mathrm{JKR}} = \gamma_{1,3,2}\delta(z - z_0)$ (Figure 3.9 B). This assumption is valid for systems featuring

- elastic materials,
- strong adhesion,
- and a 'larger scale'.

A huge advantage of the JKR theory was that it explained finite contact radii at negative loads. A critical load of

$$F_{\mathrm{JKR}} = -\frac{3}{2}\pi\gamma R \tag{3.18}$$

has to be applied to separate the sphere from the surface. The limitation, however, is that long-range forces are neglected .

To account for long-range forces, Derjaguin *et al.* introduced a completely different extension of the Hertzian theory, the **Derjaguin-Muller-Toporov (DMT) theory** [Der1975]. The basic idea was that long-range forces act in a ring-shaped region outside of the contact area, but do not deform the Hertzian contact profile (Figure 3.9 C). By superposing these additional forces on the applied load, the contact radius is modified to

$$a_{\mathrm{DMT}} = \left(\frac{R}{K}\right)^{\frac{1}{3}} \cdot [L + 2\pi\gamma R]^{\frac{1}{3}} \tag{3.19}$$

and the critical load is

$$F_{\mathrm{DMT}} = -2\pi\gamma R. \tag{3.20}$$

This model, however, is only valid for systems with

- stiff materials,
- weak adhesion,
- and a 'smaller scale'.

Hence, the JKR and the DMT model can be seen as two limiting cases of the interaction spectrum. To describe the intermediate regime, Maugis approximated the 'actual' potential by a square well Dugdale potential (cf. Figure 3.9 D) [Dug1960, Mau1992]. In the **Maugis-Dugdale (MD) theory**, a transition parameter

$$\lambda = 2\sigma_0 \left(\frac{R}{\pi\gamma K^2}\right)^{\frac{1}{3}} \tag{3.21}$$

is defined, where σ_0 matches the minimum adhesive force per unit area in the 'actual' potential. In the case of $\lambda \longrightarrow 0$ the JKR model applies, and in the case of $\lambda \longrightarrow \infty$, the DMT model applies. To predict values for the transition regime, Maugis introduced three dimensionless prefactors: β, $\hat{a}$, and α. Thus, the critical load is given by

$$F_{\mathrm{MD}} = -\beta\pi\gamma R, \tag{3.22}$$

the contact radius at zero load by

$$a_{\mathrm{MD},0} = \hat{a}\left(\frac{\pi\gamma R^2}{K}\right)^{\frac{1}{3}}, \tag{3.23}$$

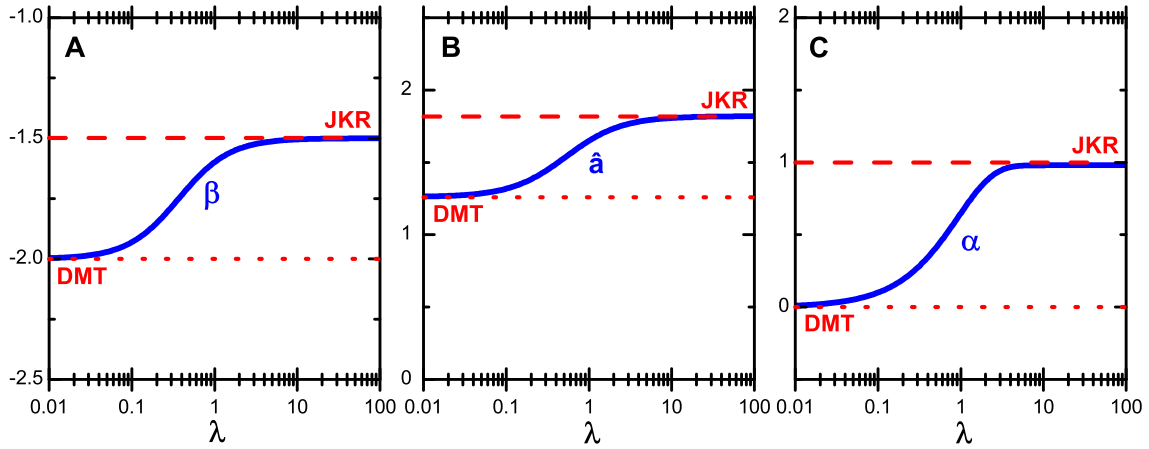

Figure 3.11: Correlation between the Maugis transition parameter λ and the dimensionless MD prefactors: A) β, B) $\hat{a}$, and C) α.

and the general contact radius as a function of the applied load by

$$a_{\mathrm{MD}} = a_{\mathrm{MD},0} \cdot \left(\frac{\alpha + \sqrt{1 - \frac{L}{F_{\mathrm{MD}}}}}{1 + \alpha} \right)^{\frac{2}{3}} . \tag{3.24}$$

The prefactors β, $\hat{a}$, and α are related to the transition parameter λ. Unfortunately, there are no analytic expressions for these relations. Carpick *et al.*, however, provided approximate empirical relations that fit the experimentally determined values reasonably well (within 1% accuracy or better) [Car1999]:

$$\beta = \frac{1}{4} \cdot \left(\frac{4.04 \cdot \lambda^{1.4} - 1}{4.04 \cdot \lambda^{1.4} + 1} \right) - \frac{7}{4}, \tag{3.25}$$

$$\hat{a} = 1.54 + 0.279 \cdot \left(\frac{2.28 \cdot \lambda^{1.3} - 1}{2.28 \cdot \lambda^{1.3} + 1} \right), \tag{3.26}$$

$$\alpha = \frac{1}{1.02} \cdot \left[1 - \exp\left(\frac{\lambda}{-0.924} \right) \right]. \tag{3.27}$$

As shown in Figure 3.11 , in the DMT-limit (roughly $\lambda < 0.1$) the prefactors approach $\beta \longrightarrow -2$, $\hat{a} \longrightarrow \sqrt[3]{2}$, and $\alpha \longrightarrow 0$ and the Equations 3.22 - 3.24 resemble the DMT case (Equations 3.19 and 3.20). Contrariwise, in the JKR-limit (roughly $\lambda > 5$), the prefactors become $\beta \longrightarrow -\frac{3}{2}$, $\hat{a} \longrightarrow \sqrt[3]{6}$, and $\alpha \longrightarrow 1$ and the Equations 3.22 - 3.24 resemble the JKR case (Equations 3.17 and 3.18).

A more detailed overview of the theory of contact mechanics and single-asperity nanotribology is given by the references [Mau1999, Nos2007, Szl2008].

Contact mechanic theories are of relevance for multiple topics in this thesis. On the one hand, the DMT theory is used to model the nanoscale contact between AFM tips and samples: Thus, by fitting the force distance curves acquired in PeakForce QNM® with the DMT model, the local elasticity of the sample, for instance, can be extracted (cf. section 4.2.4 and section 6.2). On the other hand, the MD model is applied to model the adhesive contact of the gecko spatulae with a sample (cf. section 5.1.3).

4 Materials and Methods

4.1 Substrates

4.1.1 Silicon wafers

To allow for a separate variation of surface properties and subsurface composition, a set of model substrates was utilized (cf. Figure 4.1). The model substrates are based on silicon wafers[1] with two different types of oxide layers: 'type N' wafers with a native silicon oxide layer of 1.7(3) nm (Wacker Siltronic AG, Burghausen, Germany and Si-Mat, Landsberg, Germany) and 'type T' wafers with a thick thermally grown silicon oxide layer with a thickness of 150(1) nm (Silchem, Freiberg, Germany and Si-Mat, Landsberg, Germany). The surfaces of both wafer types are identical as shown by a thorough characterization using AFM, ellipsometry, contact angle and ζ-potential measurements (cf. Table 4.1 and Figure 4.2). Furthermore, X-ray reflectivity and XPS data provided in the **publication in Addendum I** corroborate that the native oxide layers do not differ in their density from the thermally grown layers and that the stochiometry of the uppermost layer is indeed SiO_2. Thus, the two types of silicon wafers in combination feature the targeted characteristics: They differ in the subsurface composition but resemble each other in terms of their surface properties.

Immediately prior to use, the substrates were cleaned by immersing them for 30 min in freshly prepared 'piranha solution', a 1:1 mixture of sulfuric acid H_2SO_4 (conc.) and unstabilized hydrogen-peroxide H_2O_2 (30%). To remove residues of the acids, the wafers were put in boiling deionized water for 90 min, changing the water four times in between. In addition to the chemical cleaning process, a mechanical cleaning step was employed, during which the wafers were exposed to a 'Snow-Jet'—a focused jet of CO_2 crystals that removes micro- and macroscopic particles [She1994].

A second pair of substrates linked by the same characteristics was obtained by hydrophobizing both wafers—immediately after the cleaning procedure—using a self-assembled monolayer of silane molecules with a CH_3 tailgroup (octadecyltrichlorosi-

[1] The silicon wafers are polished and feature a 1-0-0 crystal orientation, a thickness of 525(20) µm, a specific resistance of $10 - 20\,\Omega\,cm^{-1}$, and a boron (p) doping.

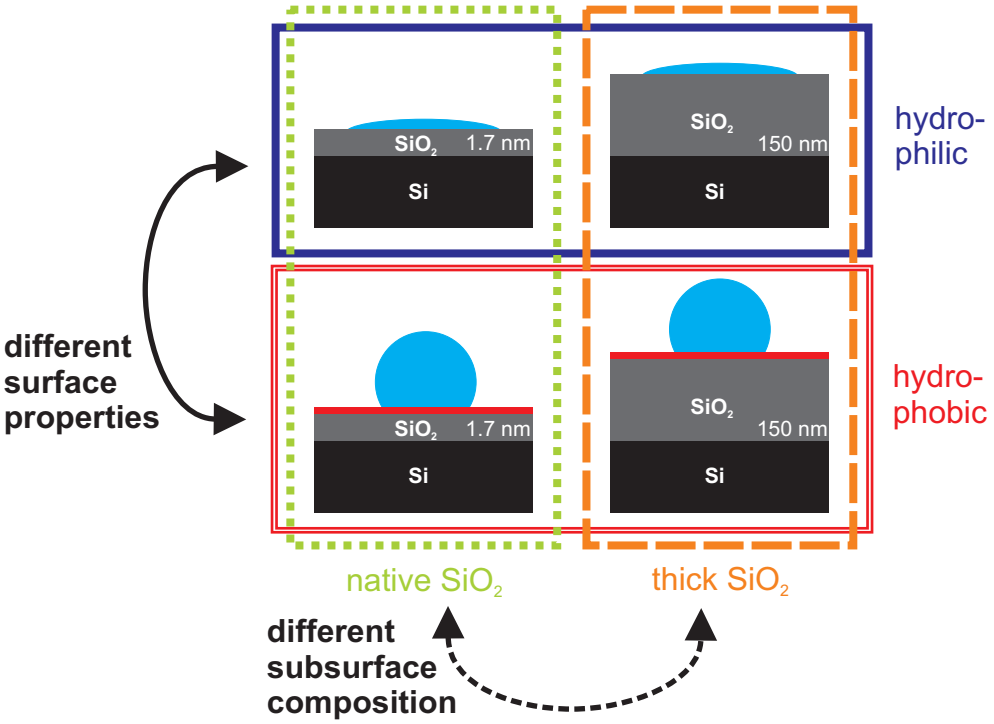

Figure 4.1: Model substrates based on silicon wafers with different thicknesses of oxide layers that allow for a separation of interactions depending on surface parameters and interactions arising from subsurface materials. The surface chemistry is tuned by a silanization of the wafers that renders them hydrophobic. The blue droplets illustrate the different water contact angles.

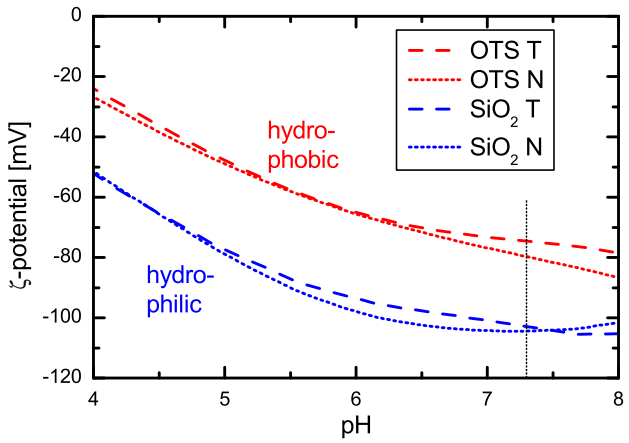

Figure 4.2: ζ potentials of hydrophobic (OTS) and hydrophilic (SiO_2) type T and type N wafers as function of pH, giving insight into the strength of electrostatic interactions.

Table 4.1: Surface properties of the set of tailored Si wafers: root mean square (rms) roughness, advancing (adv) and receding (rec) water contact angles, and Lifshitz-van der Waals (LW) as well as Lewis acid-base (AB) components of the surface energy γ obtained from contact angles of three different liquids [Myk2003].

d_{oxide} (nm)	rms (nm)	γ^{LW} (mJ m^{-2})	γ^{AB} (mJ m^{-2})	Θ_{adv} (°)	Θ_{rec} (°)	
OTS T	150(1)	0.19(3)	24(1)	0	111(3)	103(4)
OTS N	1.7(3)	0.17(0)	24(1)	0	111(2)	103(2)
SiO_2 T	150(1)	0.13(3)	43(1)	20(1)	5(2)	compl. wetting
SiO_2 N	1.7(3)	0.09(2)	43(1)	21(1)	7(2)	compl. wetting

lane, OTS, Sigma-Aldrich, Germany) following a modified recipe [Les2012] based on standard procedures [Brz1994, Was1989]. The produced OTS surfaces were also characterized using AFM, ellipsometry, contact angle and ζ-potential measurements (cf. Table 4.1 and Figure 4.2). Additionally, the high quality of the achieved OTS monolayers was affirmed by X-ray reflectivity measurements: The obtained values of the measurements shown in the **publication in Addendum II** agree well with literature values [Mez2006]. Altogether, the characterization shows that the OTS layers feature a thickness of approximately 2.6 nm, an rms roughness below 0.2 nm, and a uniform coverage, whereby a homogenous, dense, almost upright (tilt angles of $4° - 5°$ [Ger2012]) all-trans configuration of the molecules is indicated. In preparation for experiments, the hydrophobic wafers were cleaned by immersing them subsequently into ethanol and acetone (5 min each) in an ultrasonic bath. Afterwards, the wafers were in some cases—if specifically noted in the respective study—rinsed for 30 min in boiling deionized water in order to remove residues of the solvents.

In summary, the set of tailored Si wafers contains combinations of two different surface chemistries—hydrophilic 'SiO_2' and hydrophobic 'OTS' wafers—and two different subsurface compositions—'type N' wafers with a native thin oxide layer and 'type T' wafers with a thick oxide layer. Hence, the set allows for a separate study of interactions depending on surface parameters and interactions arising from subsurface material.

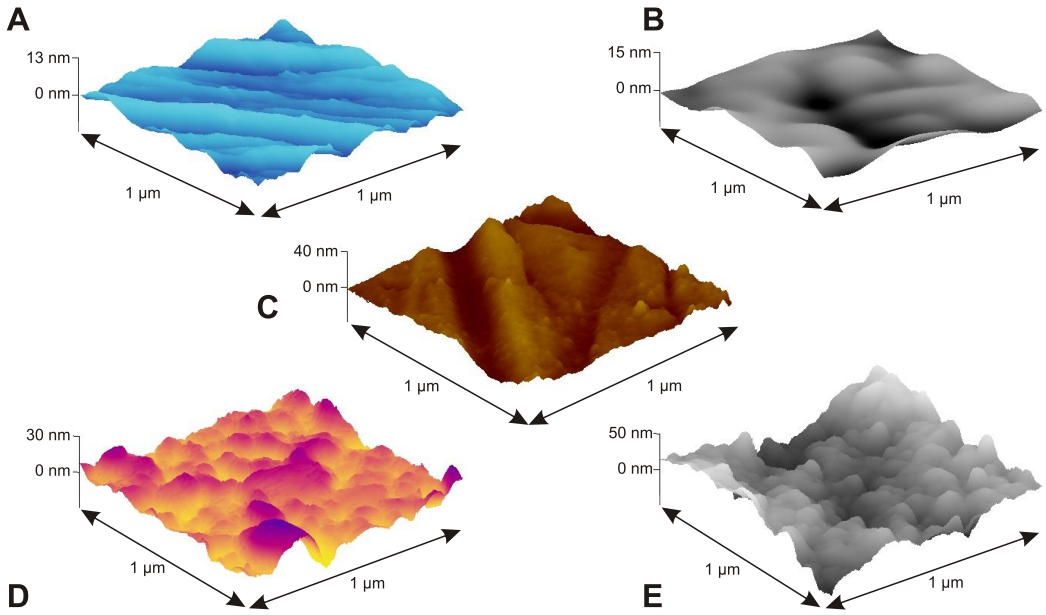

Figure 4.3: AFM topography images of $1m \times 1m$ sections of the 'everyday substrates' A) polished stainless steel, B) aluminum, C) copper, D) gold, and E) a part of a yoghurt cup (PP). Note the different height scales.

Table 4.2: Root mean square (rms) roughness and advancing water contact angles of the selection of 'everyday substrates': stainless steel, aluminum (Al), copper (Cu), gold (Au), and a part of a yoghurt cup (PP).

	stainless steel	Al	Cu	Au	yoghurt cup (PP)
rms (nm)	2.20(4)	4(1)	9(2)	5.13(1)	16(1)
Θ_{adv} (°)	< 10	< 10	< 10	< 10	$65 < \Theta < 110$

4.1.2 'Everyday Substrates'

Besides the systematic studies using the set of tailored Si wafers, this thesis includes an applied study on a selection of 'everyday substrates'[2]: Stainless steel, aluminum, copper, and a part of a yoghurt cup (PP) were chosen as 'everyday substrates' (cf. Figure 4.3).

To achieve comparable smooth surfaces with a nanometer scale roughness (cf. Table 4.2), different preparation and polishing techniques were applied:

[2]The preparation and characterization of the substrates in this section were performed by Sebastian Hümbert during his work as a diploma student tutored by Peter Loskill (cf. [Hue2010]).

The stainless steel, aluminum, and copper samples were treated using abrasive paper with four different grits. Following the abrasion process, the samples were cleaned by immersing them subsequently into toluol, acetone, and ethanol in an ultrasonic bath (5 min each). In between the cleaning steps, the samples were carefully dried in a nitrogen stream.

The gold surfaces were prepared by a vapor deposition process (UNIVEX, Leybold-Heraeus GmbH, Cologne, Germany). Silicon wafers—cleaned as described in section 4.1.1—were coated with a roughly 4 nm thick chromium layer that enables a strong adhesion between the subsequent gold layer and the underlaying wafer. To prevent any influence of the underlying material on the investigated surface processes, the gold layer was prepared to achieve a thickness of roughly 100 nm. The thickness of the deposited layer was thereby monitored using a quartz crystal microbalance (XTM/2 Deposition Monitor, Inficon, New York, USA).

A yoghurt cup consisting of **polypropylene (PP)** was selected as a real everyday sample. The off-the-shelf yoghurt cup was cut up in millimeter sized pieces. The pieces were then cleaned by immersing them in deionized water and ethanol in an ultrasonic bath (5 min each) and subsequently dried in a nitrogen stream.

4.2 Atomic Force Microscopy

The first atomic force microscope (AFM) was introduced already more than two decades ago by Gerd Binnig [Bin1986a, Bin1986b]. Since then, AFMs have developed to one of the most important microscopy techniques in nanoscience. The fundamental principle of an AFM is based on the scanning of a small pyramidal tip across a surface. Since the actual contact between the tip and the surface is made by only a few atoms, it is possible to achieve atomic resolution with an AFM. The tip itself is placed at the end of a cantilever, which is moved by piezo motors relative[3] to a sample in x, y, and z direction, whereby the deflection of the cantilever is monitored. The monitoring is commonly achieved using the beam-bounce method: A laser is focused on the backside of the cantilever and the reflection detected by a four-quadrant photodiode. Besides, there are several other detection methods available such as interferometry or scanning tunneling microscopy[4]. Based on the deflection data, the AFM is operated using a feedback loop. As feedback signal, several parameters can be used, depending on the targeted application. In general, two fundamental modi of operation exist: static AFM and dynamic AFM.

The most common static AFM mode is the contact mode with constant force: While the tip scans across the sample, the feedback loop keeps the applied force, viz. the

[3] Depending on the AFM model, either the cantilever, the sample or both are moved.
[4] In the original design by Binnig, a scanning tunneling microscopy was used.

deflection of the cantilever, constant. To achieve this, the z-position of the cantilever is varied by a piezo motor. This variation directly reflects the topography of the sample and is used as the output signal. The disadvantage of static AFM in general is that while scanning, a normal and a lateral force are applied to the sample. Thus, deformations of the sample can occur, possibly inducing imaging artifacts, and both tip and sample can get damaged.

In dynamic AFM, the cantilever is oscillated close to its resonance frequency. Interactions between tip and sample impose an additional spring and therefore modify the resonance frequency of the system. Since these interactions, viz. the spring constant of the 'extra spring', are dependent on the distance between the tip and the surface, the resonance frequency shift[5] can be utilized as well to maintain a constant height above the sample surface. In the most common dynamic AFM mode[6], the tapping mode™ (TM), also referred to as intermittent contact mode or amplitude modulation atomic force microscopy (AM-AFM), the excitation frequency is kept constant and the separation between cantilever and substrate decreased until a specified setpoint for the oscillation amplitude is reached. While scanning, the z-position of the cantilever is varied—in an analogous manner as in the contact mode—to maintain the specified amplitude setpoint. In principle, the z-movement again corresponds to the topography of the sample[7]. Benefits of TM-AFM are that no lateral forces are applied and that normal forces are exerted only when 'tapping' onto the sample in the reversal points of the oscillations[8]. Thereby, the risk of a deformation or alteration of the sample is reduced. For this reason, TM-AFM is commonly used to study soft and damageable samples.

Yet, the biggest advantage of dynamic AFM is the so-called phase image. The energy dissipated while oscillating induces a phase shift relative to the driving force. Hence, the phase image is a map of the dissipated energy at the respective point on the sample. The dissipated energy, however, is influenced inter alia by the properties of the imaged material (e. g. adhesion, elasticity). Consequently, the phase image reflects a map of the material properties of the sample—if the setpoint is kept constant throughout the imaging. This ability to not only image the topography of the sample, but also to probe its properties provides an unique selling point to AFM that distinguishes it from other microscopy techniques.

Today, AFM is not only employed in physics or material science; in microbiological research, AFM has emerged as a very powerful tool in recent years [Duf2002, Duf2004,

[5] The resonance frequency shift results in a shift in the oscillation amplitude if the excitation frequency is not changed.

[6] An introduction in dynamic AFM modi in general is given in the reference [Gar2002].

[7] Yet, this is strictly speaking only true for chemically homogenous samples. Otherwise, if the tip 'taps' on the surface, differences in mechanical properties can cause a change in the amplitude as well and thereby induce an apparent topography.

[8] Dynamic AFM enables pure non-contact modes as well, preventing even these 'tapping' forces.

Duf2008, Kas2008, Wri2010]. Due to its high-resolution paired with the possibility to work in buffers and to map material properties, AFM provides considerable advantages over conventional microscopy techniques. It is, for instance, possible to quantitatively study the elasticity of bacterial and eukaryotic cells [Mat2001, Tou2003b, Duf2004, Ric2005] or to image DNA *in-situ* [Han1992, Mou1995, Lyu1997].

A more comprehensive introduction in AFM is given in the references [Gie2003, Los2009]. In this work, AFMs of the types BioScope Catalyst™ and Dimension® Icon® (both Bruker, Santa Barbara, USA) were employed.

4.2.1 Force Spectroscopy

As mentioned above, it is possible to extract data on mechanical properties from the phase image in TM-AFM. Yet, the informative value of these data is restricted. The knowledge of the dissipated energy is not directly transferable into quantitative data on, for instance, elasticity or adhesion. Hence, to gain quantitative data on the mechanical properties of a sample, the force spectroscopy mode is commonly used. In this mode, the AFM cantilever is moved solely along the vertical axis and is not scanned over the sample surface. Thereby, the vertical force field is characterized and quantitative data on the maximum adhesion force between the tip and the sample can be extracted (cf. Figure 4.4): The maximum negative deflection[9], also referred to as the adhesion peak, can directly be converted to the maximum adhesion force by means of the cantilever spring constant [Car2007]. Moreover, by pressing the AFM tip onto the sample up to a specified force threshold, additional information about the mechanical properties such as the elasticity of the sample are gained [Wei1993, Heu1995, Vin1998, Nor2006, Den2011].

The drawback of the force spectroscopy mode, however, is that it lacks any lateral resolution. A straightforward improvement is provided by the force volume mode, in which multiple force/distance curves are performed on a grid with adjustable spacing. Thereby, the force field is mapped in three dimensions and hence some kind of lateral resolution as well as an image of the topography[10] are gained. A more comprehensive disquisition on AFM force spectroscopy is given in the references [But2005, Car2007, Seo2008].

[9] The maximum negative deflection is usually obtained at the moment of the breakaway of the tip from the surface.

[10] The point of contact in each force/distance curve provides information of the sample height in this point.

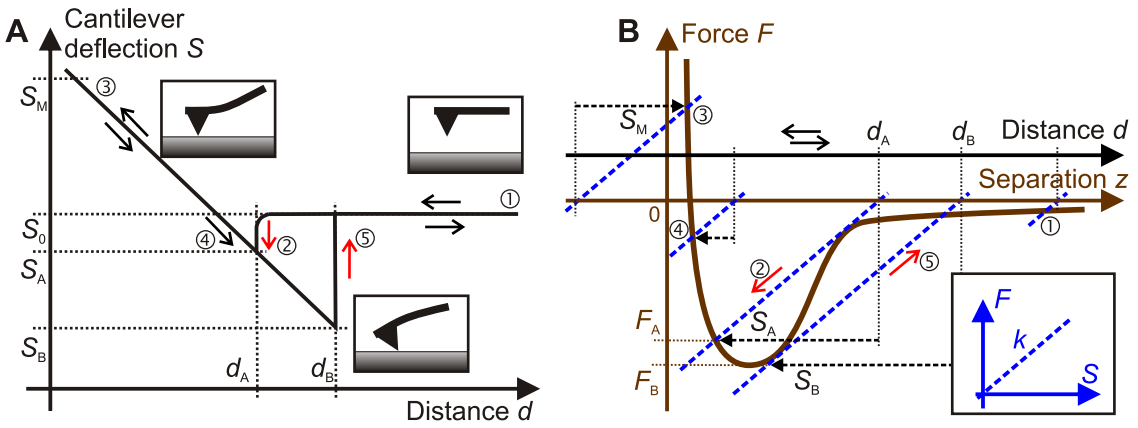

Figure 4.4: A) Scheme of a force/distance curve, whereby the cantilever deflection S is plotted against the distance d between sample and mounting of the cantilever. B) Typical plot of the force F acting between the AFM tip and a sample against their separation z. The blue dashed lines represent the force/deflection relations of an AFM cantilever for selected (①-⑤) distances d between sample and mounting of the cantilever. For typical deflections, an AFM cantilever can be described by Hooke's law (with cantilever spring constant k; cf. inset). Since the mounting of the cantilever is moved along the z-axis, the zero-point of its force/deflection relation is shifted as well. At any time, the deflection S can be obtained from the point of intersection of the respective cantilever force/deflection relation and the interaction force curve (balance of forces). Usually, two discontinuities exist: During the approach phase (at a distance d_a), the deflection of the cantilever increases suddenly (up to S_a) when the slope of the interaction force curve exceeds the cantilever spring constant (②, 'snap-in contact'). During the retract phase exists a bistable point as well: Often, an adhesion keeps the tip in contact with the surface until the cantilever force exceeds the adhesion force. There (at a distance d_b), the cantilever snaps off the sample, resulting in the so-called adhesion peak in the force/distance curve (⑤, 'snap-off contact'). The transition between approach and retract phase occurs when a specified force threshold, viz. a maximum positive deflection S_M, is reached (③).

Force Spectroscopy with Surface Delay

In the course of a force/distance curve, the actual time during which the tip is in contact with the surface is in the range of a few hundreds of milliseconds—in the case of usual ramp rates of a few Hz. To investigate if the adhesion force is contact time dependent, measurements with an adjustable surface delay (SD) can be performed. In this thesis, SDs in the range of 0 s to 10 s are used. 0 s SD thereby stands for a standard force/distance curve with no break at the trigger threshold, viz. no additional contact time. In order to compare different experiments that comprise multiple series of measurements with increasing SD, Boks *et al.* used

$$F(t_{SD}) = F_0 + (F_\infty - F_0)\left(1 - \exp -\frac{t_{SD}}{\tau}\right) \tag{4.1}$$

to fit their data, whereby F_0 is the adhesion force in the case of 0 s SD, F_∞ is the maximum adhesion force after strengthening, and τ is the characteristic time needed for the adhesion to strengthen [Bok2008a, Mei2009]. However, in the case of force/distance curves, these parameters have no specific physical or biological meaning and serve only as a tool for comparison.

Force Spectroscopy with Functionalized Tips

The adhesion forces usually determined in the force spectroscopy mode arise from the interaction of the sample and the AFM tip, which is typically made of SiO_2 [Wol1991, Ran1994] or Si_3N_4 [Alb1990]. Yet, in many cases it is necessary to determine the adhesion between a selected probe material and a sample. Thereto, functionalized AFM cantilevers are necessary.

The most straightforward type of functionalization is the modification of the surface chemistry of the entire tip: This is usually achieved by the application of self assembled monolayers (SAMs) of thiols or silanes with defined tail group such as hydroxyl (-OH), carboxyl (-COOH), or amino (-NH_2) groups [Fri1994, Noy1995, Noy1997, Cle1999, Dag2007, Dor2008].

A more complicated kind of functionalization is the immobilization of single macromolecules on the apex of an AFM tip. By using these types of tips, single molecule force spectroscopy can be performed and the forces between single molecules can be measured [Hin2006, Neu2008]. Since the pioneering work of Merkel *et al.*, where they studied receptor ligand interactions [Mer1999], a wide variety of molecules have been investigated in terms of their adhesion properties: The adhesion of, for instance, fibronectin to surfaces, cells, or integrins has been studied extensively [Li2003, Vel2008, Ver2009, Yon2007, Buc2010]. Other studies investigated the adhesion of molecules such as single amino acids [Lee2006], antigens [Ber2005], antibiotics [Gil2007], or further proteins [Tou2003a, Dup2005]. Besides measuring adhesion forces, however, the AFM can also be used to stretch or unfold a protein—or a macromolecule in genera: By attaching the macromolecule not only to the tip, but also to the substrate, its intrinsic energy landscape can be explored [Rie1997, Car1999, Car2000, Fis2000].

The complexity of the functionalization, however, is not limited to single molecules. Complex microscopic objects can also be attached to AFM cantilevers; for instance, nano- and microparticles of arbitrary material [Yon2006, Ong2007, Gan2007, Bus2008], air bubbles [Tab2011], and gecko [Hub2005] or abalone setae [Lin2009]. It is even possible to immobilize alive organisms such as eukariotic cells [Ben2000, Bow2001, Hel2008] or bacteria [Ong1999, Low2000, Eme2004]. In this thesis, AFM force spectroscopy experiments with bacterial probes play a major role. Hence, the design and preparation of bacterial probes are described in more detail in the following section.

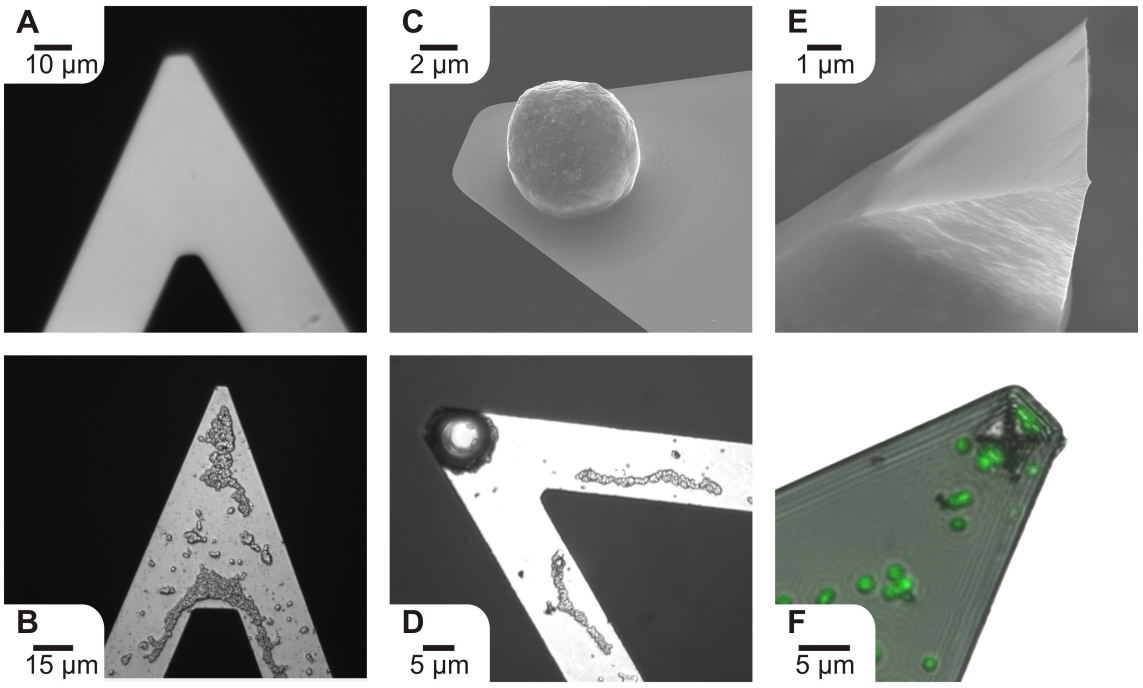

Figure 4.5: Examples of typical AFM cantilevers featuring different tip geometries. All types of cantilevers can be used for the preparation of bacterial probes, thereby displaying different advantages and disadvantages. Optical microscopy of A) a bare tipless cantilever and B) a tipless cantilever coated with *S. carnosus*, C) SEM image of a spherical probe cantilever and D) optical microscopy of a spherical probe cantilever coated with *S. carnosus*, E) SEM image of a standard pyramidal tip cantilever and F) confocal fluorescence microscopy image of a pyramidal tip cantilever coated with fluorescently labeled *S. carnosus*.

4.2.2 Bacterial Probes for AFM Force Spectroscopy

To perform AFM force spectroscopy experiments with bacterial probes, single bacteria or clusters of bacteria have to be immobilized onto the AFM cantilever. For the immobilization, two parameters are of major importance, namely the geometry of the AFM tip and the selection of an appropriate glue.

The geometry of the tip affects the size of the contact area and—closely related—the amount of bacteria that makes contact with the sample under study. Various tip geometries are possible. In the studies in the references [Los2009, Hue2010], the applicability of multiple different geometries and preparation procedures is investigated. Figure 4.5 shows some typical examples with standard geometries.

The most common tip geometry is the absence of a tip (cf. Figure 4.5 A, B) [Bow2001, Bok2008a, Mei2009, Kan2009, Zha2011]. These so-called **tipless cantilevers** feature a large and accessible contact area. Thereby, they have the advantages of an easy

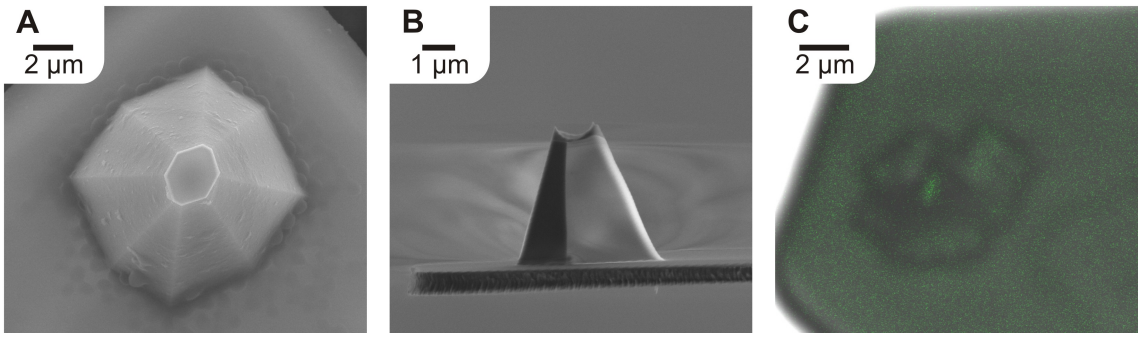

Figure 4.6: Specifically designed tip geometries that are especially suitable for the preparation of bacterial probes: A) SEM image of a cantilever featuring a plateau tip, B) SEM image of a cantilever featuring a 'bacteria saddle' tip, achieved by modification of a standard pyramidal tip using a focused ion beam (FIB), and C) confocal fluorescence microscopy image of a single bacterium immobilized in the 'bacteria saddle' tip.

functionalization with a glue and of a straightforward fixation of bacteria at suitable positions. The disadvantage, however, is that the number of bacteria that are in contact with the substrate's surface is uncertain due to the large contact area. Therefore, it is not possible to compare measurements with different cantilevers. Measurements with the same cantilever on different substrates, however, are comparable.

Further common tip geometries utilized as basis for bacterial probes are spherical probes (cf. Figure 4.5 C, D) [Low2000, Low2001] and pyramidal tips (cf. Figure 4.5 E, F) [Raz1998, Eme2006, Cao2006]. Both have the benefit of a controlled contact area and an accessible and hence controlled number of bacteria that are in contact with the substrate's surface. Thus, measurements with different cantilevers are comparable[11]. The preparation of bacterial probes based on these types of cantilevers, however, is much more complicated compared to tipless cantilevers. Both—spherical probes and pyramidal tips—offer only a small contact area to the bacteria due to the respective—curved or pointed—geometry. Therefore, a high adhesive strength of the glue holding the bacteria onto the cantilevers is necessary. Moreover, it is harder to place single bacteria at the respective spot, the apex of the tip or the topmost part of the sphere (cf. Figure 4.5 D, F).

A compromise between controlled contact area and straightforward preparation is to employ specifically designed geometries. Commercially available are plateau cantilevers (e. g. PL2-CONTR-10, NANOSENSORS™, Neuchâtel, Switzerland), which provide a flat contact area to a small number of bacteria (cf. Figure 4.6 A). An even more controlled contact area that enables the immobilization of a single bacterium can be achieved by a modification of standard pyramidal tips. Using a focused ion beam (FIB), it is possible to remove the apex of the tip and to generate a 'saddle'-like

[11] Results from measurements with spherical probes have to be scaled with the probe radius.

structure (cf. Figure 4.6 B). By choosing an adequate[12] diameter of the saddle, a single bacterium can be immobilized in it (cf. Figure 4.6 C). Unfortunately, these 'special' types of cantilevers are costly in terms of either labor or money. Hence, they are only restrictedly suitable for experiments that require a certain amount of statistics, such as AFM force spectroscopy.

The glue selection is especially challenging due to two major requirements: On the one hand, the bacteria must be firmly attached to the cantilever by a force that exceeds the adhesion force to the substrate under study. On the other hand, the viability and the properties of the bacterial cell wall that is not in contact with the cantilever must not be affected.

Various types of glues based on different binding mechanisms have been presented in the literature[13]:

- Positively charged polymer coatings such as polyethyleneimine (PEI) [Raz1998, Ong1999] and poly-L-lysine (PLL) [Bok2008a, Qu2011] can be used, since the surfaces of both, the bacterium and the cantilever, are negatively charged at a physiological pH.
- By using aminosilanes, -thiols [Low2001, Nea2005], or poly(dopamine) (PDA) [Lee2009a, Kan2009], the cantilevers can be functionalized with amino groups that form strong, unspecific, covalent bonds with the carboxyl groups in the bacterial cell wall.
- Specific linkage can be achieved by coating the cantilevers with proteins such as fibronectin [Kuu1978, Buc2010].

Although approaches such as the use of regular glue have also been reported in the literature [Bow2001, Bow2002], the general satisfaction of the second requirement—the prevention of any alteration of the bacterium—is highly doubtful. The same is true for procedures involving the crosslinking via glutaraldehyde [Raz1998, Ong1999], which is known to have an effect on the surface properties of the entire bacterium [Vel2002, Bur2003].

In the experiments presented in this thesis, the employed bacterial probes are all based on triangular shaped tipless cantilevers (PNP-TR-TL, Nanoworld, Neuchâtel, Switzerland and NP-0, Bruker, Santa Barbara, USA). The fixation of the bacteria was achieved primarily using PLL, a polymer with positively charged side chains that is known to form adhesive interlayers [Voe1995, Wes1997]. In some studies[14], however, PDA was utilized. PDA is produced by the self-polymerization of dopamine [Lee2007a,

[12] Saddle diameters that are equal to the diameter of the respective type of bacteria or slightly above give the best chances of success.

[13] An extensive disquisition on the advantages and disadvantages of various types of glues can be found in the refs. [Los2009, Hue2010].

[14] The applied coating is always mentioned in the respective studies.

Lee2007b]. Dopamine is closely related to the catecholic amino acid 3,4-dihydroxy-L-phenylalanine (DOPA), which is secreted by mussels and is capable to form strong coordination bonds with inorganic materials and covalent bonds with organic surfaces [Lee2006].

The preparation procedures for both glues were preceded by a cleaning step, during which the cantilevers were treated with an air plasma.

The PLL coating was then applied by immersing the AFM cantilever in a droplet of PLL (MP Biomedicals, Solon, USA) solution (0.1 mg/ml) for 1 h. Subsequently, the cantilever was carefully rinsed with phosphate buffered saline (PBS).

The PDA coating was achieved by immersing the cantilever vertically into a solution of dopamine hydrochloride (Sigma-Aldrich, Steinheim, Germany) in 10 mM tris(hydroxymethyl)aminomethane (TRIS)/HCl-buffer (pH 8.3 at 23 °C) for 1 h at 4 °C. Following this, the cantilever was rinsed with deionised water and dried in vacuum for 10 min.

Immediately after the preparation of the respective adhesive interlayer, the cantilevers were placed in a droplet of bacteria solution for 1 h at 4 °C. To remove unbound bacteria, the probes were then rinsed with PBS. In general, bacterial probes were freshly prepared prior to the experiments.

4.2.3 Implementation of Force Spectroscopy Experiments

The AFM force spectroscopy experiments with bacterial probes in this work consist of multiple series of force measurements on each substrate under study. Each series usually[15] consists of 50-100 single force/distance curves. In order to avoid inaccuracy due to local irregularities in the substrate, every single force/distance curve was carried out at a different spot[16] on the surface. If not indicated otherwise, single force/distance curves were carried out with a ramp size of 1 µm, a ramping speed of 1 Hz and a maximal force trigger threshold of 1 nN.

To convert the measured photodiode signal first into cantilever deflection and then into force, the deflection sensitivity and the cantilever spring constant of the system have to be quantified. The deflection sensitivity was determined by a force/distance curve on a hard substrate: After the tip makes contact with such a surface, the engaged distance directly translates into a deflection of the cantilever. The cantilever spring constant is obtained by the thermal tune method [Hut1993, Ser2005]. Since the

[15] Some series in the SD experiments consist of 30-40 single measurements to decrease the stress on the bacterial probe.

[16] The probed surface spots are arranged along a grid with 0.5 µm to 5 µm spacing.

bacterial probe could get damaged in the course of these two calibration steps, the entire procedure was carried out subsequent to the experiment. Hence, typical values for the respective system were used as calibration constants prior to the experiment and afterwards replaced by the obtained values.

An essential task when working with bacterial probes is to ensure the integrity of the bacterial probe throughout the entire experiment—irrespective of the glue or the type of cantilever used for the bacterial probes. Therefore, a detaching of bacteria or any other probe alteration must be detected. In this work, the integrity of the bacterial probes was controlled either by optical microscopy prior and after the experiment or by control measurements: Consecutive series of force/distance measurements were taken alternately on the substrates under study, ending always on the substrate and with the respective parameters (e. g. surface delay) that had been probed first.

4.2.4 PeakForce QNM®

As can be inferred from the preceding sections, the AFM modes commonly used to study physical properties of the surface have severe limitations:

- TM-AFM provides a high spatial resolution, but is limited in terms of quantitative analysis.
- The force spectroscopy mode allows for a quantitative analysis, but lacks any spatial resolution.
- The force volume mode seems to be a good compromise: It produces quantitative data and enables spatial resolution. The achieved resolution, however, is usually very low and the imaging time very long.

PeakForce tapping mode with quantitative nanomechanical property mapping (PeakForce QNM®) is a recently introduced mode that combines the advantages of the three classical modes mentioned: It allows for simultaneous quantitative mapping of topography and multiple mechanical properties (e. g. elasticity, adhesion, deformation), featuring the typical resolution and scan speed of the tapping mode [Ple2010, Pit2010, Ber2011]. PeakForce QNM® can be employed for various types of biological or artificial samples [Ber2010, Ada2011, Su2012, Ple2012, Trt2012, Bit2012].

From a technical point of view, PeakForce QNM® is basically a combination of force volume mapping and TM-AFM. In contrast to the latter, the drive frequency is far below the resonance frequency of the cantilever and the feedback loop keeps the maximum cantilever deflection and thereby the maximum applied force constant instead of the vibration amplitude. Thereby, a force/distance curve is produced each time the tip taps on the surface. By analyzing the force/distance curve in each point

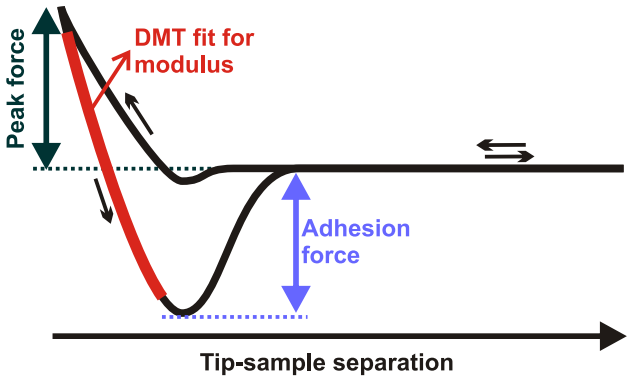

Figure 4.7: In PeakForce QNM® mode, each time the tip taps on the surface, a force/distance curve is acquired. Thereby, information about multiple mechanical properties in each point can be collected. The adhesion force can be extracted as the height difference between the negative adhesion peak and the zero force baseline. The peak force is defined as the vertical distance between the baseline and the turn-away point. The Young's modulus is obtained by a DMT fit [Der1975, Mau1999] of the retract part of the force/distance curve (Scheme adapted from [Pit2010]).

(cf. Figure 4.7), a map of mechanical properties such as elasticity (Young's modulus) or adhesion force is achieved. The adhesion forces between tip and sample are thereby gained the same way as in classical force spectroscopy: The height differences between the negative adhesion peaks and the respective zero force baselines are determined for each single force/distance curve. The Young's moduli are obtained by a DMT fit [Der1975, Mau1999] of the retract part[17] of the force/distance curves described by

$$F - F_{\mathrm{Adh}} = \frac{4}{3}\frac{E}{(1-\nu^2)}\sqrt{R}\,(d-d_0)^{3/2}, \tag{4.2}$$

with the determined force relative to the adhesion force $F - F_{\mathrm{Adh}}$, the Poisson's ratio ν, the radius R of the tip, the deformation $d - d_0$ of the sample, and the targeted Young's modulus E.

4.3 Parallel Plate Flow Chambers

In order to study bacterial adhesion on bacteria in a free swimming (planctonic) state as well, parallel plate flow chamber experiments were conducted in addition to the

[17] In contrast to typical simple Hertz fits, the DMT fit takes long-range attractive forces into account. Thus, the reference point is the point of maximum adhesion—in the retract part—and not the point of zero indentation—in the approach part. The correct determination of the latter is often delicate.

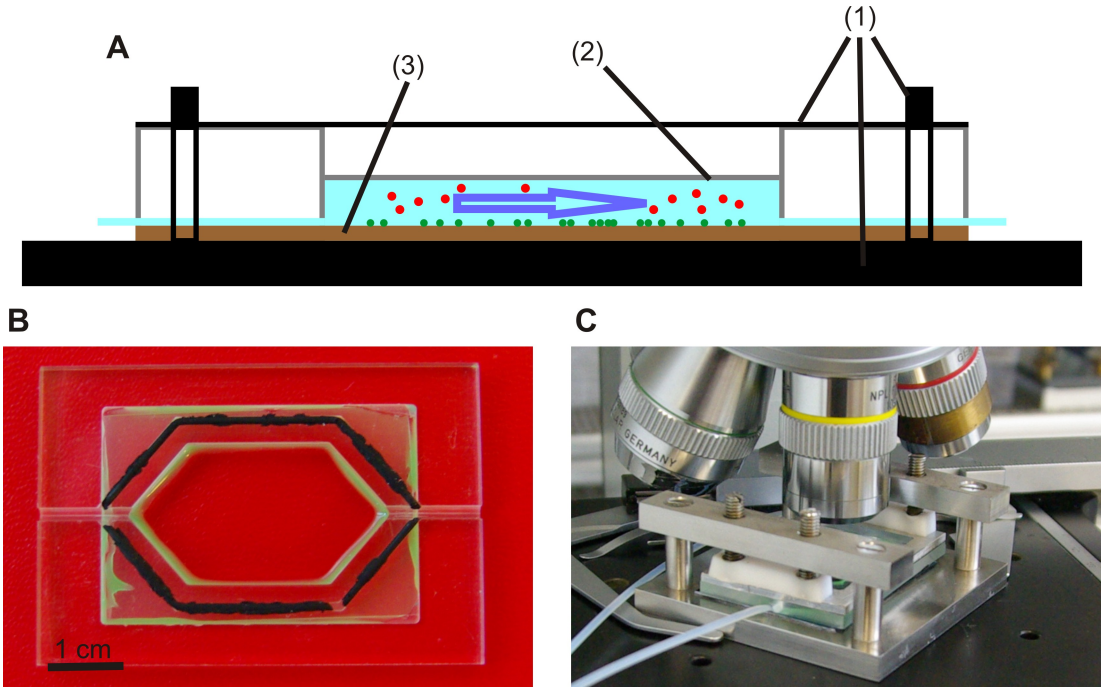

Figure 4.8: Custom build parallel plate flow chamber used in this work: A) Side view scheme showing the chamber embedded in the cleanable holder system (1), sealed on the upper side with a cover slide (2), and pressed with the lower side on the substrate (3); B) optical top view image of the chamber; C) photograph of the flow chamber and the holder system.

AFM force spectroscopy experiments with bacterial probes. Parallel plate flow chambers are a classical microbiological method commonly employed to investigate the adhesion of (bacterial) cells on a macroscopic scale [vanKoo1992, Mei1992, Mei1995, Tho2002, Har2006, Ros2008]. The analysis of flow chamber experiments usually comprises solely the counting of the number of bacteria on the substrate. Therefore, strictly speaking, not the adhesion, but the adsorption process is investigated. The main requirement on a flow chamber is that an area of constant shear force, viz. a uniform flow profile, exists. Such a profile is gained if the flow is steady, incompressible, laminar and established, which depends on the geometry of the chamber [vanWag1980, Bow1985, vanKoo1992, Usa1993, Mun1994, Bak2003]: A rectangular chamber can be described by the characteristic length

$$Le = a\, h\, Re \tag{4.3}$$

with a proportionality constant a, the chamber height h, and the Reynolds number Re. The latter is given by

$$Re = \rho \frac{Q}{\eta\,(w+h)} \tag{4.4}$$

with the fluid density ρ, the viscosity η, the flow rate Q, and the chamber width w. The value of the proportionality constant a is reported differently to 0.013 [vanWag1980]

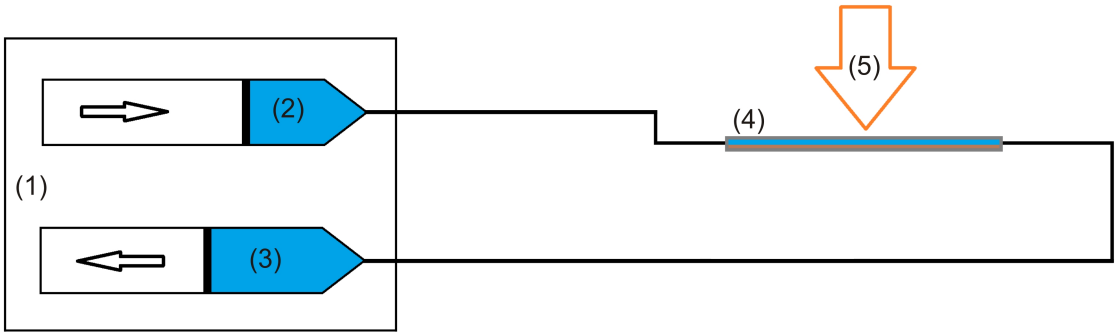

Figure 4.9: Scheme of the flow system in which the flow chamber is embedded. A step motor (1) pumps the bacteria solution at an adjustable constant flow rate from one syringe (2) through the chamber (4) into the second syringe (3). The sample in the flow chamber is thereby monitored by means of an optical microscope (5).

and 0.044 [Bow1985]. In general, an adequate uniform flow profile is achieved if Le is small enough compared to the chamber length l, described by

$$Le \leq b\, l \tag{4.5}$$

whereby b is a further proportionality constant. Equation 4.5, however, can also be interpreted differently in terms of strictness, since different values for b were introduced in the literature ($b = 0.1$ [Bow1985] and $b = 0.025$ [vanWag1980]). To sum up, the maximum flow rate for which a uniform flow profile is achieved depends on the dimensions of the flow chamber—for a specified liquid.

The flow chamber system used in this thesis is a custom build parallel plate flow chamber (cf. Figure 4.8). It features a $1.6 \times 1.6\,\mathrm{cm}^2$ base area and an effective height of 0.2 cm. Due to these dimensions, a uniform flow profile is achieved for flow rates[18], $Q \leq 81.9\,\mu\mathrm{l\,s}^{-1}$ (viz. $Re \leq 4.55$), according[19] to Equation 4.3 and Equation 4.5. The chamber itself is based on a disposable skeletal structure made of acrylic glass (poly(methyl methacrylate), PMMA), which is pressed on the sample substrate by a cleanable holder system made of stainless steel and aluminum. The lower side of the chamber—the connection with the substrate—is sealed with a standard sealing band. The upper side of the chamber is covered with a cover slip, which is glued to the chamber using a biocompatible rubber glue (Reprorubber Thin Pour, Flexbar Machine Corporation, Islandia, USA).

The chamber is incorporated in a flow system (cf. Figure 4.9) consisting of two syringes ($d = 16.22\,\mathrm{mm}$, $V_{\max} = 12\,\mathrm{ml}$, type Omnifex®, B|BRAUN Melsungen AG,

[18] For the calculations, $\eta = 1\,\mathrm{mPa\,s}$ and $\rho = 1\,\mathrm{kg\,l}^{-1}$ are used as solution properties, similar to the properties of water at room temperature. This is a reasonably safe assumption, since the bacteria solution is dilute.

[19] Thereby, the most rigorous combination of the proportionality constants is used. Using the weakest combination, the limit increases up to $Q \leq 1.1\,\mathrm{ml\,s}^{-1}$ (viz. $Re \leq 61.1$).

Melsungen, Germany) that are connected with the chamber via polytetrafluorethylene (PTFE) tubes ($d_{\text{interior}} = 1\,\text{mm}$, $d_{\text{exterior}} = 1.6\,\text{mm}$, Bohlender GmbH, Grünsfeld, Germany). A stepper motor (KDS Model 200 Serie S, KD Scientific Inc., Holliston, USA) pumps the bacteria solution with an adjustable constant flow rate through the system. Measurements on the substrates under study are always carried out using the same bacteria solution and in random order of the substrates.

During an experiment, the surface of the studied substrate was monitored by optical microscopy using a 10× objective and images taken at a frame rate of 0.1 Hz. Two different combinations of camera and microscope were employed in this study: a Pixelfly CCD-camera (PCO, Kelheim, Germany) on an Axiophot light microscope (Zeiss, Oberkochen, Germany) and a Cool SNAP™-Pro Digital Kit (Media Cybernetics® Inc., Bethesda, USA) on a Laborlux 12 ME S light microscope (Leica Camera AG, Solms, Germany).

The number of adhering bacteria was determined using an image analysis software (Image Pro Plus, Media Cybernetics, Bethesda, MD). To circumvent problems arising from deviations in brightness and contrast close to the edges of the images, an area of interest (AOI) in the center was chosen. The position and size of the AOI were kept constant over one experiment.

5 Influence of Substrate Properties on Surface Processes

5.1 The "Subsurface Energy"

As reviewed in the **publication in Addendum I**, the potential of the vdW interactions between a probe object and a stratified material is composed of a term describing the interaction with the surface and terms arising from interactions with the interfaces below the surface. The latter terms will in the following be referred to as the 'subsurface energy'. This interaction property features an important characteristic, namely that two superficially alike samples with the same surface chemistry may differ strongly in their subsurface energy. Moreover, this disparity can have a notable influence on the interactions with probe objects, as will be revealed in the following sections. An elegant way to independently study the impact of the subsurface energy is the set of tailored Si wafers introduced in section 4.1.1 (cf. the **publication in Addendum I**).

Especially in biological systems, researchers predominantly focused on coatings and surfaces so far. Thus, it is a crucial question to determine the role of the subsurface energy in these systems. In this thesis, three different types of biological objects were studied with regard to their adhesion/adsorption behavior onto the set of tailored Si wafers. By choosing (*nanoscopic*) proteins, (*microscopic*) bacteria, and (*macroscopic*) geckos, a wide range of scales is covered.

5.1.1 Impact on Protein Adsorption

First, the influence of the subsurface energy of the substrate on the adsorption of proteins was investigated. Previous studies have already shown that changes in the subsurface energy affect the kinetics of the protein adsorption process [Bel2008, Qui2008, Sch2010]. To determine whether these different kinetics implicate differences in the final structure of the adsorbed protein films, *in situ* X-ray reflectivity experiments were performed. Thereby, the adsorption of three different globular proteins (α-amylase,

lysozyme, and BSA) onto the set of tailored Si wafers was investigated. The experiments described in the **publication in Addendum II** reveal that the electron density profile of the adsorbate—i. e. its structure—varies, dependent on the thickness of the oxide layer: A different adsorbate structure on the type N and the type T wafer was observed, regardless of the studied protein and whether or not the substrates were hydrophobized. That is to say, irrespective of the surface chemistry, the subsurface energy impacts the protein adsorbate.

5.1.2 Impact on Bacterial Adhesion

Since bacterial adhesion is mediated by proteins, an analogous influence of the subsurface energy is conceivable. To probe the adhesion of model bacteria (*S. carnosus*) onto the set of tailored Si wafers on a single cell level, AFM force spectroscopy experiments with bacterial probes were performed. The findings presented in the **publication in Addendum III** show that the bacteria adhere stronger to the substrates with the thin oxide layers. In both cases—hydrophilic and hydrophobic—the adhesion forces on the type N wafers are roughly twice as high as on the type T wafers. By using a qualitative theoretical model based on considerations of the different Hamaker constants, the experimental results were backed up. Moreover, the **publication in Addendum III** addressed the question whether the differences in adhesion forces on a single cell level measurably affect the adsorption process on a macroscale. Adsorption experiments performed with a custom-built parallel plate flow chamber setup corroborated the AFM experiments: The number of adsorbed bacteria grows faster on the SiO_2 type N than on the SiO_2 type T wafers, independent of the concentration of the bacterial solution. In short, not only nanoscopic proteins but also microscopic bacteria are affected by variations in the subsurface energy.

5.1.3 Impact on Gecko Adhesion

To test if the subsurface properties of the substrate are relevant for macroscopic objects as well, isolated gecko setal arrays were used as an adhesion probe. Using the 'Robotoe' testing platform [Aut2006a, Gra2010], the setal arrays were dragged across the surfaces of the model substrates, mimicking a gecko's footfall. As shown in the **publication in Addendum IV**, the adhesion forces are significantly higher on type N than on type T wafers. Even when the setal array and the oxide layer are separated by a hydrophobic OTS monolayer, the adhesion is stronger on the OTS type N substrates. This trend is independent of humidity, drag speed, and array size. To support the experimental findings, theoretical approximations were performed. By incorporating oxide thickness dependent vdW potentials into the MD friction model (cf. section 3.5) an extensive MD model was developed. Therewith, it was shown that

the (vdW) pull-off force on Si wafers with oxide layers of thicknesses d in the range of $0.5\,\text{nm} \leq d \leq 5\,\text{nm}$ is remarkably higher in comparison to type T wafers. Hence, also on a macroscopic scale, the subsurface properties have an influence on the adhesion forces.

5.2 Influence of the Fluoridation of Hydroxyapatite on Bacterial Adhesion

In the **publication in Addendum V** the influence of the fluoridation of dental material on bacterial adhesion was characterized. As therein reviewed, it is known since many decades that the application of fluoride compounds to dental material has a cariostatic effect, which is mostly traced back to a change in the demineralization characteristics of the teeth. However, to address the question whether bacterial adhesion is also affected by the fluoridation, the adhesion forces between bacteria and hydroxyapatite surfaces—treated and untreated with fluoride solution—were determined on a single bacterial level. AFM force spectroscopy experiments with bacterial probes were performed to study the adhesion of the cariogenic pathogens *Streptococcus mutans* and *Streptococcus oralis*, and the apathogenic species *Staphylococcus carnosus*. As revealed in the **publication in Addendum V**, all bacterial species exhibit lower adhesion forces after fluoridation of the surfaces. These findings show that the adhesion of bacteria is indeed directly affected by the fluoridation of dental material. Consequently, it seems likely that this decrease of adhesion properties is another origin of the cariostatic effect of fluoride.

5.3 Bacterial Adhesion to 'Everyday Surfaces'

The studies presented in the preceding sections investigated surface interactions on a fundamental level by changing single parameters of model substrates separately. In this section, however, a more applied work[1] is presented: The characterization of the adhesion of bacteria to various 'everyday substrates'. For this purpose, AFM force spectroscopy experiments were performed using bacterial probes based on tipless cantilevers (PNP-TR-TL) coated with poly(dopamine) and covered with *S. carnosus*. As 'everyday substrates', stainless steel, aluminum, copper, and a part of a yoghurt cup (PP) were chosen (details for surface roughness and contact angle cf. section 4.1.2) and supplemented by the model substrates SiO_2 type N and OTS type N.

[1]The AFM force spectroscopy experiments in this section were performed by Sebastian Hümbert during his work as a diploma student tutored by Peter Loskill (cf. [Hue2010]).

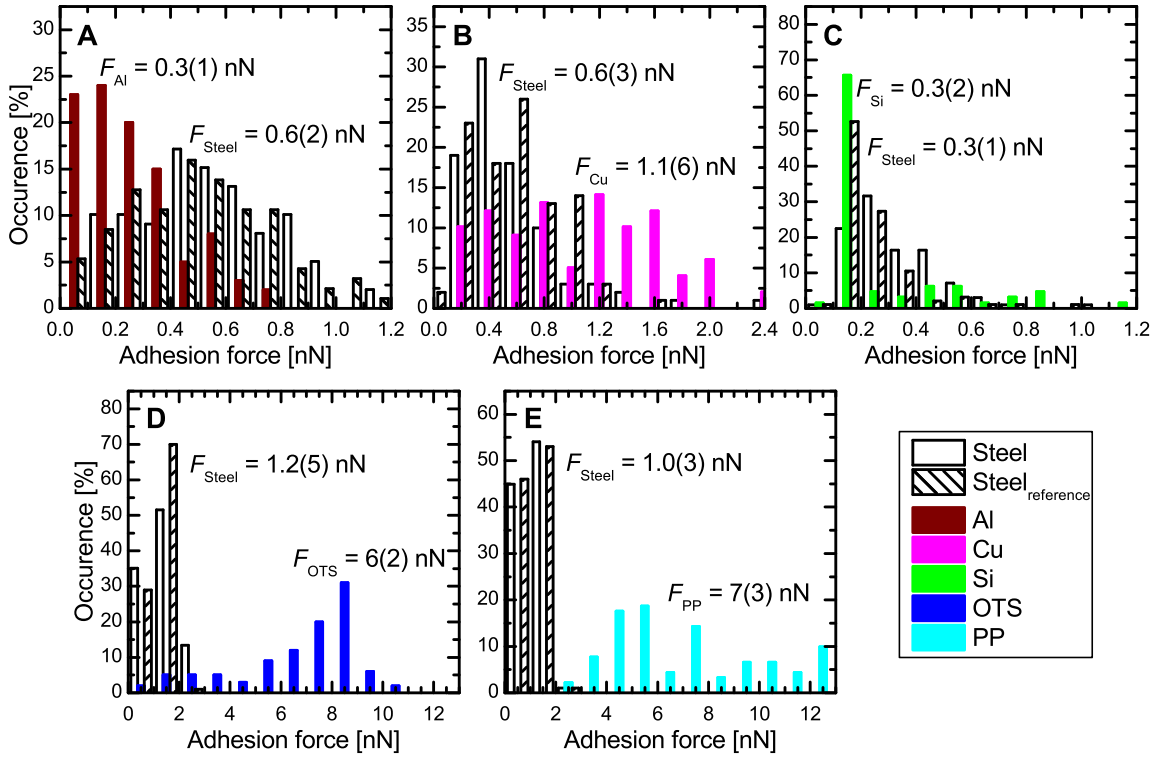

Figure 5.1: Results of AFM force spectroscopy experiments with bacterial probes (*S. carnosus*) on various 'everyday substrates'. The experiments consist of two series of measurements on stainless steel separated by a series of measurement on A) Al, B) Cu, C) SiO_2 type N, D) OTS type N, or E) PP. Since the first and last series of the experiments are comparable, the integrity of the bacterial probes can be granted.

Each experiment consisted of two series of measurements on stainless steel separated by a series of measurement on one of the other substrates. Thereby, the ratio of the adhesion forces on stainless steel and all other substrates was determined (cf. Figure 5.1). By normalizing the force values with respect to the corresponding value on stainless steel, the results of the different experiments—with different cantilevers—can be compared. The combination of the normalized values of all characterized 'everyday substrates' in Figure 5.2 clearly shows that the bacteria adhere stronger to the hydrophobic substrates (OTS type N wafer and the yoghurt cup) than to the hydrophilic substrates: $F_{\mathrm{OTS\,N}} \approx 6 \cdot F_{\mathrm{Steel}}$ and $F_{\mathrm{PP}} \approx 7 \cdot F_{\mathrm{Steel}}$. Within the hydrophilic substrates, the variations in adhesion forces are smaller: $F_{\mathrm{Al}} \approx 0.5 \cdot F_{\mathrm{Steel}}$, $F_{\mathrm{Si}} \approx F_{\mathrm{Steel}}$ and $F_{\mathrm{Cu}} \approx 2 \cdot F_{\mathrm{Steel}}$.

An explanation for the strong difference between hydrophobic and hydrophilic substrates is given by the hydrophobic effect. Although the hydrophobicity of bacteria varies strongly, even for the same strain [Mam1987], a difference in the wettability of the substrate can change the interaction energy significantly. Within the hydrophilic and hydrophobic substrates, it is hardly possible to isolate the origin for the differ-

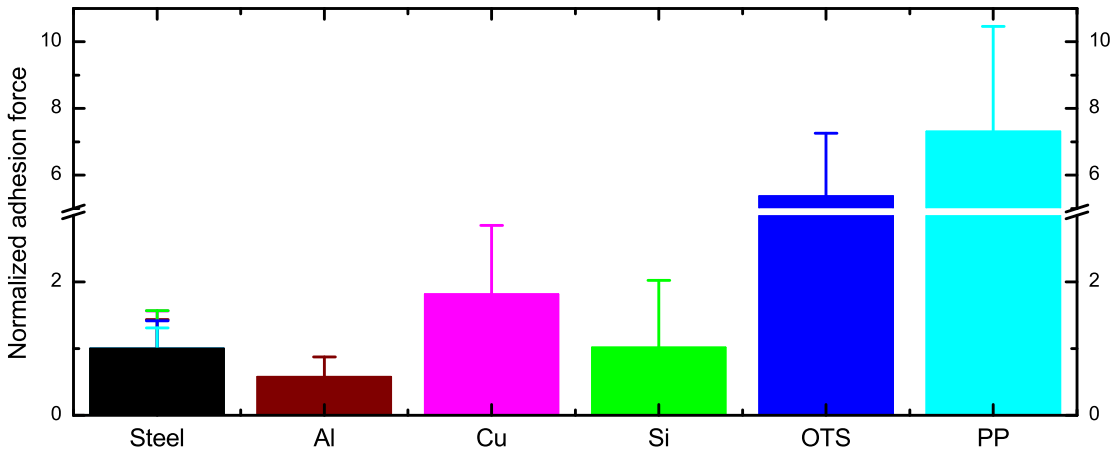

Figure 5.2: Average adhesion force values between *S. carnosus* and all characterized 'everyday substrates' normalized with respect to the corresponding value on stainless steel.

ent adhesion forces. The substrates differ in multiple properties such as roughness, isoelectric point, polarizability, and surface energy (cf. section 4.1.2)—properties that can all influence bacterial adhesion (cf. section 3.3.2) [Plo2010, An1998].

While this type of study is a demonstrative and straightforward procedure often applied to compare a limited amount of substrates, the gain of scientific insight is restricted. Moreover, this section highlights the importance of the type of studies presented in the preceding sections: To achieve a comprehensive understanding of the involved interactions, single parameters have to be studied independently.

6 Surface Properties of Bacteria

6.1 Dynamic Adhesion of Different *Staphylococci* Species

As soon as a bacterium makes contact with a surface, various processes in- and outside the cell are initiated (cf. section 3.3.2). Some of these processes directly affect the adhesion force leading to dynamics in the adhesion process. Here, the dynamic adhesion of bacteria of the genus *Staphylococcus* was investigated by carrying out AFM force spectroscopy experiments with bacterial probes using different surface delays (SDs). The main focus thereby was the comparison of the apathogenic *S. carnosus* with the highly pathogenic species *S. aureus*.

AFM experiments[1] with viable *S. carnosus*, viable *S. aureus*, and by formaldehyde inactivated *S. aureus* on OTS type T substrates were performed under physiological conditions. Each experiment consisted of series of measurements with a SD of 0 s, 1 s, 5 s, and 10 s, whereby in the course of the experiment, the SD was first gradually increased from 0 s to 10 s and subsequently decreased to 0 s again. For a better comparability, the mean adhesion forces of each experiment were normalized with respect to the value of the corresponding initial 0 s SD series. Moreover, to allow for a quantitative interpretation, the change in the mean adhesion force while increasing the SD was fitted with a function introduced by Boks *et al.* [Bok2008a] (cf. section 4.2.1), hereinafter called 'Boks-function'.

At first, the dynamic adhesion of viable *S. carnosus* was investigated. The determined average force values demonstrate that the adhesion strengthens with increasing SD (Figure 6.1 A). The fit with the Boks-function reveals a saturation value of the adhesion force of $F^{\infty}_{S.\ carnosus}/F^{0}_{S.\ carnosus} = 2.30(8)$ and a characteristic time of the adhesion strengthening of $\tau_{S.\ carnosus} = 1.8(3)$ s. Moreover, the corresponding values in the two parts of the experiments—the SD increasing and the SD decreasing part—are comparable within the experimental error, inducing a symmetrical shape of the results.

[1] The SD experiments in this paragraph were performed by Nicolas Thewes during his work as a diploma student tutored by Peter Loskill (cf. [The2012]).

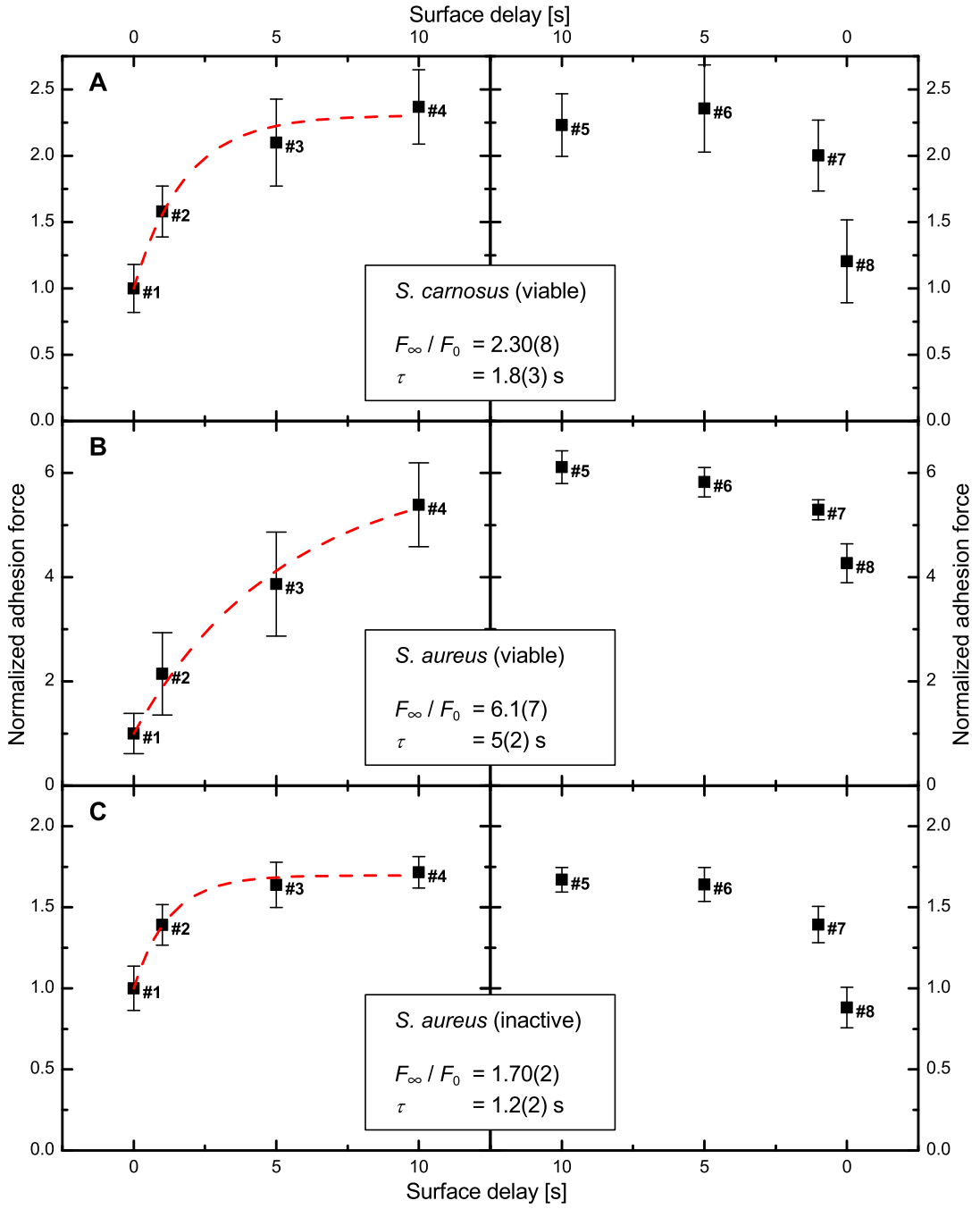

Figure 6.1: Results of AFM force spectroscopy experiments with bacterial probes on OTS type T substrates. The experiments consist of series of measurements with different SDs, whereby in the first part of the experiment, the SD was gradually increased and in the second part decreased again. The adhesion dynamics of A) viable *S. carnosus*, B) viable *S. aureus*, and C) by formaldehyde inactivated *S. aureus* were characterized. The numbers on the data points denote the order of the measurements taken.

Species	F^∞/F^0	τ [s]
S. carnosus (viable)	2.30(8)	1.8(3)
S. aureus (viable)	6.1(7)	5(2)
S. aureus (inactive)	1.70(2)	1.2(2)

Table 6.1: Summary of the resulting fit parameters of the Boks-function.

Next, viable *S. aureus* were characterized in terms of the adhesion dynamics. Analogous to the results for *S. carnosus*, the adhesion of *S. aureus* strengthens with increasing SD (Figure 6.1 B), with a saturation force value of $F^\infty_{S.\ aureus;\text{viable}}/F^0_{S.\ aureus;\text{viable}} = 6.1(7)$ and a characteristic time of $\tau_{S.\ aureus;\text{viable}} = 5(2)\,\text{s}$. Yet, for 10 s SD, the determined adhesion force $F^{10\,\text{s}}_{S.\ aureus;\text{viable}} = 5.4(8)$ is still lower than the saturation force value. Hence, the adhesion never reaches saturation during the measurement. Moreover, combining the first—SD increasing—and the second—SD decreasing—part of the experiment reveals a major difference between the viable *S. aureus* and *S. carnosus*. The adhesion force of *S. aureus* in the second part, is always stronger than the corresponding value in the first part, giving the results an asymmetrical shape.

Inactivating the *S. aureus* with formaldehyde changes the adhesion dynamics notably. The adhesion still strengthens with increasing SD (Figure 6.1 C). The saturation force, however, dropped down to $F^\infty_{S.\ aureus;\text{inactive}}/F^0_{S.\ aureus;\text{inactive}} = 1.70(2)$ and the characteristic time down to $\tau_{S.\ aureus;\text{inactive}} = 1.2(2)\,\text{s}$. Moreover, the combination of both parts of the experiment is redolent of the *S. carnosus* results and differs from the viable *S. aureus* results: The corresponding force values in both parts are comparable within the experimental error; the shape of the results is symmetrical.

Discussion

Comparing the results of the experiments with the different species, the following conclusions can be drawn:

- The adhesion forces for viable *S. carnosus* and inactive *S. aureus* are roughly doubled by increasing SD. The adhesion force for viable *S. aureus*, however, increases to a much larger extend, to a factor between 5 and 6.

- The characteristic time needed for the adhesion of viable *S. aureus* to strengthen is considerably longer than for the adhesion of viable *S. carnosus* and inactive *S. aureus*. A finding that is especially emphasized by the fact that no indications for a saturation of the force values were observed, in the case of viable *S. aureus*.

- The adhesion dynamics of *S. aureus* reveal a kind of 'memory effect': As earlier noticed, the combination of SD increasing and SD decreasing part is asymmetrical for the experiments with viable *S. aureus*: The force values in the second—SD decreasing—part are always higher than their corresponding values in the first—SD increasing—part (cf. Figure 6.2 B). In the adhesion dynamics of viable *S. carnosus* and inactive *S. aureus*, no such effect was observed: The experiments resulted in symmetrical dynamics (cf. Figure 6.2 A and C).

To sum up, the adhesion dynamics of viable *S. carnosus*, viable *S. aureus*, and by formaldehyde inactivated *S. aureus* on OTS type T substrates were investigated and significant differences were observed (cf. Table 6.1): Experiments with viable *S. aureus* revealed a strong increase of the adhesion for longer contact times indicating some kind of adaption of the bacterial cell. Moreover, the existence of a 'memory effect' in *S. aureus* indicates that this adaption process is not instantly reversible. Treating the *S. aureus* with formaldehyde changed the results significantly. Similar to *S. carnosus*, the adhesion of inactive *S. aureus* increased only weakly and no 'memory effect' was observed. In fact, the increase was just slightly stronger than observed for bare AFM probes (roughly 50% [Los2009]) suggesting that the dynamics do not arise from a 'real' biological origin, but most likely from hydrodynamic and equilibration effects.

To give a possible explanation for the different adhesion dynamics, the structure of the apathogenic *S. carnosus* and the highly pathogenic species *S. aureus* have to be taken into account. As reviewed in section 3.3.3, *S. aureus* possess various adhesive molecules, bound and unbound to the cell wall, which *S. carnosus* are lacking and which are inactivated due to the formaldehyde treatment. Based on this, feasible types of adaption processes are

1. conformational changes of membrane proteins,
2. the secretion of SERAMs by the bacterial cells, or
3. the migration of adhesion 'amplifying' cell wall compounds to the contact region.

As the time scale of conformational changes of proteins is typically very fast—usually in the range of a few ns[2] [Bon2004, Hen2007]—these changes would most likely already occur during the measurements with 0 s SD[3]. Yet, since protein relaxation processes on time scales of several minutes have been reported previously as well [Wer1999, Häh2011, Hof2012], a contribution to the adhesion dynamics can not be ruled out completely.

[2] Large scale conformational changes can take 'longer times'—up to ms [Hen2007]. Yet, this is still magnitudes below the used SDs in the experiments.

[3] Even during the 0 s SD measurements, the bacteria are in contact with the surface for a finite time (range of ms) until the force trigger is reached.

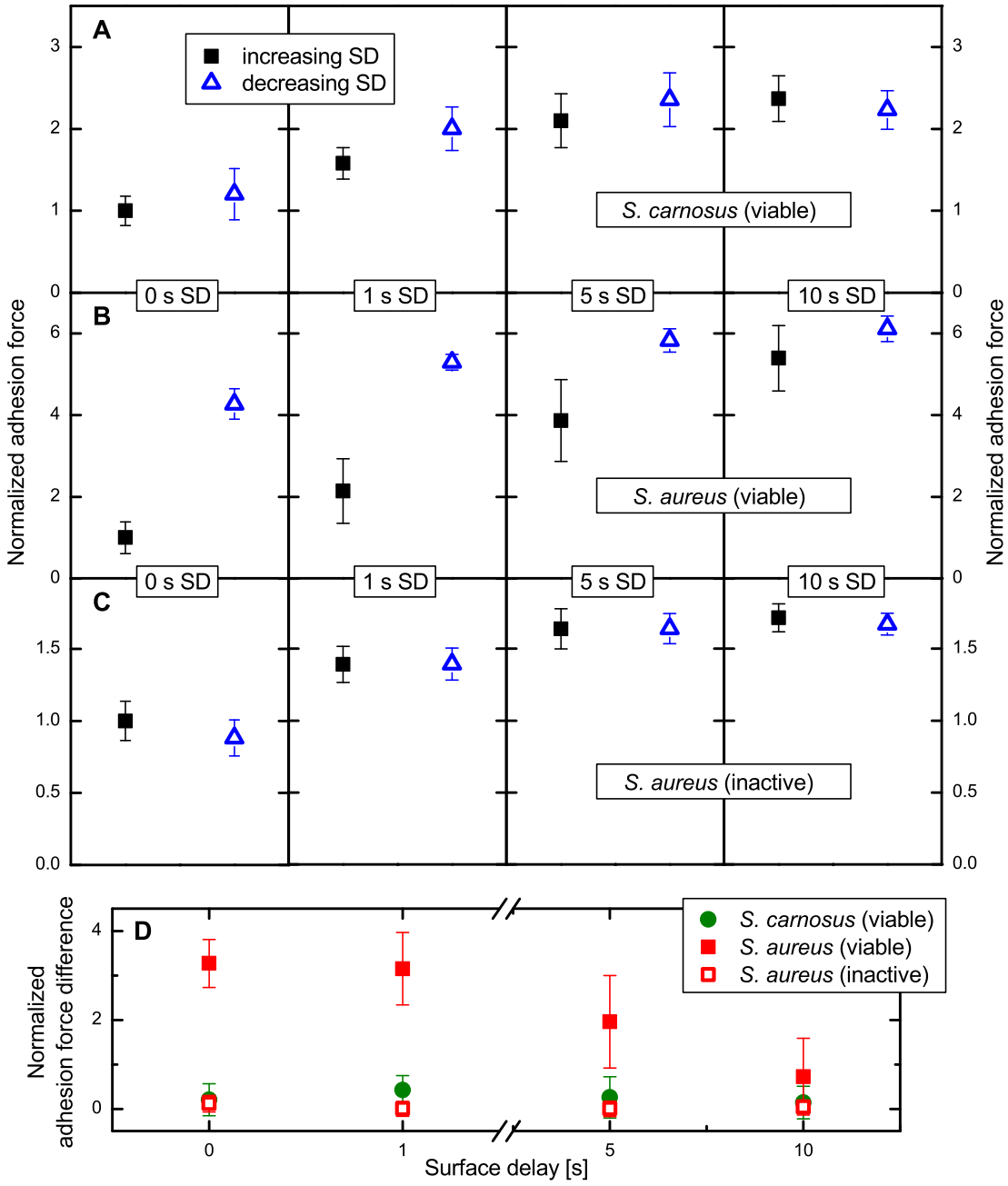

Figure 6.2: Alternative arrangement of the results of the AFM force spectroscopy experiments presented in Figure 6.1. Corresponding adhesion force values for the same SD from both parts—the SD increasing (left, solid symbol) and the decreasing (right, open symbol) part—of the experiment are combined. A dissimilarity in the 'memory effect' of A) viable *S. carnosus*, B) viable *S. aureus*, and C) by formaldehyde inactivated *S. aureus* can be observed. This dissimilarity becomes especially evident in D) the absolute value of the difference between the corresponding adhesion force values. All values are normalized with the respective first 0 s SD value.

The secretion of SERAMs can be excluded as a major factor for the dynamic adhesion studied in this section. Although this process would lead to increased adhesion forces, it usually occurs on a different (much slower) time scale and cannot explain the 'memory effect', since every single measurement is carried out on a different spot of the surface.

The time scale of the migration of adhesion 'amplifying' cell wall compounds to the contact region, however, can be in the same order of magnitude as the applied SDs [Cus1997, Til2003]. Moreover, these processes would also explain both the strong increase in adhesion forces as well as the 'memory effect'. As reviewed in section 3.3.1, the bacterial cell wall features relatively mobile compounds such as covalently unbound proteins and Lipoteichoic acids. Both of these could act as adhesion 'amplifying' molecules. Hence, the possibility of cell wall compounds migrating[4] to the contact region should be considered as a factor boosting the adhesion of the highly pathogenic *S. aureus*.

6.2 Dependence of the Cell Wall Elasticity on the Degree of Peptidoglycan Crosslinking

In the **publication in Addendum VI**, the effect of a reduction in the crosslinking of the PG on the elasticity of the cell wall of highly virulent and resistant prototype strains of *S. aureus* was investigated. Using AFM PeakForce tapping under physiological conditions, the cell wall elasticity of viable, genetically defined cells and their isogenic mutants was characterized. The mutants lack the non-essential transpeptidase PBP4 and thereby feature a modified secondary PG crosslinking, as detected by high-performance liquid chromatography (HPLC) and fluorescence microscopy. Associating these findings with the AFM results reveals that alterations in the secondary PG crosslinking trigger changes in the mechanical properties of the *S. aureus* cell wall: More precisely, the absence of PBP4, and the concomitant reduction of the PG crosslinking leads to a reduced stiffness of the cell wall.

Furthermore, the **publication in Addendum VI** compares the effect on community acquired-MRSA (CA-MRSA) and on hospital acquired-MRSA (HA-MRSA) strains. PBP4 is essential for beta-lactam resistance in CA-MRSA but not in HA-MRSA. The reduction in cell wall stiffness due to the absence of PBP4, however, was observed both in CA- and HA-MRSA strains. This indicates that the requirement of PBP4 for beta-lactam resistance—as solely observed in CA-MRSA—is not directly related to

[4] Whether this process is an active cell response or whether it is due to physical long-range interactions cannot be determined based on the herein presented results. Yet, follow-up projects investigating the dynamic adhesion of *S. aureus* inactivated by different means (metabolic or structural) could answer this question.

changes in the mechanical properties of the PG. Still, a correlation is conceivable, since the effect of the reduction of the secondary crosslinking on the mechanical properties of the cell wall in CA-MRSA strains is stronger than in HA-MRSA strains.

7 Summary and Outlook

The goal of this thesis is to unravel the influence of different—subsurface and surface—parameters of a material on biological surface processes. The major focus, thereby, lies on the impact of vdW forces arising from subsurface layers. Therefore, various biological objects covering a wide-range of scales are studied. It is shown that, independent of the scale, the adhesion process is always affected by differences in the vdW forces arising from subsurface layers—viz. the subsurface composition of the substrate.

Experimentally, the unravelling of vdW forces arising from subsurface layers from all other types of interactions is possible by using a set of tailored Si wafers consisting of four different types of substrates that can be classified in a hydrophilic and a hydrophobic pair. As hydrophilic substrates, silicon wafers with (thin) native and (thick) thermally grown oxide layers are selected and as hydrophobic substrates, the same pair of silicon wafers functionalized with an OTS monolayer. As a result, the surface chemistry and the subsurface composition of the substrates are varied separately in a well-defined manner.

By performing *in situ* X-ray reflectometry, the structure of protein films adsorbed on the set of tailored Si wafers is analyzed. The results reveal an influence of the subsurface material on the protein adsorbates. More precisely, a distinct influence of the topmost surface layer and the subsurface material is observed. The topmost surface layer is responsible for the level of denaturation of the proteins and determines the protein layer thickness. The subsurface material influences the density of the protein layer and thereby the final adsorbed amount of protein. The trends in the density and the final adsorbed amount are the same for all studied proteins (BSA, lysozyme, and α-amylase) and for all pH values tested.

AFM force spectroscopy experiments with bacterial probes in conjunction with flow chamber experiments demonstrate that bacterial adhesion and adsorption is also influenced by the subsurface composition of a substrate. The results of the AFM experiments show that the adhesion force of *S. carnosus* is about a factor of two stronger on the wafers with the thin oxide layer, irrespective if covered by a molecular-sized hydrophobic layer or not. The AFM results are corroborated by flow chamber experiments displaying a higher adsorption rate on the wafers with the thin oxide layer.

Using a custom mechanical testing platform ('Robotoe'), the adhesion of setal arrays from alive tropical geckos (*Gekko gecko*) onto the set of tailored Si wafers is tested. Again, the adhesion force is higher on the wafers with the thinner oxide layer for both—hydrophilic and hydrophobic—pairs of substrates. The measured trend in adhesion force agrees with theoretical predictions from a modified MD model, in which vdW potentials with a oxide layer thickness dependency are integrated.

Besides the influence of vdW interactions, the impact of the fluoridation of artificial tooth material on the attachment of bacteria is studied. The results of AFM force spectroscopy experiments with bacterial probes show that the adhesion force of oral bacteria is lowered due to the fluoridation. This finding suggests that the decrease of bacterial adhesion is another origin of the cariostatic effect of fluoride.

In addition to the properties of the artificial, inorganic substrate, the properties of the interacting biological objects are investigated:

AFM force spectroscopy experiments with bacterial probes and varied contact times reveal that the dynamics of the adhesion forces are significantly different for pathogenic and nonpathogenic *Staphylococcal* species. Pathogenic *S. aureus* display a strong increase in adhesion and a memory effect. Both is absent in the case of nonpathogenic *S. carnosus* and dead *S. aureus*. These findings indicate that during the attachment of *S. aureus* a rearrangement process of cell wall compounds takes place that *S. carnosus* is lacking.

By employing AFM in peak force tapping mode, the topography and elasticity of live *S. aureus* cells is mapped. The results indicate that the mechanical properties of the *S. aureus* cell wall are changed due to alterations in the secondary PG crosslinking. The overall elasticity of both HA and CA-MRSA bacteria is enhanced when lacking the non-essential transpeptidase PBP4. The effect of the reduction of the secondary crosslinking on the elasticity of the cell wall is stronger in CA-MRSA strains than in HA-MRSA strains. Interestingly, this correlates with β-lactam resistance; CA-MRSA strains require PBP4 for the resistance.

In short, this thesis reveals that the material hidden below the topmost surface layer can have an influence on biological surface processes, that the fluoridation of artificial teeth decreases the initial bacterial attachment, that rearrangement processes occur in bacteria triggered by surface contact, and that a reduced crosslinking of the peptiodglycan results in an increased elasticity of the bacterial cell wall. Furthermore, it is also demonstrated why a thorough separation of parameters is important to achieve a comprehensive understanding of biological adhesion. For the future, this thesis opens up a variety of possible follow-up studies; some of which are already ongoing.

Concerning the influence of vdW interactions on biological systems, a thorough theoretical description is necessary. Full spectral methods for complete Lifshitz calcu-

lations are challenging in the case of biological materials which are too complex to include all necessary parameters. Yet, a promising starting point could be the use of spectral data for fixed model proteins (e. g. keratin) representing the gecko system. Based on this, the more complex system of mobile single proteins could be tackled. Finally, a mixture of proteins and polysaccharides, representing the bacterial cell wall could be addressed. From an experimental point of view, various follow-up experiments are conceivable: In general, intermediate thicknesses of silicon oxide layers could be studied to determine a 'critical' thickness, necessary to 'shield' the subsurface compound of the vdW interactions. Moreover, different tailored systems featuring, for instance, a higher clinical relevance are of interest. For the studied biological systems, follow-up questions arise as well: In the case of the protein adsorption, a direct observation of the surface mobility on the hydrophilic surfaces is intriguing. In the case of bacteria, a very applied experiment could be the coating of different materials (e. g. gold, polymers, ceramics) with thin layers that are reputed to have antifouling properties and study their efficiency. Additionally, the mixture of protein adsorption and bacterial adhesion exposes important questions, such as the effect of different conformations of adsorbed proteins on subsequently adhering bacteria.

Regarding the consequence of the fluoridation of hydroxyapatite surfaces, a necessary follow-up study should investigate the adsorption of proteins, followed by a combination with the bacterial adhesion.

The nanoscale mapping of the local elasticity of the bacterial cell wall is a powerful and novel tool that can be used to tackle many significant questions. Similar to the herein presented study, the comparison of further mutant/wild-type system could help answering various questions of microbiology and medicine. As a direct follow-up of the presented findings, an in-depth analysis of the correlation of cell wall crosslinking, elasticity and resistance to antimicrobial agents is highly interesting.

In general, the combination of physical tools with biological objects is very promising and has the potential to help tackling many important questions in microbiology and medicine.

Bibliography

[Abk1994] V. I. Abkevich, A. M. Gutin, and E. I. Shakhnovich, *Free Energy Landscape for Protein Folding Kinetics: Intermediates, Traps, and Multiple Pathways in Theory and Lattice Model Simulations*, J Chem Phys **101** (1994) 6052–6062. ↑7

[Abs1983] D. R. Absolom, F. V. Lamberti, Z. Policova, W. Zingg, C. J. van Oss, and A. W. Neumann, *Surface Thermodynamics of Bacterial Adhesion*, Appl Environ Microbiol **46** (1983) 90–97. ↑3.3.2

[Ada2011] J. Adamcik, A. Berquand, and R. Mezzenga, *Single-Step Direct Measurement of Amyloid Fibrils Stiffness by Peak Force Quantitative Nanomechanical Atomic Force Microscopy*, Appl Phys Lett **98** (2011) 193701. ↑4.2.4

[Alb1990] T. R. Albrecht, S. Akamine, T. E. Carver, and C. F. Quate, *Microfabrication of Cantilever Styli for the Atomic Force Microscope*, J Vac Sci Technol A **8** (1990) 3386. ↑4.2.1

[An1998] Y. H. An and R. J. Friedman, *Concise Review of Mechanisms of Bacterial Adhesion to Biomaterial Surfaces*, J Biomed Mater Res, Part A **43** (1998) 338–348. ↑3.3.2, 5.3

[And2008] G. G. Anderson and G. A. O'Toole, *Innate and Induced Resistance Mechanisms of Bacterial Biofilms*, Curr Top Microbiol **322** (2008) 85–105. ↑3.3.3

[Ans2010] K. Anselme, P. Davidson, A. M. Popa, M. Giazzon, M. Liley, and L. Ploux, *The Interaction of Cells and Bacteria with Surfaces Structured at the Nanometre Scale*, Acta Biomater **6** (2010) 3824–3846. ↑3.3.2

[Arc1998] G. L. Archer, *Staphylococcus aureus: a Well-Armed Pathogen*, Clin infect dis, 1998, pp. 1179–1181. ↑3.3.3

[Arz2003] E. Arzt, S. N. Gorb, and R. Spolenak, *From Micro to Nano Contacts in Biological Attachment Devices*, Proc Natl Acad Sci **100** (2003) 10603–10606. ↑3.4.1

[Asa2005] D. B. Asay and S. H. Kim, *Evolution of the Adsorbed Water Layer Structure on Silicon Oxide at Room Temperature*, J Phys Chem B **109** (2005) 16760–16763. ↑3.1.8

[Ash1970] A. Ashkin, *Acceleration and Trapping of Particles by Radiation Pressure*, Phys Rev Lett **24** (1970) 156–159. ↑3.3.2

[Ash1986] A. Ashkin, J. M. Dziedzic, J. E. Bjorkholm, and S. Chu, *Observation of a Single-Beam Gradient Force Optical Trap for Dielectric Particles*, Opt Lett **11** (1986) 288–290. ↑3.3.2

[Ash1987] A. Ashkin and J. M. Dziedzic, *Optical Trapping and Manipulation of Viruses and Bacteria*, Science **235** (1987) 1517–1520. ↑3.3.2

[Aut2002a] K. Autumn and A. M. Peattie, *Mechanisms of Adhesion in Geckos*, Integr Comp Biol **42** (2002) 1081–1090. ↑3.4.1

[Aut2002b] K. Autumn, M. Sitti, Y. A. Liang, A. M. Peattie, W. R. Hansen, S. Sponberg, T. W. Kenny, R. S. Fearing, J. N. Israelachvili, and R. J. Full, *Evidence for Van Der Waals Adhesion in Gecko Setae*, Proc Natl Acad Sci **99** (2002) 12252–12256. ↑3.4.1

[Aut2006a] K. Autumn, A. Dittmore, D. Santos, M. Spenko, and M. Cutkosky, *Frictional Adhesion: a New Angle on Gecko Attachment*, J Exp Biol **209** (2006) 3569–3579. ↑5.1.3

[Aut2006b] K. Autumn, C. Majidi, R. E. Groff, A. Dittmore, and R. S. Fearing, *Effective Elastic Modulus of Isolated Gecko Setal Arrays*, J Exp Biol **209** (2006) 3558–3568. ↑3.4.1

[Bak2003] D. P. Bakker, A. van der Mats, G. J. Verkerke, H. J. Busscher, and H. C. van der Mei, *Comparison of Velocity Profiles for Different Flow Chamber Designs Used in Studies of Microbial Adhesion to Surfaces*, Appl Environ Microbiol **69** (2003) 6280–6287. ↑4.3

[Ban2003] J. A. Banas and M. M. Vickerman, *Glucan-Binding Proteins of the Oral Streptococci*, Crit Rev Oral Biol M **14** (2003) 89–99. ↑3.3.4

[Bar1968] F. F. Barrett, R. F. McGehee, and M. Finland, *Methicillin-Resistant Staphylococcus aureus at Boston City Hospital: Bacteriologic and Epidemiologic Observations*, New Engl J Med **279** (1968) 441–448. ↑3.3.3

[Bar2011] W. J. P. Barnes, P. J. P. Goodwyn, M. Nokhbatolfoghahai, and S. N. Gorb, *Elastic Modulus of Tree Frog Adhesive Toe Pads*, J Comp Physiol A (2011). ↑1

[Bau1986] A. M. Bauer and A. P. Russell, *Hoplodactylus delcourti n. sp. (Reptilia: Gekkonidae), the Largest Known Gecko*, New Zeal J Zool **13** (1986) 141–148. ↑3.4

[Bay1998] K. W. W. Bayles, C. A. Wesson, L. E. Liou, L. K. Fox, G. A. Bohach, and W. R. Trumble, *Intracellular Staphylococcus aureus Escapes the Endosome and Induces Apoptosis in Epithelial Cells*, Infect Immun **66** (1998) 336–342. ↑3.3.3

[Bay2009] S. Bayoudh, A. Othmane, L. Mora, and H. Ben Ouada, *Assessing Bacterial Adhesion Using DLVO and XDLVO Theories and the Jet Impingement Technique*, Colloids Surf B **73** (2009) 1–9. ↑3.3.2

[Bea1981] E. H. Beachey, *Bacterial Adherence: Adhesion-Receptor Interactions Mediating the Attachment of Bacteria to Mucosal Surfaces*, J Infect Dis **143** (1981) 325–345. ↑3.3.2

[Bel2008] M. Bellion, L. Santen, H. Mantz, H. Hähl, A. Quinn, A. M. Nagel, C. Gilow, C. Weitenberg, Y. Schmitt, and K. Jacobs, *Protein Adsorption on Tailored Substrates: Long-Range Forces and Conformational Changes*, J Phys: Condens Matter **20** (2008) 404226. ↑3.2.1, 5.1.1

[Bel2012] M. Bellion, *Die Monte Carlo Methode für komplexe Fluide - Adsorptionsphänomene und Cluster Algorithmen*, Dissertation, 2012, Saarbrücken. ↑3.2.1

[Ben2000] M. Benoit, D. Gabriel, G. Gerisch, and H. E. Gaub, *Discrete Interactions in Cell Adhesion Measured by Single-Molecule Force Spectroscopy*, Nat Cell Biol **2** (2000) 313–317. ↑4.2.1

[Ber1981] M. S. Bergdoll, B. A. Crass, R. F. Reiser, R. N. Robbins, and J. P. Davis, *A New Staphylococcal Enterotoxin, Enterotoxin F, Associated with Toxic-Shock-Syndrome Staphylococcus aureus Isolates*, Lancet **1** (1981) 1017–1021. ↑3.3.3

[Ber2005] A. Berquand, N. Xia, D. G. Castner, B. H. Clare, N. L. Abbott, V. Dupres, Y. Adriaensen, and Y. F. Dufrene, *Antigen Binding Forces of Single Antilysozyme Fv Fragments Explored by Atomic Force Microscopy*, Langmuir **21** (2005) 5517–5523. ↑4.2.1

[Ber2010] A. Berquand, C. Roduit, S. Kasas, A. Holloschi, L. Ponce, and M. Hafner, *Atomic Force Microscopy Imaging of Living Cells*, Micros Today **18** (2010) 8–14. ↑4.2.4

[Ber2011] A. Berquand, *Quantitative Imaging of Living Biological Samples by PeakForce QNM Atomic Force Microscopy*, Bruker Corporation Application Note AN135, 2011. ↑4.2.4

[Bel1990] M.-N. Bellon-Fontaine, N. Mozes, H. C. van der Mei, J. Sjollema, O. Cerf, P. G. Rouxhet, and H. J. Busscher, *A Comparison of Thermodynamic Approaches to Predict the Adhesion of Dairy Microorganisms to Solid Substrata*, Cell Biophys **17** (1990) 93–106. ↑3.3.2

[Bin1986a] G. Binnig, *Atomic Force Microscope and Method for Imaging Surfaces with Atomic Resolution* (1986). ↑4.2

[Bin1986b] G. Binnig, C. F. Quate, and C. Gerber, *Atomic Force Microscope*, Phys Rev Lett **56** (1986) 930–933. ↑4.2

[Bit2012] A. Bitler, R. Dover, and Y. Shai, *Fractal Properties of Macrophage Membrane Studied by AFM*, Micron (2012). ↑4.2.4

[Blo1992] S. M. Block, *Making Light Work with Optical Tweezers*, Nature **360** (1992) 493–495. ↑3.3.2

[Bod1989] M. K. Bodén and J.-I. Flock, *Fibrinogen-Binding Protein/Clumping Factor from Staphylococcus aureus*, Infect Immun **57** (1989) 2358–2363. ↑3.3.3

[Bod1992] M. K. Bodén and J.-I. Flock, *Evidence for Three Different Fibrinogen-Binding Proteins with Unique Properties from Staphylococcus aureus Strain Newman.*, Microb Pathogenesis **12** (1992) 289–298. ↑3.3.3

[Bod1994] M. K. Bodén and J.-I. Flock, *Cloning and Characterization of a Gene for a 19kDa Fibrinogen-Binding Protein from Staphylococcus aureus*, Mol Microbiol **12** (1994) 599–606. ↑3.3.3

[Boe2010] L. F. Boesel, C. Greiner, E. Arzt, and A. del Campo, *Gecko-Inspired Surfaces: A Path to Strong and Reversible Dry Adhesives*, Adv Mater **22** (2010) 2125–2137. ↑1

[Bok2008a] N. P. Boks, H. J. Busscher, H. C. van der Mei, and W. Norde, *Bond-Strengthening in Staphylococcal Adhesion to Hydrophilic and Hydrophobic Surfaces Using Atomic Force Microscopy*, Langmuir **24** (2008) 12990–12994. ↑4.2.1, 4.2.2, 4.2.2, 6.1

[Bok2008b] N. P. Boks, W. Norde, H. C. van der Mei, and H. J. Busscher, *Forces Involved in Bacterial Adhesion to Hydrophilic and Hydrophobic Surfaces*, Microbiology **154** (2008) 3122–3133. ↑3.3.2

[Bon2000] I. G. Boneca, Z.-H. Huang, D. A. Gage, and A. Tomasz, *Characterization of Staphylococcus aureus Cell Wall Glycan Strands, Evidence for a New β-N-Acetylglucosaminidase Activity*, J Biol Chem **275** (2000) 9910–9918. ↑3.3.3

[Bon2004] P. J. Bond and M. S. P. Sansom, *The Simulation Approach to Bacterial Outer Membrane Proteins (Review)*, Mol Membr Biol **21** (2004) 151–161. ↑6.1

[Bow1964] F. P. Bowden and D. Tabor, *Friction and Lubrication of Solids: Part 2*, Oxford University Press, Oxford, USA, 1964. ↑3.5

[Bow1985] B. D. Bowen, *Streaming Potential in the Hydrodynamic Entrance Region of Cylindrical and Rectangular Capillaries*, J Colloid Interface Sci **106** (1985) 367–376. ↑4.3, 4.3, 4.3

[Bow2001] W. R. Bowen, R. W. Lovitt, and C. J. Wright, *Atomic Force Microscopy Study of the Adhesion of Saccharomyces cerevisiae*, J Colloid Interface Sci **237** (2001) 54–61. ↑3.3.2, 4.2.1, 4.2.2, 4.2.2

[Bow2002] W. R. Bowen, A. S. Fenton, R. W. Lovitt, and C. J. Wright, *The Measurement of Bacillus mycoides Spore Adhesion using Atomic Force Microscopy, Simple Counting Methods, and a Spinning Disk Technique*, Biotechnol Bioeng **79** (2002) 170–179. ↑4.2.2

[Boy1990] J. M. Boyce, *Increasing Prevalence of Methicillin-resistant Staphylococcus aureus in the United States*, Infect Cont Hosp Ep **11** (1990) 639–642. ↑3.3.3

[Bri1982] P. D. Bridge and P. H. A. Sneath, *Streptococcus gallinarum sp. nov. and Streptococcus oralis sp. nov.*, Int J Syst Bacteriol **32** (1982) 410–415. ↑3.3.4

[Bru1983] L. W. Bruch, *Theory of Physisorption Interactions*, Surf Sci **125** (1983) 194–217. ↑8

[Bru1997] R. Bruckner, *Gene Replacement in Staphylococcus carnosus and Staphylococcus xylosus*, FEMS Microbiol Lett **151** (1997) 1–8. ↑3.3.3

[Bru2001] G. M. Bruinsma, H. C. van der Mei, and H. J. Busscher, *Bacterial Adhesion to Surface Hydrophilic and Hydrophobic Contact Lenses*, Biomaterials **22** (2001) 3217–3224. ↑3.3.2

[Bry2008] J. D. Bryers, *Medical Biofilms*, Biotechnol Bioeng **100** (2008) 1–18. ↑3.2.1

[Brz1994] J. B. Brzoska, I. B. Azouz, and F. Rondelez, *Silanization of Solid Substrates: A Step toward Reproducibility*, Langmuir **10** (1994) 4367–4373. ↑4.1.1

[Buc2010] A. W. Buck, V. G. Fowler Jr, R. Yongsunthon, J. Liu, A. C. DiBartola, Y.-A. Que, P. Moreillon, and S. K. Lower, *Bonds between Fibronectin and Fibronectin-Binding Proteins on Staphylococcus aureus and Lactococcus lactis*, Langmuir **26** (2010) 10764–10770. ↑4.2.1, 4.2.2

[Bur2003] G. A. Burks, S. B. Velegol, E. Paramonova, B. E. Lindenmuth, J. D. Feick, and B. E. Logan, *Macroscopic and Nanoscale Measurements of the Adhesion of Bacteria with Varying Outer Layer Surface Composition*, Langmuir **19** (2003) 2366–2371. ↑4.2.2

[Bus1983] H. J. Busscher, A. W. J. van Pelt, H. P. de Jong, and J. Arends, *Effect of Spreading Pressure on Surface Free Energy Determinations by Means of Contact Angle Measurements*, J Colloid Interface Sci **95** (1983) 23–27. ↑3.1.6

[Bus1984] H. J. Busscher, A. H. Weerkamp, H. C. van der Mei, A. W. J. van Pelt, H. P. de Jong, and J. Arends, *Measurement of the Surface Free Energy of Bacterial Cell Surfaces and Its Relevance for Adhesion*, Appl Environ Microbiol **48** (1984) 980–983. ↑3.3.2

[Bus1990] H. J. Busscher, M.-N. Bellon-Fontaine, N. Mozes, H. C. van der Mei, J. Sjollema, A. J. Leonard, P. G. Rouxhet, and O. Cerf, *An Interlaboratory Comparison of Physico-Chemical Methods for Studying the Surface Properties of Microorganisms - Application to Streptococcus thermophilus and Leuconostoc mesenteroides*, J Microbiol Meth **12** (1990) 101–115. ↑3.3.2

[Bus2008] H. J. Busscher, R. J. B. Dijkstra, D. E. Langworthy, D. I. Collias, D. W. Bjorkquist, M. D. Mitchell, and H. C. van der Mei, *Interaction Forces Between Waterborne Bacteria and Activated Carbon Particles*, J Colloid Interface Sci **322** (2008) 351–357. ↑4.2.1

[But2005] H. J. Butt, B. Cappella, and M. Kappl, *Force Measurements with the Atomic Force Microscope: Technique, Interpretation and Applications*, Surf Sci Rep **59** (2005) 1–152. ↑4.2.1

[Cam2000] T. A. Camesano and B. E. Logan, *Probing Bacterial Electrosteric Interactions Using Atomic Force Microscopy*, Environ Sci Technol **34** (2000) 3354–3362. ↑3.3.2, 3.3.2

[Cao2006] T. Cao, H. Tang, X. Liang, A. Wang, G. W. Auner, S. O. Salley, and K. Y. S. Ng, *Nanoscale Investigation on Adhesion of E. coli Surface Modified Silicone Using Atomic Force Microscopy*, Biotechnol Bioeng **94** (2006) 167–176. ↑4.2.2

[Car1997] R. W. Carpick and M. Salmeron, *Scratching the Surface: Fundamental Investigations of Tribology with Atomic Force Microscopy*, Chem Rev **97** (1997) 1163–1194. ↑3.5

[Car1999] R. W. Carpick, D. F. Ogletree, and M. Salmeron, *A General Equation for Fitting Contact Area and Friction vs Load Measurements*, J Colloid Interface Sci **211** (1999) 395–400. ↑3.10, 3.5

[Car2007] R. W. Carpick, J. Batteas, and M. P. de Boer, *Scanning Probe Studies of Nanoscale Adhesion Between Solids in the Presence of Liquids and Monolayer Films*, Handbook of nanotechnology, 2007, pp. 951–979. ↑4.2.1, 4.2.1

[Cha1913] D. L. Chapman, *LI. A Contribution to the Theory of Electrocapillarity*, Phil Mag **25** (1913) 475–481. ↑3.1.2

[Cha1983] W. G. Characklis and K. E. Cooksey, *Biofilms and Microbial Fouling*, Adv Appl Microbiol **29** (1983) 93–138. ↑3.2.1

[Cha2002] T. Chavakis, M. Hussain, S. M. Kanse, G. Peters, R. G. Bretzel, J. I. Flock, M. Herrmann, and K. T. Preissner, *Staphylococcus aureus Extracellular Adherence Protein Serves as Anti-Inflammatory Factor by Inhibiting the Recruitment of Host Leukocytes*, Nat Med **8** (2002) 687–693. ↑3.3.3

[Cha2005] T. Chavakis, K. Wiechmann, K. T. Preissner, and M. Herrmann, *Staphylococcus aureus Interactions with the Endothelium - the Role of Bacterial "Secretable Expanded Repertoire Adhesive Molecules" (SERAM) in Disturbing Host Defense Systems*, Thromb Haemostasis **94** (2005) 278–285. ↑3.3.3

[Chh2002] G. S. Chhatwal, *Anchorless Adhesins and Invasins of Gram-Positive Bacteria: a New Class of Virulence Factors*, Trends Microbiol **10** (2002) 205–208. ↑3.3.2

[Chi1919] H. T. Chickering and J. H. Park, *Staphylococcus aureus Pneumonia*, JAMA **72** (1919) 617–626. ↑3.3.3

[Cla1924] J. K. Clarke, *On the Bacterial Factor in the Aetiology of Dental Caries*, British journal of experimental pathology **5** (1924) 141–147. ↑3.3.4

[Cla2006] S. R. Clarke and S. J. Foster, *Surface Adhesins of Staphylococcus aureus*, Advances in Microbial Physiology **51** (2006) 187–224. ↑3.3.3

[Cle1999] S. C. Clear and P. F. Nealey, *Chemical Force Microscopy Study of Adhesion and Friction Between Surfaces Functionalized with Self-Assembled Monolayers and Immersed in Solvents*, J Colloid Interface Sci **213** (1999) 238–250. ↑4.2.1

[Cos1987] J. W. Costerton, K. J. Cheng, G. G. Geesey, T. I. Ladd, J. C. Nickel, M. Dasgupta, and T. J. Marrie, *Bacterial Biofilms in Nature and Disease*, Annu Rev Microbiol **41** (1987) 435–464. ↑3.3.2

[Cos2008] D. Costa, A. Tougerti, F. Tielens, C. Gervais, L. Stievano, and J. F. Lambert, *DFT Study of the Adsorption of Microsolvated Glycine on a Hydrophilic Amorphous Silica Surface*, Phys Chem Chem Phys **10** (2008) 6360–6368. ↑3.2.1

[Cuc2001] C. Cucarella, C. Solano, J. Valle, B. Amorena, I. Lasa, and J. R. Penades, *Bap, a Staphylococcus aureus Surface Protein Involved in Biofilm Formation*, J Bacteriol **183** (2001) 2888–2896. ↑3.3.3

[Cus1997] E. L. Cussler, *Diffusion, Mass Transfer in Fluid Systems*, 2. Aufl., Cambridge University Press, New York, 1997. ↑6.1

[Car1999] M. Carrion-Vazquez, A. F. Oberhauser, S. B. Fowler, P. E. Marszalek, S. E. Broedel, J. Clarke, and J. M. Fernandez, *Mechanical and Chemical Unfolding of a Single Protein: a Comparison*, Proc Natl Acad Sci **96** (1999) 3694–3699. ↑4.2.1

[Car2000] M. Carrion-Vazquez, A. F. Oberhauser, T. E. Fisher, P. E. Marszalek, H. Li, and J. M. Fernandez, *Mechanical Design of Proteins Studied by Single-Molecule Force Spectroscopy and Protein Engineering*, Prog Biophys Mol Bio **74** (2000) 63–91. ↑4.2.1

[Dag2007] E. Dague, D. Alsteens, J.-P. Latge, C. Verbelen, D. Raze, A. R. Baulard, and Y. F. Dufrene, *Chemical Force Microscopy of Single Live Cells*, Nano Lett **7** (2007) 3026–3030. ↑4.2.1

[Den2011] Y. Deng, M. Sun, and J. Shaevitz, *Direct Measurement of Cell Wall Stress Stiffening and Turgor Pressure in Live Bacterial Cells*, Phys Rev Lett **107** (2011). ↑4.2.1

[Der1941] B. V. Derjaguin and L. Landau, *Theory of the Stability of Strongly Charged Lyophobic Sols and of the Adhesion of Strongly Charged Particles in Solutions of Electrolytes*, Acta Physicochim URS **14** (1941) 633–662. ↑3.3.2

[Der1975] B. V. Derjaguin, V. M. Muller, and Yu. P. Toporov, *Effect of Contact Deformations on the Adhesion of Particles*, J Colloid Interface Sci **53** (1975) 314–326. ↑3.5, 4.7, 4.2.4

[Des2006] M. Desvaux, E. Dumas, I. Chafsey, and M. Hebraud, *Protein Cell Surface Display in Gram-Positive Bacteria: from Single Protein to Macromolecular Protein Structure*, FEMS Microbiol Lett **256** (2006) 1–15. ↑3.3.1

[Dij1987] J. Dijk, F. Herkstroter, H. J. Busscher, A. H. Weerkamp, H. Jansen, and J. Arends, *Surface-Free Energy and Bacterial Adhesion — An in Vivo Study in Beagle Dogs*, J Clin Periodontol **14** (1987) 300–304. ↑3.3.2

[Din2000] A. R. Dinner, A. Šali, L. J. Smith, C. M. Dobson, and M. Karplus, *Understanding Protein Folding via Free-Energy Surfaces from Theory and Experiment*, TiBS **25** (2000) 331–339. ↑7

[deJon1992] B. L. M. de Jonge, Y.-S. Chang, D. A. Gage, and A. Tomasz, *Peptidoglycan Composition of a Highly Methicillin-Resistant Staphylococcus aureus Strain—the Role of Penicillin Binding Protein-2a*, J Biol Chem **267** (1992) 11248–11254. ↑3.3.3

[Don2002] R. M. Donlan and J. W. Costerton, *Biofilms: Survival Mechanisms of Clinically Relevant Microorganisms*, Clin Microbiol Rev **15** (2002) 167–193. ↑3.3.2, 3.3.3

[Dor2008] L. S. Dorobantu, S. Bhattacharjee, J. M. Foght, and M. R. Gray, *Atomic Force Microscopy Measurement of Heterogeneity in Bacterial Surface Hydrophobicity*, Langmuir **24** (2008) 4944–4951. ↑4.2.1

[Dor2009] L. S. Dorobantu, S. Bhattacharjee, J. M. Foght, and M. R. Gray, *Analysis of Force Interactions between AFM Tips and Hydrophobic Bacteria Using DLVO Theory*, Langmuir **25** (2009) 6968–6976. ↑3.3.2

[Dre2011] A. Dreisbach, J. M. van Dijl, and G. Buist, *The Cell Surface Proteome of Staphylococcus aureus*, Proteomics **11** (2011) 3154–3168. ↑3.3.3, 3.7

[DeSou2008] E. J. De Souza, M. Brinkmann, C. Mohrdieck, A. J. Crosby, and E. Arzt, *Capillary Forces between Chemically Different Substrates*, Langmuir **24** (2008) 10161–10168. ↑3.1.8

[Duf2002] Y. F. Dufrene, *Atomic Force Microscopy, a Powerful Tool in Microbiology*, J Bacteriol **184** (2002) 5205–5213. ↑3.3.2, 4.2

[Duf2004] Y. F. Dufrene, *Using Nanotechniques to Explore Microbial Surfaces*, Nat Rev Microbiol **2** (2004) 451–460. ↑4.2

[Duf2008] Y. F. Dufrene, *Towards Nanomicrobiology Using Atomic Force Microscopy*, Nat Rev Microbiol **6** (2008) 674–680. ↑3.3.2, 4.2

[Dug1960] D. S. Dugdale, *Yielding of Steel Sheets Containing Slits*, J Mech Phys Solids **8** (1960) 100–104. ↑3.5

[Dup2005] V. Dupres, F. D. Menozzi, C. Locht, B. H. Clare, N. L. Abbott, S. Cuenot, C. Bompard, D. Raze, and Y. F. Dufrene, *Nanoscale Mapping and Functional Analysis of Individual Adhesins on Living Bacteria*, Nat Methods **2** (2005) 515–520. ↑4.2.1

[Elw1998] H. Elwing, *Protein Absorption and Ellipsometry in Biomaterial Research*, Biomaterials **19** (1998) 397–406. ↑3.2.1

[Eme2004] R. J. Emerson and T. A. Camesano, *Nanoscale Investigation of Pathogenic Microbial Adhesion to a Biomaterial*, Appl Environ Microbiol **70** (2004) 6012–6022. ↑4.2.1

[Eme2006] R. J. Emerson, T. S. Bergstrom, Y. Liu, E. R. Soto, C. A. Brown, W. G. McGimpsey, and T. A. Camesano, *Microscale Correlation Between Surface Chemistry, Texture, and the Adhesive Strength of Staphylococcus epidermidis*, Langmuir **22** (2006) 11311–11321. ↑3.3.2, 4.2.2

[Ern1966] V. Ernst and R. Ruibal, *Structure and Development of Digital Lamellae of Lizards*, J Morphol **120** (1966) 233–265. ↑3.4.1

[Eus2004] S. R. Euston, *Computer Simulation of Proteins: Adsorption, Gelation and Self-Association*, Curr Opin Colloid Interface Sci **9** (2004) 321–327. ↑3.2.1

[Eve2008] F. Evers, K. Shokuie, M. Paulus, C. Sternemann, C. Czeslik, and M. Tolan, *Exploring the Interfacial Structure of Protein Adsorbates and the Kinetics of Protein Adsorption: an in Situ High-Energy X-Ray Reflectivity Study*, Langmuir **24** (2008) 10216–10221. ↑3.2.1

[Fre2006] L. Freeman-Cook and K. D. Freeman-Cook, *Staphylococcus aureus Infections*, 2006. ↑3.3.3

[Fed2001] W. Federle, E. L. Brainerd, T. A. McMahon, and B. Hölldobler, *Biomechanics of the Movable Pretarsal Adhesive Organ in Ants and Bees*, Proc Natl Acad Sci **98** (2001) 6215–6220. ↑1

[Fis2000] T. E. Fisher, P. E. Marszalek, and J. M. Fernandez, *Stretching Single Molecules Into Novel Conformations Using the Atomic Force Microscope*, Nat Struct Biol **7** (2000) 719–724. ↑4.2.1

[For1982] M. A. Fortes, *Axisymmetric Liquid Bridges Between Parallel Plates*, J Colloid Interface Sci **88** (1982) 338–352. ↑3.1.8

[Fos1998] T. J. Foster and M. Hook, *Surface Protein Adhesins of Staphylococcus aureus*, Trends Microbiol **6** (1998) 484–488. ↑3.3.3, 3.3.3

[Fos2005] T. J. Foster, *Immune Evasion by Staphylococci*, Nat Rev Microbiol **3** (2005) 948–958. ↑3.3.3, 3.3.3

[Fra2005] B. W. Frazee, J. Lynn, E. D. Charlebois, L. Lambert, D. Lowery, and F. Perdreau-Remington, *High Prevalence of Methicillin-Resistant Staphylococcus aureus in Emergency Department Skin and Soft Tissue Infections*, Annals of emergency medicine **45** (2005) 311–320. ↑3.3.3

[Fre1995] R. H. French, R. M. Cannon, L. K. Denoyer, and Y.-m. Chiang, *Full Spectral Calculation of Nonretarded Hamaker Constants for Ceramic Systems from Interband Transition Strengths*, Solid State Ionics **75** (1995) 13–33. ↑3.1

[Fre2010] R. H. French, V. A. Parsegian, R. Podgornik, R. F. Rajter, A. Jagota, J. Luo, D. Asthagiri, M. K. Chaudhury, Y.-m. Chiang, S. Granick, S. Kalinin, M. Kardar, R. Kjellander, D. C. Langreth, J. Lewis, S. Lustig, D. Wesolowski, J. S. Wettlaufer, W.-Y. Ching, M. Finnis, F. Houlihan, O. A. von Lilienfeld, C. J. Van Oss, and T. Zemb, *Long Range Interactions in Nanoscale Science*, Rev Mod Phys **82** (2010) 1887–1944. ↑3.1

[Fri1994] C. D. Frisbie, L. F. Rozsnyai, A. Noy, M. S. Wrighton, and C. M. Lieber, *Functional Group Imaging by Chemical Force Microscopy*, Science **265** (1994) 2071–2074. ↑4.2.1

[Gab2008] F. Gaboriaud, M. L. Gee, R. A. Strugnell, and J. F. L. Duval, *Coupled Electrostatic, Hydrodynamic, and Mechanical Properties of Bacterial Interfaces in Aqueous Media*, Langmuir **24** (2008) 10988–10995. ↑3.3.2

[Gan2007] Y. Gan, *A Review of Techniques for Attaching Micro- and Nanoparticles to a Probe's Tip for Surface Force and Near-field Optical Measurements*, Rev Sci Instrum **78** (2007) 081101. ↑4.2.1

[Gar2002] R. Garcia and R. Perez, *Dynamic Atomic Force Microscopy Methods*, Surf Sci Rep **47** (2002) 197–301. ↑6

[Gar2008] T. R. Garrett, M. Bhakoo, and Z. Zhang, *Bacterial Adhesion and Biofilms on Surfaces*, Prog Nat Sci **18** (2008) 1049–1056. ↑3.2.1

[Gat2009] S. Gatermann and K. Miksits, *Staphylokokken*, Medizinische mikrobiologie und infektiologie, 2009, pp. 191–202. ↑14

[Gei2003] A. K. Geim, S. V. Dubonos, I. V. Grigorieva, K. S. Novoselov, A. A. Zhukov, and S. Y. Shapoval, *Microfabricated Adhesive Mimicking Gecko Foot-Hair*, Nature Mater **2** (2003) 461–463. ↑1, 3.4.1

[Ger2012] S. Gerth, M. Lessel, O. Bäumchen, M. Klimczak, H. G. Steinrück, K. Jacobs, and A. Magerl, *On The Structure of Self-Assembled Silane Coatings*, submitted (2012). ↑4.1.1

[Gib1973] R. J. Gibbons and J. van Houte, *On the Formation of Dental Plaques*, Journal of Periodontology **44** (1973) 347–360. ↑3.3.4

[Gib1975] R. J. Gibbons and J. van Houte, *Bacterial Adherence in Oral Microbial Ecology*, Annu Rev Microbiol **29** (1975) 19–44. ↑3.3.4

[Gie2003] F. J. Giessibl, *Advances in Atomic Force Microscopy*, Rev Mod Phys **75** (2003) 949–983. ↑4.2

[Gil2007] Y. Gilbert, M. Deghorain, L. Wang, B. Xu, P. D. Pollheimer, H. J. Gruber, J. Errington, B. Hallet, X. Haulot, C. Verbelen, P. Hols, and Y. F. Dufrene, *Single-Molecule Force Spectroscopy and Imaging of the Vancomycin/D-Ala-D-Ala Interaction*, Nano Lett **7** (2007) 796–801. ↑4.2.1

[Göt1990] F. Götz, *Staphylococcus carnosus: a New Host Organism for Gene Cloning and Protein Production*, J Appl Bacteriol **69** (1990) S49–S53. ↑3.3.3

[Göt2002] F. Götz, *Staphylococcus and Biofilms*, Mol Microbiol **43** (2002) 1367–1378. ↑3.3.3

[Gou1910] M. Gouy, *Sur La Constitution De La Charge Electrique a La Surface D'un Electrolyte*, J Phys Theor Appl **9** (1910) 457–468. ↑3.1.2

[Gra1884] C. Gram, *Ueber die isolierte Faerbung der Schizomyceten: In Schnitt- und Trockenpraeparaten*, Fortschritte der Medizin **2** (1884) 185. ↑3.3

[Gra2010] N. Gravish, M. Wilkinson, S. Sponberg, A. Parness, N. Esparza, D. Soto, T. Yamaguchi, M. Broide, M. Cutkosky, C. Creton, and K. Autumn, *Rate-Dependent Frictional Adhesion in Natural and Synthetic Gecko Setae*, J R Soc Interface **7** (2010) 259–269. ↑5.1.3

[Gre2000] R. J. Green, R. A. Frazier, K. M. Shakesheff, M. C. Davies, C. J. Roberts, and S. J. B. Tendler, *Surface Plasmon Resonance Analysis of Dynamic Biological Interactions with Biomaterials*, Biomaterials **21** (2000) 1823–1835. ↑3.2.1

[Gri1987] A. G. Gristina, *Biomaterial-Centered Infection: Microbial Adhesion Versus Tissue Integration*, Science **237** (1987) 1588–1595. ↑3.3.2

[Gro2001] M. Gross, S. E. Cramton, F. Götz, and A. Peschel, *Key Role of Teichoic Acid Net Charge in Staphylococcus aureus Colonization of Artificial Surfaces*, Infect Immun **69** (2001) 3423–34233426. ↑3.3.1

[Häh2011] H. Hähl, *Proteinadsorption an Grenzflaechen: Bestimmung von Adsorptionskinetik und Adsorbatstruktur mittels Reflexionsmethoden*, Dissertation, 2011. ↑3.2.1, 6.1

[Ham1980] S. Hamada and H. D. Slade, *Biology, Immunology, and Cariogenicity of Streptococcus mutans*, Microbiol Rev **44** (1980) 331–384. ↑3.3.4

[Han1992] H. G. Hansma, J. Vesenka, C. Siegerist, G. Kelderman, H. Morrett, R. L. Sinsheimer, V. Elings, C. Bustamante, and P. K. Hansma, *Reproducible Imaging and Dissection of Plasmid DNA Under Liquid with the Atomic Force Microscope*, Science **256** (1992) 1180–1184. ↑4.2

[Han2005] W. R. Hansen and K. Autumn, *Evidence for Self-Cleaning in Gecko Setae*, Proc Natl Acad Sci **102** (2005) 385–389. ↑1

[Har2003] N. Harraghy, M. Hussain, A. Haggar, T. Chavakis, B. Sinha, M. Herrmann, and J.-I. Flock, *The Adhesive and Immunomodulating Properties of the Multifunctional Staphylococcus aureus Protein Eap*, Microbiology **149** (2003) 2701–2707. ↑3.3.3

[Har2006] N. Harraghy, S. Seiler, K. Jacobs, M. Hannig, M. D. Menger, and M. Herrmann, *Advances in in vitro and in vivo Models for Studying the Staphylococcal Factors Involved in Implant Infections*, Int J Artif Organs **29** (2006) 368–378. ↑3.3.2, 4.3

[Hed2001] S. B. Hedges and R. Thomas, *At the Lower Size Limit in Amniote Vertebrates: a New Diminutive Lizard from the West Indies*, Caribb J Sci **37** (2001) 168–173. ↑3.4

[Hel2008] J. Helenius, C.-P. Heisenberg, H. E. Gaub, and D. J. Muller, *Single-Cell Force Spectroscopy*, J Cell Sci **121** (2008) 1785–1791. ↑3.3.2, 4.2.1

[Her1882] H. Hertz, *Ueber die Berührung fester elastischer Körper.*, Journal für die reine und angewandte Mathematik (Crelles Journal) **1882** (1882) 156–171. ↑3.5

[Her1999] M. Hermansson, *The DLVO Theory in Microbial Adhesion*, Colloids Surf B **14** (1999) 105–119. ↑3.3.2

[Heu1995] M. Heuberger, G. Dietler, and L. Schlapbach, *Mapping the Local Young's Modulus by Analysis of the Elastic Deformations Occurring in Atomic Force Microscopy*, Nanotechnology **6** (1995) 12–23. ↑4.2.1

[Hil1968] U. Hiller, *Untersuchungen zum Feinbau und zur Funktion der Haftborsten von Reptilien*, Zoomorphology **62** (1968) 307–362. ↑3.4.1, 3.4.1

[Hil1969] U. Hiller, *Correlation Between Corona-Discharge of Polyethylene-Films and the Adhering Power of Tarentola M. mauritanica (Rept.)*, Forma et functio **1** (1969) 350–352. ↑3.4.1

[Hin2006] P. Hinterdorfer and Y. F. Dufrene, *Detection and Localization of Single Molecular Recognition Events Using Atomic Force Microscopy*, Nat Methods **3** (2006) 347–355. ↑4.2.1

[Hof2012] A. M. G. Hoffmann, *Proteinadsorption auf hydrophobisierten Oberflächen: Bestimmung und Modellierung von Adsorptionskinetiken und deren Abhängigkeit von Prozessparametern*, Diplomarbeit, 2012. ↑3.2, 6.1

[Hou1980] D. B. Hough and L. R. White, *The Calculation of Hamaker Constants from Liftshitz Theory with Applications to Wetting Phenomena*, Adv Colloid Interface Sci **14** (1980) 3–41. ↑*e*

[Hub2005] G. Huber, H. Mantz, R. Spolenak, K. Mecke, K. Jacobs, S. N. Gorb, and E. Arzt, *Evidence for Capillarity Contributions to Gecko Adhesion from Single Spatula Nanomechanical Measurements*, Proc Natl Acad Sci **102** (2005) 16293–16296. ↑3.4.1, 4.2.1

[Hue2010] S. Huembert, *Herstellung und Erprobung von AFM-Bakteriensonden auf definierten Oberflächen*, Diplomarbeit, 2010. ↑2, 4.2.2, 13, 1

[Hus2001] M. Hussain, C. Heilmann, G. Peters, and M. Herrmann, *Teichoic Acid Enhances Adhesion of Staphylococcus epidermidis to Immobilized Fibronectin*, Microb Pathogenesis **31** (2001) 261–270. ↑3.3.1

[Hut1993] J. L. Hutter and J. Bechhoefer, *Calibration of Atomic-Force Microscope Tips*, Rev Sci Instrum **64** (1993) 1868–1873. ↑4.2.3

[Hen2007] K. Henzler-Wildman and D. Kern, *Dynamic Personalities of Proteins*, Nature **450** (2007) 964–972. ↑6.1, 2

[Ish2000] N. Ishida, T. Inoue, M. Miyahara, and K. Higashitani, *Nano Bubbles on a Hydrophobic Surface in Water Observed by Tapping-Mode Atomic Force Microscopy*, Langmuir **16** (2000) 6377–6380. ↑3.1.4

[Isr1982] J. N. Israelachvili and R. M. Pashley, *The Hydrophobic Interaction Is Long-Range, Decaying Exponentially with Distance*, Nature **300** (1982) 341–342. ↑3.1.4

[Isr1984] J. N. Israelachvili and R. M. Pashley, *Measurement of the Hydrophobic Interaction Between Two Hydrophobic Surfaces in Aqueous Electrolyte Solutions*, J Colloid Interface Sci **98** (1984) 500–514. ↑3.1.4

[Isr1992] J. N. Israelachvili, *Intermolecular and Surface Forces*, 2. Aufl., Academic Press, San Diego, 1992. ↑3.1, 3.1, 3.1.1, 3.1.2

[Isr1996] J. N. Israelachvili and H. Wennerström, *Role of Hydration and Water Structure in Biological and Colloidal Interactions*, Nature **379** (1996) 219–225. ↑3.1.4

[Jan2004] J. Jang, G. C. Schatz, and M. A. Ratner, *Capillary Force in Atomic Force Microscopy*, J Chem Phys **120** (2004) 1157. ↑3.1.8

[Joh1971] K. L. Johnson, K. Kendall, and A. D. Roberts, *Surface Energy and the Contact of Elastic Solids*, Proc R Soc Lond A **324** (1971) 301–313. ↑3.5

[Jon1924] J. E. Jones, *On the Determination of Molecular Fields.—II. From the Equation of State of a Gas*, Proc R Soc Lond A **106** (1924) 463–477. ↑3.1.5

[Jon1982] G. W. Jones and R. E. Isaacson, *Proteinaceous Bacterial Adhesins and Their Receptors*, CRC Critical Reviews in Microbiology **10** (1982) 229–260. ↑3.3.2

[Jos2009] C. Josenhans, H. Hahn, and R. E. Streeck, *Bakterien: Definition und Aufbau*, Medizinische mikrobiologie und infektiologie, 2009, pp. 175–185. ↑3.3, 12

[Kal2010] S. Kalasin, J. Dabkowski, K. Nuesslein, and M. M. Santore, *The Role of Nano-Scale Heterogeneous Electrostatic Interactions in Initial Bacterial Adhesion from Flow: a Case Study with Staphylococcus aureus*, Colloids Surf B **76** (2010) 489–495. ↑3.3.2

[Kan2009] S. Kang and M. Elimelech, *Bioinspired Single Bacterial Cell Force Spectroscopy*, Langmuir **25** (2009) 9656–9659. ↑4.2.2, 4.2.2

[Kar2002] M. Karplus and J. A. McCammon, *Molecular Dynamics Simulations of Biomolecules*, Nat Struct Biol **9** (2002) 646–652. ↑3.2.1

[Kas2008] S. Kasas and G. Dietler, *Probing Nanomechanical Properties from Biomolecules to Living Cells*, Pflug Arch Eur J Phy **456** (2008) 13–27. ↑4.2

[Kes1975] S. W. Kessler, *Rapid Isolation of Antigens from Cells with a Staphylococcal Protein A-Antibody Adsorbent: Parameters of Interaction of Antibody-Antigen Complexes with Protein A*, J Immunol **115** (1975) 1617–1624. ↑3.3.3

[Kir2004] B. J. Kirby and E. F. Hasselbrink, *Zeta Potential of Microfluidic Substrates: 1. Theory, Experimental Techniques, and Effects on Separations*, Electrophoresis **25** (2004) 187–202. ↑3.1.2

[Kle2000] P. Klemm and M. A. Schembri, *Bacterial Adhesins: Function and Structure*, Int J Med Microbiol **290** (2000) 27–35. ↑3.3.2

[Kle2006] R. M. Klevens, J. R. Edwards, F. C. Tenover, L. C. McDonald, T. Horan, R. P. Gaynes, and National Nosocomial Infections Surveillance System, *Changes in the Epidemiology of Methicillin-Resistant Staphylococcus aureus in Intensive Care Units in US Hospitals, 1992-2003*, Clinical Infectious Diseases **42** (2006) 389–391. ↑3.3.3

[Klu1997] J. Kluytmans, A. van Belkum, and H. Verbrugh, *Nasal Carriage of Staphylococcus aureus: Epidemiology, Underlying Mechanisms, and Associated Risks*, Clin Microbiol Rev **10** (1997) 505–&. ↑3.3.3

[Kro1999] I. Kroes, P. W. Lepp, and D. A. Relman, *Bacterial Diversity Within the Human Subgingival Crevice*, Proc Natl Acad Sci **96** (1999) 14547–14552. ↑3.3.4

[Kum1998] C. G. Kumar and S. K. Anand, *Significance of Microbial Biofilms in Food Industry: a Review*, Int J Food Microbiol **42** (1998) 9–27. ↑1

[Kuu1978] P. Kuusela, *Fibronectin Binds to Staphylococcus aureus*, Nature **276** (1978) 718–720. ↑4.2.2

[Laa1988] M. Laatikainen and M. Lindström, *Determination of Adsorption Isotherms with Quartz Crystal Microbalance in Liquid Phase*, J Colloid Interface Sci **125** (1988) 610–614. ↑3.2.1

[Lam1916] I. Lamgmuir, *The Constitution and Fundamental Properties of Solids and Liquids. Part 1*, J Am Chem Soc **38** (1916) 2221–2295. ↑3.2.1

[Lan1918] I. Langmuir, *The Adsorption of Gases on Plane Surfaces of Glass, Mica and Platinum.*, J Am Chem Soc **40** (1918) 1361–1403. ↑3.2.1

[Lap1806] P. S. Laplace, *Supplement Au Dixieme Livre Du Traite De Mecaniqe Celeste Sur L'Action Capillaire*, Courcier, Paris, 1806. ↑3.1.8

[Lat2008] R. A. Latour, *Molecular Simulation of Protein-Surface Interactions: Benefits, Problems, Solutions, and Future Directions (Review)*, Biointerphases **3** (2008) FC2–FC12. ↑3.2.1

[Lec2001] D. Leckband and J. N. Israelachvili, *Intermolecular Forces in Biology*, Q Rev Biophys **34** (2001) 105–267. ↑3.1, 3.3

[Lee2006] H. Lee, *Single-Molecule Mechanics of Mussel Adhesion*, Proc Natl Acad Sci **103** (2006) 12999–13003. ↑3.3.2, 4.2.1, 4.2.2

[Lee2007a] H. Lee, S. M. Dellatore, W. M. Miller, and P. B. Messersmith, *Mussel-Inspired Surface Chemistry for Multifunctional Coatings*, Science **318** (2007) 426–430. ↑4.2.2

[Lee2007b] H. Lee, B. P. Lee, and P. B. Messersmith, *A Reversible Wet/Dry Adhesive Inspired by Mussels and Geckos*, Nature **448** (2007) 338–U4. ↑1, 4.2.2

[Lee2008] J. Lee and R. S. Fearing, *Contact Self-Cleaning of Synthetic Gecko Adhesive from Polymer Microfibers*, Langmuir **24** (2008) 10587–10591. ↑1

[Lee2009a] H. Lee, J. Rho, and P. B. Messersmith, *Facile Conjugation of Biomolecules onto Surfaces via Mussel Adhesive Protein Inspired Coatings*, Adv Mater **21** (2009) 431–+. ↑4.2.2

[Lee2009b] J. Lee, B. G. Bush, R. Maboudian, and R. S. Fearing, *Gecko-Inspired Combined Lamellar and Nanofibrillar Array for Adhesion on Nonplanar Surface*, Langmuir **25** (2009) 12449–12453. ↑3.4.1

[Les2012] M. Lessel, O. Bäumchen, M. Klos, H. Hähl, R. Fetzer, and K. Jacobs, *Self-Assembled Silane Monolayers: a Step-by-Step Recipe for High-Quality, Low Energy Surfaces*, in preparation (2012). ↑4.1.1

[Lew2008] K. Lewis, *Multidrug Tolerance of Biofilms and Persister Cells*, Curr Top Microbiol **322** (2008) 107–131. ↑3.3.3

[Li2003] F. Li, S. D. Redick, H. P. Erickson, and V. T. Moy, *Force Measurements of the $\alpha(5)\beta(1)$ Integrin-Fibronectin Interaction*, Biophys J **84** (2003) 1252–1262. ↑4.2.1

[Lia2000] M. N. Liang, S. P. Smith, S. J. Metallo, I. S. Choi, M. Prentiss, and G. M. Whitesides, *Measuring the Forces Involved in Polyvalent Adhesion of Uropathogenic Escherichia coli to Mannose-Presenting Surfaces*, Proc Natl Acad Sci **97** (2000) 13092–13096. ↑3.3.2

[Lin2009] A. Y. M. Lin, R. Brunner, P. Y. Chen, F. E. Talke, and M. A. Meyers, *Underwater Adhesion of Abalone: the Role of Van der Waals and Capillary Forces*, Acta Mater **57** (2009) 4178–4185. ↑4.2.1

[Liu2007] Y. Liu, J. Strauss, and T. A. Camesano, *Thermodynamic Investigation of Staphylococcus epidermidis Interactions with Protein-Coated Substrata*, Langmuir **23** (2007) 7134–7142. ↑3.3.2

[Liu2011] C. Liu and Q. Zhao, *Influence of Surface-Energy Components of Ni-P-TiO_2-PTFE Nanocomposite Coatings on Bacterial Adhesion*, Langmuir **27** (2011) 9512–9519. ↑3.3.2

[Loe1986] W. J. Loesche, *Role of Streptococcus mutans in Human Dental Decay*, Microbiol Rev **50** (1986) 353–380. ↑3.3.4

[Lon1937] F. London, *The General Theory of Molecular Forces*, T Faraday Soc **33** (1937) 8–26. ↑3.1.1

[Los2009] P. Loskill, *Einfluss langreichweitiger Van der Waals-Wechselwirkungen auf die Adhäsion von Bakterien—Eine AFM Studie*, Diplomarbeit, 2009. ↑4.2, 4.2.2, 13, 6.1

[Low1998] F. D. Lowy, *Medical Progress - Staphylococcus aureus Infections*, New Engl J Med **339** (1998) 520–532. ↑3.3.3

[Low2000] S. K. Lower, C. J. Tadanier, and M. F. Hochella Jr, *Measuring Interfacial and Adhesion Forces Between Bacteria and Mineral Surfaces with Biological Force Microscopy*, Geochim Cosmochim Acta **64** (2000) 3133–3139. ↑4.2.1, 4.2.2

[Low2001] S. K. Lower, M. F. Hochella Jr, and T. J. Beveridge, *Bacterial Recognition of Mineral Surfaces: Nanoscale Interactions Between Shewanella and α-FeOOH*, Science **292** (2001) 1360–1363. ↑4.2.2, 4.2.2

[Lu2007] J. R. Lu, X. Zhao, and M. Yaseen, *Protein Adsorption Studied by Neutron Reflection*, Curr Opin Colloid Interface Sci **12** (2007) 9–16. ↑3.2.1

[Lyk1991] J. Lyklema, *Fundamentals of Interface and Colloid Science*, 1. Aufl., Fundamentals, Band 1, Academic Press, Cornwall, 1991. ↑3.1, 3

[Lyn2007] D. J. Lynch, T. L. Fountain, J. E. Mazurkiewicz, and J. A. Banas, *Glucan-Binding Proteins Are Essential for Shaping Streptococcus mutans Biofilm Architecture*, FEMS Microbiol Lett **268** (2007) 158–165. ↑3.3.4

[Lyu1997] Y. L. Lyubchenko and L. S. Shlyakhtenko, *Visualization of Supercoiled DNA with Atomic Force Microscopy in situ.*, Proc Natl Acad Sci **94** (1997) 496–501. ↑4.2

[Mad1964] P. F. A. Maderson, *Keratinized Epidermal Derivatives as Aid to Climbing in Gekkonid Lizards*, Nature **203** (1964) 780–&. ↑3.4.1

[Mad2006] M. T. Madigan and J. M. Martinko, *Brock Mikrobiologie*, 11. Aufl., Pearson Studium, München, 2006. ↑14, 3.3.4

[Mah1941] B. C. Mahendra, *Contributions to the Bionomics, Anatomy, Reproduction and Development of the Indian House-Gecko, Hemidactylus flaviviridis Rüppel*, Proceedings: Plant Sciences **13** (1941) 288–306. ↑3.4.1

[Mah2008] A. Mahdavi, L. Ferreira, C. Sundback, J. W. Nichol, E. P. Chan, D. J. D. Carter, C. J. Bettinger, S. Patanavanich, L. Chignozha, E. Ben-Joseph, A. Galakatos, H. Pryor, I. Pomerantseva, P. T. Masiakos, W. Faquin, A. Zumbuehl, S. Hong, J. Borenstein, J. Vacanti, R. Langer, and J. M. Karp, *A Biodegradable and Biocompatible Gecko-Inspired Tissue Adhesive*, Proc Natl Acad Sci **105** (2008) 2307–2312. ↑3.4.1

[Mal2003] M. Malmsteen, *Biopolymers at Interfaces*, 2. Aufl., Marcel Dekker, Inc, New York, 2003. ↑3.2.1

[Mam1987] W. Mamo, F. Rozgonyi, A. Brown, S. Hjerten, and T. Wadstrom, *Cell Surface Hydrophobicity and Charge of Staphylococcus aureus and Coagulase-Negative Staphylococci from Bovine Mastitis*, J Appl Bacteriol **62** (1987) 241–249. ↑3.3.2, 5.3

[Mar1971] K. C. Marshall, R. Stout, and R. Mitchell, *Mechanism of Initial Events in Sorption of Marine Bacteria to Surfaces*, J Gen Microbiol **68** (1971) 337–348. ↑3.3.2

[Mat2001] R. Matzke, K. Jacobson, and M. Radmacher, *Direct, High-Resolution Measurement of Furrow Stiffening During Division of Adherent Cells*, Nat Cell Biol **3** (2001) 607–610. ↑4.2

[Mat2006] V. R. F. Matias and T. J. Beveridge, *Native Cell Wall Organization Shown by Cryo-Electron Microscopy Confirms the Existence of a Periplasmic Space in Staphylococcus aureus*, J Bacteriol **188** (2006) 1011–1021. ↑3.3.3

[Mat2007] V. R. F. Matias and T. J. Beveridge, *Cryo-Electron Microscopy of Cell Division in Staphylococcus aureus Reveals a Mid-Zone Between Nascent Cross Walls*, Mol Microbiol **64** (2007) 195–206. ↑3.3.3

[Mau1992] D. Maugis, *Adhesion of Spheres: The JKR-DMT Transition Using a Dugdale Model*, J Colloid Interface Sci **150** (1992) 243–269. ↑3.5

[Mau1999] D. Maugis, *Contact, Adhesion and Rupture of Elastic Solids*, 1. Aufl., Springer, Berlin, 1999. ↑3.5, 4.7, 4.2.4

[May1998] E. Mayr, *Two Empires or Three?*, Proc Natl Acad Sci **95** (1998) 9720–9723. ↑10

[Maz1999] S. K. Mazmanian, G. Liu, H. Ton-That, and O. Schneewind, *Staphylococcus aureus Sortase, an Enzyme That Anchors Surface Proteins to the Cell Wall*, Science **285** (1999) 760–763. ↑3.3.3

[Mei1992] J. M. Meinders, J. Noordmans, and H. J. Busscher, *Simultaneous Monitoring of the Adsorption and Desorption of Colloidal Particles During Deposition in a Parallel Plate Flow Chamber*, J Colloid Interface Sci **152** (1992) 265–280. ↑4.3

[Mei1995] J. M. Meinders, H. C. van der Mei, and H. J. Busscher, *Deposition Efficiency and Reversibility of Bacterial Adhesion Under Flow*, J Colloid Interface Sci **176** (1995) 329–341. ↑3.3.2, 4.3

[Mei2009] L. Mei, H. C. van der Mei, Y. Ren, W. Norde, and H. J. Busscher, *Poisson Analysis of Streptococcal Bond Strengthening on Stainless Steel with and without a Salivary Conditioning Film*, Langmuir **25** (2009) 6227–6231. ↑4.2.1, 4.2.2

[Mer1999] R. Merkel, P. Nassoy, A. Leung, K. Ritchie, and E. Evans, *Energy Landscapes of Receptor-Ligand Bonds Explored with Dynamic Force Spectroscopy*, Nature **397** (1999) 50–53. ↑3.3.2, 4.2.1

[Mey2005] E. E. Meyer, Q. Lin, T. Hassenkam, E. Oroudjev, and J. N. Israelachvili, *Origin of the Long-Range Attraction Between Surfactant-Coated Surfaces*, Proc Natl Acad Sci **102** (2005) 6839–6842. ↑3.1.4

[Mey2006] E. E. Meyer, K. J. Rosenberg, and J. N. Israelachvili, *Recent Progress in Understanding Hydrophobic Interactions*, Proc Natl Acad Sci **103** (2006) 15736–15738. ↑3.1.4

[Mez2006] M. Mezger, H. Reichert, S. Schoder, J. Okasinski, H. Schroder, H. Dosch, D. Palms, J. Ralston, and V. Honkimaki, *High-Resolution in situ X-ray Study of the Hydrophobic Gap at the Water-Octadecyl-Trichlorosilane Interface*, Proc Natl Acad Sci **103** (2006) 18401–18404. ↑4.1.1

[Mil2008] B. C. Millar, B. D. Prendergast, and J. E. Moore, *Community-Associated MRSA (CA-MRSA): an Emerging Pathogen in Infective Endocarditis*, Journal of Antimicrobial Chemotherapy **61** (2008) 1–7. ↑3.3.3

[Min2008] Y. Min, M. Akbulut, K. Kristiansen, Y. Golan, and J. N. Israelachvili, *The Role of Interparticle and External Forces in Nanoparticle Assembly*, Nature Mater **7** (2008) 527–538. ↑3.1.8

[Mo2009] Y. Mo, K. T. Turner, and I. Szlufarska, *Friction Laws at the Nanoscale*, Nature **457** (2009) 1116–1119. ↑3.5

[Mof2008] J. R. Moffitt, Y. R. Chemla, S. B. Smith, and C. Bustamante, *Recent Advances in Optical Tweezers*, Annu Rev Biochem **77** (2008) 205–228. ↑3.3.2

[Mor1983] C. Moritz, *Parthenogenesis in the Endemic Australian Lizard Heteronotia binoei (Gekkonidae)*, Science **220** (1983) 735–737. ↑3.4

[Mor2006] J. Morgan, J. Notte, R. Hill, and B. Ward, *An Introduction to the Helium Ion Microscope*, Micros Today **14** (2006) 24–31. ↑3.8

[Mou1995] J. Mou, D. M. Czajkowsky, Y. Zhang, and Z. Shao, *High-Resolution Atomic-Force*

Microscopy of DNA: the Pitch of the Double Helix, FEBS Lett **371** (1995) 279–282. ↑4.2

[Mun1994] L. L. Munn, R. J. Melder, and R. K. Jain, *Analysis of Cell Flux in the Parallel-Plate Flow Chamber - Implications for Cell Capture Studies*, Biophys J **67** (1994) 889–895. ↑4.3

[Mur2007] M. P. Murphy, B. Aksak, and M. Sitti, *Adhesion and Anisotropic Friction Enhancements of Angled Heterogeneous Micro-Fiber Arrays with Spherical and Spatula Tips*, J Adhes Sci Technol **21** (2007) 1281–1296. ↑3.4.1

[Myk2003] T. A. Mykhaylyk, S. D. Evans, C. M. Fernyhough, I. W. Hamley, and J. R. Henderson, *Surface Energy of Ethylene-co-1-butene Copolymers Determined by Contact Angle Methods*, J Colloid Interface Sci **260** (2003) 234–239. ↑4.1

[Nav1999] W. W. Navarre and O. Schneewind, *Surface Proteins of Gram-Positive Bacteria and Mechanisms of Their Targeting to the Cell Wall Envelope*, Microbiol Mol Biol R **63** (1999) 174–229. ↑3.3.1

[Nea2005] A. L. Neal, T. L. Bank, M. F. Hochella Jr, and K. M. Rosso, *Cell Adhesion of Shewanella oneidensis to Iron Oxide Minerals: Effect of Different Single Crystal Faces*, Geochem T **6** (2005) 77–84. ↑4.2.2

[Neu1974] A. W. Neumann, R. J. Good, C. J. Hope, and M. Sejpal, *An Equation-of-State Approach to Determine Surface Tensions of Low-Energy Solids from Contact Angles*, J Colloid Interface Sci **49** (1974) 291–304. ↑3.1.6

[Neu1992] H. C. Neu, *The Crisis in Antibiotic Resistance*, Science **257** (1992) 1064–1073. ↑3.3.3

[Neu2003] F. C. Neuhaus and J. Baddiley, *A Continuum of Anionic Charge: Structures and Functions of D-Alanyl-Teichoic Acids in Gram-Positive Bacteria*, Microbiol Mol Biol R **67** (2003) 686–723. ↑3.3.1

[Neu2008] K. C. Neuman and A. Nagy, *Single-Molecule Force Spectroscopy: Optical Tweezers, Magnetic Tweezers and Atomic Force Microscopy*, Nat Methods **5** (2008) 491–505. ↑3.3.2, 4.2.1

[Ner2006] I. Neria-González, E. T. Wang, F. Ramírez, J. M. Romero, and C. Hernández-Rodríguez, *Characterization of Bacterial Community Associated to Biofilms of Corroded Oil Pipelines from the Southeast of Mexico*, Anaerobe **12** (2006) 122–133. ↑1

[Nie2008] P. H. Niewiarowski, S. Lopez, L. Ge, E. Hagan, and A. Dhinojwala, *Sticky Gecko Feet: The Role of Temperature and Humidity*, PLoS ONE **3** (2008) e2192. ↑3.4.1

[Nor1990] J. K. Norskov, *Chemisorption on Metal Surfaces*, Rep Prog Phys **53** (1990) 1253–1295. ↑9

[Nor2006] D. Norouzi, M. M. Mueller, and M. Deserno, *How to Determine Local Elastic Properties of Lipid Bilayer Membranes from Atomic-Force-Microscope Measurements: a Theoretical Analysis*, Phys Rev E **74** (2006) 061914. ↑4.2.1

[Nos2007] M. Nosonovsky and B. Bhushan, *Multiscale Friction Mechanisms and Hierarchical Surfaces in Nano- and Bio-Tribology*, Mat Sci Eng R **58** (2007) 162–193. ↑3.5

[Noy1995] A. Noy, C. D. Frisbie, L. F. Rozsnyai, M. S. Wrighton, and C. M. Lieber, *Chemical Force Microscopy: Exploiting Chemically-Modified Tips to Quantify Adhesion, Friction, and Functional Group Distributions in Molecular Assemblies*, J Am Chem Soc **117** (1995) 7943–7951. ↑4.2.1

[Noy1997] A. Noy, D. V. Vezenov, and C. M. Lieber, *Chemical Force Microscopy*, Annu Rev Mater Sci **27** (1997) 381–421. ↑4.2.1

[Olo2005] A.-C. Olofsson, M. Hermansson, and H. Elwing, *Use of a Quartz Crystal Microbalance to Investigate the Antiadhesive Potential of N-acetyl-L-cysteine*, Appl Environ Microbiol **71** (2005) 2705–2712. ↑3.3.2

[Ols2009] A. L. J. Olsson, H. C. van der Mei, H. J. Busscher, and P. K. Sharma, *Influence of Cell Surface Appendages on the Bacterium-Substratum Interface Measured Real-Time Using QCM-D*, Langmuir **25** (2009) 1627–1632. ↑3.3.2

[Ols2010] A. L. J. Olsson, H. C. van der Mei, H. J. Busscher, and P. K. Sharma, *Novel Analysis of Bacterium-Substratum Bond Maturation Measured Using a Quartz Crystal Microbalance*, Langmuir **26** (2010) 11113–11117. ↑3.3.2

[Ong1999] Y.-L. Ong, A. Razatos, G. Georgiou, and M. M. Sharma, *Adhesion Forces Between E. coli Bacteria and Biomaterial Surfaces*, Langmuir **15** (1999) 2719–2725. ↑4.2.1, 4.2.2

[Ong2007] Q. K. Ong and I. Sokojov, *Attachment of Nanoparticles to the AFM Tips for Direct Measurements of Interaction Between a Single Nanoparticle and Surfaces*, J Colloid Interface Sci **310** (2007) 385–390. ↑4.2.1

[Ott2008] M. Otto, *Staphylococcal Biofilms*, Curr Top Microbiol **322** (2008) 207–228. ↑3.3.3

[Owe1969] D. K. Owens and R. C. Wendt, *Estimation of Surface Free Energy of Polymers*, J Appl Polym Sci **13** (1969) 1741–1747. ↑3.1.6

[Pal1998] M. Palma, D. Wade, M. Flock, and J.-I. Flock, *Multiple Binding Sites in the Interaction Between an Extracellular Fibrinogen-binding Protein from Staphylococcus aureus and Fibrinogen*, J Biol Chem **273** (1998) 13177–13181. ↑3.3.3

[Pal1999] M. Palma, A. Haggar, and J.-I. Flock, *Adherence of Staphylococcus aureus Is Enhanced by an Endogenous Secreted Protein with Broad Binding Activity*, J Bacteriol **181** (1999) 2840–2845. ↑3.3.3

[Pan1992] A. L. Panlilio, D. H. Culver, R. P. Gaynes, S. Banerjee, T. S. Henderson, J. S. Tolson, W. J. Martone, and t. N. N. I. S. System, *Methicillin-Resistant Staphylococcus aureus in U.S. Hospitals, 1975-1991*, Infect Cont Hosp Ep **13** (1992) 582–586. ↑3.3.3

[Pas1982] R. M. Pashley, *Hydration Forces Between Mica Surfaces in Electrolyte Solutions*, Adv Colloid Interface Sci **16** (1982). ↑3.1.4

[Pit2010] B. Pittenger, N. Erina, and C. Su, *Quantitative Mechanical Property Mapping at the Nanoscale with PeakForce QNM*, Bruker Corporation Application Note AN128, 2010. ↑4.2.4, 4.7

[Ple2010] G. Pletikapić, A. Berquand, and S. Vesna, *Peak Force Tapping AFM, State of the Art Tool for Quantitative Nanomechanical Mapping*, Charge density waves: small scales and ultrashort time, 2010, pp. 1–1. ↑4.2.4

[Ple2012] G. Pletikapić, A. Berquand, T. M. Radić, and V. Svetličić, *Quantitative Nanomechanical Mapping of Marine Diatom in Seawater Using Peak Force Tapping Atomic Force Microscopy*, J Phycol **48** (2012) 174–185. ↑4.2.4

[Plo2010] L. Ploux, A. Ponche, and K. Anselme, *Bacteria/Material Interfaces: Role of the Material and Cell Wall Properties*, J Adhes Sci Technol **24** (2010) 2165–2201. ↑5.3

[Poo2002] A. T. Poortinga, R. Bos, W. Norde, and H. J. Busscher, *Electric Double Layer Interactions in Bacterial Adhesion to Surfaces*, Surf Sci Rep **47** (2002) 3–32. ↑3.3.2, 3.3.2

[Put2010] J. B. Puthoff, M. S. Prowse, M. Wilkinson, and K. Autumn, *Changes in Materials Properties Explain the Effects of Humidity on Gecko Adhesion*, J Exp Biol **213** (2010) 3699–3704. ↑3.4.1

[Qu2011] W. Qu, H. J. Busscher, J. M. M. Hooymans, and H. C. van der Mei, *Surface Thermodynamics and Adhesion Forces Governing Bacterial Transmission in Contact Lens Related Microbial Keratitis*, J Colloid Interface Sci **358** (2011) 430–436. ↑4.2.2

[Qui2008] A. Quinn, H. Mantz, K. Jacobs, M. Bellion, and L. Santen, *Protein Adsorption Kinetics in Different Surface Potentials*, EPL **81** (2008) 56003. ↑5.1.1

[Rab2010] M. Rabe, D. Verdes, and S. Seeger, *Understanding Cooperative Protein Adsorption Events at the Microscopic Scale: A Comparison between Experimental Data and Monte Carlo Simulations*, J Phys Chem B **114** (2010) 5862–5869. ↑3.2.1

[Rab2011] M. Rabe, D. Verdes, and S. Seeger, *Understanding Protein Adsorption Phenomena at Solid Surfaces*, Adv Colloid Interface Sci **162** (2011) 87–106. ↑3.2.1, 3.2.1

[Ram1994] J. J. Ramsden, *Experimental Methods for Investigating Protein Adsorption-Kinetics at Surfaces*, Q Rev Biophys **27** (1994) 41–105. ↑3.2.1

[Ran1994] I. W. Rangelow, *Sharp Silicon Tips for AFM and Field Emission*, Microelectron Eng **23** (1994) 369–372. ↑4.2.1

[Raz1998] A. Razatos, Y.-L. Ong, M. M. Sharma, and G. Georgiou, *Molecular Determinants of Bacterial Adhesion Monitored by Atomic Force Microscopy*, Proc Natl Acad Sci **95** (1998) 11059–11064. ↑4.2.2, 4.2.2

[Rei2011] N. T. Reichmann and A. Grundling, *Location, Synthesis and Function of Glycolipids and Polyglycerolphosphate Lipoteichoic Acid in Gram-Positive Bacteria of the Phylum Firmicutes*, FEMS Microbiol Lett **319** (2011) 97–105. ↑3.3.1

[Ric2005] F. Rico, P. Roca-Cusachs, N. Gavara, R. Farre, M. Rotger, and D. Navajas, *Probing Mechanical Properties of Living Cells by Atomic Force Microscopy with Blunted Pyramidal Cantilever Tips*, Phys Rev E **72** (2005) 021914. ↑4.2

[Rie1997] M. Rief, M. Gautel, F. Oesterhelt, J. M. Fernandez, and H. E. Gaub, *Reversible Unfolding of Individual Titin Immunoglobulin Domains by AFM*, Science **276** (1997) 1109–1112. ↑4.2.1

[Rij1995] H. H. M. Rijnaarts, W. Norde, E. J. Bouwer, J. Lyklema, and A. J. B. Zehnder, *Reversibility and Mechanism of Bacterial Adhesion*, Colloids Surf B **4** (1995) 5–22. ↑3.3.2

[Rim2008] A. Rimola, M. Corno, C. M. Zicovich-Wilson, and P. Ugliengo, *Ab Initio Modeling of Protein/Biomaterial Interactions: Glycine Adsorption at Hydroxyapatite Surfaces*, J Am Chem Soc **130** (2008) 16181–16183. ↑3.2.1

[Riz2005] N. W. Rizzo, K. H. Gardner, D. J. Walls, N. M. Keiper-Hrynko, T. S. Ganzke, and D. L. Hallahan, *Characterization of the Structure and Composition of Gecko Adhesive Setae*, J R Soc Interface **3** (2005) 441–451. ↑3.4.1

[Rob1979] R. B. Roberts, A. G. Krieger, N. L. Schiller, and K. C. Gross, *Viridans Streptococcal Endocarditis: The Role of Various Species, Including Pyridoxal-Dependent Streptococci*, Clin Infect Dis **1** (1979) 955–966. ↑3.3.4

[Ros1884] F. J. Rosenbach, *Mikro-organismen bei den Wund-Infections-Krankheiten des Menschen*, J. F. Bergmann, 1884. ↑3.3.3

[Ros2008] M. Rosentritt, S. Hahnel, G. Groeger, B. Muehlfriedel, R. Buergers, and G. Handel, *Adhesion of Streptococcus mutans to Various Dental Materials in a Laminar Flow Chamber System*, J Biomed Mater Res, Part B **86B** (2008) 36–44. ↑4.3

[Rot1996] C. M. Roth, B. L. Neal, and A. M. Lenhoff, *Van der Waals Interactions Involving Proteins*, Biophys J **70** (1996) 977–987. ↑3.1

[Rub1999] R. J. Rubin, C. A. Harrington, A. Poon, K. Dietrich, J. A. Greene, and A. Moiduddin, *The Economic Impact of Staphylococcus aureus Infection in New York City Hospitals*, Emerg Infect Dis **5** (1999) 9–17. ↑3.3.3

[Rui1965] R. Ruibal and V. Ernst, *The Structure of the Digital Setae of Lizards*, J Morphol **117** (1965) 271–293. ↑3.4.1

[Sch1972] K. H. Schleifer and O. Kandler, *Peptidoglycan Types of Bacterial Cell Walls and Their Taxonomic Implications*, Bacteriol Rev **36** (1972) 407–477. ↑3.3.1

[Sch1982] K. H. Schleifer and U. Fischer, *Description of a New Species of the Genus Staphylococcus: Staphylococcus carnosus*, Int J Syst Bacteriol **32** (1982) 153–156. ↑3.3.3

[Sch1996] P. M. Schneeberger, M. Janssen, and A. Voss, *α-Hemolytic Streptococci: a Major Pathogen of Iatrogenic Meningitis Following Lumbar Puncture. Case Reports and a Review of the Literature*, Infection **24** (1996) 29–33. ↑3.3.4

[Sch2009] K. Schroeder, M. Jularic, S. M. Horsburgh, N. Hirschhausen, C. Neumann, A. Bertling, A. Schulte, S. J. Foster, B. E. Kehrel, G. Peters, and C. Heilmann, *Molecular Characterization of a Novel Staphylococcus aureus Surface Protein (SasC) Involved in Cell Aggregation and Biofilm Accumulation*, PLoS ONE **4** (2009) e7567. ↑3.3.3

[Sch2010] Y. Schmitt, H. Hähl, C. Gilow, H. Mantz, K. Jacobs, O. Leidinger, M. Bellion, and L. Santen, *Structural Evolution of Protein-Biofilms: Simulations and Experiments*, Biomicrofluidics **4** (2010) 032201. ↑5.1.1

[Sch2011] M. P. Schultz, J. A. Bendick, E. R. Holm, and W. M. Hertel, *Economic Impact of Biofouling on a Naval Surface Ship*, Biofouling **27** (2011) 87–98. ↑1

[Sco2006] J. R. Scott and T. C. Barnett, *Surface Proteins of Gram-Positive Bacteria and How They Get There*, Annu Rev Microbiol **60** (2006) 397–423. ↑3.3.1

[Seo2008] Y. Seo and W. Jhe, *Atomic Force Microscopy and Spectroscopy*, Rep Prog Phys **71** (2008) 016101. ↑4.2.1

[Ser2005] F. M. Serry, *The Thermal Tune Solution to the Cantilever Spring Constant Problem*, Bruker Corporation Application Note AN90, 2005. ↑4.2.3

[Sha1989] N. Sharon and H. Lis, *Lectins as Cell Recognition Molecules*, Science **246** (1989) 227–234. ↑3.3.2

[She1994] R. Sherman, D. Hirt, and R. Vane, *Surface Cleaning with the Carbon Dioxide Snow Jet*, J Vac Sci Technol A **12** (1994) 1876. ↑4.1.1

[Sin2011] A. V. Singh, V. Vyas, R. Patil, V. Sharma, P. E. Scopelliti, G. Bongiorno, A. Podestà, C. Lenardi, W. N. Gade, and P. Milani, *Quantitative Characterization of the Influence of the Nanoscale Morphology of Nanostructured Surfaces on Bacterial Adhesion and Biofilm Formation*, PLoS ONE **6** (2011) e25029. ↑3.3.2

[Sjö1977] J. Sjödahl, *Repetitive Sequences in Protein A from Staphylococcus aureus. Arrangement of Five Regions within the Protein, Four being Highly Homologous and Fc-Binding*, Eur J Biochem **73** (1977) 343–351. ↑3.3.3

[Ste1924] O. Stern, *Zur Theorie der Elektrolytischen Doppelschicht*, Zeitschrift für Elektrochemie und angewandte physikalische Chemie **30** (1924) 508–516. ↑3.1.2

[Ste2009] M. J. Stevens, L. J. Donato, S. K. Lower, and N. Sahai, *Oxide-Dependent Adhesion of the Jurkat Line of T Lymphocytes*, Langmuir **25** (2009) 6270–6278. ↑3.3.2

[Str2009] J. Strauss, Y. Liu, and T. A. Camesano, *Bacterial Adhesion to Protein-Coated Surfaces: an AFM and QCM-D Study*, Jom-Us **61** (2009) 71–74. ↑3.3.2

[Su2012] H.-N. Su, Z.-H. Chen, S.-B. Liu, L.-P. Qiao, X.-L. Chen, H.-L. He, X. Zhao, B.-C. Zhou, and Y.-Z. Zhang, *Bacterial Capsules under Atomic Force Microscopy: Characterization of the Bacterial Polysaccharide Capsules and Detection of the Capsules in the Presence of Deliquescent Water*, Appl Environ Microbiol (2012). ↑4.2.4

[Sun2005] W. Sun, P. Neuzil, T. S. Kustandi, S. Oh, and V. D. Samper, *The Nature of the Gecko Lizard Adhesive Force*, Biophys J **89** (2005) L14–L17. ↑3.4.1

[Svo1994] K. Svoboda and S. M. Block, *Biological Applications of Optical Forces*, Annu Rev Bioph Biom **23** (1994) 247–285. ↑3.3.2

[Szl2008] I. Szlufarska, M. Chandross, and R. W. Carpick, *Recent Advances in Single-Asperity Nanotribology*, J Phys D: Appl Phys **41** (2008) 123001. ↑3.5

[Tab2011] R. F. Tabor, R. Manica, D. Y. C. Chan, F. Grieser, and R. R. Dagastine, *Repulsive van der Waals Forces in Soft Matter: Why Bubbles Do Not Stick to Walls*, Phys Rev Lett **106** (2011). ↑4.2.1

[Tan1992] C. Tancrede, *Role of Human Microflora in Health and Disease*, Eur J Clin Microbiol **11** (1992) 1012–1015. ↑3.3

[Tan2005] G. L. Tan, M. F. Lemon, D. J. Jones, and R. H. French, *Optical Properties and London Dispersion Interaction of Amorphous and Crystalline SiO_2 Determined by Vacuum Ultraviolet Spectroscopy and Spectroscopic Ellipsometry*, Phys Rev B **72** (2005) 205117. ↑3.1

[Tay1998] R. L. Taylor, J. Verran, G. C. Lees, and A. J. P. Ward, *The Influence of Substratum Topography on Bacterial Adhesion to Polymethyl Methacrylate*, J Mater Sci Mater Med **9** (1998) 17–22. ↑3.3.2

[Tel2006] J. L. Telford, M. A. Barocchi, I. Margarit, R. Rappuoli, and G. Grandi, *Pili in Gram-Positive Pathogens*, Nat Rev Microbiol **4** (2006) 509–519. ↑3.3.1

[Tet2001] H. Tettelin, K. E. Nelson, I. T. Paulsen, J. A. Eisen, T. D. Read, S. Peterson, J. Heidelberg, R. T. DeBoy, D. H. Haft, R. J. Dodson, A. S. Durkin, M. Gwinn, J. F. Kolonay, W. C. Nelson, J. D. Peterson, L. A. Umayam, O. White, S. L. Salzberg, M. R. Lewis, D. Radune, E. Holtzapple, H. Khouri, A. M. Wolf, T. R. Utterback, C. L. Hansen, L. A. McDonald, T. V. Feldblyum, S. Angiuoli, T. Dickinson, E. K. Hickey, I. E. Holt, B. J. Loftus, F. Yang, H. O. Smith, J. C. Venter, B. A. Dougherty, D. A. Morrison, S. K. Hollingshead, and C. M. Fraser, *Complete Genome Sequence of a Virulent Isolate of Streptococcus pneumoniae*, Science **293** (2001) 498–506. ↑3.3.4

[Tha2005] M. Thanbichler, S. C. Wang, and L. Shapiro, *The Bacterial Nucleoid: a Highly Organized and Dynamic Structure*, J Cell Biochem **96** (2005) 506–521. ↑3.3

[The2012] N. Thewes, *Kraftspektroskopie zur bakteriellen Adhäsion: Was unterscheidet pathogene von apathogenen Staphylokokken?*, Diplomarbeit, 2012. ↑1

[Tho2002] W. E. Thomas, E. Trintchina, M. Forero, V. Vogel, and E. V. Sokurenko, *Bacterial Adhesion to Target Cells Enhanced by Shear Force*, Cell **109** (2002) 913–923. ↑4.3

[Til2003] R. D. Tilton, *Mobility of Biomolecules at Interfaces*, Biopolymers at interfaces, 2003, pp. 221–258. ↑6.1

[Tou2003a] A. Touhami, B. Hoffmann, A. Vasella, F. A. Denis, and Y. F. Dufrene, *Probing Specific Lectin-Carbohydrate Interactions Using Atomic Force Microscopy Imaging and Force Measurements*, Langmuir **19** (2003) 1745–1751. ↑4.2.1

[Tou2003b] A. Touhami, B. Nysten, and Y. F. Dufrene, *Nanoscale Mapping of the Elasticity of Microbial Cells by Atomic Force Microscopy*, Langmuir **19** (2003) 4539–4543. ↑4.2

[Trt2012] P. Trtik, J. Kaufmann, and U. Volz, *On the Use of Peak-Force Tapping Atomic Force Microscopy for Quantification of the Local Elastic Modulus in Hardened Cement Paste*, Cem Concr Res **42** (2012) 215–221. ↑4.2.4

[Usa1993] S. Usami, Y. H. Zhao, H.-H. Chen, S. Chien, and R. Skalak, *Design and Construction of a Linear Shear-Stress Flow Chamber*, Ann Biomed Eng **21** (1993) 77–83. ↑4.3

[Vel2002] S. B. Velegol and B. E. Logan, *Contributions of Bacterial Surface Polymers, Electrostatics, and Cell Elasticity to the Shape of AFM Force Curves*, Langmuir **18** (2002) 5256–5262. ↑4.2.2

[Vel2008] E. Velzenberger, I. Pezron, G. Legeay, M.-D. Nagel, and K. el Kirat, *Probing Fibronectin-Surface Interactions: A Multitechnique Approach*, Langmuir **24** (2008) 11734–11742. ↑4.2.1

[Ver1948] E. J. W. Verwey and J. T. G. Overbeek, *Theory of the Stability of Lyophobic Colloids*, 1. Aufl., Elsevier Publishing Co, Amsterdam, 1948. ↑3.3.2

[Ver2009] C. Verbelen and Y. F. Dufrene, *Direct Measurement of Mycobacterium-Fibronectin Interactions*, Integr Biol **1** (2009) 296–300. ↑4.2.1

[Vij2005] K. Vijayanand, D. K. Pattanayak, T. R. Rama Mohan, and R. Banerjee, *Interpreting Blood-Biomaterial Interactions from Surface Free Energy and Work of Adhesion*, Trends Biomater Artif Organs **18** (2005) 1873–1881. ↑3.3.2

[Vin1998] A. Vinckier and G. Semenza, *Measuring Elasticity of Biological Materials by Atomic Force Microscopy*, FEBS Lett **430** (1998) 12–16. ↑4.2.1

[vanKoo1992] T. G. van Kooten, J. M. Schakenraad, H. C. van der Mei, and H. J. Busscher, *Development and Use of a Parallel-Plate Flow Chamber for Studying Cellular Adhesion to Solid-Surfaces*, J Biomed Mater Res, Part A **26** (1992) 725–738. ↑3.3.2, 4.3

[vanLoo1987] M. C. M. van Loosdrecht, J. Lyklema, W. Norde, G. Schraa, and A. J. B. Zehnder, *The Role of Bacterial Cell Wall Hydrophobicity in Adhesion*, Appl Environ Microbiol **53** (1987) 1893–1897. ↑3.3.2

[vanLoo1990] M. C. M. van Loosdrecht, W. Norde, and A. J. B. Zehnder, *Physical Chemical Description of Bacterial Adhesion*, J Biomater Appl **5** (1990) 91–106. ↑3.3.2

[VanOss1986] C. J. Van Oss, R. J. Good, and M. K. Chaudhury, *The Role of van der Waals Forces and Hydrogen Bonds in "Hydrophobic Interactions" between Biopolymers and Low Energy Surfaces*, J Colloid Interface Sci **111** (1986) 378–390. ↑3.1.6

[VanOss1989] C. J. Van Oss, *Energetics of Cell-Cell and Cell-Biopolymer Interactions*, Cell Biochem Biophys **14** (1989) 1–116. ↑3.3.2

[VanOss1990] C. J. Van Oss, R. F. Giese, and P. M. Costanzo, *DLVO and Non-DLVO Interactions in Hectorite*, Clay Clay Miner **38** (1990) 151–159. ↑3.3.2

[vanOss2006] C. J. van Oss, *Interfacial Forces in Aqueous Media*, 2. Aufl., Taylor & Francis, Boca Raton, 2006. ↑3.3.2

[Voe1995] D. Voet and J. Voet, *Biochemistry*, John Wiley & Sons, New York, 1995. ↑4.2.2

[Vol2008] W. Vollmer, D. Blanot, and M. A. de Pedro, *Peptidoglycan Structure and Architecture*, FEMS Microbiol Rev **32** (2008) 149–167. ↑3.3.1

[Vol2010] W. Vollmer and S. J. Seligman, *Architecture of Peptidoglycan: More Data and More Models*, Trends Microbiol **18** (2010) 59–66. ↑3.3.3

[vanWag1980] R. A. van Wagenen and J. D. Andrade, *Flat Plate Streaming Potential Investigations: Hydrodynamics and Electrokinetic Equivalency*, J Colloid Interface Sci **76** (1980) 305–314. ↑3.3.2, 4.3, 4.3, 4.3

[Wah1995] M. Wahlgren, T. Arnebrant, and I. Lundström, *The Adsorption of Lysozyme to Hydrophilic Silicon Oxide Surfaces: Comparison Between Experimental Data and Models for Adsorption Kinetics*, J Colloid Interface Sci **175** (1995) 506–514. ↑3.2.1

[Wah1997] M. Wahlgren and U. Elofsson, *Simple Models for Adsorption Kinetics and Their Correlation to the Adsorption of β-Lactoglobulin A and B*, J Colloid Interface Sci **188** (1997) 121–129. ↑3.2.1

[Was1989] S. R. Wasserman, G. M. Whitesides, I. M. Tidswell, B. M. Ocko, P. S. Pershan, and J. D. Axe, *The Structure of Self-Assembled Monolayers of Alkylsiloxanes on Silicon: A Comparison of Results from Ellipsometry and Low-Angle X-ray Reflectivity*, J Am Chem Soc **111** (1989) 5852–5861. ↑4.1.1

[Wei1993] A. L. Weisenhorn, M. Khorsandi, S. Kasas, V. Gotzos, and H. J. Butt, *Deformation and Height Anomaly of Soft Surfaces Studied with an AFM*, Nanotechnology **4** (1993) 106–113. ↑4.2.1

[Wer1999] C. F. Wertz and M. M. Santore, *Adsorption and Relaxation Kinetics of Albumin and Fibrinogen on Hydrophobic Surfaces: Single-Species and Competitive Behavior*, Langmuir **15** (1999) 8884–8894. ↑6.1

[Wer2002] C. F. Wertz and M. M. Santore, *Adsorption and Reorientation Kinetics of Lysozyme on Hydrophobic Surfaces*, Langmuir **18** (2002) 1190–1199. ↑3.2.1

[Wes1997] J. K. West, R. A. Latour, and L. L. Hench, *Molecular Modeling Study of Adsorption of Poly-L-lysine onto Silica Glass*, J Biomed Mater Res, Part A **37** (1997) 585–591. ↑4.2.2

[Wha2000] A. M. Whatmore, A. Efstratiou, A. P. Pickerill, K. Broughton, G. Woodard, D. Sturgeon, R. George, and C. G. Dowson, *Genetic Relationships Between Clinical Isolates of Streptococcus pneumoniae, Streptococcus oralis, and Streptococcus mitis: Characterization of "Atypical" Pneumococci and Organisms Allied to S. mitis Harboring S. pneumoniae Virulence Factor-encoding Genes*, Infect Immun **68** (2000) 1374–1382. ↑3.3.4

[Whi1998] W. B. Whitman, D. C. Coleman, and W. J. Wiebe, *Prokaryotes: the Unseen Majority*, Proc Natl Acad Sci **95** (1998) 6578–6583. ↑3.3

[Whi2006] K. A. Whitehead, D. Rogers, J. Colligon, C. J. Wright, and J. Verran, *Use of the Atomic Force Microscope to Determine the Effect of Substratum Surface Topography on the Ease of Bacterial Removal*, Colloids Surf B **51** (2006) 44–53. ↑3.3.2

[Wil1979] B. J. Wilkinson, P. K. Peterson, and P. G. Quie, *Cryptic Peptidoglycan and the Antiphagocytic Effect of the Staphylococcus aureus Capsule: Model for the Antiphagocytic Effect of Bacterial Cell Surface Polymers*, Infect Immun **23** (1979) 502–508. ↑3.3.3

[Woe1990] C. R. Woese, O. Kandler, and M. L. Wheelis, *Towards a Natural System of Organisms: Proposal for the Domains Archaea, Bacteria, and Eucarya*, Proc Natl Acad Sci **87** (1990) 4576–4579. ↑3.3

[Woe1998] C. R. Woese, *Default Taxonomy: Ernst Mayr's View of the Microbial World*, Proc Natl Acad Sci **95** (1998) 11043–11046. ↑10

[Wol1991] O. Wolter, T. Bayer, and J. Greschner, *Micromachined Silicon Sensors for Scanning Force Microscopy*, J Vac Sci Technol B **9** (1991) 1353. ↑4.2.1

[Wol2008] S. Wolff, H. Hahne, M. Hecker, and D. Becher, *Complementary Analysis of the Vegetative Membrane Proteome of the Human Pathogen Staphylococcus aureus*, Molecular & Cellular Proteomics **7** (2008) 1460–1468. ↑3.3.3

[Wri2010] C. J. Wright, M. K. Shah, L. C. Powell, and I. Armstrong, *Application of AFM from Microbial Cell to Biofilm*, Scanning **32** (2010) 134–149. ↑3.3.2, 4.2

[Yan2011] J. Yang, J. B. Puthoff, and K. Autumn, *HIM Imaging of Uncoated Adhesive Foot Structures of Gecko and Spider*, Carl Zeiss NTS GmbH, 2011. ↑3.8

[Yon2006] R. Yongsunthon and S. K. Lower, *Force Spectroscopy of Bonds That Form Between a Staphylococcus Bacterium and Silica or Polystyrene Substrates*, J Electron Spectrosc **150** (2006) 228–234. ↑3.3.2, 4.2.1

[Yon2007] R. Yongsunthon, V. G. Fowler Jr, B. H. Lower, F. P. Vellano, E. Alexander, L. B. Reller, G. R. Corey, and S. K. Lower, *Correlation Between Fundamental Binding Forces and Clinical Prognosis of Staphylococcus aureus Infections of Medical Implants*, Langmuir **23** (2007) 2289–2292. ↑4.2.1

[Zha2008] H. Zhang and K.-K. Liu, *Optical Tweezers for Single Cells*, J R Soc Interface **5** (2008) 671–690. ↑3.3.2

[Zha2011] W. Zhang, A. G. Stack, and Y. Chen, *Interaction Force Measurement Between E. coli Cells and Nanoparticles Immobilized Surfaces by Using AFM*, Colloids Surf B **82** (2011) 316–324. ↑4.2.2

[Zho2004] J. Zhou, H.-K. Tsao, Y.-J. Sheng, and S. Jiang, *Monte Carlo Simulations of Antibody Adsorption and Orientation on Charged Surfaces*, J Chem Phys **121** (2004) 1050. ↑3.2.1

[Zhu2003] X. Y. Zhu, J. Lubeck, and J. J. Kilbane II, *Characterization of Microbial Communities in Gas Industry Pipelines*, Appl Environ Microbiol **69** (2003) 5354–5363. ↑1

Publications

Addendum I - Is adhesion superficial?! Silicon wafers as a model system to study van der Waals interactions

Authors: P. Loskill, H. Hähl, T. Faidt, S. Grandthyll, F. Müller, and K. Jacobs

Department of Experimental Physics, Saarland University, 66041 Saarbrücken, Germany.

Advances in Colloid and Interface Sciences **179–182**, 107–113 (2012).
(http://dx.doi.org/10.1016/j.cis.2012.06.006)

Author contributions:
Experiments were performed by P. Loskill, H. Hähl, T. Faidt, S. Grandthyll, and F. Müller. The article was written by P. Loskill, F. Müller, and K. Jacobs. Research was directed by K. Jacobs.

Abstract - Adhesion is a key issue for researchers of various fields, it is therefore of uppermost importance to understand the parameters that are involved. Commonly, only surface parameters are employed to determine the adhesive forces between materials. Yet, van der Waals forces act not only between atoms in the vicinity of the surface, but also between atoms in the bulk material. In this review, we describe the principles of van der Waals interactions and outline experimental and theoretical studies investigating the influence of the subsurface material on adhesion. In addition, we present a collection of data indicating that silicon wafers with native oxide layers are a good model substrate to study van der Waals interactions with coated materials.

ARTICLE IN PRESS
CIS-01235; No of Pages 7
Advances in Colloid and Interface Science xxx (2012) xxx–xxx
Contents lists available at SciVerse ScienceDirect
Advances in Colloid and Interface Science
journal homepage: www.elsevier.com/locate/cis

Is adhesion superficial? Silicon wafers as a model system to study van der Waals interactions

Peter Loskill, Hendrik Hähl, Thomas Faidt, Samuel Grandthyll, Frank Müller, Karin Jacobs *

Department of Experimental Physics, Saarland University, 66041 Saarbrücken, Germany

ARTICLE INFO

Available online xxxx

Keywords:
Adhesion
Multilayer
van der Waals-interactions
Silicon oxide layer

ABSTRACT

Adhesion is a key issue for researchers of various fields, it is therefore of uppermost importance to understand the parameters that are involved. Commonly, only surface parameters are employed to determine the adhesive forces between materials. Yet, van der Waals forces act not only between atoms in the vicinity of the surface, but also between atoms in the bulk material. In this review, we describe the principles of van der Waals interactions and outline experimental and theoretical studies investigating the influence of the subsurface material on adhesion. In addition, we present a collection of data indicating that silicon wafers with native oxide layers are a good model substrate to study van der Waals interactions with coated materials.

Contents

1. Introduction

Stimulating or preventing adhesion is a key issue for researchers of various fields. To solve these problems, a comprehensive understanding of the prevailing adhesion mechanism is indispensable. Yet, not only various adhesion mechanisms, but also plenty of parameters that can affect adhesion exist: nanoscale or microscale roughness [1,2], static charges or the zeta-potential at the interface [3,4], surface energies [5,6], and contact shapes [7] are a few frequently-studied examples. All these parameters, however, have in common that they are describing the surface of a material. Hence, the question arises whether adhesion is really only 'superficial'. This question is of great importance since commonly used photoresists, coatings, adhesion promoters or other functionalized surface layers are often in the range of just a few nanometers. These dimensions are smaller than the range of interactions such as van der Waals (vdW) interactions. Hence, the material right underneath the surface might indeed have an effect on adhesion mediated by vdW interactions. In this paper, we review experimental and theoretical studies investigating the influence of subsurface material on vdW forces. Additionally, we provide a collection of experimental data highlighting the suitability of stratified substrates based on silicon wafers to study vdW interactions.

2. Van der Waals interactions

Already more than hundred years ago van der Waals introduced his theory of an attraction between neutral atoms in order to explain non-ideal gases [8]. Later, three types of interactions were identified to contribute to the vdW interactions:

- *Keesom interactions* characterize dipol–dipol interactions of molecules that carry permanent dipoles [9].

* Corresponding author. Fax: +49 681 302 70499.
E-mail address: k.jacobs@physik.uni-saarland.de (K. Jacobs).

0001-8686/$ – see front matter © 2012 Elsevier B.V. All rights reserved.
doi:10.1016/j.cis.2012.06.006

Please cite this article as: Loskill P, et al, Is adhesion superficial? Silicon wafers as a model system to study van der Waals interactions, Adv Colloid Interface Sci (2012), doi:10.1016/j.cis.2012.06.006

- *Debye interactions* describe forces between a permanent dipole that induces a dipole moment in an otherwise unpolar molecule [9].
- *London interactions*, also called dispersion interactions, describe forces between instantaneously induced dipoles [10].

All three types have in common that the interaction energy scales with $-1/d^6$. Hence, the vdW potentials ϕ for the interactions between two single atoms separated by a distance d can be written as

$$\phi(d) = -C/d^6. \tag{1}$$

Due to this scaling, vdW interactions are often considered as short-range.

Hamaker, however, calculated energy–distance relations for macroscopic objects by pairwise summation over all atoms, continuing the work of Bradley and DeBoer [11–13]. Depending on the geometry, different scaling laws apply (cf. Fig. 1). To account for the properties of the involved materials, Hamaker introduced a coefficient A, also called 'Hamaker constant', which he defined to

$$A = \pi^2 C \rho_1 \rho_2 \tag{2}$$

where ρ_i are the number of atoms per unit volume of the two materials. The controversial subject of Hamaker's theory was that he assumes a pairwise additivity of the vdW interactions, which is generally speaking not valid. A few years later, Casimir used a completely different ansatz to calculate the force between two ideally conducting semi-infinite half-spaces in vacuum [14]. On the basis of Planck's famous theory, he summed up the allowed electromagnetic modes between two conducting plates. Lifshitz extended Casimir's idea and presented a theory for arbitrary materials, based on quantum field theory [15]. In principle, although many studies differentiate between Lifshitz-vdW and Casimir interactions, Lifshitz and Casimir essentially described the same effect, but with different foci [16,17]. By treating the interacting objects as continuous media, Casimir's and Lifshitz' theories circumvent the question of pairwise additivity. Interestingly, Lifshitz' ansatz led to the same scaling laws as the classical Hamaker ansatz (cf. Fig. 1). Only the way the Hamaker constants are derived is different. Following Lifshitz' theory, they are calculated from the optical properties of the involved materials. Thereto, the full optical spectra over an infinite range of frequencies are necessary. Nowadays, suitable datasets are available for many different materials, obtained both experimentally and from ab initio theory [18–23]. Still, in some systems – especially in biological systems – the full spectra of all involved materials are hardly accessible. In these cases, the Hamaker constants can be approximated (see Appendix A) by

$$A_{12-32} \approx \frac{3}{4} k_B T \left(\frac{\varepsilon_1-\varepsilon_2}{\varepsilon_1+\varepsilon_2}\right)\left(\frac{\varepsilon_3-\varepsilon_2}{\varepsilon_3+\varepsilon_2}\right) + \frac{3\hbar\omega_e}{8\sqrt{2}} \frac{\left(n_1^2-n_2^2\right)\left(n_3^2-n_2^2\right)}{\sqrt{\left(n_1^2+n_2^2\right)}\sqrt{\left(n_3^2+n_2^2\right)}\cdot\left[\sqrt{\left(n_1^2+n_2^2\right)}+\sqrt{\left(n_3^2+n_2^2\right)}\right]} \tag{3}$$

with the dielectric constants ε_i, the refractive indices in the visible regime n_i, and the main electronic absorption frequency ω_e.

The works of Hamaker, Casimir and Lifshitz demonstrate that vdW–Casimir interactions can indeed be regarded as long-range, since for mesoscopic and macroscopic objects, the absolute value of the exponent of the scaling law is decreased (the interaction between two semi-infinite half slabs scales with $-1/d^2$, for instance). Yet, the long-range character is restricted due to the finite speed of light [24]. This retardation effect increases the absolute value of the exponent of the scaling law by up to one (for $d \gg 20$ nm). For separations smaller than 10 nm, however, the retardation can usually be neglected [25,26].

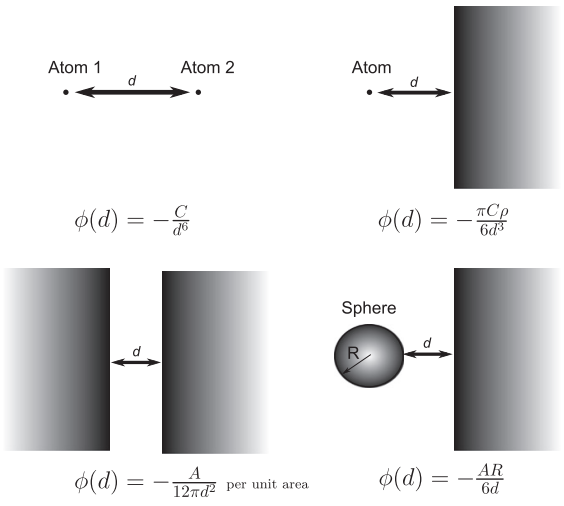

Fig. 1. VdW potentials $\phi(d)$ for different geometries. Adapted from [9].

3. Van der Waals interactions with coated substrates

Using the equations given by the theories mentioned above, it is usually possible to predict the potentials for the interactions of two uniform objects. Yet, many systems consist of coated substrates. However, vdW interactions act not only between atoms in the vicinity of the surface, but also between atoms in the bulk material. Early experiments of Israelachvili and Tabor showed that in the case of mica substrates covered with a monomolecular layer of stearic acids, both the acids and the mica contribute to the vdW interactions [27]. These experimental studies were in agreement with theoretical predictions of Langbein, who postulated that the interactions with the surface layer dominate for separations d smaller than the layer thickness D ($D \gg d$) and the interactions with the bulk material dominate in the opposing limit ($D \ll d$) [28,29]. More recent studies showed that variations in the thickness of a surface layer induce differences in the vdW potentials and influence e.g. the stability of thin liquid coatings [30–33]. These thin film dewetting studies moreover demonstrated quantitatively the impact of the subsurface composition to the effective interface potential [34]: the impact was measured experimentally by determining the differences in the preferred wavelength of spinodally dewetting thin films with variable subsurface composition [30,35].

3.1. Interactions in biological systems

VdW interactions also play a major role in biological systems [36]. Particularly non specific adhesion is governed by vdW interactions in conjunction with electric double layer interactions, usually described using the DLVO-theory [3,37] or extended DLVO-theory [38]. Many biological processes, such as the aggregation of proteins [39], the unspecific adhesion of cells and bacteria [40–42], the adherence of abalones [43], and the sticking of geckos [44–46] are influenced and sometimes dominated by vdW interactions. Moreover, in the case of biological objects – just as for rough objects, in general – adhesion does not occur at 'zero separation'. As a logical consequence, these processes are also not 'purely superficial', viz. not solely dependent on the properties of the surface. It could be shown that, when interacting with a coated substrate, proteins indeed sense both, the surface

Please cite this article as: Loskill P, et al, Is adhesion superficial? Silicon wafers as a model system to study van der Waals interactions, Adv Colloid Interface Sci (2012), doi:10.1016/j.cis.2012.06.006

layer and the underlying material: Adsorption experiments on tailored silicon wafers with differences in the thickness of the oxide layer on top of the wafers revealed qualitatively different adsorption kinetics of multiple types of proteins [47,48]. Based on Monte-Carlo simulations featuring surface processes such as surface mobility and conformational changes, the distinctions were invoked by the influence of the vdW-interactions on the time scale of these processes [49]. X-ray reflectivity experiments corroborated these findings [50]. Recent studies discovered that the influence of the subsurface material on adhesion is sensed by larger biological objects, too: the unspecific adhesion of bacteria from the *Staphylococcus* genus is affected by the properties of the subsurface material, as could be shown by AFM force spectroscopy measurements [51]. Moreover, adhesion experiments with setal arrays of live geckos revealed that the adhesion force was significantly varied by a change in the substrates subsurface composition [52].

3.2. Theoretical description of multilayer systems

For a comprehensive theoretical description of the vdW potentials for systems involving multilayer structures, not only the surface layer, but also the composition of the entire substrate has to be taken into account.

Substantial theoretical work has been done in recent years concerning the description of van der Waals interactions in multilayer systems [53–56] and graded interfaces [57,58]. Still, often experimentalists of various fields do not take into consideration that the interactions with coated materials may be affected by the subsurface and characterize substrates only by their surface properties. Moreover, by using strict cutoff radii for vdW interactions, most MD simulations also do not account for interactions with stratified substrates.

In general, the drawback of tailored systems is that the applying scaling laws are not as simple as the ones in Fig. 1, since the Hamaker constants depend on the separation. The vdW potential for the interaction of two layered semi-infinite half slabs, for instance, must be modified to

$$\phi(d) = -\frac{A(d)}{12\pi d^2} \tag{4}$$

per unit area. For the case of non-retarded interactions between infinite planar coated substrates, however, straightforward approximations are available that (qualitatively) describe many systems quite well. For instance, combining rules (geometric mean) may be used to calculate 'effective' Hamaker constants for a multilayer system. These relations, that are derived from the combining rules for surface energies, are a common way to find out unknown Hamaker constants [59]. Yet, these relations break down whenever the Keesom and Debye parts (the zero frequency terms) cannot be neglected [9]. Especially in multilayer systems, where multiple Hamaker constants are necessary, combining rules are not applicable.

On the basis of the Lifshitz theory, Ninham and Parsegian approximated the potentials for the interactions of symmetrical triple layer films (cf. Fig. 2A) by [60–62]

$$\phi_{\mathrm{vdW}}(d) = -\frac{1}{12\pi}\cdot\left(\frac{A_{23-23}}{d^2} + 2\frac{A_{23-12}}{(d+D)^2} + \frac{A_{12-12}}{(d+2D)^2}\right) \tag{5}$$

with A_{ij-kl} the constants for the interactions of the two different interfaces. Using the same ansatz, the vdW potential of the interactions between a probe material and a substrate coated with a layer of thickness D (cf. Fig. 2B) is given by [61,17]

$$\phi_{\mathrm{vdW}}(d) = -\frac{1}{12\pi}\cdot\left(\frac{A_{12-32}}{d^2} + \frac{A_{12-43}}{(d+D)^2}\right). \tag{6}$$

For larger separations $D \ll d$, however, Eq. (6) is no longer valid.

For the description of an experimental system with a variable D (e.g. the thickness of a coating), we have previously chosen an alternative approximation [30,32]: By assuming a scaling of the interaction with $\frac{C_a}{d^2} + \frac{C_b}{(d+D^2)}$ and a continuous transition between the boundary cases $D \ll d$ and $D \gg d$, we gained

$$\phi(d) = -\frac{1}{12\pi}\cdot\left(\frac{A_{12-32}}{d^2} + \frac{A_{12-42}-A_{12-32}}{(d+D)^2}\right), \tag{7}$$

where A_{12-42} stands for the interaction of material 1 via medium 2 with material 4 in the case that $D = 0$, viz. medium 3 is nonexistent.

4. Silicon wafers as a model system

Most of the studies mentioned above used silicon wafers as a model system to study vdW interactions with coated materials. This model system has the advantage of the feasibility to manufacture silicon wafers with defined oxide layer thicknesses that feature all the same surface properties. Hence, silicon wafers provide the possibility to tune the composition of the subsurface – viz. the vdW interactions arising from the subsurface – independent of all other interactions. As described earlier, vdW interactions are essentially dependent on the optical properties of the involved materials (Eq. (3)). In the case of pure SiO_2, these properties are well-known for various atomic structures [21]. The properties of thin silicon oxide films, however, have been discussed controversially for decades, e.g. in terms of the oxidation state of the silicon atoms. In the following, the term "silicon oxide" stands for SiO_x. The use of SiO_2 bulk values for oxide films

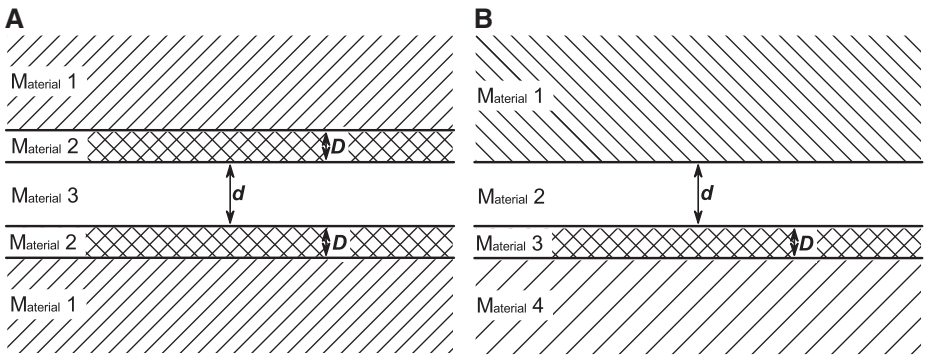

Fig. 2. Schemes of two multilayer configurations: A) symmetrical triple layers and B) interaction between a uniform material and a coated material.

Please cite this article as: Loskill P, et al, Is adhesion superficial? Silicon wafers as a model system to study van der Waals interactions, Adv Colloid Interface Sci (2012), doi:10.1016/j.cis.2012.06.006

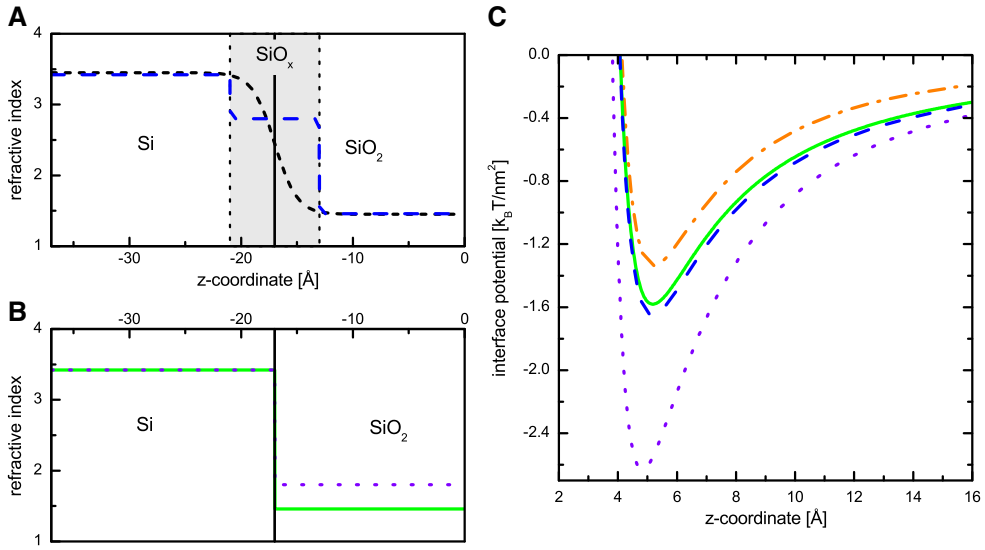

Fig. 3. Properties of thin oxide layers: A) Theoretically expected transition of the refractive index (short dashes) and a proposed double layer oxide model (long dashes). B) Single layer oxide models whereby the oxide layer has i) SiO_2 bulk-like properties (solid line) or ii) properties expected by optical studies with limited resolution (dotted line). C) Calculated potentials of the van der Waals interactions between a semi-infinite half-space of polystyrene ($n_{vis}=1.585, \epsilon_0=2.6$) and a silicon wafer with a thin oxide layer for the three model configurations (cf. A and B) and a bulk silicon dioxide substrate ($n_{vis}=1.46$, $\epsilon_0=3.9$ [63]) as a comparison (dash-dotted line). To include the short-range repulsive interaction a second term C/d^8 (maintaining the difference in exponents of the Lennard–Jones potential) was added. The parameter C was kept constant for all configurations, since the surface is essentially the same.

thicker than 100 nm is generally accepted. Yet, the validity of these values for thin film has been questioned numerous times and especially the optical properties, such as the refractive index, are disputed. In general, thin silicon oxide layers may be described by two different models:

- *Single layer model*: by assuming a sharp transition between the bulk Si and the oxide, the latter can be described by a single layer (cf. Fig. 3A). In this case, the oxide layer may have the same refractive index as bulk SiO_2 or an increased refractive index.
- *Double layer model*: since a sharp transition between the materials is highly unphysical, a continuous transition or an interface roughness is very likely. As the thickness of this transition region is of the same order of magnitude as the oxide layer thickness, a double layer configuration is an obvious approximation (cf. Fig. 3B).

The van der Waals interactions sensed by a probe object should differ strongly for these different model configurations (cf. Fig. 3C).

By applying the single layer model,[1] Jellison observed an increase in the refractive index of the whole oxide layer [64]. Using spectroscopic polarization modulation ellipsometry, the refractive index of very thin layers was determined to be $1.5-1.8$ (at $\lambda=800$ nm). These findings were later on confirmed by other studies [65,66].

Experimental support for the double layer model, viz. the observation of an interfacial transition layer, is also given by previous studies. Experimental studies noticed a thin ($\approx 6-7$ Å) region of atomically mixed Si and O with a refractive index of $n\approx 2.8-3.2$ (at 546.1 nm) [67,68]. High-resolution core-level and XPS spectroscopy [69,70] also confirmed that "the interface is not abrupt, as evidenced by the high density of intermediate-oxidation states (about two monolayers of Si) and by their nonideal distribution" [71]. These findings were matched by predictions of theoretical models [72,73].

[1] Jellison indeed assumed a transition layer. Yet, at some point (for thin films) he started to neglect this layer, whereby the increase in refractive index began exactly around this point.

The results of these studies, however, are not contradictory, but arise from the different methods applied. A problem of optical reflectivity methods, such as ellipsometry, is that they are not able to determine the density and the thickness of thin films (≤ 5 nm) independently (not to mention to distinguish between two of such films). Thus, the usage of the single layer model for these methods is the only possible way. Yet, for thinner silicon oxide films, the transition layer fraction of the total oxide layer is increased resulting in an observation of a higher overall refractive index.

Another limitation of all of the mentioned studies is, that they are performed on silicon wafers with thermally grown silicon oxide layers. Especially for thin (≤ 10 nm) films, the process parameters of the artificial growing process can have a significant influence on the density and the optical properties of the silicon oxide (decreased vs. increased refractive index) [74,75]. Yet, already without any pretreatment, silicon wafers are covered with a native oxide layer of 1.5 nm to 2 nm thickness. Since only limited data is available for the optical properties of native oxide layers, we present a brief summary of the properties of these layers containing previously unpublished data.

4.1. Properties of thin native oxide layers

The increase in refractive index to values up to $n=1.8$, as predicted by several studies [64–66], is highly unlikely for native oxide layers as polymer dewetting studies have shown via an indirect way

Table 1
Surface properties of a native oxide layer and of a thermally grown thick oxide layer as a comparison: thickness (d), root mean square (rms) roughness (by 1 μm^2 AFM scan), advancing (adv) and receding (rec) water contact angle, and surface energy γ (obtained from contact angle measurements of three different liquids [77]).

Oxide layer	d [nm]	rms [nm]	Θ_{adv} [°]	Θ_{rec} [°]	γ [mJ/m^2]
Native	1.7 (3)	0.13 (3)	5 (2)	Compl. wetting	63 (1)
Thick	150 (1)	0.09 (2)	7 (2)	Compl. wetting	64 (1)

Please cite this article as: Loskill P, et al, Is adhesion superficial? Silicon wafers as a model system to study van der Waals interactions, Adv Colloid Interface Sci (2012), doi:10.1016/j.cis.2012.06.006

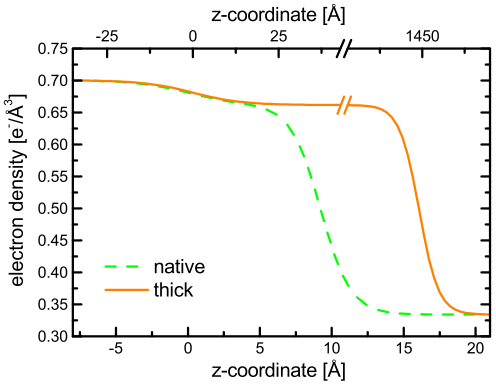

Fig. 4. Electron density profiles of a native (dashed line) and a thick oxide layer (solid line) determined by high energy X-ray reflectivity. The z-coordinate has been set to zero at the center of the transition between Si and its oxide. Data from [50].

[30]: thin liquid polystyrene (PS) films prepared on Si wafers with native oxide layers (D_{SiO} = 2.4 nm) were unstable and dewetted spinodally. Since this process is driven by the minimization of the free energy determined by the vdW potential [76,9] the refractive index of the oxide cannot be higher than the one of PS (≈1.59), as shown by Eq. (3).

A more direct ansatz is to compare native oxide layers to thick oxide layers in terms of the material properties, such as surface roughness, surface chemistry, homogeneity, electron density and stoichiometry: the surface characterization via atomic force microscopy (AFM) and contact angle (CA) measurements shows that – within the experimental error – the roughness and chemical homogeneity of the surface of a native oxide layer on Si wafers does not differ from the properties of a thick SiO_2 layer (cf. Table 1). The analysis of high energy X-ray reflectivity measurements on native and thick oxide layers leads to electron densities that are again similar (Fig. 4). Especially the topmost part (0–5 Å) of the native oxide layer resembles the density of the thicker layer.

The stoichiometry of the native oxide layer was studied by X-ray photoelectron spectroscopy (XPS) combined with Ar ion etching in order to reveal the depth profiles for different oxidation states/valencies Si^{k+} (k = 0,…,4). Fig. 5A shows the Si-2p spectra recorded in normal emission mode (take-off angle 0° along the surface normal) with two components representing Si^0 and Si^{4+} at lower and higher binding energy, respectively. Contributions from Si^{1+}, Si^{2+} and Si^{3+} could not be resolved, but have to be treated as a third peak in the background between the Si^0 and Si^{4+} signals. For stepwise ablation of the surface, the intensity of the Si^{4+} peak decreases asymmetrically, i.e., it is shifted towards the Si^0 signal, forming a shoulder in the intermediate state before vanishing (for calibration of ablation see, e.g., Ref. [78]). For ablation of about 1.5 nm, contributions from oxide species can no longer be observed, which is in accordance with the thickness of the native oxide measured by other methods (Fig. 4 and Table 1). The asymmetry in the Si oxide related part of the spectra is characteristic for intensity contributions from Si^{4+} and (Si^{1+}, Si^{2+}, Si^{3+}) when distributed in a double layer model as depicted in Fig. 5B. For this type of stacking, the simulation of intensity distributions within the Si-2p spectra in Fig. 5C shows the same characteristics, namely the asymmetric decrease of the intensity from the oxide species as the experimental data in

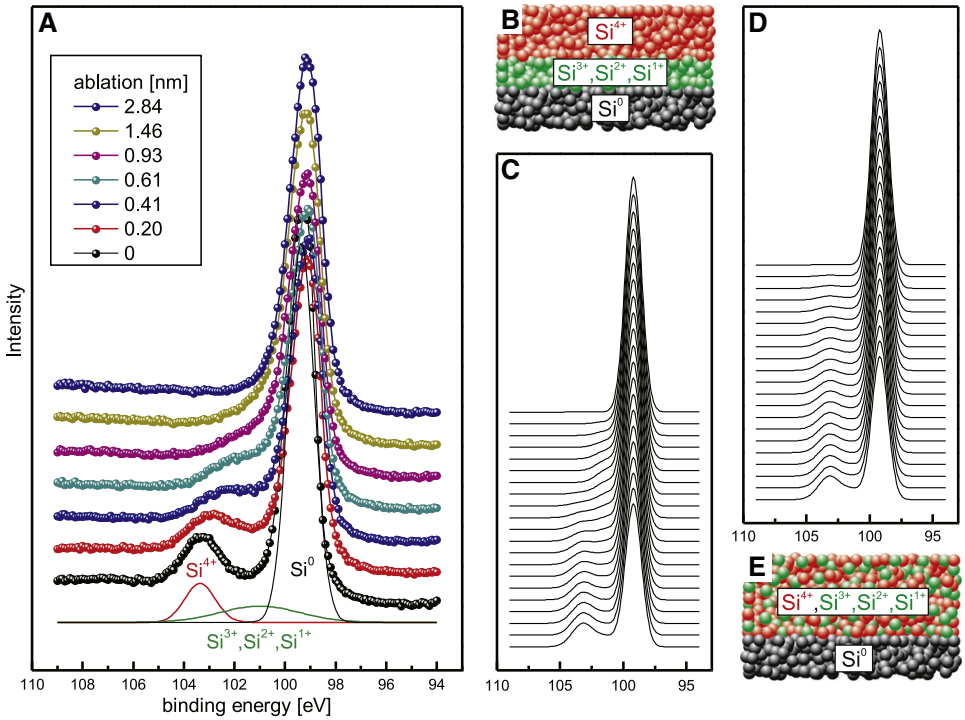

Fig. 5. A) XPS core level spectra for Si-2p (Al–Kα radiation, $\hbar\omega$ = 1486.6 eV, normal emission) for different stages of surface ablation by Ar ion etching with asymmetric decrease of intensity contributions from oxide species. B) Double layer oxide model with Si^0–(Si^{1+}, Si^{2+}, Si^{3+})–Si^{4+} stacking (from bulk to surface). C) Simulation of spectra for the double layer model from B) with the same asymmetric decrease of oxide intensities as observed in the experiment. D) Simulation of spectra for the single layer model depicted in E) with uniform decrease of oxide intensities. E) Single layer model with a homogeneous (Si^{1+}, Si^{2+}, Si^{3+}, Si^{4+}) surface layer.

Please cite this article as: Loskill P, et al, Is adhesion superficial? Silicon wafers as a model system to study van der Waals interactions, Adv Colloid Interface Sci (2012), doi:10.1016/j.cis.2012.06.006

Fig. 5A. A similar asymmetry was reported in previous studies on thermally grown oxide layers [70]. For comparison, Fig. 5E shows a second model with a homogeneous distribution of the oxidation states within the oxide layer. For this scenario, the simulation in Fig. 5D predicts a uniform disappearance of the oxide contributions, in contrast to the experimental observations in Fig. 5A.

In summary, these results show that native silicon oxide layers can be approximated by a double layer system as depicted in Figs. 3A and 5B, where adjacent to the bulk Si a transition layer and then a bulk-like SiO_2 layer follows. Since all characterized material properties of the SiO_2 part are similar to the properties of thick oxide layers, there are no hints to assume different optical properties. The transition layer, however, will most likely display increased polarizability [67,68,73]. That means, differences in the vdW potentials of wafers featuring native and thick oxide layers arouse indeed from subsurface contributions, since the uppermost material is the same, namely SiO_2. Hence, silicon wafers with native oxide layers are indeed good model substrates to study van der Waals interactions with coated materials.

Acknowledgement

This work was supported by the graduate college GRK 1276 of the Deutsche Forschungsgemeinschaft DFG, the DAAD PROMOS, Saarland University and Saarland Ministry of Economy. K.J. thanks John Ralston for his encouragement to pursue an academic career and for intense discussions of soft matter problems, e.g. the physics of skiing.

Appendix A. Calculation of Hamaker constants

Based on the Lifshitz theory, the Hamaker constant can be calculated by[2]

$$A_{12-32} = \frac{3}{2} kT \sum_{n=0}^{\infty}{}' \Delta_{1,2}(i\xi_n)\Delta_{3,2}(i\xi_n) \tag{A.1}$$

with

$$\Delta_{a,b}(i\xi) = \frac{\varepsilon_a(i\xi) - \varepsilon_b(i\xi)}{\varepsilon_a(i\xi) + \varepsilon_b(i\xi)} \tag{A.2}$$

whereby $\varepsilon_a(i\xi)$ are the values of the dielectric function of material a at the imaginary (Matsubara) frequencies

$$\xi_n = n \cdot 2\pi k_B T/h. \tag{A.3}$$

Using the Ninham–Parsegian approximation it is possible to obtain the $\varepsilon(i\xi)$ from the adsorption spectrum [79,60], more precisely the relative strengths and the frequencies of the peaks, by

$$\varepsilon(i\xi) = 1 + \sum_{j=0}^{N} \frac{C_j}{1 + \left(\xi/\omega_j\right)^2} \tag{A.4}$$

with

$$C_j = \frac{2f_j}{\pi\omega_j} \tag{A.5}$$

where f_j is the strength of an oscillator, ω_j its relaxation frequency, and N is the total number of oscillators. For dielectric materials Eq. (A.4) reduces to [80,81]

$$\varepsilon(i\xi) \approx 1 + \frac{\varepsilon(0) - \varepsilon(\omega_{vis})}{1 + (\xi/\omega_{rot})^2} + \frac{\varepsilon(\omega_{vis}) - 1}{1 + (\xi/\omega_e)^2} \tag{A.6}$$

[2] The prime denotes that the zero term has to be multiplied with $\frac{1}{2}$.

with ω_{rot} the molecular rotational relaxation frequency (typically in the IR regime), ω_e the main electronic absorption frequency (typically $\approx 3 \cdot 10^{15}\ s^{-1}$, in the UV regime), and $\varepsilon(\omega_{vis}) = n_{vis}^2$ the refractive index in the visible regime. As usually $\xi_1 \gg \omega_{rot}$ (cf. Eq. (A.3)) the first term in Eq. (A.6) can be neglected and Eq. (A.1) may be approximated by Eq. (3) if the adsorption frequencies of the three materials are similar [9].

References

[1] Fuller KNG, Tabor D. The effect of surface roughness on adhesion of elastic solids. Proc R Soc Lond A 1975;345:327–42.
[2] Persson BNJ, Tosatti E. The effect of surface roughness on the adhesion of elastic solids. J Chem Phys 2001;115:5597–610.
[3] Derjaguin BV, Landau L. Theory of the stability of strongly charged lyophobic sols and of the adhesion of strongly charged particles in solutions of electrolytes. Acta Physicochim URS 1941;14:633–62.
[4] Yoon BJ, Lenhoff AM. Computation of the electrostatic interaction energy between a protein and a charged surface. J Phys Chem-Us 1992;96:3130–4.
[5] Johnson KL, Kendall K, Roberts AD. Surface energy and the contact of elastic solids. Proc R Soc A 1971;324:301–13.
[6] Good RJ. Contact angle, wetting, and adhesion: a critical review. J Adhes Sci Technol 1992;6:1269–302.
[7] Spolenak R, Gorb SN, Gao H, Arzt E. Effects of contact shape on the scaling of biological attachments. Proc R Soc A 2005;461:305–19.
[8] Van der Waals, J.D. Die Kontinuität des gasformigen und des flüssigen Zustandes. Ph.D. thesis; Leiden; 1873.
[9] Israelachvili JN. Intermolecular and surface forces. 2 ed. San Diego: Academic Press; 1992.
[10] London F. The general theory of molecular forces. T Faraday Soc 1937;33:8–26.
[11] de Boer JH. The influence of van der Waals' forces and primary bonds on binding energy, strength and orientation, with special reference to some artificial resins. T Faraday Soc 1936;32:10–37.
[12] Bradley RS. The cohesive force between solid surfaces and the surface energy of solids. LXXIXPhil Mag 1932;13:853–62.
[13] Hamaker HC. The London-van der Waals attraction between spherical particles. Physica 1937;4:1058–72.
[14] Casimir HBG. On the attraction between two perfectly conducting plates. Proc K Ned Akad Wet 1948;51:793.
[15] Dzyaloshinskii IE, Lifshitz EM, Pitaevskii LP. The general theory of van der Waals forces. Adv Phys 1961;10:165–209.
[16] French RH, Parsegian VA, Podgornik R, Rajter RF, Jagota A, Luo J, et al. Long range interactions in nanoscale science. Rev Mod Phys 2010;82:1887–944.
[17] Parsegian VA. Van der Waals forces. A handbook for biologists, chemists, engineers, and physicists1 ed. . New York: Cambridge University Press; 2006.
[18] French RH, Cannon RM, Denoyer LK, Chiang Ym. Full spectral calculation of non-retarded Hamaker constants for ceramic systems from interband transition strengths. Solid State Ionics 1995;75:13–33.
[19] French RH, Mullejans H, Jones DJ, Duscher G, Cannon RM, Ruhle M. Dispersion forces and Hamaker constants for intergranular films in silicon nitride from spatially resolved-valence electron energy loss spectrum imaging. Acta Mater 1998;46:2271–87.
[20] Ahuja R, Osorio-Guillen JM, de Almeida JS, Holm B, Ching WY, Johansson B. Electronic and optical properties of γ-Al_2O_3 from ab initio theory. J Phys Condens Matter 2004;16:2891–900.
[21] Tan GL, Lemon MF, Jones DJ, French RH. Optical properties and London dispersion interaction of amorphous and crystalline SiO2 determined by vacuum ultraviolet spectroscopy and spectroscopic ellipsometry. Phys Rev B 2005;72:205117.
[22] Rajter RF, Podgornik R, Parsegian VA, French RH, Ching WY. van der Waals–London dispersion interactions for optically anisotropic cylinders: Metallic and semiconducting single-wall carbon nanotubes. Phys Rev B 2007;76:045417.
[23] Masuda T, Matsuki Y, Shimoda T. Spectral parameters and Hamaker constants of silicon hydride compounds and organic solvents. J Colloid Interface Sci 2009;340:298–305.
[24] Casimir HBG, Polder D. The Influence of Retardation on the London–van der Waals Forces. Phys Rev 1948;73:360–72.
[25] Tabor D, Winterton RHS. The direct measurement of normal and retarded van der Waals forces. Proc Roy Soc A 1969;312:435–50.
[26] Israelachvili JN, Tabor D. Measurement of van der Waals dispersion forces in the range 1.4 to 130 nm. Nature 1972;236:106.
[27] Israelachvili JN, Tabor D. The measurement of van der Waals dispersion forces in the range 1.5 to 130 nm. Proc R Soc A 1972;331:19–38.
[28] Langbein D. Non-retarded dispersion energy between macroscopic spheres. J Phys Chem Solids 1971;32:1657–67.
[29] Langbein D. Van der Waals attraction in multilayer structures. J Adhes 1972;3:213–35.
[30] Seemann R, Herminghaus S, Jacobs K. Dewetting patterns and molecular forces: a reconciliation. Phys Rev Lett 2001;86:5534–7.
[31] Seemann R, Herminghaus S, Jacobs K. Gaining control of pattern formation of dewetting liquid films. J Phys Condens Matter 2001;13:4925–38.
[32] Jacobs K, Seemann R, Herminghaus S. Stability and dewetting of thin liquid films. In: Tsui OKC, Russel TP, editors. Polymer thin films. Singapore: World Scientific; 2008. p. 243–66.

Please cite this article as: Loskill P, et al, Is adhesion superficial? Silicon wafers as a model system to study van der Waals interactions, Adv Colloid Interface Sci (2012), doi:10.1016/j.cis.2012.06.006

[33] Bäumchen O, Jacobs K. Slip effects in polymer thin films. J Phys Condens Matter 2010;22:033102.
[34] Vrij A. Possible mechanism for the spontaneous rupture of thin, free liquid films. Discuss Faraday Soc 1966;42:23–33.
[35] Herminghaus S, Jacobs K, Mecke K, Bischof J, Fery A, Ibn-Elhaj M, et al. Spinodal dewetting in liquid crystal and liquid metal films. Science 1998;282:916–9.
[36] Leckband D, Israelachvili JN. Intermolecular forces in biology. Q Rev Biophys 2001;34:105–267.
[37] Verwey EJW, Overbeek JTG. Theory of the stability of lyophobic colloids. 1 ed. Amsterdam: Elsevier Publishing Co.; 1948.
[38] Van Oss CJ. Energetics of cell–cell and cell–biopolymer interactions. Cell Biochem Biophys 1989;14:1–116.
[39] Leckband D, Schmitt F, Israelachvili JN, Knoll W. Direct force measurements of specific and nonspecific protein interactions. Biochemistry-Us 1994;33:4611–24.
[40] Nir S, Andersen M. Van der Waals interactions between cell surfaces. J Membrane Biol 1977;31:1–18.
[41] Nir S. Van der Waals interactions between surfaces of biological interest. Prog Surf Sci 1977;8:1–58.
[42] Ploux L, Ponche A, Anselme K. Bacteria/material interfaces: role of the material and cell wall properties. J Adhes Sci Technol 2010;24:2165–201.
[43] Lin AYM, Brunner R, Chen PY, Talke FE, Meyers MA. Underwater adhesion of abalone: the role of van der Waals and capillary forces. Acta Mater 2009;57:4178–85.
[44] Autumn K, Sitti M, Liang YCA, Peattie AM, Hansen WR, Sponberg S, et al. Evidence for van der Waals adhesion in gecko setae. Proc Natl Acad Sci 2002;99:12252–6.
[45] Autumn K, Peattie AM. Mechanisms of adhesion in geckos. Integr Comp Biol 2002;42:1081–90.
[46] Huber G, Mantz H, Spolenak R, Mecke K, Jacobs K, Gorb SN, et al. Evidence for capillarity contributions to gecko adhesion from single spatula nanomechanical measurements. Proc Natl Acad Sci 2005;102:16293–6.
[47] Quinn A, Mantz H, Jacobs K, Bellion M, Santen L. Protein adsorption kinetics in different surface potentials. Europhys Lett 2008;81:56003.
[48] Schmitt Y, Hähl H, Gilow C, Mantz H, Jacobs K, Leidinger O, et al. Structural evolution of protein-biofilms: simulations and experiments. Biomicrofluidics 2010;4:032201.
[49] Bellion M, Santen L, Mantz H, Hähl H, Quinn A, Nagel AM, et al. Protein adsorption on tailored substrates: long-range forces and conformational changes. J Phys Condens Matter 2008;20:404226.
[50] Hähl H, Evers F, Grandthyll S, Paulus M, Sternemann C, Loskill P, et al. Subsurface influence on the structure of protein adsorbates revealed by in situ X-ray reflectivity. Langmuir 2012;28:7747–56.
[51] Loskill P, Hähl H, Kreis CT, Thewes N, Bischoff M, Herrmann M, et al. The influence of the subsurface composition of a material on the adhesion of Staphylococci. Langmuir 2012;28:7242–8.
[52] Loskill, P., Puthoff, J.B., Wilkinson, M., Mecke, K., Jacobs, K., Autumn, K. Adhesion of gecko setae reflects nanoscale differences in subsurface energy. submitted for publication.
[53] Tomaš M. Casimir force in absorbing multilayers. Phys Rev A 2002;66:052103.
[54] Podgornik R, Hansen PL, Parsegian VA. On a reformulation of the theory of Lifshitz–van der Waals interactions in multilayered systems. J Chem Phys 2003;119:1070.
[55] Podgornik R, Parsegian VA. van der Waals interactions across stratified media. J Chem Phys 2004;120:3401.
[56] Podgornik R, French RH, Parsegian VA. Nonadditivity in van der Waals interactions within multilayers. J Chem Phys 2006;124:044709.
[57] van Benthem K, Tan G, DeNoyer LK, French RH, Ruhle M. Local optical properties, electron densities, and London dispersion energies of atomically structured grain boundaries. Phys Rev Lett 2004;93:227201.
[58] van Benthem K, Tan G, French R, DeNoyer L, Podgornik R, Parsegian VA. Graded interface models for more accurate determination of van der Waals–London dispersion interactions across grain boundaries. Phys Rev B 2006;74:205110.
[59] Van Oss CJ, Chaudhury MK. Interfacial Lifshitz-van der Waals and polar interactions in macroscopic systems. Chem Rev 1988;88:927–41.
[60] Ninham BW, Parsegian VA. Van der Waals forces across triple-layer films. J Chem Phys 1970;52:4578–87.
[61] Parsegian VA, van der Ninham BW. Waals forces in many-layered structures: generalizations of the Lifshitz result for two semi-infinite media. J Theor Biol 1973;38:101–9.
[62] Parsegian VA. Reconciliation of Van-Der-Waals force measurements between phosphatidylcholine bilayers in water and between bilayer-coated mica surfaces. Langmuir 1993;9:3625–8.
[63] Sze SM, Ng KK. Physics of semiconductor devices. 3 ed. New York: John Wiley & Sons; 2006.
[64] Jellison Jr GE. Examination of thin SiO_2-films on si using spectroscopic polarization modulation ellipsometry. J Appl Phys 1991;69:7627–34.
[65] Wang Y, Irene EA. Consistent refractive index parameters for ultrathin SiO_2 films. J Vac Sci Technol B 2000;18:279–82.
[66] Hebert KJ, Zafar S, Irene EA, Kuehn R, McCarthy TE, Demirlioglu EK. Measurement of the refractive index of thin SiO_2 films using tunneling current oscillations and ellipsometry. Appl Phys Lett 1996;68:266–8.
[67] Taft E, Cordes L. Optical evidence for a silicon–silicon oxide interlayer. J Electrochem Soc 1979;126:131–4.
[68] Aspnes DE, Theeten JB. Optical-properties of the interface between Si and its thermally grown oxide. Phys Rev Lett 1979;43:1046–50.
[69] Hollinger G, Himpsel FJ. Probing the transition layer at the SiO_2-Si interface using core level photoemission. Appl Phys Lett 1984;44:93–5.
[70] Grunthaner FJ, Grunthaner PJ, Vasquez RP, Lewis BF, Maserjian J, Madhukar A. Local atomic and electronic-structure of oxide-GaAs and SiO_2–Si interfaces using high-resolution XPS. J Vac Sci Technol 1979;16:1443–53.
[71] Himpsel FJ, McFeely FR, Taleb-Ibrahimi A. Microscopic structure of the SiO_2/Si interface. Phys Rev B Condens Matter 1988;38:6084–96.
[72] Ohdomari I, Akatsu H, Yamakoshi Y, Kishimoto K. Study of the interfacial structure between Si (100) and thermally grown SiO_2 using a ball-and-spoke model. J Appl Phys 1987;62:3751–4.
[73] Giustino F, Bongiorno A, Pasquarello A. Atomistic models of the Si(100)–SiO_2 interface: structural, electronic and dielectric properties. J Phys Condens Matter 2005;17:S2065–74.
[74] Irene E, Tierney E, Angilello J. A viscous-flow model to explain the appearance of high-density thermal SiO_2 at low oxidation temperatures. J Electrochem Soc 1982;129:2594–7.
[75] Cai QY, Zheng YX, Mao PH, Zhang RJ, Zhang DX, Liu MH, et al. Evolution of optical constants of silicon dioxide on silicon from ultrathin films to thick films. J Phys D: Appl Phys 2010;43:445302.
[76] Geoghegan M, Krausch G. Wetting at polymer surfaces and interfaces. Prog Polym Sci 2003;28:261–302.
[77] Mykhaylyk TA, Evans SD, Fernyhough CM, Hamley IW, Henderson JR. Surface energy of ethylene-co-1-butene copolymers determined by contact angle methods. J Colloid Interface Sci 2003;260:234–9.
[78] Müller F, Zeitz C, Mantz H, Ehses KH, Soldera F, Schmauch J, et al. Elemental depth profiling of fluoridated hydroxyapatite: saving your dentition by the skin of your teeth? Langmuir 2010;26:18750–9.
[79] Parsegian VA, Ninham BW. Application of the Lifshitz theory to the calculation of Van der Waals forces across thin lipid films. Nature 1969;224:1197–8.
[80] Mahanty J, Ninham BW. Dispersion forces. 1 ed. London: Academic Press; 1976.
[81] Hough DB, White LR. The calculation of Hamaker constants from Liftshitz theory with applications to wetting phenomena. Adv Colloid Interface Sci 1980;14:3–41.

Please cite this article as: Loskill P, et al, Is adhesion superficial? Silicon wafers as a model system to study van der Waals interactions, Adv Colloid Interface Sci (2012), doi:10.1016/j.cis.2012.06.006

Addendum II - Subsurface Influence on the Structure of Protein Adsorbates as Revealed by in Situ X-ray Reflectivity

Authors: H. Hähl[1], F. Evers[2], S. Grandthyll[1], M. Paulus[2], C. Sternemann[2], P. Loskill[1], M. Lessel[1], A. K. Hüsecken[2], T. Brenner[2], M. Tolan[2], and K. Jacobs[1]

[1] Department of Experimental Physics, Saarland University, 66041 Saarbrücken, Germany. [2] Fakultät Physik/DELTA, TU Dortmund, 44221 Dortmund, Germany

Langmuir **28**, 7747–7756 (2012).
(http://dx.doi.org/10.1021/la300850g)

Author contributions:
Experiments were conceived and designed by H. Hähl and K. Jacobs. Experiments were performed by H. Hähl, F. Evers, S. Grandthyll, M. Paulus, C. Sternemann, P. Loskill, M. Lessel, A. K. Hüsecken, and T. Brenner. Data was analyzed by F. Evers. The article was written by H. Hähl and F. Evers. Research was directed by K. Jacobs and M. Tolan.

Abstract - The adsorption process of proteins to surfaces is governed by the mutual interactions between proteins, solution and substrate. Interactions arising from the substrate are usually attributed to the uppermost atomic layer. This 'actual surface' defines the surface chemistry and hence steric and electrostatic interactions. For a comprehensive understanding, however, also the interactions arising from the bulk material have to be considered. Our protein adsorption experiments with globular proteins (α-amylase, bovine serum albumin, and lysozyme) clearly reveal the influence of the subsurface material via van der Waals forces. Thereby, the used set of functionalized silicon wafers enables a distinction between effects of the surface chemistry and the subsurface composition of the substrate: Whereas the surface chemistry controls whether or not the individual proteins are denatured, the strength of the van der Waals forces affects the final layer density and hence the adsorbed amount of proteins. The results imply that van der Waals forces mainly influence surface processes, which govern the structure formation of the protein adsorbates, such as surface diffusion or spreading.

Langmuir

Subsurface Influence on the Structure of Protein Adsorbates as Revealed by in Situ X-ray Reflectivity

Hendrik Hähl,[†] Florian Evers,[‡,§] Samuel Grandthyll,[†] Michael Paulus,[‡] Christian Sternemann,[‡] Peter Loskill,[†] Matthias Lessel,[†] Anne K. Hüsecken,[‡] Thorsten Brenner,[‡] Metin Tolan,[‡] and Karin Jacobs*[,†]

[†]Department of Experimental Physics, Saarland University, 66041 Saarbrücken, Germany

[‡]Fakultät Physik/DELTA, TU Dortmund, 44221 Dortmund, Germany

Supporting Information

ABSTRACT: The adsorption process of proteins to surfaces is governed by the mutual interactions among proteins, the solution, and the substrate. Interactions arising from the substrate are usually attributed to the uppermost atomic layer. This actual surface defines the surface chemistry and hence steric and electrostatic interactions. For a comprehensive understanding, however, the interactions arising from the bulk material also have to be considered. Our protein adsorption experiments with globular proteins (α-amylase, bovine serum albumin, and lysozyme) clearly reveal the influence of the subsurface material via van der Waals forces. Here, a set of functionalized silicon wafers enables a distinction between the effects of surface chemistry and the subsurface composition of the substrate. Whereas the surface chemistry controls whether the individual proteins are denatured, the strength of the van der Waals forces affects the final layer density and hence the adsorbed amount of proteins. The results imply that van der Waals forces mainly influence surface processes, which govern the structure formation of the protein adsorbates, such as surface diffusion and spreading.

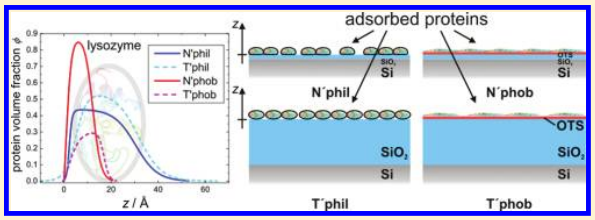

INTRODUCTION

The unspecific adsorption of proteins on solid/liquid interfaces is a well-known and often studied phenomenon.[1−4] Its importance in and influence on clinical, biological, and technical applications is enormous. For instance, biofilm formation on surfaces adherent to biological solutions (saliva, blood, etc.) begins with and depends on the primary adsorption by the proteins. Therefore, to control the biofilm development, it is desirable to gain control of the protein adsorption process.

Recent studies have shown that the substrate strongly influences the enzymatic activity of adsorbed proteins,[5] their orientation on the surface,[6,7] and the kinetics of the adsorption process.[5,8,9] The latter studies have shown that slight changes in the substrate's subsurface composition (i.e., the material composition below the uppermost surface layer) influence the kinetics of adsorption. It is the aim of our study to yield structural information about the adsorption process and the influence of the subsurface composition of the substrate and connect the results to kinematical studies.[8−10]

Parameters that influence protein adsorption are numerous: the pH value, ionic strength, temperature, protein concentration, and the concentration of cosolvents and additives are the most prominent properties of the solution.[2−4,11−13] The influence of the substrate on adsorption is in most studies described by and restricted to the sign and value of the surface charge, the roughness of the surface, and the surface free energy (i.e., the chemical composition of the surface).[4,14−16]

The above-named substrate properties belong to the actual surface of the offered substrate. Nevertheless, the influence of the bulk substrate should not be neglected because van der Waals forces range over tens of nanometers, depending mainly on the geometry of the interacting objects.[17,18] It could already be shown that van der Waals forces govern the stability of thin films.[19,20] Furthermore, they influence the adhesion strength even in wet surroundings.[21,22] Thus, their influence on protein adsorbates is expected.

In recent studies, it was shown that the adsorption kinetics of large, deformable proteins such as α-amylase and bovine serum albumin (BSA) are affected by different van der Waals forces.[8,9] By using silicon wafers with different silicon oxide thicknesses, the van der Waals forces can be varied while keeping the surface free energy constant. On thick silicon oxide wafers, regardless of whether they were hydrophilic or hydrophobic, the proteins showed Langmuir-like kinetics, whereas on thin silicon oxide "stepped" kinetics was observed with a distinct change in the adsorption rate at low coverage. Such behavior was not recorded for the lysozyme,[8] which is generally regarded as a stiff

Received: February 28, 2012
Revised: April 25, 2012
Published: April 25, 2012

protein (Gibbs energy for unfolding: 60 kJ/mol).[2] On the basis of this fact, it is expected that the final state of the protein films also diversifies (e.g., in protein orientation or conformation) with different subsurface compositions. There are only a few techniques, however, that allow us to resolve in situ the structure of films with thicknesses of only a few nanometers. In this study, we applied X-ray reflectometry at high X-ray energies to analyze the film structure with angström resolution. In former studies,[23−25] this technique has proven to be able to resolve the film structure of similar protein films.

EXPERIMENTAL SECTION

Materials and Setup. As substrates for protein adsorption, two types of silicon wafers were used: wafers with a natural silicon oxide layer of 1.7(3) nm (Wacker Siltronic AG, Burghausen, Germany) and wafers with a thermally grown amorphous silicon oxide layer with a thickness of 150(3) nm (Silchem, Freiberg, Germany), as characterized by ellipsometry. Prior to use, the wafers were cleaned for 30 min in a fresh 1:1 H_2SO_4(conc)/H_2O_2(30%) solution and subsequently rinsed in hot deionized water to remove hydrocarbon residues from the polishing process. After this procedure, the wafers were hydrophilic with a water contact angle of <5°. The wafers were stored in deionized water until they were used. Additionally, both types of wafers could be covered with a self-assembled monolayer of octadecyltrichlorosilane (OTS, Sigma-Aldrich, Germany) using standard procedures.[26,27] After this treatment, the substrates exhibit hydrophobic surfaces with water contact angles of 107 to 112° with a contact angle hysteresis of <5°. The quality of the achieved hydrophobic layers could additionally be affirmed by X-ray reflectivity measurements. The obtained values agree well with the literature,[28,29] indicating densely packed and homogeneous layers. As the cleaning procedure for these wafers, sonication in ethanol and acetone turned out to be fully sufficient.

Thus, a set of four different substrates was obtained: hydrophilic and hydrophobic wafers (abbreviated as "phil" and "phob", respectively) with either a natively thin (called "N") or a thick (called "T") silicon oxide layer. In previous studies, it could be shown by streaming potential measurements that substrates from this set with the same surface chemistry also showed the same zeta potential regardless of their silicon oxide thickness[9] and thus have the same surface charge. The isoelectric points (IEP) of these surfaces are 1.9(2) for the hydrophilic and 3.0(2) for the hydrophobic surfaces. The roughness, as measured via atomic force microscopy in a 0.5 × 0.5 μm^2 area, was below 0.2 nm for all types of wafers. This set of four wafer types allows for a separate variation of short- and long-range forces (i.e., by providing the same surface chemistry, as indicated by identical zeta potentials,[9] but different silicon oxide thicknesses, where only long-range forces arising from the different subsurface compositions are varied). The hydrophobization process changes only the short-range forces, as a molecularly thick silane layer affects the van der Waals interaction only marginally.[30]

The proteins used in this study were α-amylase from human saliva (prod. no. A0521), bovine serum albumin (BSA, prod. no. A3059), and lysozyme from hen egg white (prod. no. 62971, all purchased from Sigma-Aldrich, Steinheim, Germany). The proteins were received as a lyophilized powder and used without further treatment. (The α-amylase powder, however, contains only approximately 10% protein. The rest of the mass consists, as shown by a crude precipitation test, mainly of stabilizing salts such as sulfates. This results in final protein solutions with a consequently decreased protein content and marginally increased ionic strength of the solution.) BSA and lysozyme were stored at 2 °C and α-amylase was stored at −20 °C until used.

Table 1. Characteristics of the Substrates

	N'phob	T'phob	N'phil	T'phil
surface material	OTS	OTS	SiO_2	SiO_2
surface energy/mJ/m^2	24(1)	24(1)	64(1)	64(1)
roughness (rms)/nm	0.12(2)	0.15(2)	0.09(2)	0.13(2)
SiO_2 layer thickness/nm	1.7(3)	150(3)	1.7(3)	150(3)
isoelectric point (IEP)	3.0(2)	3.0(2)	1.9(2)	1.9(2)

Table 2. Characteristics of the Proteins Studied

	α-amylase[31]	BSA[34]	lysozyme[32]
molar mass/kg/mol	56.0	66.3	14.3
molar volume/cm^3/mol	38 071	48 600	10 057
electron density/e/Å^3	0.47125[a]	0.43866[34]	0.45582[24]
isoelectric point (IEP)	6.9[35]	4.7[36]	11[37]
diameters/Å^3	80(2) × 48(2) × 47(2)	83(2) × 81(2) × 45(2)	48(2) × 30(2) × 28(2)

[a]Calculated from the protein structure.

Their molecular masses and other properties are listed in Table 2. All are globular proteins and can roughly be described as prolate or, in the case of BSA, as oblate ellipsoids.[31−33] The length of the shortest axis is thereby similar for BSA and α-amylase and coincides with the long axis of lysozyme (Table 2). Because of their respective IEP values, the electric properties of these proteins differ greatly: at pH 7, α-amylase carries a close to zero net charge, whereas the net charge is negative for BSA and positive for lysozyme.

As a solution for the proteins, a 10 mM phosphate buffer solution with a pH of 7 was prepared using ultrapure water. No salt was added, resulting in a calculated ionic strength of I = 20 mM because of the buffer components. Additionally, different buffer systems were used to achieve stable pH values at the respective IEP of the proteins: an acetate buffer system at pH 4.7 was used for BSA, and CAPS (3-(cyclohexylamino)-1-propanesulfonic acid) adjusted with NaOH to pH 11 was utilized for lysozyme. Appropriate amounts of NaCl were added to obtain the same ionic strength as for the phosphate buffer solutions.

For the X-ray measurements, the substrates were put into a closed Teflon sample cell with Kapton windows. Prior to the measurement, the cell was rinsed and flooded with buffer solution. Subsequently, the cell was connected to a flow system containing a syringe pump and a switch with a sample loop (Rheodyne Manual Sample Injector) prior to the cell. The protein solution was injected into the sample loop, which could be inserted into the flow system at a specific time by using the switch. This system allowed for an injection of the protein solution with a minimum disturbance of the system. The protein concentration of the solution in the sample loop was chosen to result in a final concentration inside the sample cell of 0.1 g/L (with a smaller concentration in the case of α-amylase, see above).

To achieve stable protein film conditions during the measurements, the films were allowed to equilibrate for at least 1 h before starting the reflectivity scans. By comparing subsequent scans of the same system, these stable conditions were affirmed.

X-ray Reflectivity Technique. The X-ray scattering experiments were conducted at beamline BL9 at synchrotron light source DELTA (Dortmund, Germany).[23] The sample cell was illuminated with a monochromatic X-ray beam with a wavelength λ of 0.459 Å (corresponding to a photon energy of 27 keV). The wavelength was chosen to balance between a high transmission signal through water and minimal radiation damage on the biological samples.[38−40] Specular reflectivity scans are performed in $\theta-2\theta$ geometry. The wave vector transfer is directed perpendicular to the surface and is given by

$$q_z = \frac{4\pi}{\lambda} \sin\theta \quad (1)$$

The angle between the surface and the X-ray beam is denoted as θ. To obtain the true specular reflectivity, the diffuse scattering has been measured by longitudinal, diffuse scans with a constant angular

detector offset of 0.1°. A typical X-ray reflectivity measurement was recorded within 0.5 h, including an offset scan reaching a maximum q_z value of 0.5 Å^{-1} and covering a dynamic range of 6 to 7 orders of magnitude.

The reflectivity, $R(q_z)$, is in the Born approximation given by

$$R(q_z) = R_F(q_z)\left|\frac{1}{\rho_{ref}}\int\left(\frac{d\rho(z)}{dz}\right)e^{iq_z z}\,dz\right|^2 \quad (2)$$

R_F, $\rho(z)$, and ρ_{ref} denote the Fresnel reflectivity of a sharp interface, the electron density profile (EDP), and the electron density of the subphase (buffer solution), respectively. Hence, X-ray reflectivity measurements probe the EDP of the sample averaged over the illuminated area.[41,42]

Analysis of the X-ray Reflectivity Data. The raw data were background-corrected, normalized, and scaled as a function of q_z. Because of the rapid decay of the reflected X-ray intensity, it is common to present reflectivity data in the form R/R_F versus q_z (cf. Figure 1) in order to increase the visibility of features stemming from the molecularly thin layers at the surface (i.e., from the adsorbed protein films or the OTS structure). To obtain the EDP from the reflectivity data, a model of the vertical structure of the studied system is proposed from which a reflectivity is calculated by Parratt's recursive method.[43] The proposed EDP is varied in such a way that the mean square variation, χ^2, between calculated and observed reflectivity curves is minimized using a least-squares fitting routine. The EDP is described in terms of the effective density model, which guarantees for continuous profiles even if the roughness is not small compared to the layer thickness.[41] In general, the EDP can be described by a stack of homogeneous layers each with a distinct electron density, ρ, layer thickness, d, and interfacial roughness, σ.

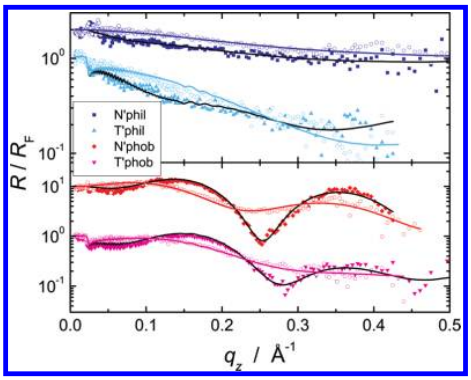

Figure 1. X-ray reflectivity data of BSA adsorbates presented as R/R_F vs q_z on the four different types of substrates (from top to bottom): N'phil (blue), T'phil (cyan), N'phob (red), and T'phob (purple). Open circles represent the reference measurements, and solid symbols represent the final state with the adsorbed protein layer. The lines show the calculated reflectivity values as obtained from the respective model fits. The curves were shifted for clarity.

In our study, one layer is sufficient to explain the structure of the protein adsorbate film adequately. The EDP structure of the hydrophilic substrates is described as "silicon/silicon oxide/aqueous buffer solution". For the hydrophobic substrates, two layers are introduced into the model representing the head and the tail of the OTS film.[28,44] Moreover, for the characterization of an OTS/water interface, an additional layer accounting for the electron density depletion at the hydrophobic gap has to be introduced,[28] yielding an EDP structure described as "silicon/silicon oxide/OTS head/OTS tail/gap/aqueous buffer solution" (Figure 2).

To minimize the number of fitting parameters, the following strategies are applied. First, each substrate is characterized under pure buffer without protein. Because no changes in the substrate's properties are expected during the subsequent protein adsorption, the EDP structure obtained for the substrate is kept constant when fitting the data after protein adsorption. Thus, only the parameters of the adsorbed protein layer and, in the case of hydrophobic substrates, the parameters of the hydrophobic gap have to be varied when refining the corresponding reflectivity curves. Furthermore, the electron density of the silicon substrate, the silicon oxide layer, and the water subphase are set to the theoretical values of 0.702, 0.663, and 0.334 e$^-$/Å^3, respectively.[45] To model the structure of the OTS films, values from the literature[28] are used as starting values and varied over a narrow range. The thickness of the silicon oxide layer is varied between 10 and 15 Å for native SiO_2, and a value of 1500 Å is used as a starting value for the thickness of the thermally grown SiO_2 layer, as was obtained by ellipsometry.

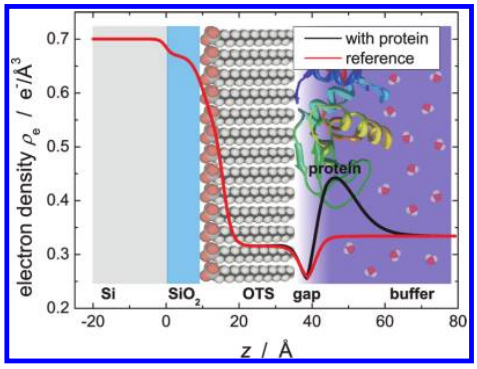

Figure 2. Electron density profile of an N'phob substrate in buffer without (red line) and with (black line) an adsorbed lysozyme layer.

Typically, when studying protein adsorption phenomena, only the amount of adsorbed protein per unit area, Γ, is determined. However, from the X-ray reflectivity data, not only Γ can be obtained but also the volume fraction profile along the surface normal[25,46] $\phi(z)$ is defined by subtracting the EDP without protein adsorbate, $\rho_{ref}(z)$, from the EDP with protein adsorbate, $\rho(z)$, and dividing this difference by the contrast between the protein and reference medium

$$\phi(z) = \frac{\rho(z) - \rho_{ref}(z)}{\rho_{protein} - \rho_{sub}} \quad (3)$$

where ρ_{sub} is the electron density of the aqueous buffer solution (subphase, 0.334 e$^-$/Å^3) and $\rho_{protein}$ is the electron density of the protein (Table 2). Thus, the adsorbed amount is given by

$$\Gamma = \frac{m}{\nu}\int\phi(z)\,dz \quad (4)$$

with the molar mass, m, and the molar volume, ν, of the proteins as listed in Table 2. It is important to note that the roughness between the adsorbed layer (with thickness d_{ads}) and the subphase, σ_{sub}, contributes to the effective layer thickness, d_{eff}, of the adsorbed protein film,[24,46] which is given by

$$d_{eff} = d_{ads} + \sigma_{sub} \quad (5)$$

In the following text, we will use d_{eff} for the characterization of the adsorbate thickness.

Error bars of each fitting parameter are determined by allowing a variation of 5% from the χ^2 of the best fit.[24] The error in Γ is assessed by setting each fitting parameter equal to the value that increases χ^2 by 5% and combining these values to the EDP of maximum χ^2.

RESULTS

Protein Adsorbates in Different Surface Potentials. The adsorption of α-amylase, BSA, and lysozyme has been studied on four different types of substrates. Therefore,

dx.doi.org/10.1021/la300850g | Langmuir 2012, 28, 7747−7756

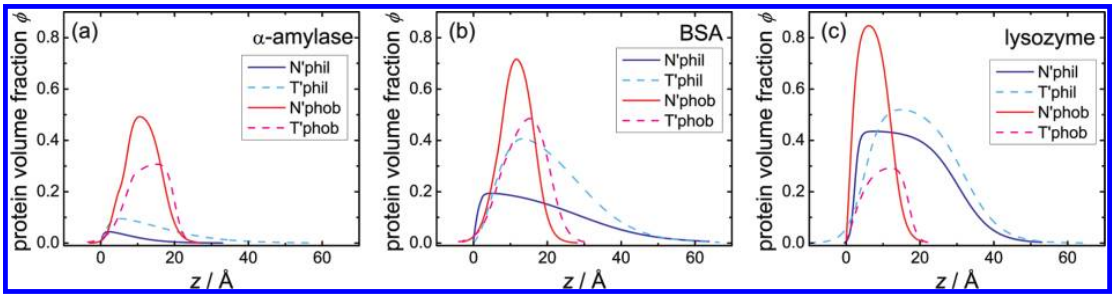

Figure 3. Volume fraction profiles $\phi(z)$ as given by eq 3 for (a) α-amylase, (b) BSA, and (c) lysozyme on the four different types of substrates at pH 7 as received from the fitting procedure.

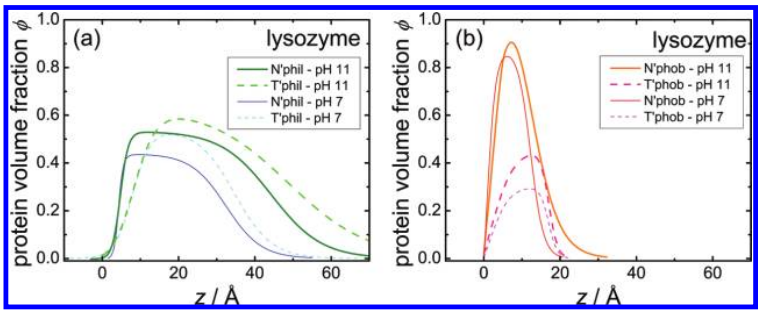

Figure 4. Protein volume fraction $\phi(z)$ of lysozyme on (a) hydrophilic and (b) hydrophobic substrates at its IEP (pH 11) (thick lines). For comparison, the profiles at pH 7 on the respective substrates are also shown (thin lines).

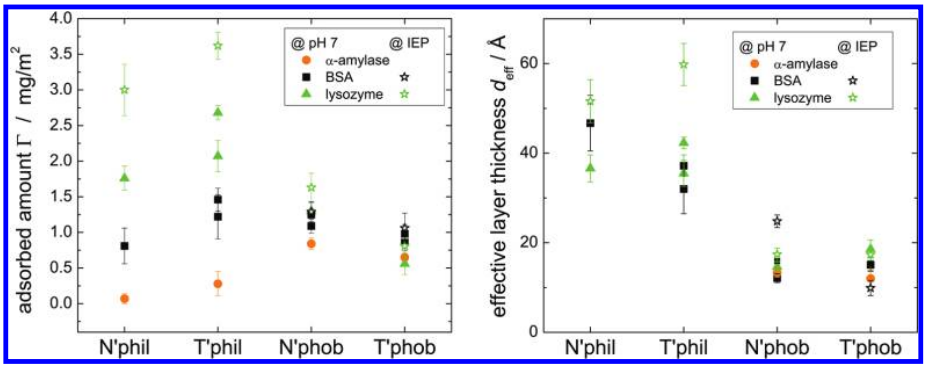

Figure 5. Adsorbed amount, Γ, (left) and effective film thickness, d_{eff}, (right) as obtained from X-ray reflectometry.

reflectivity measurements of the substrates without and with an adsorbed protein layer have been performed. The reference measurements (i.e., scans of a substrate in pure buffer solution) display the specific features of the different substrates (Figure 1 and Supporting Information, SI): The hydrophobic substrates in solution exhibit oscillations in the reflectivity curves (Kiessig fringes) that can be related to the OTS layer and a depletion layer in the electron density above the OTS coating.[28] Furthermore, high-frequency oscillations are observed in the reflectivities of the thick oxide wafers, which could be reproduced in the refinement procedure of the model (SI), yielding the actual layer thickness of the silicon oxide.

When we compare the raw reference data (open symbols) and final measurements (solid symbols, see Figure 1), the effect of an additional protein layer is visible on all types of substrates. On the hydrophilic surfaces, this effect is mainly a reduction of the reflectivity. On the hydrophobized silicon wafers, however, measurements before and after adsorption differ more drastically: the Kiessig fringes are enhanced and the positions of the extrema are shifted by adsorption.

A detailed analysis and modeling of the data yield the respective EDPs. The contributions of the respective protein layers to the final EDPs are depicted in Figures 3 and 4. (The reflectivity data corresponding to these profiles are shown in the SI.) Several trends can immediately be extracted from these volume fraction profiles and hold true for all three studied proteins: by comparing protein layers on hydrophilic and hydrophobic surfaces, one notices that the volume fraction profiles on the hydrophilic surfaces extend to higher z values, representing higher film thicknesses than on the hydrophobic surfaces (cf. Figure 5). Additionally, these profiles also decay more gradually to the buffer phase (Figures 3 and 4), which indicates a high interfacial roughness.

On the hydrophobic surfaces, the thickness of any of the protein films does not exceed 25 Å. When comparing this value with the dimensions of the proteins used, one notices that the

film thicknesses on the hydrophobic surfaces are noticeably smaller than even the smallest diameter of every protein in this study, therefore implying changes in the protein structure due to adsorption. Furthermore, the profiles are nearly symmetrical with steep flanks and high maximum protein volume fractions.

When we calculate the adsorbed amount Γ (Figure 5), another tendency becomes visible: in contrasting the values for Γ of the protein layers on thin and thick silicon oxide wafers, we notice that trends in the data of hydrophobic and hydrophilic surfaces differ significantly. On the hydrophobic surfaces, the adsorbed amount Γ is higher on substrates with a thin SiO_2 layer. This trend in Γ (Figure 5) is inverted when changing the surface chemistry from hydrophobic to hydrophilic. On the hydrophilic substrates, thin oxide layers are covered by less adsorbed proteins compared to the thick oxide samples.

Upon comparing the different proteins, we find that the above-described trends exist in every case, although the surface coverage differs. This fact may be attributed to the different IEPs of the proteins (Table 2) and surfaces used (pH 1.9(2) for bare SiO_2 and pH 3.0(2) for the OTS surface.[9]) Thus, interprotein as well as protein−surface Coulomb forces differ for every combination of protein and surface. To adjust at least the interprotein Coulomb interactions, the measurements for BSA and lysozyme have been repeated at their respective IEPs. The results of these experiments reveal that the differences between layers on thin and thick oxide wafers are also conserved when changing the pH value to the IEP of the protein.

DISCUSSION

The presented results reveal clear trends indicating that the subsurface composition affects the adsorbing proteins and the structure of the formed adsorbate. The data moreover contains a wealth of information that will be discussed in the following text.

Influence of the Surface Chemistry. The effect of different surface chemistry is most obvious in the values for the protein layer thickness: on the hydrophobic surfaces in this study, we reproducibly observe protein film thicknesses smaller than 30 Å, whereas on the hydrophilic ones the films are thicker. The very low film thickness on hydrophobic surfaces indicates a substantial variation of the shape (i.e., conformation) of the proteins. For every protein studied, the smallest diameter of the protein is still larger than the respective layer thickness of the adsorbate. Furthermore, on the hydrophobic samples, the protein layers are characterized by a low roughness for both interfaces as well as a high protein fraction, which characterizes a dense protein film with little water content. Both a low film thickness and a high density indicate a strong denaturation of the proteins adsorbed on the OTS surfaces. Additionally, the low interfacial roughness, indicated by the steep slope in the profiles, can be accomplished only by nearly complete denaturation and proteins that interdigitate into each other. A similar drastic denaturation was found in neutron reflectivity studies and in simulations concerning the adsorption of lysozyme on OTS.[47,48]

In discussing the leading forces, two aspects can be extracted from Figures 3−5: (i) Despite the different size, geometry, and conformational stability of α-amylase, BSA and lysozyme, their adsorbates on hydrophobic surfaces have remarkably similar, low film thicknesses. (ii) At pH 7, a similar mass of adsorbed protein per area is observed for all used proteins, though at this pH value BSA and lysozyme carry opposing net charges and α-amylase possesses a net charge that is close to zero. Both aspects together imply only a secondary role of Coulomb forces in the adsorption process on the hydrophobic surfaces. Instead, the hydrophobic effect governs the structure formation of the protein films. The level of denaturation and hence the deduced influence of the hydrophobic effect seem to be determined by the interfacial energy of the surface. This hypothesis is also supported by a study in which polystyrene (interfacial energy in between those of hydrophilic and hydrophobic wafers in this study) was used as a surface material.[25]

On the hydrophilic surfaces, however, the degree of conformational changes that can be deduced from the relatively high film thickness values is much lower than on hydrophobic surfaces. The thicknesses of BSA and α-amylase films are roughly twice as high as on hydrophobic samples yet are still thinner than the smallest diameter of the respective protein (ca. 45 Å). Additionally, the profiles in $\phi(z)$ are highly asymmetric for all proteins, reflecting a much higher roughness for the protein/buffer interface than for the substrate/protein interface. The profiles can be interpreted by assuming adsorbed protein molecules that are flattened on the adsorption side and retain a more native, globular configuration to the solution side. This interpretation is further corroborated by contrasting the maximum protein content on hydrophilic and hydrophobic surfaces. On hydrophilic surfaces, a maximum of $\phi = 0.6$ is observed (lysozyme on T'phil at pH 11), whereas on hydrophobic surfaces, with denatured proteins, up to $\phi = 0.9$ could be recorded (lysozyme on N'phob at pH 11).

What does a measured protein fraction of $\phi = 0.6$ mean? Because in the measurements the hydration shell is indistinguishable from the surrounding free water molecules, we consider densely packed (i.e., a surface coverage of $\gtrsim$90%), side-on-adsorbed colloids with the typical dimension of native lysozyme including its hydration shell. To allow for a measured protein fraction of only 60%, the resulting hydration shell must be assumed to be only about 2 Å thick. This is below the thickness of the native hydration shell (up to 10 Å[49]) and even below the thickness of a water monolayer (~3 Å). Thus, the hydration shells of individual proteins have to overlap. Assumptions of less-perfect ordering even reduce the calculated hydration shell thickness, which justifies the above-made assumption of ordering. It remains open whether this ordering stems from clustering[50,51] or collective effects[10,52] on the surface. Furthermore, the lysozyme film thickness at pH 11 (at its IEP) is a few angströms larger than even the largest diameter of the protein (cf. Figure 4). This large film thickness permits the assumption of bilayer adsorption, which was also found in other studies (Figure 6).[24,53−55] An end-on adsorption of the lysozyme molecules should not result in a film thickness above ca. 50 Å, which is the protein's largest diameter. Additionally, end-on adsorbed proteins would exhibit a lower protein fraction because of the lower protein/hydration shell area fraction of their surface projection compared to that of side-on adsorbed proteins. At the lower pH value of 7, where a net electrostatic attraction between a surface and a protein and a net repulsion between individual proteins exist, thinner films and lower adsorbed amounts are recorded (cf. Figure 5).

BSA exhibits a much lower protein fraction in the layer than does lysozyme (Figure 3) on hydrophilic samples. When we consult the colloidal picture once more, the low maximum values of $\phi(z)$ of BSA on hydrophilic surfaces indicate higher interprotein distances (41 Å if one assumes hexagonal

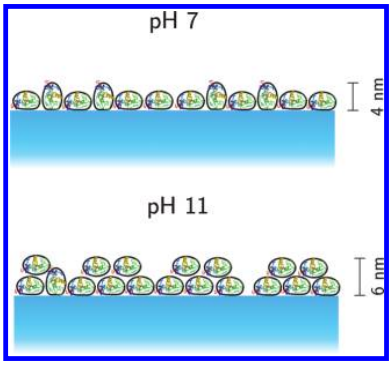

Figure 6. Schematic representation of the lysozyme molecules in the adsorbate at pH 7 and 11 according to the interpretation of the reflectivity data (cf. Su et al.[55] and Evers et al.[24]).

ordering) than in the case of lysozyme. This is most probably due to the repulsive electrostatic forces between the highly negatively charged BSA molecules.[56] In the case of α-amylase, the overall adsorbed amount on the hydrophilic surfaces is very low in comparison to the cases of BSA and lysozyme. In combination with the low electron density contrast, it renders the electron density profile hard to interpret. Therefore, the thickness values for the α-amylase adsorbates on N'phil and T'phil have been omitted in Figure 5. The profiles, however, are presented because their integral gives the adsorbed amount of protein, which is, although small, a reliable value. The reason for the low adsorbed amount is most probably due to the aforementioned composition of the protein powder. The salts contained in this powder increase the ionic strength and hence the screening of the electrostatic forces between the protein and substrate. Moreover, sulfate ions have kosmotropic character, stabilizing the native structure of proteins,[57] and it has recently been reported that kosmotropic salts can lead to reduced protein adsorption.[58] Additionally, the protein concentration in the solution is reduced by about 1 order of magnitude. When we assume partially reversible adsorption, this reduction of dissolved proteins reduces the adsorbed amount. However, because the adsorbed amount is lowered only on the hydrophilic substrates, it hints at the conclusion that the adsorption on the hydrophobic substrates is not affected by dissolved ions and is also completely irreversible. Nevertheless, the trends in the adsorbed amount resemble the trends for BSA and lysozyme and are discussed in the next section.

So far we have reported on the impact of surface chemistry on protein adsorption. The results for the adsorbed mass and film thickness are in accordance with recent studies,[24,47,48,53−55] yet with the in-layer characterization by the protein fraction $\phi(z)$, we are able to obtain further insight into the protein layer structure. Therefore, it is now possible to go one step further and probe the effect of subsurface composition, a factor that is neglected by most recent studies and will be discussed in the following section.

Influence of the Subsurface Composition. The influence of the subsurface material on protein adsorbates is elucidated in this study by contrasting protein layers on samples with the same surface energy but different silica layer thicknesses. Thereby, the used set of substrates provides the possibility to test the influence of long-range forces in combination with different surface chemistry. The effect of different subsurface composition is revealed by the final adsorbed amounts of protein.

Figure 5 (left) presents the adsorbed amount Γ, calculated via eq 4, of all measurements in this study. This overview exposes clear trends in the value of the adsorbed amount for every protein species used. On hydrophobic surfaces, the adsorbed amount on substrates with thin silica layers (N'phob) is higher than on substrates with thick silica layers (T'phob), whereas this tendency is inverted on the hydrophilic, bare silica substrates.

Because the experimental conditions for adsorption on substrates with thin and thick SiO_2 layers, either hydrophilic or hydrophobic, were identical, the only difference lies in the different subsurface composition of the substrate. From these subsurface differences, varied dispersion forces arise. On thin SiO_2-layer samples, an interaction with the silicon beneath is possible, at least for molecules in direct contact with the surface. Here, the screening of the dispersion interactions by ionic solutes is weakest (if not zero). On samples with a thick silicon oxide layer, however, the distance to the silicon is too large for the interaction with the silicon to have a significant influence. These samples may be regarded as being solely composed of silicon oxide (with a silane layer in the case of the hydrophobic samples), thus resembling simple (hydrophobized) glass substrates. Because the polarizability (or relevant parts of the dielectric function $\varepsilon(i\xi)$)[59] is higher for silicon than for silica, the strength of the interaction of molecules the size of proteins with the sample substrate is higher for composite substrates N'phil and N'phob than for their respective counterparts T'phil and T'phob.

The calculation of the correct van der Waals interaction constant (i.e., the Hamaker constant), however, is already difficult for proteins in solution.[60] Additionally, the strength of the interaction also depends strongly on the geometry of the interacting objects.[59] However, the protein geometry in the adsorbed state is not known and can only be assumed, which produces large errors in the estimation of the interaction energy, especially at short distances. This means in sum that it is presently not possible to give numbers for the differences in the protein/substrate interaction between substrates with thin and thick oxide layers. Instead, a more qualitative approach to the effect of the variation of dispersion forces is chosen.

Because the variation in the dispersion force has the opposite effect on the adsorbed amount Γ on hydrophilic and hydrophobic surfaces, it is clear that different subprocesses of the entire adsorption process are affected. In ellipsometry studies,[10] qualitatively different adsorption kinetics were observed on the thin and thick oxide wafers, especially for large proteins like α-amylase and BSA. These measurements indicated that the variation in the subsurface composition changes the time scale of a surface process such that its influence on the adsorption rate could be seen. With the data from the present study, however, it becomes obvious that, although not clearly resolved in the kinetics, the lysozyme adsorption is also affected and, even more importantly, that the affected surface processes are of a different type on hydrophilic and hydrophobic surfaces. The restriction to surface processes is motivated by the fact that the initial adsorption rate showed no variation due to subsurfaces changes[9] and by the notion that the dispersion forces and hence their differences are strongest in direct contact with the surface. Currently, however, we cannot exclude additional variations in the possibly nonzero desorption rate by the dispersion forces because these

variations are hardly distinguishable from surface diffusion by a mere inspection of the determined protein adsorbates.

The surface processes in question are the surface diffusion of the proteins[61] and surface spreading or conformational changes.[48,62] In the case of the latter process, there is even direct evidence from the data, especially on the hydrophobic surfaces. On the hydrophilic surfaces in this study, however, where only small conformational changes in the proteins can be deduced from the data, we assume the surface diffusivity to be the relevant process that is affected by changing the substrate's subsurface composition.

Nonzero surface diffusivities for proteins are reported in the literature (Tilton[61] and references therein) and are a necessary condition allowing for high packing densities (e.g., lysozymes on hydrophilic samples), where protein surface concentrations that reflect a nearly hexagonal close packing are reached.[61,63] Even BSA, which in our study is the protein with the largest interfacial contact area as a result of its oblate shape, shows measurable surface diffusion on glassy surfaces.[64,65] However, in most experiments mobile and immobile proteins are found. The reason for the coexistence of mobile and immobile protein species is believed to result from different conformations or orientations of the adsorbed proteins.[66]

These findings stimulate the following hypothesis for the explanation of the subsurface influence on the adsorbed amount on the hydrophilic surfaces: higher attractive forces to the substrate (as on the N'phil substrate compared to on T'phil) result in stronger binding to the surface and may also trigger an augmented flattening of the proteins at the solid surface. This stronger binding and the small conformational differences then lead to a reduced surface diffusivity and/or a higher nonmobile protein fraction. Eventually, higher attractive surface forces would result in reduced desorption, slower and less ordering, and hence a higher occupied space per protein (Figure 7). Thus, the higher amount on T'phil in comparison to that on N'phil can be understood. Ellipsometry studies[9] support this hypothesis because a faster saturation of the adsorbed layer is reported on the thick oxide.

On the hydrophobic surfaces, conformational changes (we propose spreading) of the proteins seem to be the dominating surface process. Protein layers of the same protein on thin and thick oxide samples differ only in their maximum protein fraction (Figures 3 and 4). These differences appear for every protein studied but are most pronounced for the lysozyme. From the adsorbed amounts and the film thickness values, a surface coverage can be calculated, which the adsorbed proteins would have had in their native state (i.e., before spreading). For BSA and lysozyme on T'phob, values of about 20% can be calculated, whereas on N'phob values of 30% for BSA and 55% for lysozyme are found (12 and 20% for α-amylase). Because these values do not exceed the jamming limit of a random sequential adsorption model (ca. 55%),[67] the assumption of surface diffusion is not necessary. However, they encourage the following hypothesis: in the course of the spreading of the proteins, the interprotein distances will be reduced. Thus, the repulsive forces between the charged protein molecules increase and hence promote the desorption of less spread or later adsorbed proteins. A higher attractive force between the proteins and substrate would decrease this tendency because of higher adhesion and by enhancing and accelerating the spreading process,[62] thereby leading to a higher adsorbed amount (Figure 7).

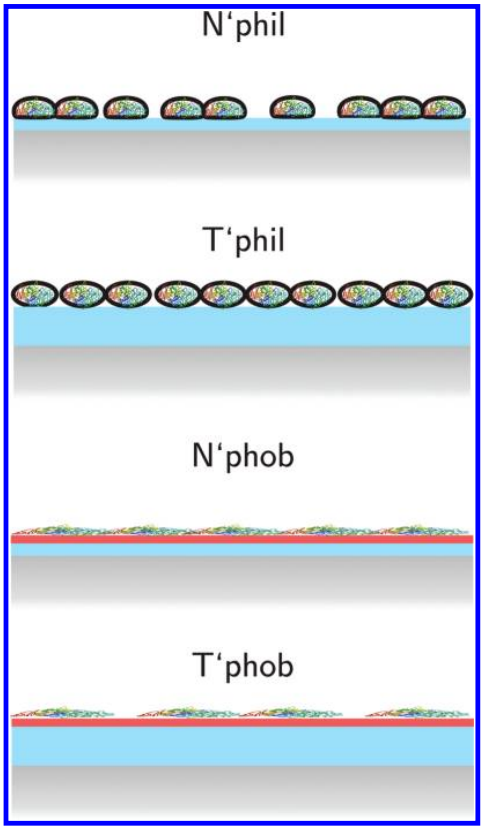

Figure 7. Schematic representation of the adsorbates on the four different wafer types according to the interpretation of the reflectivity data: flattened proteins on hydrophobic wafers and proteins with only slight changes in their conformation on hydrophilic wafers. A higher density is recorded on T'phil compared to that on N'phil and on N'phob compared to that on T'phob, yielding a higher adsorbed amount on the respective substrates. The interprotein distances vary with the protein species (not shown).

Remarks on the Behavior of the Hydrophobic Gap. The hydrophobic gap above an OTS layer submerged in water has become a topic of many recent studies.[28,68,69] Because this gap is a layer with a low-density contrast, it requires reflectivity curves up to higher q_z values than reached in this study to draw valid conclusions. However, because it is expected that proteins tend to expose their hydrophobic residues to the OTS layer, induced by the hydrophobic effect, we note the following interesting observation: the depth and width of the depletion zone seem to be influenced by the quality of the OTS layer, as was inferred from measurements with a batch of OTS-covered samples exhibiting a slightly higher water contact angle hysteresis than usual. The adsorption of proteins can decrease or increase this depletion zone, depending again on the layer quality. Thus, the interfacial roughness between the protein and substrate is also influenced; however, the adsorbed amount is not, as could be shown in repeated measurements (Figure 5 and SI).

In this section, we have put forward several hypotheses concerning processes involved in adsorbate formation. To support these, further experiments are highly desirable (e.g., a time-resolved characterization of the buildup of the film). In the

SI, a brief outlook is given as to how this may be achieved in the future with X-ray reflectivity measurements.

CONCLUSIONS

This study analyzed the interfacial structure of adsorbed protein films by in situ X-ray reflectometry. From the analysis of the scattering curves, the film structure and the adsorbed amounts of α-amylase, BSA, and lysozyme on four different types of substrates are retrieved at high resolution. Silicon wafers with native and thermally grown oxide layers are chosen as hydrophilic substrates and coated with an OTS layer to gain hydrophobic substrates. Thus, the surface chemistry and subsurface composition of the substrates can be varied separately in a well-defined manner. The influence of the van der Waals forces between the substrate and proteins can be tested by varying the silicon oxide thickness.

Irrespective of the actual surface chemistry, the results clearly exhibit evidence of the influence of the subsurface material on the protein adsorbates up to several nanometers below the solid/liquid interface. More precisely, the properties of the uppermost surface layer are responsible for the extent of denaturation of the proteins determining the protein layer thickness; the subsurface composition, however, influences the density of the layer and thereby the final adsorbed amount of protein. When we compare the different surfaces, the trends in the adsorbed amount are sustained for every protein species (reflecting different charges, geometries, sizes, and conformational stabilities) and for all pH values tested. These trends are inverse on hydrophilic and hydrophobic surfaces and therefore indicate that surface processes after the initial adsorption are involved in the structure formation of the protein films.[61,62]

To conclude, surface processes after the initial adsorption may vary with the surface chemistry, yet surface processes and their time constant are sensitive to van der Waals forces arising from buried layers.

A future challenge will be to directly identify the involved surface processes and measure and simulate the respective influence of the attractive surface potential.

ASSOCIATED CONTENT

Supporting Information

Reflectivity data corresponding to the presented volume fraction profiles. Electron density profiles addressing the behavior of the electron depletion zone. X-ray reflectivity measurements of the adsorption kinetics together with corresponding ellipsometric studies and considerations concerning the strength of the van der Waals forces between proteins and stratified substrates. This material is available free of charge via the Internet at http://pubs.acs.org.

AUTHOR INFORMATION

Corresponding Author

*E-mail: k.jacobs@physik.uni-saarland.de.

Present Address

[§]Condensed Matter Physics Laboratory, Heinrich Heine University Düsseldorf, 40225 Düsseldorf, Germany.

Notes

The authors declare no competing financial interest.

ACKNOWLEDGMENTS

We acknowledge financial support from the German Science Foundation under grant numbers GRK 1276 and GRK 532 and technical support by Wacker Siltronic AG (Burghausen, Germany). The DELTA machine group is gratefully acknowledged for providing synchrotron radiation and technical support. A.K.H. and T.B. thank the NRW Forschungsschule "Forschung mit Synchrotronstrahlung in den Nano- und Biowissenschaften" for financial support.

REFERENCES

(1) Norde, W. My voyage of discovery to proteins in flatland... and beyond. *Colloids Surf., B* **2008**, *61*, 1−9.
(2) Czeslik, C. Factors ruling protein adsorption. *Z. Phys. Chem.* **2004**, *218*, 771−801.
(3) Wahlgren, M.; Arnebrant, T. Protein adsorption to solid-surfaces. *Trends Biotechnol.* **1991**, *9*, 201−208.
(4) Malmsten, M., Ed. *Biopolymers at Interfaces*, 2nd ed.; Surfactant Science Series; Marcel Dekker: New York, 2003; Vol. *110*.
(5) Michael, K.; Vernekar, V.; Keselowsky, B.; Meredith, J.; Latour, R. A.; Garcia, A. Adsorption-induced conformational changes in fibronectin due to interactions with well-defined surface chemistries. *Langmuir* **2003**, *19*, 8033−8040.
(6) Anand, G.; Sharma, S.; Dutta, A. K.; Kumar, S. K.; Belfort, G. Conformational transitions of adsorbed proteins on surfaces of varying polarity. *Langmuir* **2010**, *26*, 10803−10811.
(7) Wertz, C.; Santore, M. Adsorption and reorientation kinetics of lysozyme on hydrophobic surfaces. *Langmuir* **2002**, *18*, 1190−1199.
(8) Quinn, A.; Mantz, H.; Jacobs, K.; Bellion, M.; Santen, L. Protein adsorption kinetics in different surface potentials. *Europhys. Lett.* **2008**, *81*, 56003.
(9) Bellion, M.; Santen, L.; Mantz, H.; Haehl, H. A.; Quinn, A.; Nagel, A.; Gilow, C.; Weitenberg, C.; Schmitt, Y.; Jacobs, K. Protein adsorption on tailored substrates: long-range forces and conformational changes. *J. Phys.: Condens. Matter* **2008**, *20*, 404226.
(10) Schmitt, Y.; Haehl, H.; Gilow, C.; Mantz, H.; Jacobs, K.; Leidinger, O.; Bellion, M.; Santen, L. Structural evolution of proteinbiofilms: simulations and experiments. *Biomicrofluidics* **2010**, *4*, 032201.
(11) Déjardin, P., Ed. *Proteins at Solid-Liquid Interfaces: Principles and Practice*; Springer: Heidelberg, Germany, 2006.
(12) Koo, J.; Gutberlet, T.; Czeslik, C. Control of protein interfacial affinity by nonionic cosolvents. *J. Phys. Chem. B* **2008**, *112*, 6292−6295.
(13) Evers, F.; Steitz, R.; Tolan, M.; Czeslik, C. Reduced protein adsorption by osmolytes. *Langmuir* **2011**, *27*, 6995−7001.
(14) Sharp, J.; Forrest, J.; Jones, R. Surface denaturation and amyloid fibril formation of insulin at model lipid-water interfaces. *Biochemistry* **2002**, *41*, 15810−15819.
(15) Roach, P.; Farrar, D.; Perry, C. Interpretation of protein adsorption: surface-induced conformational changes. *J. Am. Chem. Soc.* **2005**, *127*, 8168−8173.
(16) Roach, P.; Farrar, D.; Perry, C. Surface tailoring for controlled protein adsorption: effect of topography at the nanometer scale and chemistry. *J. Am. Chem. Soc.* **2006**, *128*, 3939−3945.
(17) Munday, J. N.; Capasso, F.; Parsegian, V. A. Measured long-range repulsive Casimir-Lifshitz forces. *Nature* **2009**, *457*, 170−173.
(18) Israelachvili, J. N. *Intermolecular and Surface Forces*, 2nd ed.; Academic Press: London, 1991; p 480.
(19) Seemann, R.; Herminghaus, S.; Jacobs, K. Dewetting patterns and molecular forces: a reconciliation. *Phys. Rev. Lett.* **2001**, *86*, 5534−5537.
(20) Herminghaus, S.; Jacobs, K.; Mecke, K. R.; Bischof, J.; Fery, A.; Ibn-Elhaj, M.; Schlagowski, S. Spinodal dewetting in liquid crystal and liquid metal films. *Science* **1998**, *282*, 916−919.
(21) Loskill, P.; Hähl, H.; Thewes, N.; Kreis, C. T.; Bischoff, M.; Herrmann, M.; Jacobs, K. Influence of the Subsurface Composition of a Material on the Adhesion of Staphylococci. *Langmuir* **2012**, *28*, 7242−7248.
(22) Huber, G.; Mantz, H.; Spolenak, R.; Mecke, K. R.; Jacobs, K.; Gorb, S.; Arzt, E. Evidence for capillarity contributions to gecko

adhesion from single spatula nanomechanical measurements. *Proc. Natl. Acad. Sci. U.S.A.* **2005**, *102*, 16293−16296.
(23) Paulus, M.; Lietz, D.; Sternemann, C.; Shokuie, K.; Evers, F.; Tolan, M.; Czeslik, C.; Winter, R. An access to buried interfaces: the X-ray reflectivity set-up of BL9 at DELTA. *J Synchrotron Radiat.* **2008**, *15*, 600−605.
(24) Evers, F.; Shokuie, K.; Paulus, M.; Sternemann, C.; Czeslik, C.; Tolan, M. Exploring the interfacial structure of protein adsorbates and the kinetics of protein adsorption: an in situ high-energy X-ray reflectivity study. *Langmuir* **2008**, *24*, 10216−10221.
(25) Evers, F.; Shokuie, K.; Paulus, M.; Tiemeyer, S.; Sternemann, C.; Czeslik, C.; Tolan, M. Characterizing the structure of protein layers adsorbed onto functionalized surfaces by means of in-situ X-ray reflectivity. *Eur. Phys. J. Spec. Top.* **2009**, *167*, 185−189.
(26) Brzoska, J.; Benazouz, I.; Rondelez, F. Silanization of solid substrates - a step toward reproducibility. *Langmuir* **1994**, *10*, 4367−4373.
(27) Wassermann, S.; Whitesides, G.; Tidswell, I.; Ocko, B. M.; Pershan, P.; Axe, J. The structure of self-assembled monolayers of alkylsiloxanes on silicon - a comparison of results from ellipsometry and low-angle X-ray reflectivity. *J. Am. Chem. Soc.* **1989**, *111*, 5852−5861.
(28) Mezger, M.; Reichert, H.; Schoeder, S.; Okasinski, J.; Schroeder, H.; Dosch, H.; Palms, D.; Ralston, J.; Honkimaeki, V. High-resolution in situ X-ray study of the hydrophobic gap at the water-octadecyltrichlorosilane interface. *Proc. Natl. Acad. Sci. U.S.A.* **2006**, *103*, 18401−18404.
(29) Tidswell, I.; Rabedeau, T.; Pershan, P.; Kosowsky, S.; Folkers, J.; Whitesides, G. X-ray grazing-incidence diffraction from alkylsiloxane monolayers on silicon-wafers. *J. Chem. Phys.* **1991**, *95*, 2854−2861.
(30) Jacobs, K.; Seemann, R.; Herminghaus, S. In *Polymer Thin Films*; Tsui, O. K., Russell, T. P., Eds.; Soft Condensed Matter; World Scientific: Singapore, 2008; Vol. *1*, Chapter 10.
(31) Ramasubbu, N.; Paloth, V.; Luo, Y.; Brayer, G.; Levine, M. Structure of human salivary alpha-amylase at 1.6 angstrom resolution: implications for its role in the oral cavity. *Acta Crystallogr., Sect. D* **1996**, *52*, 435−446.
(32) Diamond, R. Real-space refinement of structure of hen egg-white lysozyme. *J. Mol. Biol.* **1974**, *82*, 371−391.
(33) Zhang, F.; Skoda, M.W. A.; Jacobs, R.M. J.; Martin, R. A.; Martin, C. M.; Schreiber, F. Protein interactions studied by SAXS: effect of ionic strength and protein concentration for BSA in aqueous solutions. *J. Phys. Chem. B* **2007**, *111*, 251−259.
(34) Hollmann, O.; Gutberlet, T.; Czeslik, C. Structure and protein binding capacity of a planar PAA brush. *Langmuir* **2007**, *23*, 1347−1353.
(35) Hu, S.; Xie, Y.; Ramachandran, P.; Loo, R.; Li, Y.; Loo, J.; Wong, D. Large-scale identification of proteins in human salivary proteome by liquid chromatography/mass spectrometry and two-dimensional gel electrophoresis-mass spectrometry. *Proteomics* **2005**, *5*, 1714−1728.
(36) Arnebrant, T. In *Biopolymers at Interfaces*, 2nd ed.; Malmsten, M., Ed.; Surfactant Science Series; Marcel Dekker: New York, 2003; Vol. *110*, Chapter 29, pp 811−855.
(37) Roth, C. M.; Lenhoff, A. M. Electrostatic and van der Waals contributions to protein adsorption: comparison of theory and experiment. *Langmuir* **1995**, *11*, 3500−3509.
(38) Miller, C.; Majewski, J.; Gog, T.; Kuhl, T. Characterization of biological thin films at the solid-liquid interface by X-ray reflectivity. *Phys. Rev. Lett.* **2005**, *94*, 238104.
(39) Reich, C.; Hochrein, M.; Krause, B.; Nickel, B. A microfluidic setup for studies of solid-liquid interfaces using X-ray reflectivity and fluorescence microscopy. *Rev. Sci. Instrum.* **2005**, *76*, 095103.
(40) Taking the energy and flux of the beam into account, radiation damage is expected to occur only for exposure times exceeding 4 h. Subsequent scans (each recorded in ca. 0.5 h) showed no changes due to radiation damage, for example, in the increased electron density of the protein film near the surface.
(41) Tolan, M. *X-ray Scattering from Soft-Matter Thin Films*; Springer Tracts in Modern Physics 148; Springer: Heidelberg, Germany, 1999.
(42) Russell, T. P. X-ray and neutron reflectivity for the investigation of polymers. *Mater. Sci. Rep.* **1990**, *5*, 171−271.
(43) Parratt, L. G. Surface studies of solids by total reflection of X-rays. *Phys. Rev.* **1954**, *95*, 359−369.
(44) Richter, A.; Yu, C.; Datta, A.; Kmetko, J.; Dutta, P. In situ and interrupted-growth studies of the self-assembly of octadecyltrichlorosilane monolayers. *Phys. Rev. E* **2000**, *61*, 607−615.
(45) The Center for X-Ray Optics. http://www.cxro.lbl.gov/.
(46) Hüsecken, A. K.; Evers, F.; Czeslik, C.; Tolan, M. Effect of urea and glycerol on the adsorption of ribonuclease A at the air−water interface. *Langmuir* **2010**, *26*, 13429−13435.
(47) Lu, J.; Su, T.; Thirtle, P.; Thomas, R.; Rennie, A.; Cubitt, R. The denaturation of lysozyme layers adsorbed at the hydrophobic solid/liquid surface studied by neutron reflection. *J. Colloid Interface Sci.* **1998**, *206*, 212−223.
(48) Raffaini, G.; Ganazzoli, F. Protein adsorption on a hydrophobic surface: a molecular dynamics study of lysozyme on graphite. *Langmuir* **2010**, *26*, 5679−5689.
(49) Ebbinghaus, S.; Kim, S. J.; Heyden, M.; Yu, X.; Heugen, U.; Gruebele, M.; Leitner, D. M.; Havenith, M. An extended dynamical hydration shell around proteins. *Proc. Natl. Acad. Sci. U.S.A.* **2007**, *104*, 20749−20752.
(50) Ramsden, J. J.; Bachmanova, G.; Archakov, A. Kinetic evidence for protein clustering at a surface. *Phys. Rev. E* **1994**, *50*, 5072−5076.
(51) Mulheran, P. A.; Pellenc, D.; Bennett, R. A.; Green, R. J.; Sperrin, M. Mechanisms and dynamics of protein clustering on a solid surface. *Phys. Rev. Lett.* **2008**, *100*, 068102.
(52) Rabe, M.; Verdes, D.; Seeger, S. Understanding cooperative protein adsorption events at the microscopic scale: a comparison between experimental data and monte carlo simulations. *J. Phys. Chem. B* **2010**, *114*, 5862−5869.
(53) Jackler, G.; Steitz, R.; Czeslik, C. Effect of temperature on the adsorption of lysozyme at the silica/water interface studied by optical and neutron reflectometry. *Langmuir* **2002**, *18*, 6565−6570.
(54) Wahlgren, M.; Arnebrant, T.; Lundstrom, I. The adsorption of lysozyme to hydrophilic silicon-oxide surfaces: comparison between experimental-data and models for adsorption-kinetics. *J. Colloid Interface Sci.* **1995**, *175*, 506−514.
(55) Su, T.; Lu, J.; Thomas, R.; Cui, Z.; Penfold, J. The effect of solution pH on the structure of lysozyme layers adsorbed at the silica−water interface studied by neutron reflection. *Langmuir* **1998**, *14*, 438−445.
(56) Peters, T., Jr. *Adv. Protein Chem.* **1985**, *37*, 161−245.
(57) Zhang, Y.; Cremer, P. S. Chemistry of Hofmeister anions and osmolytes. *Annu. Rev. Phys. Chem.* **2010**, *61*, 63−83.
(58) Evers, F.; Steitz, R.; Tolan, M.; Czeslik, C. Analysis of Hofmeister effects on the density profile of protein adsorbates: a neutron reflectivity study. *J. Phys. Chem. B* **2009**, *113*, 8462−8465.
(59) Parsegian, V. A. *Van der Waals Forces*; Cambridge University Press: New York, 2006.
(60) Roth, C. M.; Neal, B.; Lenhoff, A. M. Van der Waals interactions involving proteins. *Biophys. J.* **1996**, *70*, 977−987.
(61) Tilton, R. D. In *Biopolymers at Interfaces*, 2nd ed.; Malmsten, M., Ed.; Surfactant Science Series; Marcel Dekker: New York, 2003; Vol. *110*, Chapter 9, pp 221−257.
(62) Wertz, C.; Santore, M. Adsorption and relaxation kinetics of albumin and fibrinogen on hydrophobic surfaces: Single-species and competitive behavior. *Langmuir* **1999**, *15*, 8884−8894.
(63) Haggerty, L.; Lenhoff, A. Analysis of ordered arrays of adsorbed lysozyme by scanning tunneling microscopy. *Biophys. J.* **1993**, *64*, 886−895.
(64) Burghardt, T.; Axelrod, D. Total internal reflection-fluorescence photobleaching recovery study of serum-albumin adsorption dynamics. *Biophys. J.* **1981**, *33*, 455−467.
(65) Tilton, R.; Robertson, C.; Gast, A. Lateral diffusion of bovine serum albumin adsorbed at the solid-liquid interface. *J. Colloid Interface Sci.* **1990**, *137*, 192−203.

(66) Tilton, R.; Gast, A.; Robertson, C. Surface diffusion of interacting proteins: effect of concentration on the lateral mobility of adsorbed bovine serum-albumin. *Biophys. J.* **1990**, *58*, 1321−1326.
(67) Hinrichsen, E.; Feder, J.; Jøssang, T. Geometry of random sequential adsorption. *J. Stat. Phys.* **1986**, *44*, 793−827.
(68) Poynor, A.; Hong, L.; Robinson, I. K.; Granick, S.; Zhang, Z.; Fenter, P. A. How water meets a hydrophobic surface. *Phys. Rev. Lett.* **2006**, *97*, 266101.
(69) Mezger, M.; Sedlmeier, F.; Horinek, D.; Reichert, H.; Pontoni, D.; Dosch, H. On the origin of the hydrophobic water gap: an X-ray reflectivity and MD simulation study. *J. Am. Chem. Soc.* **2010**, *132*, 6735−6741.

Addendum III - The Influence of the Subsurface Composition of a Material on the Adhesion of *Staphylococci*

Authors: P. Loskill[1], H. Hähl[1], N. Thewes[1], C. T. Kreis[1], M. Bischoff[2], M. Herrmann[2], and K. Jacobs[1]

[1] Department of Experimental Physics, Saarland University, 66041 Saarbrücken, Germany. [2] The Institute of Medical Microbiology and Hygiene, Saarland University, 66421 Homburg/Saar, Germany.

Langmuir **28**, 7242–7248 (2012).
(http://dx.doi.org/10.1021/la3004323)

Author contributions:
Experiments were conceived and designed by P. Loskill, H. Hähl, M. Bischoff, M. Herrmann, and K. Jacobs. AFM experiments were performed by P. Loskill and N. Thewes. Flow chamber experiments were performed by C. T. Kreis. Data was analyzed by P. Loskill. The article was written by P. Loskill and K. Jacobs. Research was directed by M. Herrmann and K. Jacobs.

Abstract - Controlling the interface between bacteria and solid materials has become an important task in biomedical science. For a fundamental and comprehensive understanding of adhesion it is necessary to seek quantitative information about the involved interactions. Most studies concentrate on the modification of the surface (chemical composition, hydrophobicity or topography), neglecting, however, the influence of the bulk material, which always contributes to the overall interaction via van der Waals forces. In this study, we applied AFM force spectroscopy and flow chamber experiments to probe the adhesion of *S. carnosus* to a set of tailored Si wafers, allowing for a separation of short- and long-range forces. We provide experimental evidence that the subsurface composition of a substrate influences bacterial adhesion. A coarse estimation of the strength of the van der Waals forces via the involved Hamaker constants substantiates the experimental results. The results demonstrate that the uppermost layer is not solely responsible for the strength of adhesion. Rather, for all kinds of adhesion studies, it is equally important to consider the contribution of the subsurface.

Langmuir

Influence of the Subsurface Composition of a Material on the Adhesion of *Staphylococci*

Peter Loskill,[†] Hendrik Hähl,[†] Nicolas Thewes,[†] Christian Titus Kreis,[†] Markus Bischoff,[‡] Mathias Herrmann,[‡] and Karin Jacobs*[,†]

[†]Department of Experimental Physics, Saarland University, Saarbrücken, 66041, Germany

[‡]The Institute of Medical Microbiology and Hygiene, Saarland University, Homburg/Saar, 66421, Germany

ABSTRACT: Controlling the interface between bacteria and solid materials has become an important task in biomedical science. For a fundamental and comprehensive understanding of adhesion it is necessary to seek quantitative information about the involved interactions. Most studies concentrate on the modification of the surface (chemical composition, hydrophobicity, or topography) neglecting, however, the influence of the bulk material, which always contributes to the overall interaction via van der Waals forces. In this study, we applied AFM force spectroscopy and flow chamber experiments to probe the adhesion of *Staphylococcus carnosus* to a set of tailored Si wafers, allowing for a separation of short- and long-range forces. We provide experimental evidence that the subsurface composition of a substrate influences bacterial adhesion. A coarse estimation of the strength of the van der Waals forces via the involved Hamaker constants substantiates the experimental results. The results demonstrate that the uppermost layer is not solely responsible for the strength of adhesion. Rather, for all kinds of adhesion studies, it is equally important to consider the contribution of the subsurface.

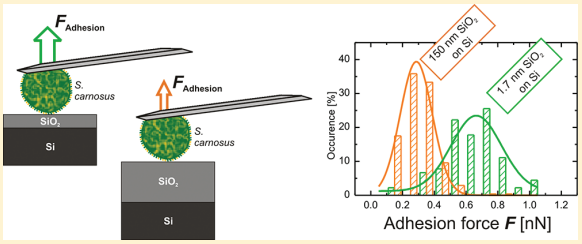

INTRODUCTION

Adhesion and adsorption of proteins and bacteria onto inorganic surfaces is crucial in various biomedical fields, such as biofilm formation or DNA arrays.[1,2] Thus, it has become an important task to control the interface between organic (macro)molecules and solid materials. The relevant interactions can be tuned by modifying the substrates: Most studies concentrate on the modification of the surface chemistry, the hydrophobicity, or the topography. That way, the short-range interactions are tuned.[3,4] The composition beneath the surface, however, is mostly overlooked and thereby long-range interactions are disregarded. Previous studies focusing on polymer dewetting[5,6] and liquid nanodroplets[7] showed an effect of differences in long-range van der Waals (vdW) interactions. These differences had been provoked by a variation of the subsurface composition. Similar observations have been reported for biological systems such as the adhesion of geckos[8] and the adsorption of proteins.[9]

Bacterial adhesion is mediated by proteins.[10] Hence, an influence of van der Waals interactions on the bacterial adhesion is also expected. Previous studies, however, were not able to separate parameters influencing short-range, electrostatic, and van der Waals interactions independently.[11,12] Yet, for a comprehensive understanding of the bacterial adhesion process it is necessary to seek quantitative information about the contributions of the involved interactions. In this study, we are able to tune van der Waals forces separately from other forces by using a set of tailored silicon wafers (Figure 1A): The set consists of wafers with a native oxide layer ["type N", d = 1.7(2) nm] and wafers with a thermally grown thick oxide layer ["type T", d = 150(2) nm]. Another pair of wafers with different surface properties was obtained by hydrophobizing the naturally hydrophilic wafers. Short-range interactions do not depend on the thickness of the silicon dioxide layer, whereas long-range vdW interactions do.[13,14]

The adhesion onto synthetic surfaces and the formation of biofilms is a key factor for the pathogenesis of bacteria from multiple different species.[1,15] Some species of the *Staphylococcus* genus, for instance, are known to adhere strongly to surfaces and are capable of forming biofilms[16] that are extremely resistant to removal and to antimicrobial drugs.[17] Here, we were interested in the unspecific interactions acting between a bacterium and a surface. Therefore, we concentrated on *Staphylococcus carnosus* strain TM300, an apathogenic member of the genus *Staphylococcus* and an important organism in food manufacturing, which usually serves as host organism for gene cloning.[18]

To characterize the adsorption of microorganisms to surfaces, typically parallel plate flow chambers are used.[19] In this macroscopic approach, adsorption, adhesion, and desorption effects are indistinguishable. In the past decades, some new tools have been introduced that allow for a quantitative study of bacterial adhesion, e.g., atomic force microscope (AFM).[20] Using the force spectroscopy mode of an AFM it is possible to

Received: January 30, 2012
Revised: March 2, 2012
Published: April 4, 2012

Langmuir Article

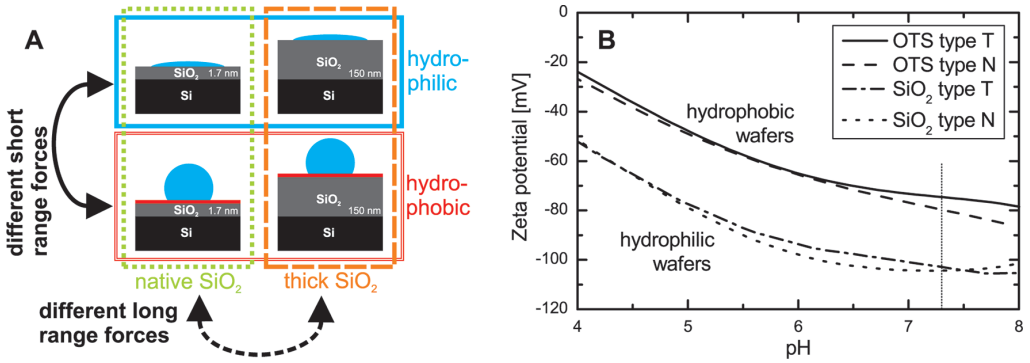

Figure 1. (A) Model substrates based on silicon wafers with different thicknesses of oxide layers that allow for a separation of effects due to short- and long-range forces. Short-range interactions are tuned by a silanization of the wafers that renders them hydrophobic. The blue droplet illustrates the different water contact angles. (B) Zeta potentials of hydrophobic and hydrophilic type T and N wafers as function of pH, giving insight into the strength of electrostatic interactions. Since the zeta potentials are indistinguishable for type T and N wafers with the same surface chemistry, differences in SiO_2 layer thickness are irrelevant for the electrostatic interactions.

probe a wide range of forces in a biologically relevant magnitude (pN to μN). A direct method to characterize bacterial adhesion onto various substrates is to use AFM probes that are covered with bacteria ("bacterial probes").[4,11,21] In this study, we used AFM force spectroscopy with bacterial probes to investigate the adhesion of *S. carnosus* (TM300) to the set of tailored silicon wafers. Since bacteria in an already adhered state (bacterial probes) might react differently as compared to bacteria in planktonic state, we also performed macroscopic flow chamber experiments with the same set of Si wafers.

MATERIALS AND METHODS

Preparation of the Substrates. The silicon wafers with the native [type N, d = 1.7(2) nm] silicon oxide layer were purchased from Wacker Siltronic AG (Burghausen, Germany) and the ones with the thick thermally grown layer [type T, d = 150(2) nm] were from Silchem (Freiberg, Germany). The substrates were cleaned by immersing them for 30 min in fresh 1:1 H_2SO_4 (conc)/H_2O_2 (30%) solution. To remove residues of the acids, the wafers were put in boiling deionized water for 90 min, the water being changed four times in between. The hydrophobic substrates were obtained by functionalizing the cleaned wafers using a liquid phase preparation of self-assembling silane molecules with a CH_3 tailgroup (octadecyltrichlorosilane, OTS, purchased from Sigma-Aldrich) following standard procedures.[22] The produced OTS surfaces feature a thickness of ≈2.6 nm, an rms roughness below 0.2 nm, and an uniform coverage, indicating a homogeneous, dense, upright, all-trans configuration of the molecules. All types of substrates were characterized by AFM, ellipsometry, zeta potential, and contact angle measurements (Figure 1B and Table 1).

Bacteria. We took stationary phase cells for the experiments. *S. carnosus* strain TM300 was cultured from blood agar plates in 5 mL of Mueller Hinton broth for 24 h at 37 °C. To remove extracellular material, bacteria were washed once with 1 mL of NaCl solution (0.9% w/v) and twice with phosphate-buffered saline (PBS, pH 7.3), each with 1 mL. Finally, the bacteria were resuspended in 300 μL of PBS and stored at 4 °C (for typically 2 h and a maximum of 48 h).

Table 1. Parameters of the Model Substrates: Root Mean Square (rms) Roughness, Advancing (adv) and Receding (rec) Contact Angles Θ of Water, and the Surface Energy γ

d_{SiO_2} (nm)	surface	rms (nm)	Θ_{adv} (deg)	Θ_{rec} (deg)	γ (mJ/m^2)
151(1)	hydrophobic	0.15(2)	112(1)	108(4)	24(1)
1.7(3)	hydrophobic	0.12(2)	111(1)	107(2)	24(1)
151(1)	hydrophilic	0.13(3)	5(2)	compl wetting	63(1)
1.7(3)	hydrophilic	0.09(2)	7(2)	compl wetting	64(1)

Preparation of Bacterial Probes. To immobilize bacteria onto tipless cantilevers we used poly-L-lysine, PLL (MP Biomedicals, Solon, OH), a polymer with positively charged side chains. Since the surfaces of both the bacterium and the cantilever are negatively charged in buffer (pH 7.3), PLL forms an adhesive interlayer.[23] Prior to the preparation procedure, the cantilevers were cleaned by treating them with an air plasma. The PLL coating was then applied by immersing the AFM cantilever in a droplet of poly-L-lysine solution (0.1 mg/mL) for 1 h. Subsequently, the cantilevers were carefully rinsed with PBS and placed in a droplet of bacteria solution for 1 h at 4 °C. To remove unbound bacteria, the probes were rinsed with PBS buffer. All probes used in this study were prepared immediately before the experiments.

AFM-Force Measurements. Experiments were conducted in PBS (pH 7.3) at room temperature with a Bioscope Catalyst (Bruker, Santa Barbara, CA). Each experiment consists of at least five series of 100 single force/distance curves. Every cantilever was calibrated using the thermal tune technique.[24] To avoid systematic errors due to local irregularities of the surface, every measurement was done on a different spot on a grid with separations of 5 μm. Single force measurements were carried out using a z-range of 1 μm, a scan rate of 1 Hz, and a relative force trigger of 1 nN. Adhesion forces were evaluated with the Nanoscope software (Bruker, Santa Barbara, CA) by calculating the difference between the adhesion peak[25] and the baseline for every single curve.[26] All single values on each substrate were fitted using a Gaussian curve. Displayed error bars describe the standard deviation.

Bacterial Probes. The bacterial probes were based on tipless cantilevers (PNP-TR-TL, Nanoworld, NeuchÃćtel, Switzerland) onto which bacteria were allowed to adsorb (Figure 2). The restricting issue of this type of probe is the comparability of serial measurements due to the uncertainty of the number of bacteria that are in contact with the substrate's surface. Therefore, it is not possible to compare measurements with different cantilevers. Measurements with the same cantilever on different substrates, however, are comparable as long as the integrity of the bacterial probe can be granted by, for example, an optical control or control measurements. We therefore always carried out the experiments on a type T and a type N wafer with the identical AFM probe. Within one experiment, consecutive series of force/distance measurements were taken alternately on the type N and T substrates, ending always on the substrate that has been probed first.

Flow Chamber Measurements. Bacteria solution of different concentrations was pumped through a custom parallel flow chamber system with dimensions 2 × 1.6 × 3 cm^3, chosen to guarantee a

Langmuir Article

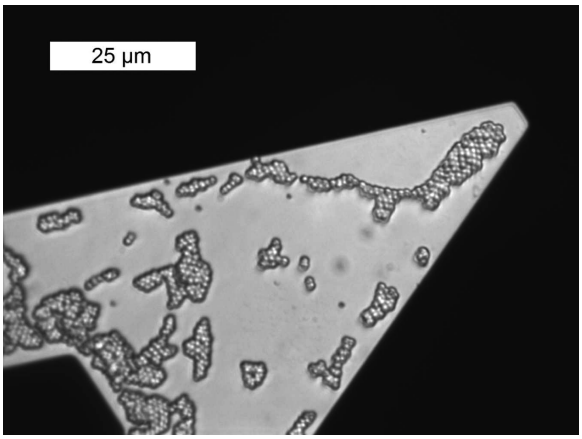

Figure 2. Optical microscopy image of *S. carnosus* immobilized by poly-L-lysine on a tipless cantilever.

uniform flow profile.[27] Measurements on type T and N substrates were always carried out using the same bacteria solution and in random order. The images were taken with a CCD-camera (Pixelfly, PCO, Kelheim, Germany), through a light microscope (Axiophot, Zeiss, Oberkochen, Germany) at a frame rate of 0.1 Hz. The number of adhering bacteria was determined using image analysis software (Image Pro Plus, Media Cybernetics, Bethesda, MD).

RESULTS

To determine whether the subsurface composition has an effect on bacterial adhesion, AFM force spectroscopy experiments with bacterial probes were carried out on all four wafer types. To distinguish from effects due to the surface chemistry, we compare the results of the two hydrophilic substrates and of the two hydrophobic substrates separately.

AFM Force Spectroscopy on Hydrophilic Substrates. Force/distance measurements on the two hydrophilic wafer types (Figure 3A) reveal a higher adhesion force on the type N than on the type T wafers. The distribution of the determined adhesion forces on the hydrophilic SiO_2 surfaces is shown in Figure 3B in the form of a histogram. We determined an average adhesion force on the hydrophilic type N wafer of F_N = 0.65(18)[28] nN and on the type T wafer of F_T = 0.30(10) nN. The integrity of the bacterial probes (detaching bacteria or other probe alteration) is controlled by two means:

(i) optical microscopy prior to and after the experiment;
(ii) control measurements, where consecutive series of force/distance measurements were taken alternately on the type N and type T substrates, ending always on the substrate that has been probed first.

In this case, (i) no detaching of bacteria was observed and (ii) the comparison of the force distribution of the different series is shown in Figure 3C,D. The means of each single series on type T wafers (I, III, V) and on type N wafers (II, IV) are identical within the experimental error.

AFM Force Spectroscopy on Hydrophobic Substrates. The determined adhesion forces on the hydrophobic substrates exhibit the same trend. The identical type of measurements including the test of the integrity of the bacterial probes was performed on the hydrophobic OTS-coated wafers. The force/distance curves (Figure 4A) resemble the ones on the hydrophilic wafers, whereby the bacterial probes stayed also intact. The average adhesion force (Figure 4B) on the hydrophobic type N wafer is F_N = 5.2(10) nN and on the type T wafer is F_T = 3.2(12) nN. Experiments with different bacterial probes lead to different absolute values (due to different densities of the bacterial layer), but the ratio is always similar (Figure 4C). The average forces on the hydrophobic substrates, however, are about one magnitude higher than the corresponding forces on the hydrophilic wafers. This

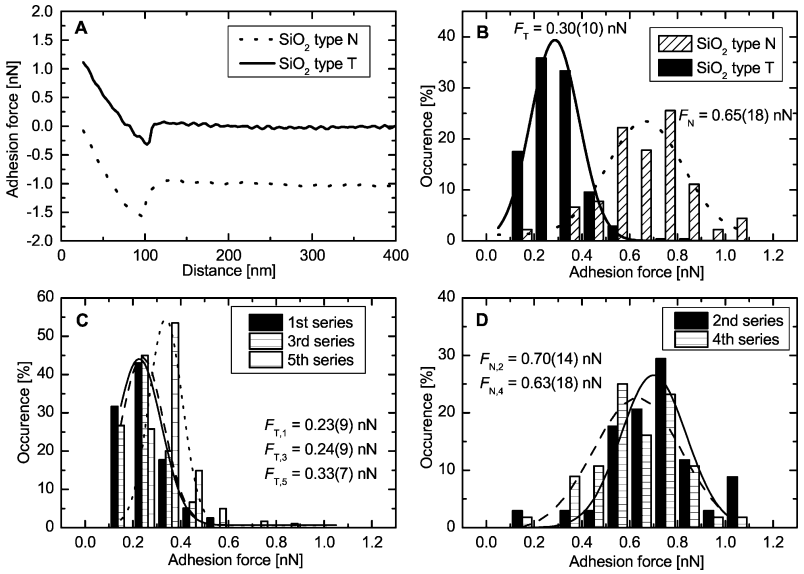

Figure 3. Results of AFM force spectroscopy experiments on bare hydrophilic substrates: (A) Retract parts of two typical force/distance measurements between a bacterial probe and a type N and a type T wafer, respectively. For a clearer display, the curve on the type N wafer is shifted by −1 nN. (B) Distribution of the determined adhesion forces. (C, D) Data of part B are shown as separated series. Odd series were performed on type T (C) and even series on type N wafers (D).

dx.doi.org/10.1021/la3004323 | Langmuir 2012, 28, 7242−7248

Langmuir Article

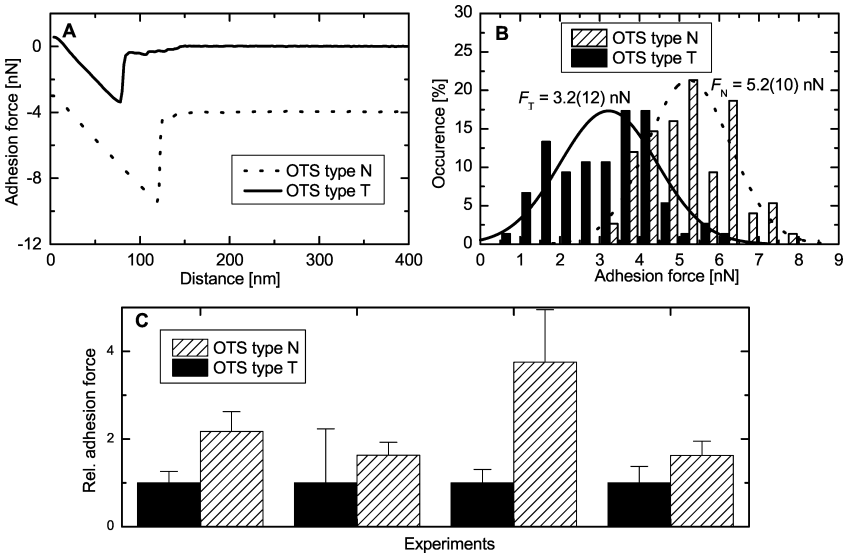

Figure 4. Results of AFM force spectroscopy experiments on hydrophobic substrates: (A) Retract parts of two typical force/distance measurements between a bacterial probe and a type N and a type T wafer, respectively. For a clearer display, the curve on the type N wafer is shifted by −4 nN. (B) Distribution of the determined adhesion forces. (C) Average force values (scaled with F_T) of multiple experiments with different cantilevers.

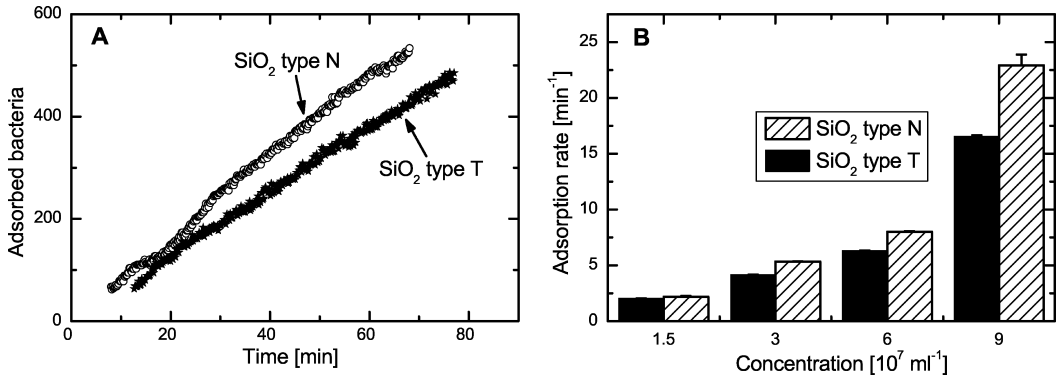

Figure 5. Results of the flow chamber experiments on the hydrophilic substrates: (A) number of the adsorbed bacteria in the field of view on type N and on type T wafers. (B) Adsorption rates of multiple experiments with different concentrations of the bacteria solution.

comparison supports the findings of previous studies, namely that increased hydrophobicity typically boosts adhesion.

Flow Chamber Experiments. Macroscopic adsorption experiments corroborate the results of the microscopic adhesion measurements. Using a custom-built parallel plate flow chamber setup, the growth of the number of bacteria adsorbed to the set of substrates was determined for multiple concentrations. The number of adsorbed bacteria grows faster on the type N than on the type T wafers (Figure 5A). The adsorption rates, i.e., the slopes of linear fits, are always higher on the type N than on the type T substrates independent of the concentration (Figure 5B).

DISCUSSION

The force spectroscopy results show that on both the hydrophilic and the hydrophobic wafers the bacterial adhesion force to the native SiO_2 layer is about twice as high as to the thick SiO_2 layer. Since the measurements were taken with the identical cantilever, the determined forces are reliable. This difference in adhesion forces is also observed for the adsorption of planktonic bacteria, as shown by the parallel plate flow chamber experiments. The surface properties that specifically influence the short-range interactions, e.g., hydrophobicity, roughness, and surface energy (Table 1), are independent of the thickness of the oxide layer. Hence, the difference in adhesion cannot be attributed to short-range forces. Also an effect of electrostatic interactions can be excluded for the explanation of the different adhesion forces, since the zeta potentials (Figure 1B) are identical within the experimental error on type T and N wafers. Therefore, only differences in van der Waals forces can explain the results. van der Waals forces are present in every system and cannot be completely shielded.[13,14,29] Often, vdW interactions are disregarded since they decrease proportional to d^{-6} with distance d, which yet is only correct for two interacting pointlike objects such as single atoms or molecules. For two macroscopic bodies, however, one obtains a lower exponent:[13,14] the nonretarded free energy between, for example, a sphere of radius R and a semifinite half-space is

dx.doi.org/10.1021/la3004323 | *Langmuir* 2012, 28, 7242−7248

Langmuir Article

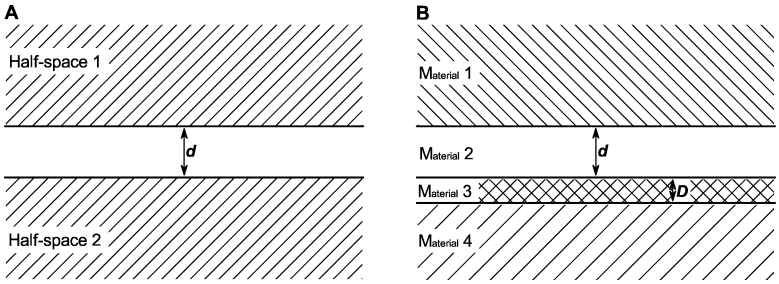

Figure 6. Schemes of two model systems: (A) interaction between two semifinite half-spaces and (B) interaction between a uniform material and a coated material.

$$W_{\mathrm{vdW}} = -R\frac{A}{6d} \tag{1}$$

and between two semifinite half-spaces (Figure 6A) is

$$w_{\mathrm{vdW}} = -\frac{A}{12\pi d^2} \tag{2}$$

per unit area, where A is the Hamaker constant of the system. It can be derived from the optical properties of the involved materials using the Lifschitz approach.[30] In the following we present a rough theoretical description of the system under study.

In principle, a bacterium can be described as a sphere of radius R consisting of two main components: the cytoplasm and the cell wall. Since the cytoplasm consists mainly of water, it has almost the same optical properties as the medium. The cell wall merely differs in its composition and consequently in its optical properties from the surrounding medium.[31] For small separations $d \ll R$, we use eq 2 and describe the system by three layers, namely, the cell wall, medium (buffer), and the substrate. In this study, the substrate is not a uniform bulk material but consists of multiple layers. In general, the vdW energy for a system (Figure 6B) consisting of a uniform half-space (M1), a medium (M2), and a half-space (M4) coated with a layer (M3) of thickness D can be calculated by[14,32]

$$w_{\mathrm{vdW}} = -\frac{1}{12\pi}\left(\frac{A_{12-32}}{d^2} + \frac{A_{12-43}}{(d+D)^2}\right) \tag{3}$$

where A_{12-32} (as well as A_{12-43}) are the Hamaker constants describing the interactions between the two interfaces M1/M2 and M2/M3 (as well as M1/M2 and M3/M4). In the system under study, the interacting interfaces are cell wall/buffer and buffer/silicon dioxide as well as cell wall/buffer and silicon dioxide/silicon. Since the cell wall features a nonuniform composition and barely accessible optical properties, we are not able to give exact theoretical values for the Hamaker constants. Nevertheless, as the polarizability of silicon dioxide (n = 1.46, ε = 3.9) is smaller than that of silicon (n = 4.13, ε = 11.8), we expect $A_{12-43} > 0$.[33] For this case, the second term in eq 3 increases the strength of the overall vdW interactions yet converges to zero for high layer thicknesses D (as on the type T substrates).

Hence, even without a comprehensive quantitative calculation, the experimental results can already be qualitatively explained by the fact that the bacterium on the type N wafer is "closer" to the strongly attractive Si bulk than if placed on a type T wafer. In other words, due to the stronger van der Waals attraction of the silicon, the bacteria experience higher adhesion forces on the wafers with a thin oxide layer. On the hydrophobic set of silicon wafers, the identical argumentation holds true, yet the contribution of an additional layer (the silane monolayer) has to be taken into account in a similar way as presented above for the oxide layer. Moreover, the results can be applied to clinical situations, where bacterial adhesion is preceded or accompanied by an adsorption of proteins, which may form a so-called conditioning layer.[34] This layer changes the surface properties of the substrate. Yet, since the thickness of the layer is usually on a nanometer scale, the unspecific adhesion forces will still be affected by the composition of the subsurface material. (The condition layer then acts like the OTS layer on the type N and T wafers.)

■ CONCLUSIONS

We have demonstrated that bacterial adhesion is influenced by the subsurface composition of a substrate. The reason for this is the strength of the vdW forces, which is given by (a) the type of geometry of two interacting objects (atom/atom or sphere/sphere), (b) their separation, (c) the composition of a stratified substrate, and (d) the polarizabilities of the involved materials. Keeping surface properties of the substrates constant, the influence of the van der Waals forces were probed by varying the subsurface composition. On Si wafers with different oxide layer thicknesses, the adhesion of *S. carnosus* was found to be about a factor of 2 stronger on the wafers with the thin oxide layer, no matter if covered by a molecular-sized hydrophobic layer or not. Consequently, for all types of adhesion studies, e.g., for the development of antibacterial substrates, it is important to characterize not only the surface properties but also the subsurface composition and to consider this in the analysis of the data. Particularly, thin coatings that promise to be antibacterial will have different effects depending on the underlying substrate! The effects could also explain inconsistent results of previous studies due to the different bulk substrates used.

■ AUTHOR INFORMATION

Corresponding Author

*E-mail: k.jacobs@physik.uni-saarland.de.

Notes

The authors declare no competing financial interest.

■ ACKNOWLEDGMENTS

This work was supported by the German Science Foundation under grant numbers GRK 1276 and INST 256/305-1 FUGG, by the German Federal Ministry for Education and Science grant 01 KI 1009E (Skin Staph), and by funds of the Federal

Langmuir Article

State of Saarland. We thank K. Hilgert for the help with handling the bacteria and R. Zimmermann for the zeta potential measurements.

REFERENCES

(1) (a) Costerton, J. W.; Stewart, P. S.; Greenberg, E. P. Bacterial biofilms: A common cause of persistent infections. *Science* **1999**, *284*, 1318−1322. (b) Costerton, J. W.; Cheng, K. J.; Geesey, G. G.; Ladd, T. I.; Nickel, J. C.; Dasgupta, M.; Marrie, T. J. Bacterial biofilms in nature and disease. *Annu. Rev. Microbiol.* **1987**, *41*, 435−464.

(2) Ramsay, G. DNA chips: State-of-the-art. *Nat. Biotechnol.* **1998**, *16*, 40−44.

(3) (a) Bowen, W. R.; Fenton, A. S.; Lovitt, R. W.; Wright, C. J. The measurement of *Bacillus mycoides* spore adhesion using atomic force microscopy, simple counting methods, and a spinning disk technique. *Biotechnol. Bioeng.* **2002**, *79*, 170−179. (b) Speranza, G.; Gottardi, G.; Pederzolli, C.; Lunelli, L.; Canteri, R.; Pasquardini, L.; Carli, E.; Lui, A.; Maniglio, D.; Brugnara, M.; Anderle, M. Role of chemical interactions in bacterial adhesion to polymer surfaces. *Biomaterials* **2004**, *25*, 2029−2037. (c) Tang, H.; Cao, T.; Liang, X.; Wang, A.; Salley, S. O.; Mcallister, J.; Ng, K. Y. S. Influence of silicone surface roughness and hydrophobicity on adhesion and colonization of *Staphylococcus epidermidis*. *J. Biomed. Mater. Res., Part A* **2009**, *88A*, 454−463. (d) Lamour, G.; Eftekhari-Bafrooei, A.; Borguet, E.; Soues, S.; Hamraoui, A. Neuronal adhesion and differentiation driven by nanoscale surface free-energy gradients. *Biomaterials* **2010**, *31*, 3762−3771.

(4) Emerson, R. J.; Bergstrom, T. S.; Liu, Y.; Soto, E. R.; Brown, C. A.; McGimpsey, W. G.; Camesano, T. A. Microscale correlation between surface chemistry, texture, and the adhesive strength of *Staphylococcus epidermidis*. *Langmuir* **2006**, *22*, 11311−11321.

(5) (a) Herminghaus, S.; Jacobs, K.; Mecke, K.; Bischof, J.; Fery, A.; Ibn-Elhaj, M.; Schlagowski, S. Spinodal dewetting in liquid crystal and liquid metal films. *Science* **1998**, *282*, 916−919. (b) Oron, A. Three-dimensional nonlinear dynamics of thin liquid films. *Phys. Rev. Lett.* **2000**, *85*, 2108−2111.

(6) Seemann, R.; Herminghaus, S.; Jacobs, K. Dewetting patterns and molecular forces: A reconciliation. *Phys. Rev. Lett.* **2001**, *86*, 5534−5537.

(7) Rauscher, M.; Dietrich, S. Nano-droplets on structured substrates. *Soft Matter* **2009**, *5*, 2997−3001.

(8) Loskill, P.; Puthoff, J. B.; Wilkinson, M.; Mecke, K.; Jacobs, K.; Autumn, K. Adhesion of gecko setae reflects nanoscale differences in subsurface energy. Submitted

(9) (a) Quinn, A.; Mantz, H.; Jacobs, K.; Bellion, M.; Santen, L. Protein adsorption kinetics in different surface potentials. *EPL* **2008**, *81*, 56003. (b) Bellion, M.; Santen, L.; Mantz, H.; Hähl, H.; Quinn, A.; Nagel, A. M.; Gilow, C.; Weitenberg, C.; Schmitt, Y.; Jacobs, K. Protein adsorption on tailored substrates: Long-range forces and conformational changes. *J. Phys.: Condens. Matter* **2008**, *20*, 404226. (c) Hähl, H.; Evers, F.; Grandthyll, S.; Paulus, M.; Sternemann, C.; Loskill, P.; Lessel, M.; Hüsecken, A. K.; Brenner, T.; Tolan, M.; Jacobs, K. Subsurface influence on the structure of protein adsorbates revealed by in situ X-ray reflectivity. Submitted

(10) Koebnik, R.; Locher, K. P.; van Gelder, P. Structure and function of bacterial outer membrane proteins: Barrels in a nutshell. *Mol. Microbiol.* **2000**, *37*, 239−253.

(11) (a) Ong, Y.-L.; Razatos, A.; Georgiou, G.; Sharma, M. M. Adhesion forces between *E. coli* bacteria and biomaterial surfaces. *Langmuir* **1999**, *15*, 2719−2725. (b) Stevens, M. J.; Donato, L. J.; Lower, S. K.; Sahai, N. Oxide-dependent adhesion of the Jurkat line of T lymphocytes. *Langmuir* **2009**, *25*, 6270−6278.

(12) Liu, C.; Zhao, Q. Influence of surface-energy components of Ni−P−TiO_2−PTFE nanocomposite coatings on bacterial adhesion. *Langmuir* **2011**, *27*, 9512−9519.

(13) Israelachvili, J. N. *Intermolecular and Surface Forces*, 2nd ed.; Academic Press: London, 1991.

(14) Parsegian, V. A. *Van der Waals forces*, 1st ed.; Cambridge University Press: New York, 2006.

(15) (a) Gristina, A. G. Biomaterial-centered infection: Microbial adhesion versus tissue integration. *Science* **1987**, *237*, 1588−1595. (b) Gristina, A. G.; Hobgood, C. D.; Webb, L. X.; Myrvik, Q. N. Adhesive colonization of biomaterials and antibiotic resistance. *Biomaterials* **1987**, *8*, 423−426.

(16) Götz, F. *Staphylococcus* and biofilms. *Mol. Microbiol.* **2002**, *43*, 1367−1378.

(17) (a) Lewis, K. Persister cells, dormancy and infectious disease. *Nat. Rev. Microbiol.* **2007**, *5*, 48−56. (b) Fux, C. A.; Costerton, J. W.; Stewart, P. S.; Stoodley, P. Survival strategies of infectious biofilms. *Trends Microbiol.* **2005**, *13*, 34−40.

(18) (a) Schleifer, K. H.; Fischer, U. Description of a New Species of the Genus *Staphylococcus*: *Staphylococcus carnosus*. *Int. J. Syst. Bacteriol.* **1982**, *32*, 153−156. (b) Götz, F. *Staphylococcus carnosus*: A new host organism for gene cloning and protein production. *J. Appl. Bacteriol.* **1990**, *69*, S49−S53.

(19) Harraghy, N.; Seiler, S.; Jacobs, K.; Hannig, M.; Menger, M.; Herrmann, M. Advances in in vitro and in vivo models for studying the staphylococcal factors involved in implant infections. *Int. J. Artif. Organs* **2006**, *29*, 368−378.

(20) Dufrene, Y. F. Atomic force microscopy, a powerful tool in microbiology. *J. Bacteriol.* **2002**, *184*, 5205−5213.

(21) (a) Razatos, A.; Ong, Y.-L.; Sharma, M. M.; Georgiou, G. Molecular determinants of bacterial adhesion monitored by atomic force microscopy. *Proc. Natl. Acad. Sci. U. S. A.* **1998**, *95*, 11059−11064. (b) Lower, S. K.; Tadanier, C. J.; Hochella, M. F. Measuring interfacial and adhesion forces between bacteria and mineral surfaces with biological force microscopy. *Geochim. Cosmochim. Acta* **2000**, *64*, 3133−3139.

(22) (a) Brzoska, J. B.; Azouz, I. B.; Rondelez, F. Silanization of solid substrates: A step toward reproducibility. *Langmuir* **1994**, *10*, 4367−4373. (b) Wasserman, S. R.; Whitesides, G. M.; Tidswell, I. M.; Ocko, B. M.; Pershan, P. S. Axe, J. D. The structure of self-assembled monolayers of alkylsiloxanes on silicon: A comparison of results from ellipsometry and low-angle X-ray reflectivity. *J. Am. Chem. Soc.* **1989**, *111*, 5852−5861.

(23) (a) Voet, D.; Voet, J. *Biochemistry*; John Wiley & Sons: New York, 1995. (b) West, J. K.; Latour, R. A.; Hench, L. L. Molecular modeling study of adsorption of poly-L-lysine onto silica glass. *J. Biomed. Mater. Res., Part A* **1997**, *37*, 585−591.

(24) Hutter, J. L.; Bechhoefer, J. Calibration of atomic-force microscope tips. *Rev. Sci. Instrum.* **1993**, *64*, 1868−1873.

(25) In the event of multiple adhesion peaks, the most pronounced one was evaluated.

(26) Carpick, R. W.; Batteas, J.; de Boer, M. P. Scanning probe studies of nanoscale adhesion between solids in the presence of liquids and monolayer films. In *Handbook of Nanotechnology*; Bhushan, B., Ed.; Springer Verlag: Berlin, 2007; pp 951−979.

(27) (a) van Wagenen, R. A.; Andrade, J. D. Flat plate streaming potential investigations: Hydrodynamics and electrokinetic equivalency. *J. Colloid Interface Sci.* **1980**, *76*, 305−314. (b) Bowen, B. D. Streaming potential in the hydrodynamic entrance region of cylindrical and rectangular capillaries. *J. Colloid Interface Sci.* **1985**, *106*, 367−376.

(28) The number in brackets gives the error bar of the last digit.

(29) French, R. H. Long range interactions in nanoscale science. *Rev. Mod. Phys.* **2010**, *82*, 1887−1944.

(30) Dzyaloshinskii, I. E.; Lifshitz, E. M.; Pitaevskii, L. P. The general theory of van der Waals forces. *Adv. Phys.* **1961**, *10*, 165−209.

(31) Nir, S.; Andersen, M. Van der Waals interactions between cell surfaces. *J. Membr. Biol.* **1977**, *31*, 1−18.

(32) Parsegian, V. A.; Ninham, B. W. Van der Waals forces in many-layered structures: Generalizations of the Lifshitz result for two semi-infinite media. *J. Theor. Biol.* **1973**, *38*, 101−109.

(33) Technically, the sign of A_{12-43} also depends on the polarizabilities of the cell wall and the buffer. Yet, a probe object featuring a lower polarizability than the medium would experience a repulsive vdW interaction.

(34) Characklis, W. G.; Cooksey, K. E. Biofilms and microbial fouling. *Adv. Appl. Microbiol.* **1983**, *29*, 93−138.

Addendum IV - Adhesion of gecko setae reflects nanoscale differences in subsurface energy

Authors: P. Loskill[1], J. Puthoff[2], M. Wilkinson[2], K. Mecke[3], K. Jacobs[1], and K. Autumn[2]

[1] Department of Experimental Physics, Saarland University, 66041 Saarbrücken, Germany. [2] Department of Biology, Lewis & Clark College, Portland, OR 97219, USA. [3] Institute for Theoretical Physics, Universität Erlangen-Nürnberg, D-91058 Erlangen, Germany

submitted to Journal of the Royal Society Interface (2012).

Author contributions:
P. Loskill and J. Puthoff contributed equally to this work. Experiments were performed by P. Loskill, J. Puthoff, and M. Wilkinson. Data were analysed by P. Loskill and J. Puthoff. Theoretical advice was given by K. Mecke. Article was written by P. Loskill, J. Puthoff, K. Jacobs, and K. Autumn. Research was directed by K. Jacobs and K. Autumn

Abstract - Surface energies are commonly employed to determine the adhesive forces between materials. However, the component of surface energy derived from long-range forces, such as van der Waals forces, depends on the material's structure below the outermost atomic layers. Prior theoretical results and indirect experimental evidence suggest that the van der Waals energies of subsurface layers will influence interfacial adhesion forces. We discovered that nanometerscale differences in the oxide layer thickness of silicon wafers result in significant macroscale differences in the adhesion of isolated gecko setal arrays. Si/SiO_2 bilayer materials exhibited stronger adhesion when the SiO_2 layer is thin (approx. 2 nm). To further explore how layered materials influence adhesion, we functionalized similar substrates with an octadecyltrichlorosilane (OTS) monolayer and again identified a significant influence of silicon dioxide layer thickness on adhesion. Our theoretical calculations describe how variation in the silicon dioxide layer thickness produces differences in the van der Waals interaction potential, and these differences are reflected in the adhesion mechanics. Setal arrays employed as tribological probes provide evidence that the 'subsurface energy' of inhomogeneous materials influences the macroscopic surface forces.

Macroscale adhesion of gecko setae reflects nanoscale differences in subsurface composition

Peter Loskill,[†] Jonathan Puthoff,[‡] Matt Wilkinson,[‡] Klaus Mecke,[¶] Karin Jacobs,[*,†] and Kellar Autumn[*,‡]

Experimental Physics, Saarland University, 66041 Saarbrücken, Germany, Department of Biology, Lewis & Clark College, Portland, OR 97219, USA, and Institute for Theoretical Physics, Universität Erlangen-Nürnberg, D-91058 Erlangen, Germany

E-mail: k.jacobs@physik.uni-saarland.de; gekkolab@gmail.com

Abstract

Surface energies are commonly employed to determine the adhesive forces between materials. However, the component of surface energy derived from long-range forces, such as van der Waals forces, depends on the material's structure below the outermost atomic layers. Prior theoretical results and indirect experimental evidence suggest that the van der Waals energies of subsurface layers will influence interfacial adhesion forces. We discovered that nanometer-scale differences in the oxide layer thickness of silicon wafers result in significant macroscale differences in the adhesion of isolated gecko setal arrays. Si/SiO_2 bilayer materials exhibited stronger adhesion when the SiO_2 layer is thin (approx. 2 nm). To further explore how layered materials influence adhesion, we functionalized similar substrates with an octadecyltrichlorosilane (OTS) monolayer and again identified a significant influence of silicon dioxide layer thickness on adhesion. Our theoretical calculations describe how variation in the silicon dioxide layer thickness produces differences in the van der Waals interaction potential, and these differences are reflected in the adhesion mechanics. Setal arrays employed as tribological probes provide evidence that the 'subsurface energy' of inhomogeneous materials influences the macroscopic surface forces.

Introduction

When describing adhesion between two materials, it is common to refer to the strength of the contribution of each material using their surface energies γ_1 and γ_2, which are the extra free energies (per unit area) possessed by atoms at a surface relative to atoms in the bulk.[1] The well-known Dupré equation gives the work of adhesion $\Delta\gamma$, the energy required to separate the dissimilar materials, as $\Delta\gamma = \gamma_1 + \gamma_2 - \gamma_{1,2}$, where $\gamma_{1,2}$ is the interfacial energy of the two contacting surfaces. The surface energy of solids typically cannot be measured directly and is usually estimated from liquid drop contact angle measurements.[2] The surface energy is largely a property of the outermost atomic layers ($\lesssim$ 1 nm deep), yet van der Waals (vdW) forces act over distances greater than 1 nm in many cases.[3–5] Thin industrial coatings like adhesion promotors, self-assembled monolayers of thiols or silanes as well as photoresists are also in the range of a few nanometers. The van der Waals forces of the underlying material should—theoretically—reach through the thin layer and influence adhesion.

Previous experiments indeed identified a significant influence of the long-range component of the interaction potential on the dewetting of thin liq-

*To whom correspondence should be addressed
†Saarland University
‡Lewis & Clark College
¶Universität Erlangen-Nürnberg

uid films,[6,7] their liquid front profiles,[8,9] and the mesoscopic organization of magnetic nanocrystals.[10] Recently, a similar influence was detected on the adsorption kinetics of proteins[11–13] and the adhesion of bacteria.[14] These experiments employed materials whose contribution to the potential had been tuned by means of surface stratification. In layered systems, the contributions of the different materials can be tuned by modifying the layer thicknesses.[15] Early work by Israelachvili and Tabor[16] measured the forces between crossed cylinders, one of which was covered with a monolayer of stearic acid, and found that the resulting dispersion forces were sensitive to the presence of the surface layer at small separations, on the order of the layer thickness. An analogous effect will apply when two materials are brought into contact, and the layer thickness is varied. The question presents itself: can stratification be used to modify the macroscopic adhesion of materials?

To tackle this question, we employed the gecko to probe adhesion and the underlying surface forces. Although the gecko is essentially a macroscopic 'object'[1], it makes use of intermolecular forces. The outstanding climbing ability of the gecko has impressed observers for hundreds of years and a technical replication is a active area of research nowadays.[18] The key adaptation that provides this ability is the hierarchical structure of a gecko foot. The underside of each toe is divided into lamellar structures that terminate in arrays of densely-packed hair-like protrusions, called seta.[19,20] Individual setae are bundles of β-keratin fibrils several hundred μm long.[21] These fibrils terminate in triangular, wedge-shaped pads about 150 nm wide at the tip, called spatulae. As a consequence of this hierarchical structure, the setal arrays have an overall compliance that allows them to closely conform to rough surfaces.[22] The nanoscopic contacts that are established at the spatular tips produce considerable overall adhesion on virtually any surface by vdW interactions.[23–25] These structures are positioned at the correct scale to establish uniform, single-asperity contacts on substrates with limited roughness below 100 nm.

[1]Tokay geckos (*Gekko gecko*) can produce an adhesion force of roughly 20 N.[17]

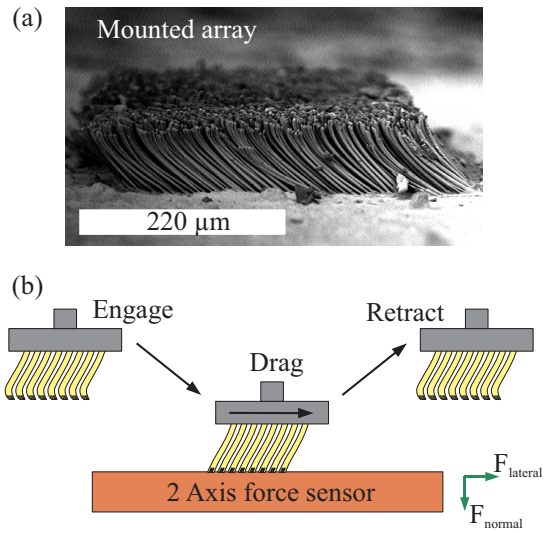

Figure 1: (a) Scanning electron microscope image of a mounted setal array. (b) A schematic diagram of the test setup for determining the adhesion (normal) forces and friction (lateral) forces between an array and a substrate.

In this study, we measured the adhesion of isolated gecko setal arrays to substrates that differed only in their subsurface composition: We used a Si wafer surface with a native ('N', 1.7(3) nm thick) oxide layer and surfaces with a thermally grown ('T', 151(1) nm thick) amorphous SiO_2 layer. In addition, we functionalized T- and N-type wafers with an octadecyltrichlorosilane (OTS) self-assembled monolayer. The OTS monolayer has optical properties that are similar to those of SiO_2, but is strongly hydrophobic. Using this set of substrates, we characterize the influence of the subsurface composition independent of surface interactions, since the latter are identical within the substrate pairs featuring the same surface chemistry.[26] A comparison between the substrates featuring different chemistries, however, is not the aim of this study, since hydrophilic and hydrophobic substrates differ in short range interactions, the characterization of which is not simply covered by one parameter (e.g. the surface energy). Comparing, however, pairs of wafers with identical short range forces, yet different thicknesses of the surface layers, will reveal the impact of van der Waals interaction and allow for a theoretical description. Our tribological probe was an isolated setal array

from a species of tropical gecko (*Gekko gecko*; Figure 1). Although the forces between each nanohair and the surface are slight, the scaling of forces implied by the 'contact-splitting effect' [24,27] yields considerable adhesion when the number of hairs packed on the array is large.

Surface forces for layered media

We address the question of whether or not subsurface differences influence the adhesion between bodies by calculating the surface interaction potential and the resulting effect on adhesion in a simple model system. Qualitatively, we expect a larger adhesive force between a probe object and a wafer with a thin oxide layer: Since Si possesses a higher index of refraction and a higher polarizability than SiO_2, the van der Waals interactions between a probe object and Si are stronger than between a probe object and SiO_2.[3] The probe will 'feel' the subsurface bulk silicon more in a type N wafer than in a type T wafer. The interaction ϕ between two bodies at a distance x can be described by a modified Lennard-Jones-type potential consisting of a short-range (SR) part and an long-range (LR) part

$$\begin{aligned}\phi(x) &= \phi_{\mathrm{SR}}(x) + \phi_{\mathrm{LR}}(x) \\ &= \frac{C_{\mathrm{SR}}}{x^m} - C_{\mathrm{C,E}} \cdot \Theta(x_0 - x) - \frac{C_{\mathrm{LR}}}{x^n}\,,\end{aligned} \tag{1}$$

where C_{SR} and C_{LR} are constants and m is typically chosen to be $n+6$ to represent the powerful repulsion between overlapping electron clouds. Short range chemical or entropic forces that act only at some separation x_0 are approximated by a Heaviside step function $\Theta(x)$ with constant strength $C_{\mathrm{C,E}}$.

In the absence of charges, the LR part is determined exclusively by the vdW interactions ϕ_{vdW}. For two infinite planes interacting[2] through a medium M, the exponent $n = 2$ and the interaction energy per unit area is given by $\phi_{\mathrm{LR}}(x) = \phi_{\mathrm{vdW}}(x) = -\frac{A_{\mathrm{i/M/j}}}{12\pi x^2}$, where $A_{\mathrm{i/M/j}}$ is the Hamaker constant for the interaction of two materials i and j through a medium (M) and can be derived from the optical properties of the materials using the Lifschitz approach.[3,28,29] In the case of a probe material (P) interacting with a substrate that consists of a bulk material (L2) and a thin coating (L1) of thickness d, the vdW part of the interface potential can be modified as[6,7]

$$\begin{aligned}\phi_{\mathrm{vdW}}(x) = -\frac{1}{12\pi}\Bigg[&\frac{A_{\mathrm{P/M/L1}}}{x^2} \\ &+ \frac{A_{\mathrm{P/M/L2}} - A_{\mathrm{P/M/L1}}}{(x+d)^2}\Bigg]\,.\end{aligned} \tag{2}$$

Hence, the relative contribution of different layers of an inhomogeneous substrate to the total LR vdW potential can be tuned by varying the thickness d of the layer L1. The second term in Eq. (2), incorporating the contribution from the lower layer, might be thought of as the 'subsurface energy' of the system. In the following, we use this term for energies that arise from vdW contributions to the interface potential due to a variable subsurface composition.

Material and Methods

Adhesion Performance Testing

We measured the tribological performance of the mounted setal arrays using a custom mechanical testing platform ('Robotoe').[30] Robotoe incorporates a 2-axis positioning stage (Aerotech, Pittsburg, PA, USA) and a piezoelectric load cell (Kistler, Amherst, NY, USA) (with a resolution of 1.3 and 2.6 mN in shear and normal forces, respectively). The mounted array is attached to the terminal end of the force sensor assembly, and the layered Si/SiO_2/OTS substrates are held rigidly in a mount on the motion stage opposite the setal array specimen chuck. All of the components are enclosed in a controlled-environment chamber. During a test, the tips of the setal arrays are dragged across the substrate in a displacement-controlled motion designed to resemble a gecko's footfall[30] (cf. Figure 1). Reported adhesion and friction values are taken from the force sensor readout during the steady-state portion of each test.[31] We can specify parameters such as the drag velocity v and approach distance during the experiment, as well as the temperature and humidity in the chamber.

[2] In this study only separations of a few nanometers are of interest. Hence, retardation can be neglected.

Table 1: Surface properties of the substrates used in this study: root mean square (rms) roughness, advancing (adv) and receding (rec) water contact angle, surface energy γ and Lifshitz-van der Waals γ^{LW} and Lewis acid-base γ^{AB} components obtained from contact angles of three different liquids.[39] The number in brackets gives the error bar of the last digit.

	rms (nm)	γ (mJ m^{-2})	γ^{LW} (mJ m^{-2})	γ^{AB} (mJ m^{-2})	Θ_{adv} (°)	Θ_{rec} (°)
OTS T	0.19(3)	24(1)	24(1)	0	111(3)	103(4)
OTS N	0.17(0)	24(1)	24(1)	0	111(2)	103(2)
SiO_2 T	0.13(3)	63(1)	43(1)	20(1)	5(2)	complete wetting
SiO_2 N	0.09(2)	64(1)	43(1)	21(1)	7(2)	complete wetting

Preparation and cleaning of substrates

The silicon wafers were purchased from Si-Mat (Landsberg, Germany). We removed residues leftover from the polishing process, as well as contaminants deposited by the atmosphere, by submerging the as-received wafers for 30 min in fresh 1:1 H_2SO_4(conc.)/H_2O_2 (30%) solution. The wafers were subsequently rinsed in boiling deionized water for 90 min, which was exchanged three times within that time. We produced a second pair of type T/type N substrates with different surface properties by hydrophobizing a series of cleaned wafers using self-assembling silane molecules with a CH_3 tail-group (octadecyl-trichlorosilane, OTS, purchased from Sigma-Aldrich, Germany) following standard procedures.[32,33] All wafer types were characterized using atomic force microscopy, ellipsometry and water contact angle measurements (cf. Table 1, further characterization data available in refs.[13,34]). Immediately prior to the experiments, the substrates were cleaned by immersing them subsequently into ethanol and acetone (5 min each) in a ultrasonic bath and rinsing them for 30 min in boiling DI water.

Setal Array Collection and Preparation

The setal arrays of *Gekko gecko* grow from lamellar strips of tissue on the ventral side of each toe. We collected entire arrays from live, unanaesthetized animals following the methods described in;[24] the keratin backing layer to which the hairs are attached can be peeled from the lamella easily. (The animal's loss of adhesive function in this digit is recovered at the next molt.) After some trimming, we affix the detached arrays to aluminum stubs, hairs facing upward at their natural resting angle, with a thin layer of cyanoacrylate glue (cf. Figure 1). These stubs are then mounted on the force sensor in Robotoe, the setal arrays facing the substrates mounted on the translation stage. The size of the arrays varies in the range of a few millimetres. The larger arrays were chosen for the experiments on the hydrophobic samples, the smaller ones for experiments on hydrophilic samples respectively.

Table 2: Optical properties of the relevant materials[35–38]

	n	ε
β-keratin	1.56	20
SiO_2	1.46	3.9
Si	4.1	11.8
OTS	1.46	2

Results

Calculation of microscopic van der Waals potentials

The optical properties of Si and SiO_2 are well-known, but only limited data on the optical properties of β-keratin is available, and, to the authors' knowledge, no studies have been done on β-keratin from geckos. Furthermore, the constant C_{SR} in the repulsive part of Eq. (1) is hardly accessible, so we cannot give rigorous theoretical values for the forces without some assumptions. We take the optical constants of β-keratin as those determined for horn keratin[35,36] (cf. Table 2). We also assume that the repulsive constant C_{SR} and $C_{C,E}$ are independent of oxide layer thickness; this is

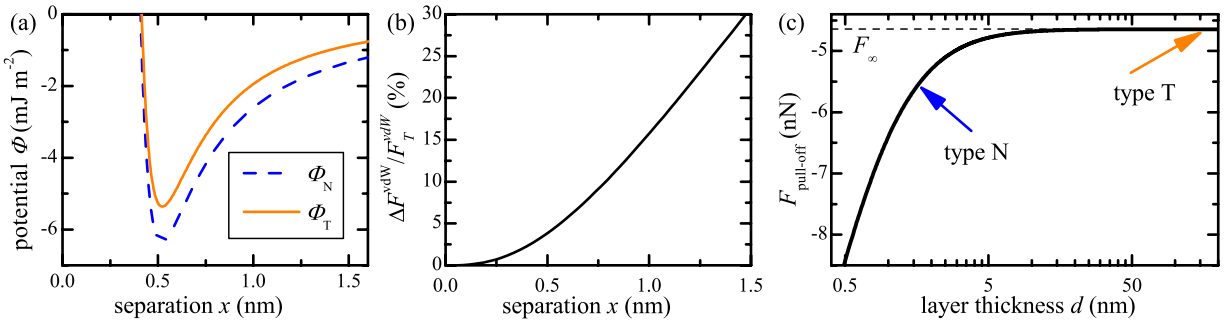

Figure 2: (a) Calculated effective interface potentials for the interaction between a keratin layer and a silicon wafer (type T and type N). The short-range constant was assumed as $C_{\mathrm{SR}} = 1 \cdot 10^{-77}\,\mathrm{J\,m^6}$ resulting in maximal forces of $F_{\mathrm{max}} \approx 10^{-2}\,\mathrm{nN\,nm^{-2}}$. (b) Relative difference in van der Waals forces on type T and type N wafers as determined using Eq. (4). (c) Estimated pull-off forces for a β-keratin sphere of radius $R = 150\,\mathrm{nm}$ on a Si/SiO_2 bilayer material with layer thickness d making use of Eq. (6).

a safe assumption since the surface properties of the substrates do not differ significantly (Table 1). Using the indices of reflection and the dielectric constants of the involved materials (cf. refTabOptProp) the Hamaker constants were calculated to $A_{\mathrm{Si}} = 61.5\,\mathrm{k_B}T$ and $A_{\mathrm{SiO_2}} = 17.8\,\mathrm{k_B}T$, confer chapter 11, Eq. 11.13 of Ref.[3] Inserting these values into Eq. (1) and Eq. (2) produces the potentials ϕ_{N} and ϕ_{T} in Figure 2*a*. As expected from the qualitative considerations before, the global minimum in the interaction potential is lower for the type N than for the type T sample. For these potentials we used $C_{\mathrm{SR}} = 10^{-77}\,\mathrm{J\,m^6}$, a value that reflects the typical magnitude given in other experiments.[6] The term $C_{\mathrm{C,E}}$, i. e. the chemical and entropic forces can be neglected in force differences because they would contribute—if significantly present at all—in the same way for type N and type T samples due to their identical surface properties. Altogether, this results in maximal forces comparable to previous experimental studies.[23] The work of adhesion for these potentials is given by $\Delta\gamma = \phi(\infty) - \phi(x_0)$.

Avoiding all of the above assumption that especially concern the SR forces, it is instructive to evaluate the system in terms of LR vdW forces only. Of significant interest is the manner in which the vdW forces differ between the N and T substrates. This difference, on a per unit area basis, is

$$\begin{aligned}\Delta F(x) &= F_{\mathrm{N}}(x) - F_{\mathrm{T}}(x) \\ &\propto \frac{A_{\mathrm{P/M/Si}} - A_{\mathrm{P/M/SiO2}}}{(x+d)^3}\,.\end{aligned} \tag{3}$$

This leads to a relative difference in vdW forces of

$$\Delta F_{\mathrm{Rel.}}(x) = \frac{\Delta F(x)}{F_{\mathrm{T}}(x)} = \frac{R_A}{(\frac{d}{x}+1)^3}\,, \tag{4}$$

where $R_A = \frac{A_{\mathrm{P/M/Si}}}{A_{\mathrm{P/M/SiO2}}} - 1$ is the shifted ratio of the Hamaker constants. The parameter R_A is useful for comparing vdW force differences between substrates with different materials or structure. The relative difference in van der Waals forces on type T and type N wafers for different separations is shown in Figure 2*b* whereby $R_A = 2.5$. Variation in the values of the refractive index and dielectric constant of β-keratin does not change these ratios significantly (c.f. supplementary material).

Influence of the potentials ϕ_{N} and ϕ_{T} on adhesion forces

Adhesion between bodies involves more phenomena than just those represented by the interaction potential. For instance, the separation of adhered structures is also influenced by the mechanical properties of the materials involved. More inclusive mechanical pictures of contact and adhesion include the Johnson-Kendall-Roberts (JKR) theory[40] and the Derjaguin-Muller-Toparov (DMT) theory[41] of contacting spheres. These models

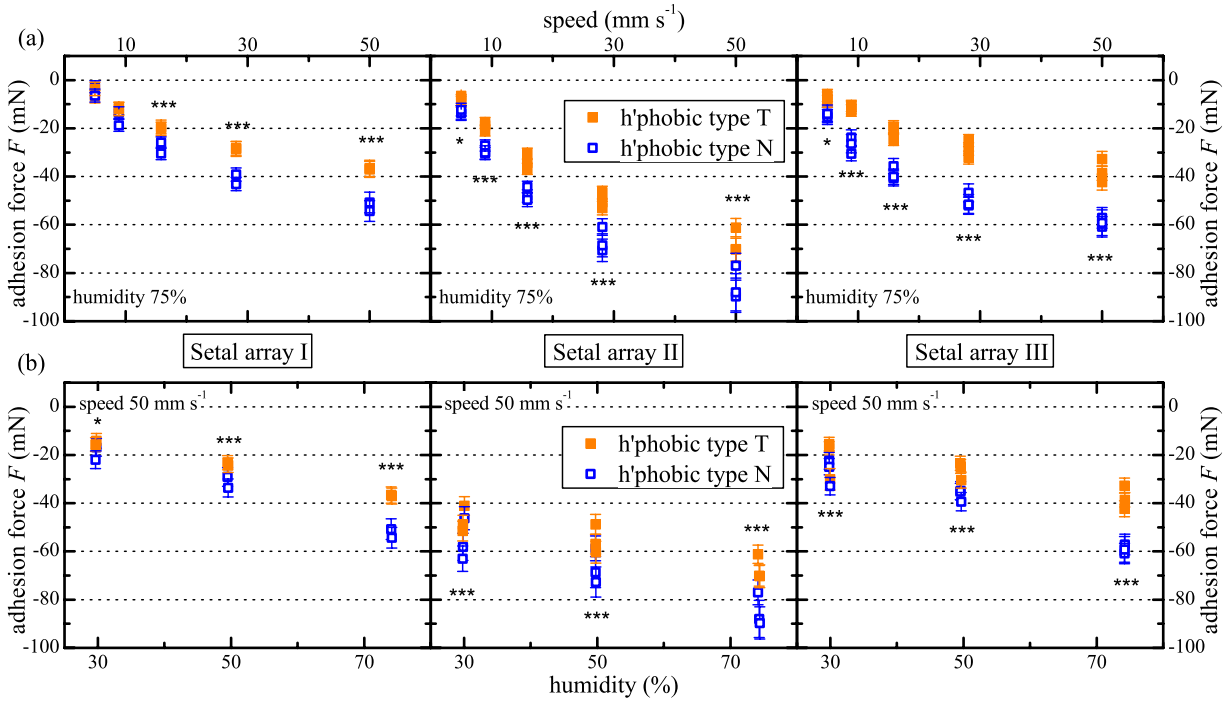

Figure 3: Results of multiple different experiments on the hydrophobic samples with different setal arrays and substrate pairs: Mean adhesion forces are plotted as a function of (a) the drag speed (at 75%RH) and (b) the humidity (with $v = 50\,\mathrm{mm\,s^{-1}}$). By convention, adhesive forces are negative. The stars indicate the level of significance.

make specific predictions of the contact areas and pull-off forces for a number of different simple contact geometries (sphere/sphere, sphere/plane) based on materials properties and surface interactions.

We investigate the influence of the interaction potential of Eq. (2) on the adhesion of a sphere of radius R to a plane using the same approach as these theories, but it is important to note that (*i*) Eq. (2) was derived for two facing half-spaces of material and (*ii*) the scaling of the adhesion forces will not be exactly linear with the changes in γ or F. We address these issues by transforming the interaction potential ϕ to a new form V amenable for contact between curved bodies using the Derjaguin approximation.[42] For contact between a body of principal curvatures κ_1, κ_2 and a plane, this gives

$$V(l) = -\frac{\alpha(\lambda)\pi}{\sqrt{\kappa_1\kappa_2}} \int_l^\infty \phi(x)\,dx \qquad (5)$$

where l is the minimum approach distance between the sphere and the plane, $\kappa_1 = \kappa_2 = \frac{1}{R}$ for the sphere, and $\frac{3}{2} \leq \alpha \leq 2$. The Maugis parameter $\lambda = 2\sigma_0 \left(\frac{R}{\pi\Delta\gamma K^2}\right)^{1/3}$ describes the transition between the JKR and DMT limiting behaviors using an approximate, square force-separation curve of depth σ_0 and integrated area $\Delta\gamma$.[43] Use of this parameter makes the adhesion properties responsive to changes in the shape of the potential V in a manner that neither the JKR or DMT solutions can capture individually. The parameter λ also introduces the elastic constants E_i, ν_i of the sphere (1) and surface (2) into the problem through the contact modulus $K = \frac{3}{4}\left(\frac{1-\nu_1^2}{E_1} + \frac{1-\nu_2^2}{E_2}\right)^{-1}$. While there is no analytical expression that relates the prefactor α to λ, there is a simple fit developed by Carpick[44] that suffices.

From Eq. (5), we can find the adhesive or 'pull-off' force for the sphere on the layered substrate. Since $F(l) = -\frac{dV}{dl} = -\alpha\pi R\phi(l)$ and the bodies are in contact at $l \approx x_0$, we have

$$\begin{aligned} F_{\text{pull-off}}(d) &= -\alpha(\lambda(d))\pi R\phi(x_0, d) \\ &= -\alpha(\lambda(d))\pi R\Delta\gamma(d). \end{aligned} \qquad (6)$$

This is the typical form for pull-off forces in ad-

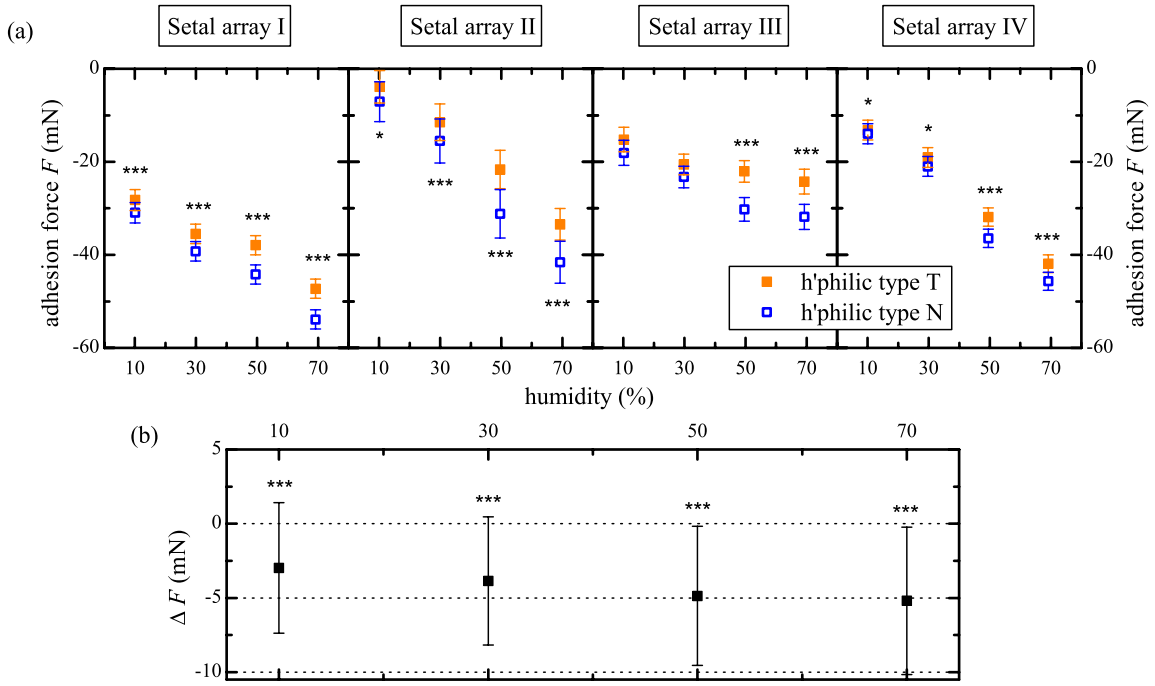

Figure 4: Results of multiple experiments (drag speed: $0.5\,\mathrm{mm\,s^{-1}}$; humidities: 10, 30, 50, 70%RH) on the hydrophilic samples with different setal arrays and substrate pairs: (a) Mean adhesion forces of the single experiments. (b) Aggregation of the experiments on the hydrophilic samples: Mean differences in adhesion forces of 'concurrent' single tests on the type N and type T wafers $\Delta F = F_\mathrm{N} - F_\mathrm{T}$ are plotted as a function of the humidity.

hesion problems, but all of the information about the potential in Eq. (1) and Eq. (2), such as the layer thickness d, is included in a consistent manner. The d-dependence enters into Eq. (6) not only in $\Delta\gamma$, but also in λ as well. Figure 2*c* shows how the pull-off forces will vary with layer thickness d. For large layer thicknesses, the influence of the second term in Eq. (2) on adhesion is negligible and the forces asymptote to the value F_∞. However, in the range $0.5\,\mathrm{nm} \leq d \leq 5\,\mathrm{nm}$, the force is significantly higher.

Adhesion forces on hydrophobic OTS-Surfaces

The predicted influence of differences in the thickness of the SiO_2 layer on adhesion forces was observable in drag experiments of setal arrays on the hydrophobic wafers. We performed multiple experiments, consisting of hundreds of individual drag tests, at five different speeds (5, 8.9, 15.8, 28.1, $50\,\mathrm{mm\,s^{-1}}$) and three humidities (30, 50, 75%RH), incorporating a number of different arrays and substrate pairs. The order of individual tests in an experiment were randomized within the constant-humidity groups. The results of typical experiments are shown in Figure 3: The mean adhesion forces of multiple different measurements at 75%RH with different setal arrays and substrate pairs are plotted as a function of drag speed (Figure 3*a*) and as a function of humidity (Figure 3*b*). The data demonstrate a clear influence of the oxide layer thickness on the adhesion force; the force on the type N substrate is always larger than the force on the type T substrate. The trend is independent of humidity and drag speed. Because of the different specimen sizes and slight variations in setal organization between individuals, absolute force values in different experiments depend on the setal array used.

Adhesion forces on hydrophilic SiO_2 Surfaces

Next, we examined whether the adhesion forces on the bare SiO_2 surfaces are also affected by

the SiO_2 layer thickness. Slow drag speeds of $0.5\,\mathrm{mm\,s^{-1}}$ were used to avoid damage to the gecko arrays from the high overall forces on the hydrophilic surfaces[3]. The experiments were performed at four different humidities (10, 30, 50, 70%RH). Similar to the results on the hydrophobic surfaces, the adhesion force on type N wafers is consistently larger than on type T wafers (Figure 4*a*). In spite of the slow drag speed, it was not entirely possible to prevent degradation of the array performance during an experiment (no degradation was observed on the hydrophobic samples). To minimize the influence of this effect in our N/T comparisons, we always carried out tests on both substrates in pairs (in a randomized order) and calculated the difference between 'concurrent' N and T measurements. The means of these differences ΔF in various experiments across multiple arrays and substrate pairs are always negative (Figure 4*b*). Therefore, the adhesion forces on the bare SiO_2 surfaces are also affected by the SiO_2 layer thickness.

Discussion

The experiments demonstrate that the subsurface energy influences macroscopic adhesion. Variation in oxide layer thickness, which causes subtle differences in the subsurface energy-distance relationship, significantly affects the force of adhesion between gecko setal arrays and Si wafers.

By using two pairs of tailored substrates, we were able to vary subsurface and surface properties independently. On the bare Si/SiO_2 substrates, the adhesion force is higher on the wafers with the thinner SiO_2 layer. This trend in adhesion force agrees with the theoretical predictions presented in Figure 2. Comparing the $F_{\text{pull-off}}(d)$ at $d = 1.7\,\mathrm{nm}$ for the hydrophilic N-type wafer with the value at $d = 151\,\mathrm{nm}$ for the T-type wafer, the pull-off force is - in absolute values - higher on the N-type sample.

On the hydrophobic Si/SiO_2/OTS materials, the overall adhesion force is lower, but the trend corroborates the results on the hydrophilic substrates. To plot $F_{\text{pull-off}}(d)$ for the hydrophobic wafers, it is not necessary to reformulate Eq. (2) with a third layer, rather, the thickness of the OTS layer ($d_{\text{OTS}} \approx 2.6\,\mathrm{nm}$)[4] is added to that of the SiO_2 layer, since both layers feature similar indexes of refraction and polarizabilities. As the top layer is still on a nanometer scale, the difference in $F_{\text{pull-off}}$ is still resolvable.

It is significant that we can distinguish these slight force differences in an essentially macroscopic experiment with the gecko material. The contact splitting effect implies that if we replace a large contact with N smaller ones,[45] the overall contact force will be multiplied by a factor of $\sim \sqrt{N}$.[27] Applying this principle magnifies the slight force differences between the N and T substrates to the point that they can be resolved macroscopically. Tokay geckos possess ≈ 14000 seta/mm^2[46] and there are ≈ 100 terminal spatulae on each seta.[21]

Furthermore, our data clearly show that adhesion is enforced with increasing drag speed and increasing humidities—on hydrophilic as well as on hydrophobic substrates—corroborating previous studies.[25,47,48] A comparison of the adhesion forces on the hydrophobic and the hydrophilic substrates is not the objective of this study; there are too many variables involved to make any specific inferences. The correlation between water contact angles and gecko adhesion was the focus of previous studies.[19,24,49–51]

Our theoretical approximations have two limitations: First, the small size, the internal structure and the unknown optical properties of the wedge-shaped β-keratin pads limit the calculations via the Lifshitz theory, which is based on continuum properties of semi-infinite parallel slabs. However, a more comprehensive and detailed theory will be able to predict more exact values for the subsurface energies of type N and type T wafers, but will not differ from our approximations in the predicted sign of the difference between the surface potentials. Second, the gecko adhesive system does not obey the idealized mechanics of the sphere-plane system. Nevertheless, the JKR/DMT solution includes all of the relevant physical concepts. The variation in the force values in Figure 2*c* derives from the difference between the surface potentials

[3] On the hydrophobic samples, an effect of wear was not observed.

[4] determined by ellipsometry and X-Ray reflectometry.

ϕ_N and ϕ_T rather than geometrical considerations, so we expect an analogous response in the gecko system. Thus, we are not able to theoretically match the absolute force values, but we were able to explain the measured differences in adhesion force on type N and type T wafers.

Conclusions

By using gecko setae as a macroscopic adhesion probe, we found evidence that differences in the interaction potential associated with the subsurface energy can produce macroscale differences in surface forces. Hence, it is indeed possible to modify the adhesion of materials by stratification. As a consequence, (i) for adhesion and adsorption experiments and simulations, van der Waals forces have to be considered and (ii) in stratified systems, subsurface and surface energies must be included accordingly.

Acknowledgement

We are grateful to Jacob Israelachvili for theoretical discussion. We thank Hendrik Hähl and Matthias Lessel for assistance with the substrates as well as Andrew Schnell and Madisen Holbrook for the gecko handling. This work was supported in part by the DAAD PROMOS and the NSF BIO awards NBM 0900723 and IOS 0847953.

References

(1) Bhushan, B. 2002 *Introduction to Tribology*, 1st edn. New York: John Wiley & Sons.

(2) Good, R. J. & Girifalco, L. A. 1960 A theory for estimation of surface and interfacial energies. III Estimation of surface energies of solids from contact angle data. *J Phys Chem-Us* **64**, 561-565.

(3) Israelachvili, J. 1991 *Intermolecular and Surface Forces*, 2nd edn. San Diego: Academic Press.

(4) Parsegian, V. A. 2006 *Van der Waals forces*, 1st edn. New York: Cambridge University Press.

(5) Delrio, F. W., de Boer, M. P., Knapp, J. A., Reedy, E. D., Clews, P. J. & Dunn, M. L. 2005 The role of van der Waals forces in adhesion of micromachined surfaces. *Nature Mater* **4**, 629-634.

(6) Seemann, R., Herminghaus, S. & Jacobs, K. 2001 Dewetting patterns and molecular forces: a reconciliation. *Phys Rev Lett* **86**, 5534-5537.

(7) Jacobs, K., Seemann, R. & Herminghaus, S. 2008 Stability and dewetting of thin liquid films. In *Polymer Thin Films* (eds. Tsui, O. K. C. & Russell, T. P.), pp. 243-265. Singapore: World Scientific Publishing Company.

(8) Indekeu, J. 1992 Line tension near the wetting transition - results from an interface displacement model. *Physica A* **183**, 439-461.

(9) Seemann, R., Herminghaus, S., Neto, C., Schlagowski, S., Podzimek, D., Konrad, R., Mantz, H. & Jacobs, K. 2005 Dynamics and structure formation in thin polymer melt films. *J Phys-Condens Mat* **17**, S267-S290.

(10) Lalatonne, Y., Richardi, J. & Pileni, M. 2004 Van der Waals versus dipolar forces controlling mesoscopic organizations of magnetic nanocrystals. *Nature Mater* **3**, 121-125.

(11) Quinn, A., Mantz, H., Jacobs, K., Bellion, M. & Santen, L. 2008 Protein adsorption kinetics in different surface potentials. *Epl-Europhys Lett* **81**, 56003.

(12) Bellion, M., Santen, L., Mantz, H., Hähl, H., Nagel, A. M., Gilow, C., Weitenberg, C., Schmitt, Y. & Jacobs, K. 2008 Protein adsorption on tailored substrates: long-range forces and conformational changes. *J Phys: Condens Matter* **20**, 404226.

(13) Hähl, H., Evers, F., Grandthyll, S., Paulus, M., Sternemann, C., Loskill, P., Lessel, M., Hüsecken, A. K., Brenner, T., Tolan, M. & Jacobs, K. 2012 Subsurface influence on the structure of protein adsorbates revealed by in situ X-ray reflectivity. *Langmuir* **28**, 7747–7756.

(14) Loskill, P., HÃd'hl, H., Kreis, C. T., Thewes, N., Bischoff, M., Herrmann, M. & Jacobs, K. 2012 The influence of the subsurface composition of a material on the adhesion of Staphylococci. *Langmuir* **28**, 7242-7248.

(15) Parsegian, V. A. 1993 Reconciliation of van-der-Waals force measurements between phosphatidylcholine bilayers in water and between bilayer-coated mica surfaces *Langmuir* **9**, 3625-3628.

(16) Israelachvili, J. N. & Tabor, D. 1972 The measurement of van der Waals dispersion forces in the range 1.5 to 130 nm. *Proc R Soc A* **331**, 19-38.

(17) Irschick, D. J., Austin, C. C., Petren, K., Fisher, R. N., Losos, J. B. & Ellers, O. 1996 A comparative analysis of clinging ability among pad-bearing lizards. *Biol J Linn Soc* **59**, 21-35.

(18) Geim, A. K., Dubonos, S. V., Grigorieva, I. V., Novoselov, K. S., Zhukov, A. A. & Shapoval, S. Y. 2003 Microfabricated adhesive mimicking gecko foot-hair. *Nature Mater* **2**, 461-463.

(19) Hiller, U. 1968 Untersuchungen zum Feinbau und zur Funktion der Haftborsten von Reptilien. *Z Morph Tiere* **62**, 307-362.

(20) Ruibal, R. & Ernst, V. 1965 The structure of the digital setae of lizards. *J Morphol* **117**, 271-293.

(21) Rizzo, N. W., Gardner, K. H., Walls, D. J., Keiper-Hrynko, N. M., Ganzke, T. S. & Hallahan, D. L. 2006 Characterization of the structure and composition of gecko adhesive setae. *J R Soc Interface* **3**, 441-451.

(22) Autumn, K., Majidi, C., Groff, R. E., Dittmore, A. & Fearing, R. 2006 Effective elastic modulus of isolated gecko setal arrays. *J Exp Biol* **209**, 3558-3568.

(23) Autumn, K., Liang, Y., Hsieh, S. T., Zesch, W., Chan, W., Kenny, T., Fearing, R. S. & Full, R. 2000 Adhesive force of a single gecko foot-hair. *Nature* **405**, 681-685.

(24) Autumn, K. & Peattie, A. M. 2002 Mechanisms of adhesion in geckos. *Integr Comp Biol* **42**, 1081-1090.

(25) Huber, G., Mantz, H., Spolenak, R., Mecke, K., Jacobs, K., Gorb, S. N. & Arzt, E. 2005 Evidence for capillarity contributions to gecko adhesion from single spatula nanomechanical measurements. *Proc Natl Acad Sci* **102**, 16293-16296.

(26) Loskill, P., Hähl, H., Faidt, T., Grandthyll, S., Müller, F. & Jacobs, K. 2012 Is adhesion superficial? Silicon wafers as a model system to study van der Waals interactions. *submitted*, arXiv:1202.6304.

(27) Arzt, E., Gorb, S. & Spolenak, R. 2003 From micro to nano contacts in biological attachment devices. *Proc Natl Acad Sci* **100**, 10603-10606.

(28) Lifshitz, E. M. 1956 The theory of molecular attractive forces between solids. *Sov Phys JETP* **2**, 73-83.

(29) Dzyaloshinskii, I. E., Lifshitz, E. M. & Pitaevskii, L. P. 1961 The general theory of van der Waals forces. *Adv Phys* **10**, 165–209.

(30) Gravish, N., Wilikinson, M. & Autumn, K. 2008 Frictional and elastic energy in gecko adhesive detachment. *J R Soc Interface* **5**, 339-348.

(31) Autumn, K., Dittmore, A., Santos, D., Spenko, M. & Cutkosky, M. 2006 Frictional adhesion: a new angle on gecko attachment. *J Exp Biol* **209**, 3569-3579.

(32) Brzoska, J. B., Ben Azouz, I. & Rondelez, F. 1994 Silanization of solid substrates: a step toward reproducibility. *Langmuir* **10**, 4367-4373.

(33) Wasserman, S. R., Whitesides, G. M., Tidswell, I. M., Ocko, B. M., Pershan, P. S. & Axe, J. D. 1989 The structure of self-assembled monolayers of alkylsiloxanes on silicon: a comparison of results from ellipsometry and low-angle x-ray reflectivity. *Int J Biol Macromol* **111**, 5852-5861.

(34) Gutfreund, P., Bäumchen, O., van der Grinten, D., Fetzer, R., Maccarini, M., Jacobs, K., Zabel, H. & Wolff, M. 2012 Surface Correlation Affects Liquid Order and Slip in a Newtonian Liquid. *submitted*, arXiv:1104.0868.

(35) Rizvi, T. Z. & Khan, M. A. 2008 Temperature-dependent dielectric properties of slightly hydrated horn keratin. *Int J Biol Macromol* **42**, 292-297.

(36) Maeda, H. 1989 Water in keratin. piezoelectric, dielectric, and elastic experiments. *Biophysical journal* **56**, 861-868.

(37) Sze, S. M. & Ng, K. K. 2006 *Physics of Semiconductor Devices*, 3rd edn. New York: John Wiley & Sons.

(38) Finklea, H., Robinson, L., Blackburn, A., Richter, B., Allara, D. & Bright, T. 1986 Formation of an organized monolayer by solution adsorption of octadecyltrichlorosilane on gold: electrochemical properties and structural characterization. *Langmuir* **2**, 239-244.

(39) Mykhaylyk, T. A., Evans, S. D., Fernyhough, C. M., Hamley, I. W. & Henderson, J. R. 2003 Surface energy of ethylene-co-1-butene copolymers determined by contact angle methods. *J Colloid Interface Sci 260*, 234-239.

(40) Johnson, K. L., Kendall, K. & Roberts, A. D. 1971 Surface energy and the contact of elastic solids. *Proc R Soc Lond A 324*, 301-313.

(41) Derjaguin, B. V., Muller, V. M. & Toporov, Y. P. 1975 Effect of contact deformations on the adhesion of particles. *J Colloid Interface Sci* **53**, 314-326.

(42) Maugis, D. 2000 *Contact, Adhesion and Rupture of Solids*, 1st edn. Berlin: Springer-Verlag.

(43) Maugis, D. 1992 Adhesion of spheres: the JKR-DMT transition using a Dugdale model. *J Colloid Interface Sci* **150**, 243-269.

(44) Carpick, R. W., Ogletree, D. F. & Salmeron, M. 1999 A general equation for fitting contact area and friction vs load measurements. *J Colloid Interface Sci* **211**, 395-400.

(45) Autumn, K., Sitti, M., Liang, Y., Peattie, A., Hansen, W. R., Sponberg, S., Kenny, T., Fearing, R. S., Israelachvili, J. N., & Full, R. 2002 Evidence for van der Waals adhesion in gecko setae. *Proc Natl Acad Sci* **99**, 12252-12256.

(46) Schleich, H. & Kästle, W. 1986 Ultrastrukturen an Gecko-Zehen (Reptilia: Sauria: Gekkonidae) *Amphibia-Reptilia* **7**, 141-166

(47) Gravish, N., Wilkinson, M., Sponberg, S., Parness, A., Esparza, N., Soto, D., Yamaguchi, T., Broide, M., Cutkosky, M., Creton, C. & Autumn, K. 2010 Rate-dependent frictional adhesion in natural and synthetic gecko setae. *J R Soc Interface* **7**, 259-269.

(48) Niewiarowski, P. H., Lopez, S., Ge, L., Hagan, E. & Dhinojwala, A. 2008 Sticky gecko feet: the role of temperature and humidity *PLoS ONE* **3**, e2192.

(49) Puthoff, J. B., Prowse, M. S., Wilkinson, M. & Autumn, K. 2010 Changes in materials properties explain the effects of humidity on gecko adhesion. *J Exp Biol* **213**, 3699-3704.

(50) Chen, B. & Gao, H. 2010 An alternative explanation of the effect of humidity in gecko adhesion: Stiffness reduction enhances adhesion on a rough surface. *Int J Appl Mech* **2**, 1-9.

(51) Kim, Y., Limanto, F., Lee, D. H., Fearing, R. S. & Maboudian, R. 2012 Role of Counter-substrate Surface Energy in Macroscale Friction of Nanofiber Arrays. *Langmuir* **28**, 2922-2927.

Addendum V - Fluoridation of hydroxyapatite leads to a reduced adhesion of oral bacteria

Authors: P. Loskill[1], C. Zeitz[1], M. Bischoff[2], M. Herrmann[2], and K. Jacobs[1]

[1] Department of Experimental Physics, Saarland University, 66041 Saarbrücken, Germany. [2] The Institute of Medical Microbiology and Hygiene, Saarland University, 66421 Homburg/Saar, Germany.

submitted to Langmuir (2012).

Author contributions:
Experiments were performed by P. Loskill. Substrates were prepared by C. Zeitz. Data was analyzed by P. Loskill. Article was written by P. Loskill, C. Zeitz, and K. Jacobs. Research was directed by M. Bischoff, M. Herrmann, and K. Jacobs.

Abstract - The mechanisms of action of fluoride have been discussed controversially for decades. The caries-preventive effect is often traced back to effects on demineralization. However, an effect on bacterial adhesion was indicated by indirect macroscopic studies. To characterize adhesion on fluoridated samples on a single bacterial level, we used AFM force-spectroscopy with bacterial probes to measure adhesion forces directly. We tested the adhesion of *Streptococcus mutans*, *Streptococcus oralis* and *Staphylococcus carnosus* onto smooth, high density hydroxyapatite surfaces, treated and untreated with fluoride solution. All bacteria species exhibit lower adhesion forces after fluoridation of the surfaces. These findings suggest that the decrease of adhesion properties is another origin of the cariostatic effect of fluoride.

Fluoridation of hydroxyapatite leads to a reduced adhesion of oral bacteria

Peter Loskill,[†] Christian Zeitz,[†] Markus Bischoff,[‡] Mathias Herrmann,[‡] and Karin Jacobs[*,†]

Experimental Physics, Saarland University, 66041 Saarbrücken, Germany, and Institute of Medical Microbiology and Hygiene, Saarland University, 66421 Homburg/Saar, Germany

E-mail: k.jacobs@physik.uni-saarland.de

Abstract

The mechanisms of action of fluoride have been discussed controversially for decades. The caries-preventive effect is often traced back to effects on demineralization. However, an effect on bacterial adhesion was indicated by indirect macroscopic studies. To characterize adhesion on fluoridated samples on a single bacterial level, we used AFM force-spectroscopy with bacterial probes to measure adhesion forces directly. We tested the adhesion of *Streptococcus mutans*, *Streptococcus oralis* and *Staphylococcus carnosus* onto smooth, high density hydroxyapatite surfaces, treated and untreated with fluoride solution. All bacteria species exhibit lower adhesion forces after fluoridation of the surfaces. These findings suggest that the decrease of adhesion properties is another origin of the cariostatic effect of fluoride.

Introduction

The campaign against caries is an always highly topical issue. Since more than seven decades it is known that the application of fluoride compounds has an cariostatic effect.[1] However, the underlying mechanisms of action of fluoride have been discussed controversially for decades and are not yet completely revealed.[2] The cariostatic impact of fluoridation is often traced back to a decreased demineralization of the teeth: Compared to hydroxyapatite (HAP), fluoroapatite (FAP) exhibits a higher resistance to acids leading to a lower demineralization (demineralization of HAP and FAP starts at pH 5.5 and pH 4.6, respectively[3]). New studies, however, showed that in the course of the fluoridation of HAP, the penetration depth of F is much lower than the previously reported micron range: FAP layer thicknesses are in the range of 10 nm.[4] In the oral cavity, chewing can shortly remove such nanometer-sized layers, which questions the explanation of the cariostatic effect of fluoridation by a decreased demineralization. Bacteria, however, are also influenced by fluoridation: The release of fluoride ions affects the bacterial metabolism,[5] the development of biofilms[6] and the behaviour of osteoplastic cells.[7] Furthermore, an effect on bacterial adhesion has been indicated by indirect macroscopic studies: Fluorapatite cement as compared to natural enamel,[8] fluoridated hydroxyapatite beads,[9] and fluoroapatite coatings[10] displayed a reduced number of adhering cells. Since fluoroapatite coatings showed to be biocompatible,[11] their antibacterial effects are not only of interest for the dental science but for all kind of implant science.

To study bacterial adhesion, classically parallel plate flow chambers are used.[12] In the past decade, however, atomic force microscopy (AFM) has been established as a powerful tool in bacterial research.[13] By means of AFM force spectroscopy with bacterial probes it is possible to study the

[*]To whom correspondence should be addressed
[†]Saarland University
[‡]Saarland University

adhesion force between bacteria and surfaces on a single bacterium level.[14] This microscopic approach is direct and quantitative in contrast to the classical macroscopic flow chamber studies.

The application of AFM force spectroscopy on enamel is problematic due to the rough and inaccessible surface. As the main compound of enamel is hydroxyapatite, we use high-density HAP pellets that feature smooth surfaces with micrometer sized patches of nanoscale roughness.

To determine whether the indicated effect of fluoridation on bacterial adhesion can be observed on a single bacterial level, we used AFM force-spectroscopy with bacterial probes to measure adhesion forces directly. We tested the adhesion of the cariogenic pathogens *Streptococcus mutans* and *Streptococcus oralis*, and of the apathogenic *Staphylococcal* species *S. carnosus* onto hydroxyapatite surfaces, treated and untreated with fluoride solution.

Experimental section

HAP and fluoridation

Using a field assisted sintering technique (FAST), commercially available hydroxyapatite (Sigma-Aldrich, Steinheim, Germany) was pressed into HAP pellets of a diameter of about 20 mm, a thickness of 5 mm and an overall density of 96% compared to a single crystal. In order to get a smooth sample surface, one side of the pellet was repeatedly treated with wet abrasive paper of increasing grain size (Struers, Willich, Germany). Subsequently, the surface was polished with diamond suspensions (DiaPro-3 μm; Struers, Willich, Germany and MSY0-0.03; Microdiamant, Lengwil, Switzerland) containing grains of 3 and 0.03 μm diameter. The procedure was performed until an RMS roughness of below 5 nm was achieved, which was determined by $(1\,\mu\mathrm{m})^2$ AFM topography scans. The pellet was then etched in a dilute acetic acid solution for 5 s with a pH of 4 in order to remove the residuals of the polishing procedure. By this step, the RMS roughness is slightly increased to 10 nm, yet the achieved surface is clean of foreign particles.[4] Fluoridation took place at pH 9, which is achieved by a fluoride solution (NaF in in de-inoized water) of 1000 ppm F^-. By thermal evaporation of Au through a mask, a strip of about 4 mm width and 100 nm thickness was prepared on the polished HAP pellet, separating it in two halves. One half was immersed into the fluoride solution for 5 min. Subsequently, the pellet was rinsed and then sonicated for 5 min in de-inoized water, in order to remove remainders of the fluoride solution.

Bacterial strains and culture conditions

The *Streptococcus mutans* and *Streptococcus oralis* clinical isolates used in this study were obtained from the Clinic of Operative Dentistry, Periodontology and Preventive Dentistry (Saarland University Hospital, Homburg/Saar, Germany). *Staphylococcus carnosus* strain TM300, used in this study as a non-pathogenic control, was obtained from the German Resource Centre for Biological Material (DSMZ, Braunschweig, Germany). The bacteria were maintained at -80 °C in tryptone soy broth (TSB; BD Biosciences, Heidelberg, Germany) containing 15% glycerol. For culturing, strains were incubated on TSB-sheep blood agar plates overnight at 37 °C. Subsequently, bacterial colonies were precultured in 5-ml MÃijller-Hinton (MH; BD Biosciences, Heidelberg, Germany) batch cultures for 6 h at 150 rpm and 37 °C. 300 μl of each preculture was used to inoculate a main culture in 10 ml MH. After 16 h of growth at 150 rpm and 37 °C, bacteria were harvested by centrifugation at 1900 g for 10 min at 20 °C and washed twice with 10 ml of phosphate-buffered saline (PBS) (10 mM potassium phosphate, 0.15 M NaCl; pH 7). The bacteria were subsequently resuspended in PBS to obtain a concentration of $1x10^9$ cells per ml.

Preparation of bacterial probes

The bacteria were immobilized onto tipless cantilevers (PNP-TR_TL; Nanoworld, NeuchÃćtel, Switzerland) by means of poly-L-lysine, PLL (MP Biomedicals, Solon, USA). Prior to the preparation procedure, the cantilevers were cleaned by treating them with an air plasma. The PLL coating was then applied by immersing the AFM cantilever in a droplet of poly-L-lysine solution

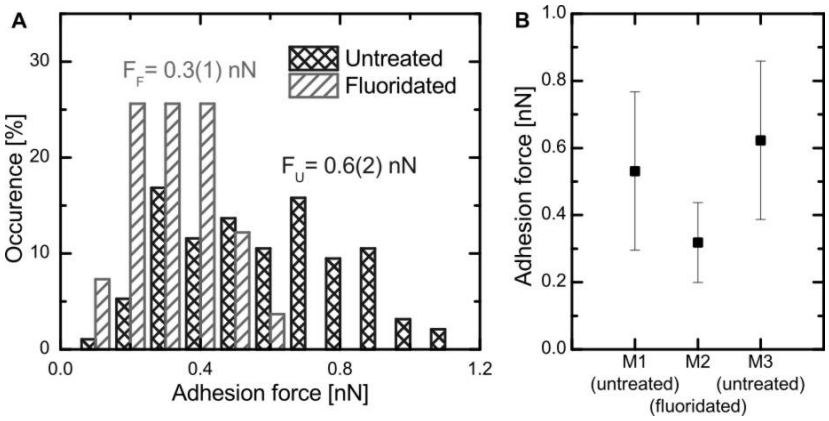

Figure 1: Results of an AFM force spectroscopy experiment with *Streptococcus oralis* and untreated or fluoridated hydroxyapatite substrates: A) Distribution of the measured adhesion forces. B) Mean adhesion forces of three subsequent series of measurements, each consisting of 50-100 force/distance curves. To assure the integrity of the bacterial probes, experiments were always started and terminated with a series of measurements on the same substrate.

(0.1 mg/ml) for 1 hour. Subsequently, the cantilevers were carefully rinsed with PBS and placed in a droplet of bacteria solution for 1 hour at 4 °C. To remove unbound bacteria, the probes were rinsed with PBS buffer. All probes used in this study were prepared immediately before the experiments.

Force spectroscopy

AFM force spectroscopy experiments were performed in PBS buffer using a Bioscope Catalyst and a Dimension Icon (both: Bruker, Santa Barbara, USA). The force measurements were performed using a z-range of 1 μm, a scan rate of 1 Hz and a relative force trigger of 1 nN. An entire experiment consists of at least 100 single measurements per substrate type. Thereby, every measurement was performed on a different spot. To control for an alteration of the bacterial probe, every experiment was terminated and started with a series of measurements on the same type of substrate. Adhesion forces were evaluated with the Nanoscope software (Bruker, Santa Barbara, USA) by calculating the difference between the adhesion peak and the baseline for every single curve.[15]

Results and discussion

To determine whether the adhesion force is influenced by fluoridation of the hydroxyapatite substrates, we carried out AFM force spectroscopy experiments with three different bacterial species.

In the case of *Streptococcus oralis*, the determined adhesion forces are lower on the fluoridated than on the untreated part of the sample (Figure 1A). The integrity of the bacterial probe can be guaranteed, since the first and the last series of measurements were performed on the same type of substrate (in this case the untreated part, cf. Figure 1B) and the respective adhesion forces were identical within the experimental error.

Further experiments with *Streptococcus mutans* and *Staphylococcus carnosus* reveal the same trend (cf. Figure 2). All bacteria species exhibit lower adhesion forces on the fluoridated part of the hydroxyapatite substrate. That is to say, fluoridation reduces the adhesion between bacteria and hydroxyapatite pellets by a factor of two, independent of the studied species and the amount of bacteria in contact.[16]

Our findings corroborate the results of simple, macroscopic counting experiments in previous studies:[8–10] Moreover, the macroscopic difference in the amount of adhering bacteria on fluoridated and untreated surfaces can now be traced back to microscopic differences in the adhesion force of

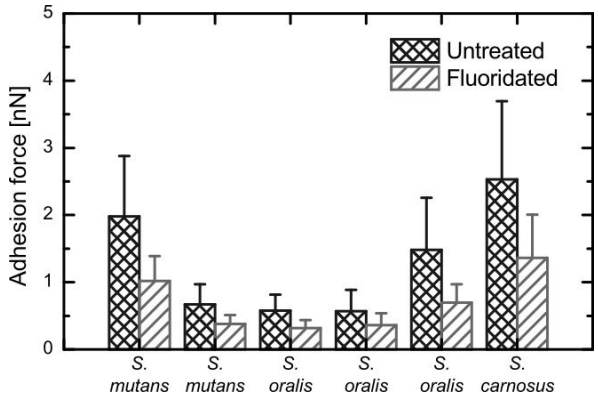

Figure 2: Aggregation of the mean adhesion forces of multiple experiments with different cantilevers and bacterial species. Consistently, the mean adhesion force is reduced by roughly 50%. Due to a different amount of bacteria in contact, independent experiments with the same species show different absolute values. The ratios, however, are consistent.

single bacteria.

The advantage of AFM force spectroscopy with bacterial probes is the possibility to directly measure adhesion forces on a microscopic scale. A restricting issue, however, is the susceptibility to local heterogeneities in the surface. By using nanoscopically smooth substrates, we circumvent problems due to topography. To account for the heterogeneity in crystallite orientation, every single measurement is carried out on a different spot on the surface. By this, we gain orientation-averaged mean adhesion forces but have to accept larger error bars. However, the observed trend is consistent and reproducible over multiple various experiments.

As all three bacterial species show the same adhesion reduction, we do not expect a specific adhesion effect or an active response of the bacterium. Especially the results for *S. carnosus*, corroborate this assumption, due to the fact that this bacterial species lacks adhesins.

Furthermore, since fluoridation only affects the outermost layer,[4] the origin of the adhesion-reducing effect of fluoride must be due to surface properties. Topography or the roughness cannot be responsible for the change in adhesion: AFM scans reveal that there are no significant differences in RMS roughness due to the fluoridation

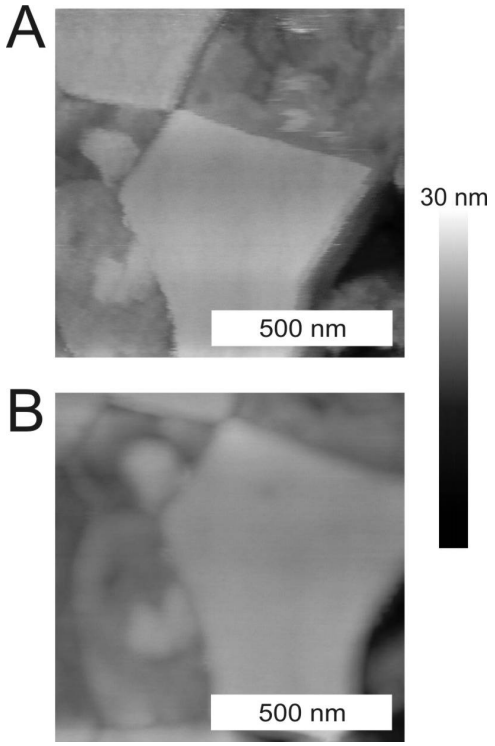

Figure 3: AFM images of a hydroxyapatite surface spot (A) before and (B) after fluoridation. The topography and RMS roughness are not affected by the fluoridation.

process (Figure 3).

The zeta-potential, however, is very likely affected by the fluoridation. At a physiological pH, the zeta-potential of HAP is negative,[17] just like the potential of most bacteria.[18] Since bacterial adsorption takes place despite this electrostatic repulsion, the adhesion process cannot be governed by the electrostatic interaction.[19] Rather, long-range attractive van der Waals forces are dominating. The overall adhesion, however, could still be reduced by a stronger electrostatic repulsion caused by a decreased zeta-potential of the substrate. Previous studies showed that the application of fluoride ions can decrease the zeta-potential of HAP[19,20] and reported an increase in the adsorbed amount of positively charged proteins.[21] Furthermore, it was shown that the adhesion of *S. mutans* to HAP was reduced by the adsorption of proteins causing an increase in surface net negative charge.[22] Consequently, a reduced zeta potential due to fluoridation should lead to a reduced adhesion force of the bacteria, since the electro-

static repulsion between bacteria and substrate is increased.

Another apparent reason for the reduction in adhesion force is a change in surface energy. The literature values for surface energies of apatites differ strongly dependent on the used methods[23] and the crystallite plane.[24] Nevertheless, since the surface energy is correlated with the zeta-potential, a change due to fluoridation is expected and has been reported previously.[7,23,24] Consequently, the determined reduce in adhesion forces could also be an effect of a fluoridation induced variation in surface energy.

Conclusions

AFM force spectroscopy with bacterial probes revealed that fluoridation of hydroxyapatite substrates reduces the adhesion force of *S. oralis*, *S. mutans* and *S. carnosus* by a factor of two. Since *S. carnosus* lacks adhesins, the origin for this general trend is likely due to an unspecific, yet surface-related effect. Fluoridation changes surface energy as well as zeta potential, which both could cause lower adhesion forces. In accordance with other studies, we expect the zeta potential and/or the surface energy to be the origin of the adhesion-reducing effect of fluoride. These findings suggest that the decrease of bacterial adhesion is another origin of the caries-preventive effect of fluoride. As a consequence, this effect could be utilized in the design of implants, potentially exceeding the oral cavity.

Acknowledgement

This work was supported by the German Science Foundation under grant numbers GRK 1276 and INST 256/305-1 FUGG, and by funds of the Federal State of Saarland. We thank K. Hilgert for the help with handling the bacteria and M. Hannig for donating the bacteria.

Notes and References

(1) Dean, H. T. *Pub. Health Rep.* **1938**, *53*, 1443–1452.

(2) (a) Ten Cate, J. M. *Acta Odontol. Scand.* **1999**, *57*, 325–329; (b) Featherstone, J. D. B. *Community Dent. Oral. Epidemiol.* **1999**, *27*, 31–40; (c) Van Loveren, C. *Caries Res.* **2001**, *35*, 65–70; (d) Buzalaf, M. A. R.; Pessan, J. P.; Honório, H. M.; Ten Cate, J. M. *Monogr. Oral Sci.* **2011**, *22*, 97–114.

(3) Featherstone, J. D. B.; Ten Cate, J. M. In *Fluoride in Dentistry*; Ekstrand, J., Fejerskov, O., Silverstone, L., Eds.; Munskgaard International Publishers: Copenhagen, 1988; pp 125–149.

(4) Müller, F.; Zeitz, C.; Mantz, H.; Ehses, K.-H.; Soldera, F.; Schmauch, J.; Hannig, M.; Hüfner, S.; Jacobs, K. *Langmuir* **2010**, *26*, 18750–18759.

(5) (a) Bibby, B. G.; Van Kesteren, M. *J. Dent. Res.* **1940**, *19*, 391–402; (b) Hamilton, I. R. *J. Dent. Res.* **1990**, *69*, 660–7 [special issue]; (c) Marquis, R. E. *Can. J. Microbiol.* **1995**, *41*, 955–964; (d) Guha-Chowdhury, N.; Clark, A. G.; Sissons, C. H. *Oral. Microbiol. Immun.* **1997**, *12*, 91–97.

(6) Li, Y. H.; Bowden, G. H. *J. Dent. Res.* **1994**, *73*, 1615–1626.

(7) Qu, H.; Wei, M. *Acta Biomater.* **2006**, *2*, 113–119.

(8) Wei, J.; Wang, J.; Shan, W.; Liu, X.; Ma, J.; Liu, C.; Fang, J.; Wei, S. *J. Mater. Sci.: Mater. Med.* **2011**, *22*, 1607–1614.

(9) Eifert, R.; Rosan, B.; Golub, E. *Infect. Immun.* **1984**, *44*, 287–291.

(10) Ge, X.; Leng, Y.; Bao, C.; Xu, S. L.; Wang, R.; Ren, F. *J. Biomed. Mater. Res., Part A* **2010**, *95A*, 588–599.

(11) (a) Dhert, W. J. A.; Klein, C. P. A. T.; Jansen, J. A.; van der Velde, E. A.; Vriesde, R. C.; Rozing, P. M.; de Groot, K. *J. Biomed. Mater. Res., Part A* **1993**, *27*, 127–138; (b) Lee, E.-J.; Kim, H.-W.; Kim, H.-E. *J. Am. Ceram. Soc.* **2005**, *88*, 1309–1311.

(12) Harraghy, N.; Seiler, S.; Jacobs, K.; Hannig, M.; Menger, M.; Herrmann, M. *Int. J. Artif. Organs* **2006**, *29*, 368–378.

(13) (a) Dufrene, Y. F. *J. Bacteriol.* **2002**, *184*, 5205–5213; (b) Dorobantu, L. S.; Gray, M. R. *Scanning* **2010**, *32*, 74–96.

(14) (a) Razatos, A.; Ong, Y.-L.; Sharma, M. M.; Georgiou, G. *Proc. Natl. Acad. Sci.* **1998**, *95*, 11059–11064; (b) Lower, S. K.; Tadanier, C. J.; Hochella, M. F. *Geochim. Cosmochim. Acta* **2000**, *64*, 3133–3139; (c) Boks, N. P.; Busscher, H. J.; van der Mei, H. C.; Norde, W. *Langmuir* **2008**, *24*, 12990–12994.

(15) Carpick, R. W.; Batteas, J.; de Boer, M. P. In *Handbook of Nanotechnology*; Bhushan, B., Ed.; Springer Verlag: Berlin, 2007; pp 951–979.

(16) The restricting issue of bacterial probes based on tipless cantilevers is the uncertainty of the number of bacteria that are in contact with the substrate's surface. Therefore, it is not possible to compare measurements with different cantilevers. Measurements with the same cantilever on different substrates, however, are comparable as long as the integrity of the bacterial probe can be granted.

(17) (a) Arends, J. *J. Dent.* **1979**, *7*, 246–253; (b) Lopes, M. A.; Monteiro, F. J.; Santos, J. D.; Serro, A. P.; Saramago, B. *J. Biomed. Mater. Res., Part A* **1999**, *45*, 370–375.

(18) Mozes, N.; Leonard, A. J.; Rouxhet, P. G. *Biochim. Biophys. Acta* **1988**, *945*, 324–334.

(19) Rao, M. K. Y.; Somasundaran, P.; Schilling, K. M.; Carson, B.; Anantha-padmanabhan, K. P. *Colloids Surf. A* **1993**, *79*, 293–300.

(20) Somasundaran, P. *J. Colloid Interface Sci.* **1968**, *27*, 659–666.

(21) Barroug, A.; Rouxhet, P. G.; Lemaitre, J. *Colloids Surfaces* **1989**, *37*, 339–355.

(22) (a) Reynolds, E. C.; Wong, A. *Infect. Immun.* **1983**, *39*, 1285–1290; (b) Weerkamp, A. H.; Uyen, H. M.; Busscher, H. J. *J. Dent. Res.* **1988**, *67*, 1483–1487.

(23) Wu, W. J.; Nancollas, G. H. *Adv. Colloid Interface Sci.* **1999**, *79*, 229–279.

(24) Busscher, H. J.; Dejong, H.; Arends, J. *Mater. Chem. Phys.* **1987**, *17*, 553–558.

Addendum VI - Reduction of the peptidoglycan crosslinking causes a decrease in stiffness of the *Staphylococcus aureus* cell envelope

Authors: P. M. Pereira[1], P. Loskill[2], P. Jung[3], M. Bischoff[3], M. Herrmann[3], M. G. Pinho[3], and K. Jacobs[2]

[1] Instituto de Tecnologia Quimica e Biologica, Universidade Nova de Lisboa, 2780-157 Oeiras, Portugal [2] Department of Experimental Physics, Saarland University, 66041 Saarbrücken, Germany. [3] The Institute of Medical Microbiology and Hygiene, Saarland University, 66421 Homburg/Saar, Germany.

submitted to PLoS ONE (2012).

Author contributions:
P. M. Pereira and P. Loskill contributed equally to this work. Experiments were conceived and designed by P. M. Pereira, P. Loskill, M. Herrmann, M. G. Pinho, and K. Jacobs. Experiments were performed by P. M. Pereira, P. Loskill, and P. Jung. Data were analyzed by P. M. Pereira and P. Loskill. Article was written by P. M. Pereira, P. Loskill, M. Herrmann, M. G. Pinho, and K. Jacobs. Research was directed by M. Bischoff, M. Herrmann, M. G. Pinho, and K. Jacobs.

Abstract - We have used atomic force microscopy (AFM) to probe the effect of peptidoglycan crosslinking reduction on the elasticity of the *Staphylococcus aureus* cell wall. PBP4 is a non-essential transpeptidase, required for the high levels of peptidoglycan crosslinking characteristic of *S. aureus*. Importantly, this protein is essential for beta-lactam resistance in community acquired-methicillin resistant *S. aureus* (CA-MRSA) strains but not in hospital acquired-MRSA (HA-MRSA) strains. Using peak force tapping AFM we observed that the absence of PBP4, and the concomitant reduction of the peptidoglycan crosslinking, resulted in a reduction in stiffness of the *S. aureus* cell wall. Importantly, the reduction in cell wall stiffness in the absence of PBP4 was observed both in CA- and HA-MRSA strains indicating that high levels of PG crosslinking modulate the overall structure and mechanical properties of the *S. aureus* cell envelope in both types of clinically relevant strains.

Reduction of the peptidoglycan crosslinking causes a decrease in stiffness of the *Staphylococcus aureus* cell envelope

Pedro M. Pereira[1], Peter Loskill[2], Philipp Jung[3], Markus Bischoff[3], Mathias Herrmann[3], Mariana G. Pinho[1,*] and Karin Jacobs[2,*]

[1] *Instituto de Tecnologia Química e Biológica, Universidade Nova de Lisboa, 2780-157 Oeiras, Portugal*
[2] *Experimental Physics, Saarland University, 66041 Saarbrücken, Germany*
[3] *Institute of Medical Microbiology and Hygiene, Saarland University, 66421 Homburg/Saar, Germany*
* To whom correspondence should be addressed: mgpinho@itqb.unl.pt and k.jacobs@physik.uni-saarland.de

We have used atomic force microscopy (AFM) to probe the effect of peptidoglycan crosslinking reduction on the elasticity of the *Staphylococcus aureus* cell wall. PBP4 is a non-essential transpeptidase, required for the high levels of peptidoglycan crosslinking characteristic of *S. aureus*. Importantly, this protein is essential for beta-lactam resistance in community acquired-methicillin resistant *S. aureus* (CA-MRSA) strains but not in hospital acquired-MRSA (HA-MRSA) strains. Using peak force tapping AFM we observed that the absence of PBP4, and the concomitant reduction of the peptidoglycan crosslinking, resulted in a reduction in stiffness of the *S. aureus* cell wall. Importantly, the reduction in cell wall stiffness in the absence of PBP4 was observed both in CA- and HA-MRSA strains indicating that high levels of PG crosslinking modulate the overall structure and mechanical properties of the *S. aureus* cell envelope in both types of clinically relevant strains.

Introduction

The cell wall (CW) is critical for cell survival in most bacteria; it functions as a protection against mechanical and osmotic lysis in addition to maintaining cell shape [1]. Furthermore, the CW controls the tactile response of bacteria, influencing a wide range of behaviours such as cell adhesion, environmental sensing or host defence evasion [2,3,4]. The major component of the CW is peptidoglycan (PG), a complex polymer composed of long glycan chains of alternating ß-1,4-linked N-acetylglucosamine (NAG) and N-acetylmuramic acid (NAM) subunits, that are cross-linked via peptide bridges to form a strong but flexible structure [5]. The last stages of PG biosynthesis are catalysed by a group of proteins called penicillin-binding proteins (PBPs), which have both transglycosylase and transpeptidase activities, required for the elongation of the glycan chains and the formation of peptide bonds, respectively [6].
As the name suggests, PBPs are the target of beta-lactam antibiotics, molecules that block the transpeptidase active site. Bacterial pathogens have evolved different mechanisms to resist the action of beta-lactams, mainly by destroying the antibiotic molecule, through the action of beta-lactamases, or by modifying its target, i.e., the PBPs. *Staphylococcus aureus* is a Gram-positive clinical pathogen which has developed a remarkable ability to resist the action of virtually all beta-lactam antibiotics. Methicillin-Resistant *S. aureus* (MRSA) strains are currently one of the major causes of antibiotic-resistant hospital acquired infections, and can also cause infections among healthy individuals in the community. Therefore the study of the *S. aureus* cell envelope is of particular importance for the development of new strategies for antimicrobial chemotherapy [7]. The CW of *S. aureus* contains not only a thick layer of PG (around 20 nm), but also other polymers like the anionic wall teichoic acids (WTA) and lipoteichoic acids (LTA), secondary modifications such as O-acetylation and several proteins attached to the PG, resulting in a structure with a total width of approximately 35 nm [3,8,9]. Studies over the last decades have focused on the biochemistry of PG biosynthesis and most steps in this pathway are now well characterized [5,10]. However, much less is known about the 3D architecture and mechanical properties of this complex polymer. In recent years, atomic force microscopy (AFM) has provided valuable information on the structure and mechanical properties of the CW in numerous biological samples [11,12,13,14,15,16]. AFM can be used not only to obtain topological information on the cell surface and the organization of the PG [13,15,16,17], but it is also a powerful tool for quantitative studies of physical properties of the surface, such as the elasticity of the bacterial CW

[18,19,20,21,22,23,24]. Classical AFM modes, such as tapping or force volume mode are limited in terms of either spatial resolution, imaging time or quantitative analysis. The recently introduced PeakForce tapping mode with its quantitative nanomechanical property mapping (PeakForce QNM), however, allows for simultaneous mapping of topography and multiple mechanical properties, featuring the typical resolution and scan speed of the tapping mode [25,26,27].

We are interested in studying the mechanical properties of the PG of live *S. aureus* cells and in identifying key enzymes essential for the final structure of this polymer. One of the characteristics of the staphylococcal PG is its very high degree of crosslinking, as up to 90% of its muropeptides are linked to adjacent glycan chains in the PG mesh. This crosslinking can be classified as (i) primary crosslinking, responsible for the first level of cross-links between different glycan chains, which is necessary in most bacteria to preserve cell integrity, and includes muropeptide species with a polymerization degree lower or equal than pentamers (see Figure 1B, peaks I to V in the HPLC chromatogram) [5]; (ii) secondary crosslinking, which is the result of same transpeptidase chemical reaction, but leads to higher levels of linkage of the PG layers, and includes muropeptide species with a polymerization degree higher than pentamers (Figure 1B, arrow) [5]. This secondary crosslinking is mainly the result of the action of *S. aureus* PBP4, a non-essential transpeptidase [28,29]. We therefore hypothesized that PBP4 could have a major role in defining the mechanical properties of *S. aureus* PG. Interestingly, although it is not essential for normal cell growth, PBP4 has been associated with resistance mechanisms against two major classes of antibiotics: glycopeptides, considered the last resort antibiotic to treat MRSA infections, where its absence was associated with low level resistance in vancomycin intermediate (VISA) *S. aureus* strains [30]; and beta-lactams, where PBP4 was shown to be required for expression of high level beta□lactam resistance in community-acquired MRSA (CA-MRSA) strains but not in hospital-acquired (HA-MRSA) strains [31].

In this work we employed AFM PeakForce QNM with viable, genetically defined prototypes of HA- and CA-MRSA strains and their *pbp4* mutants to show that the absence of PBP4 and the concomitant decrease in PG crosslinking has an effect on the overall structure and mechanical properties of the *S. aureus* CW. This effect was observed both in HA- and CA-MRSA, suggesting that the requirement of PBP4 for beta-lactam resistance - as solely observed in CA-MRSA - is not related to changes in the mechanical properties of the PG that would occur exclusively in these strains.

Results and Discussion

PBP4 localization and function is conserved in both CA-MRSA and HA-MRSA strains

The aim of this work is to study the change of the mechanical properties of the PG of live *S. aureus* cells, namely its elasticity, upon reduction of secondary PG crosslinking that results from *pbp4* deletion. Given that deletion of *pbp4* results in loss of beta-lactam resistance in CA-MRSA strains, such as MW2, but not in HA-MRSA backgrounds, such as COL, we wanted to test if lack of PBP4 had more influence on the structure of the cell surface of MW2 than of COL.

One possible source of variation in studies of PG elasticity may result from obtaining measurements on newly synthesized cell wall as well as on mature cell wall, which may have different levels of crosslinking. In the rod-shaped gram-positive model organism *B. subtilis,* cell wall synthesis occurs both at the septum, for cell division, and at the lateral wall, for cell elongation [5,6]. Although, the septum of live cells is not accessible to the AFM cantilever before separation of daughter cells,, in *B. subtilis*, measurements made at the lateral wall (side of the cylindrical cell) would include the mature PG as well as helical bands of newly synthesized PG [32]. The use of *S. aureus* as a model organism avoids this source of variation in PG composition, as round *S. aureus* cells do not elongate and therefore only synthesize cell wall at the division septum. In accordance, we determined the localization of the PG synthetic enzyme PBP4 fused to yellow fluorescent protein (YFP), expressed from its native chromosomal locus, in both MW2 and COL strains, and showed that it is localized specifically at the division septum (Figure 1A), similarly to what was previously shown for other *S. aureus* strains [33]. It follows that elasticity measurements in *S. aureus* cell surface reflect the structure of the mature CW, away from the sites of PBPs localization, i.e., the sites of synthesis of new PG. Importantly, PBP4 localization was identical in CA-MRSA and HA-MRSA backgrounds, despite its different role in beta-lactam resistance.

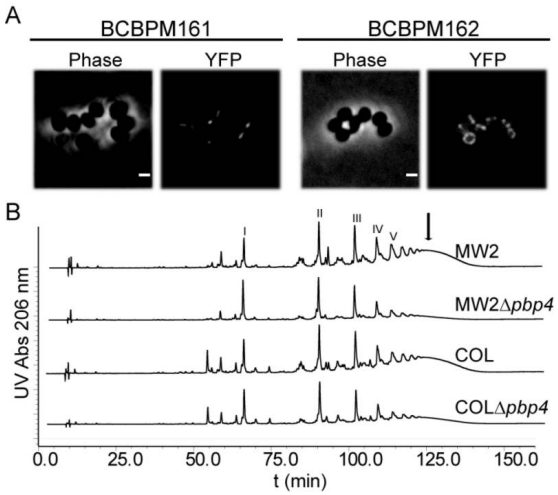

Figure 1: Localization and function of PBP4 are conserved in CA-MRSA and HA-MRSA strains. A) PBP4 is recruited to the division septa of COL and MW2 strains. Microscopy images of BCBPM161 (MW2) and BCBPM162 (COL) strains, expressing a C-terminal YFP fusion to PBP4 from its native chromosomal locus and under the control of its native promoter, show that PBP4 is recruited to the division septa in these MRSA strains. The protein can be seen as a line corresponding to a septum perpendicular to the plane of the slide, or as a ring when the septum is forming at different angles relatively to the plane of the slide (Scale bar: 1 μm). B) Chromatogram of HPLC of the muropeptide composition of PG in MW2, MW2Δpbp4, COL and COLΔpbp4, showing that deletion of pbp4 reduces the secondary crosslinking of the PG. Arrow points to highly cross-linked muropeptide species present in MW2 and COL strains but reduced in pbp4 mutants (MW2Δpbp4 and COLΔpbp4 respectively); I–V muropeptide species from monomers to pentamers.

After cell separation, the mature septum of *S. aureus* becomes one hemisphere of each daughter cell [34]. Therefore, in this organism, the entire cell surface should correspond to mature PG (although of different ages) with the possible exception of a single band around the division site corresponding to the outer edge of the septum, which can be identified on the AFM height images of dividing *S. aureus* cells [20,35] and has been shown to have different mechanical properties, such as adhesion [35]. Thus, our experimental set up enables us to map the elasticity of mature CW, in order to assess the effect of the reduction of secondary crosslinking on the mechanical properties of the *S. aureus* CW.
In order to correlate the AFM elasticity measurements with the CW structure of the *S. aureus* CA-MRSA and HA-MRSA strains, we purified the PG from parental strains COL and MW2 and their respective *pbp4* deletion mutants and analysed its composition by HPLC. We confirmed that, as previously shown [31], *pbp4* gene deletion results in significant decrease of the highly cross-linked muropeptide species that typically elute as a broad peak at the end of the HPLC chromatogram (Fig. 1B, arrow). We therefore used these isogenic pairs of bacterial strains differing in the PG crosslinking degree for AFM analysis.

Absence of secondary crosslinking contributes to a reduction in CW stiffness

Although the *S. aureus* CW is a complex heterogeneous structure composed of several polymers and proteins [3,9], it is its main component, the PG, that is thought to provide rigidity to bacterial cells, crucial for the cell to withstand the high internal osmotic pressure (20 to 30 bar) [5,8]. As stated above, PBP4 is responsible for the secondary crosslinking of the *S. aureus* PG [5]. Thus we used PBP4 mutants to test if highly cross-linked PG was in fact required for increased mechanical resistance of live *S. aureus* cells. For this purpose, we used AFM in PeakForce QNM, a method that detects material variations (such as elasticity or adhesion) at high resolution across a topographic image [25,26,27]. We used experimental conditions in which the cantilever indentation was in the range of 5-10 nm during the elasticity measurements, and therefore less than the proposed thickness of the cell wall, which is in the range of 35 nm [8]. Using this methodology, we mapped the elasticity profiles of the cell envelope of two MRSA strains, the HA-MRSA COL and the CA-MRSA MW2, as well as of the respective *pbp4* mutants COLΔ*pbp4* and MW2Δ*pbp4*. Live cells of these strains were immobilized in porous membranes (Figure 2, Panels A and C), and Young's modulus values (which reflect cell surface elasticity, and are lower for material with greater elasticity) were then measured in individual cells and mapped onto the height image. Only the top of each bacterium was analysed to avoid additional influence of a change in topography.
The first conclusion that can be obtained from our data is that the Young modulus of the cell envelope is homogeneous throughout the analysed cell surface in all strains, a finding expected given our experimental setting designed to analyse solely the mature CW and not the septal CW undergoing division.

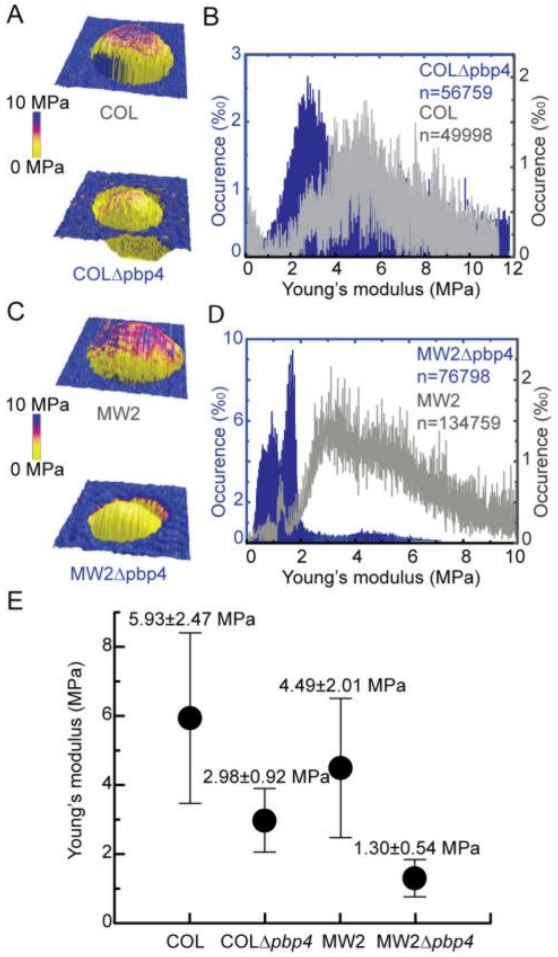

Figure 2: Young's modulus is reduced upon a reduction of secondary crosslinking. A) Height images overlaid with the distribution map of the Young's modulus values of a single COL (Top) and COLΔpbp4 (Bottom) cell trapped in a membrane pore. The increase in elasticity of the CW is homogeneous throughout the cell surface of the COLΔpbp4 mutant in comparison with the wt COL strain. B) Histogram with all the single values from each force curve obtained from all bacteria analysed. This shows that the COLΔpbp4 mutant is more elastic than the COL wt strain. Approximately 50000 single elasticity values were obtained from measurements on 11-13 single cells per strain. C) Height images with the distribution map of the Young's modulus values of a single MW2 (Top) and MW2Δpbp4 (Bottom) bacterium trapped in a membrane pore. The increase in elasticity of the MW2Δpbp4 mutant CW is homogeneous throughout the cell surface. D) Histogram with all the single values from each force curve obtained from all bacteria analysed. The MW2 wt strain is less elastic than the MW2Δpbp4 strain. Approximately 70000 to 130000 single elasticity values were obtained from measurements on 11-24 single bacteria per strain. E) All single values for each strain were fitted using a Gaussian curve and averages, with the respective errors, were calculated for each group of values, showing that the CW of mutants lacking PBP4 is more elastic than the CW of the parental strains. To avoid artifacts due to topography, only the topmost part (about 300 nm x 300 nm) of each bacterium was analysed.

The second and main conclusion of the AFM measurements relates to the significant reduction in the Young modulus of the CW in both CA-MRSA and HA-MRSA strains lacking PBP4, compared to the parental strains (MW2 4.49±2.01 MPa *Vs* MW2Δ*pbp4* 1.30±0.54 MPa; and COL 5.93±2.47 MPa *Vs* COLΔ*pbp4* 2.98±0.92 MPa; Figure 2). As the Young modulus is lower for material with greater elasticity, this data suggests that a decrease in secondary crosslinking results in increased CW elasticity (or reduced CW stiffness) both in COL and in MW2 backgrounds. This is consistent with the idea that a reduction of the number of bonds linking adjacent glycan chains results in a more pliable CW/PG structure. Accordingly, when Francius and coworkers used AFM to study the effect of lysostaphin in live *S. aureus* cells, they observed a 9.3 fold decrease in CW stiffness of lysostaphin treated cells [20]. Lysostaphin cleaves all pentaglycine bridges that crosslink *S. aureus* PG, effectively destroying both primary and secondary PG crosslinking [20]. As seen in figure 1B, the *pbp4* deletion mutants show a reduction in the levels of secondary crosslinking, but maintain PG primary crosslinking, due to the action of the other PBPs present in the cell, which justifies the fact that we observed a smaller decrease in CW stiffness (3.5 fold and 2.5 fold for MW2 and COL, respectively) compared to the action of lysostaphin. However, we cannot formally exclude the possibility that the alterations in CW stiffness are due to additional changes in the CW surface (in addition to secondary crosslinking reduction) that might result from the absence of PBP4.

Interestingly, although PG is not a rigid structure and it can withstand severe changes without compromising the overall cell envelope integrity [8,36], our data also suggest that there is a lack of a compensatory mechanism able to maintain the overall stiffness of the CW in the absence of PBP4.

Concluding remarks

We have used AFM, namely the recently introduced peak force tapping mode, to image live *S. aureus* cells, showing that alterations in the secondary PG crosslinking, caused by a lack of the non-essential transpeptidase PBP4, trigger changes in the mechanical properties of the *S. aureus* CW, enhancing the overall elasticity of staphylococcal cells both in HA and CA-MRSA strains. Interestingly, we observed a stronger

effect of the reduction of the secondary crosslinking on the mechanical properties of the CW in CA-MRSA strains (which require PBP4 for beta-lactam resistance) than in HA-MRSA strains. Thus, it might be interesting to investigate the role that these properties might play in the context of beta-lactam resistance.

Material and Methods

Staphylococcus aureus strains and growth conditions

S. aureus strains used in this study are listed in table 1. *S. aureus* strains were grown on tryptic soy agar (TSA, Difco) at 37ºC or in tryptic soy broth (TSB, Difco) at 37ºC with aeration. The medium was supplemented, when necessary, with 50 µg/ml of Kanamycin and 50 µg/ml of Neomycin (Sigma).

Table 1: S. aureus strains used in this study.

***S. aureus* strain**	**Relevant characteristics**	**Origin**
COL	HA-MRSA strain, *wild-type*	[37]
COLΔ*pbp4*	HA-MRSA strain; *pbp4* null mutant	[31]
MW2	CA-MRSA strain, *wild-type*	[38]
MW2 Δ*pbp4*	CA-MRSA strain; *pbp4* null mutant	[31]
RNPBP4YFP	RN4220 expressing PBP4-YFP C-terminal fusion; Kan^r	[33]
BCBPM161	MW2 expressing PBP4-YFP C-terminal fusion; Kan^r	This study
BCBPM162	COL expressing PBP4-YFP C-terminal fusion Kan^r	This study

Construction of *S. aureus* strains

For localization studies of PBP4 in HA-MRSA and CA-MRSA backgrounds, the gene encoding a PBP4-YFP fusion was transduced, using phage 80α, from strain RNPBP4YFP [33] into MW2 and COL strains, as previously described [39].

Fluorescence Microscopy

S. aureus strains were grown to mid-exponential phase, placed on a thin layer of 1% agarose in phosphate buffered saline (PBS; 137 mM NaCl, 10 mM phosphate, 2.7 mM KCl, pH 7.4) and analysed by fluorescence microscopy. Images were acquired using a Zeiss Axio Observer.Z1 microscope equipped with a Photometrics CoolSNAP HQ2 camera (Roper Scientific) and using Metamorph software (Meta Imaging series 7.5).

Peptidoglycan purification and HPLC Analysis

Peptidoglycan was prepared from exponentially growing cultures of COL and MW2 parental strains and corresponding *pbp4* deletion mutants, as previously described [40]. Muropeptides were obtained from purified PG digested with the muramidase mutanolysin M1 (Sigma-Aldrich), an N-acetylmuramidase that cuts glycan strands between the N-acetylmuramic and N-acetylglucosamine residues of both O-acetylated and unmodified peptidoglycan, as previously described [40]. The resulting muropeptides were reduced with sodium borohydride (Sigma) and analysed by reversed-phase HPLC using a HypersilODS column (Thermo Electron). The eluted muropeptides were detected and quantified by determination of their UV absorption at 206 nm, using the Shimadzu LC Solution software.

AFM Elasticity mapping

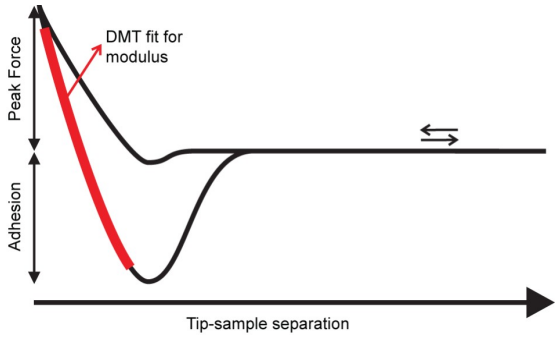

Figure 3: A single value of elasticity is obtained from each force curve acquired. By eliminating the time variable, one can plot the force versus the tip-sample distance, from which much information can be obtained. The maximum adhesion force between the tip and the sample can be extracted as the step height between the base line and the pull-off point. The peak force is defined as the vertical distance between the base line and the turn-away point. By analysing the retraction of each single force/distance curve, the Young's modulus can be determined using a DMT fit [42,43] (adapted from Pittenger, B et al.; 2010 [44]).

For AFM experiments, *S. aureus* strains were grown in 12 ml of TSB at 37ºC with aeration until mid-exponential phase (optical density OD_{600nm} = 0.6). Cells were harvested and concentrated in one third of the initial volume in fresh media. After concentration, the cell suspension was gently filtered, so that cells were immobilized by mechanical trapping into porous polycarbonate membranes with a pore size of 1.2µm (Millipore) [41]. The filter was gently rinsed with PBS, the excess of cells was removed by gently cleaning

with powder free tissue, the filter was inverted and attached to a glass slide with double-face adhesive tape. A silicone cover was used to create a hydrophobic area around the filter, which was then filled with 1:10 TSB/PBS solution.

AFM measurements were performed in the TSB/PBS solution at room temperature using a Bioscope Catalyst (Bruker, Santa Barbara, USA) in Peak Force QNM mode. The bacterial samples were freshly prepared for each series of measurements. Immediately prior to each experiment, the AFM probes (Scanasyst-Fluid+, Bruker, Santa Barbara, USA) were calibrated. Single measurements were carried out with a scan rate of 0.5 Hz, amplitude of 100-200 nm, a gain of 0.1, and a peak force threshold of 1 nN. Young's modulus mapping was obtained by a Derjaguin-Muller-Toporov (DMT) fit [42,43] of the retract part of each single force/distance curve (Figure 3) described by

$$F - F_{\mathrm{Adh}} = \frac{4}{3}\frac{E}{\left(1-\nu^2\right)}\sqrt{R}\left(d-d_0\right)^{\frac{3}{2}} \quad ,$$

where $F - F_{\mathrm{Adh}}$ is the determined force relative to the adhesion force, ν is the Poisson's ratio (for bacteria usually 0.5 [18,19]), R is the tip-radius (≈ 10 nm), $d - d_0$ is the deformation of the sample, and E is the Young's modulus. To avoid artifacts due to topography, only the topmost part (about 300 nm x 300 nm) of each bacterium was taken into account. A total of 50000 - 150000 single elasticity values were obtained from measurements on 10-25 single bacteria per strain. Multiple experiments using different bacterial cultures and AFM probes were performed for each strain.

Acknowledgments

This work was supported by grants PEst-OE/EQB/LA0004/2011 (from Fundação para a Ciência e Tecnologia) and PTDC/BIA-MIC/099151/2008 (from FCT, to M.G.P.) and fellowships SFRH/BD/41119/2007 (to P.M.P.), EMBO ASTF 427-2011 (to P.M.P) and by the German Science Foundation under grant numbers GRK 1276 and INST 256/305-1 FUGG.

We thank Ambrose Cheung for the generous gift of the *pbp4* mutant strains and Alexandre Berquand for the help with the Peak Force QNM mode.

1. Cabeen MT, Jacobs-Wagner C (2005) Bacterial cell shape. Nat Rev Microbiol 3: 601-610.
2. Beveridge TJ, Makin SA, Kadurugamuwa JL, Li Z (1997) Interactions between biofilms and the environment. FEMS Microbiol Rev 20: 291-303.
3. Foster TJ, McDevitt D (1994) Surface-associated proteins of *Staphylococcus aureus*: their possible roles in virulence. FEMS Microbiol Lett 118: 199-205.
4. Chavakis T, Wiechmann K, Preissner KT, Herrmann M (2005) *Staphylococcus aureus* interactions with the endothelium: the role of bacterial "secretable expanded repertoire adhesive molecules" (SERAM) in disturbing host defense systems. Thromb Haemost 94: 278-285.
5. Vollmer W, Blanot D, De Pedro MA (2008) Peptidoglycan structure and architecture. FEMS microbiology reviews 32: 149-167.
6. Scheffers DJ, Pinho MG (2005) Bacterial Cell Wall Synthesis: New Insights from Localization Studies. Microbiology and Molecular Biology Reviews 69: 585-607.
7. Chambers HF, DeLeo FR (2009) Waves of resistance: *Staphylococcus aureus* in the antibiotic era. Nature Reviews Microbiology 7: 629-641.
8. Matias VRF, Beveridge TJ (2006) Native Cell Wall Organization Shown by Cryo-Electron Microscopy Confirms the Existence of a Periplasmic Space in *Staphylococcus aureus*. Journal of Bacteriology 188: 1011-1021.
9. Weidenmaier C, Peschel A (2008) Teichoic acids and related cell-wall glycopolymers in Gram-positive physiology and host interactions. Nature Reviews Microbiology 6: 276-287.
10. Typas A, Banzhaf M, Gross CA, Vollmer W (2011) From the regulation of peptidoglycan synthesis to bacterial growth and morphology. Nature Reviews Microbiology 10: 123-136.
11. Andre G, Deghorain M, Bron P, van Swam I, Kleerebezem M, et al. (2011) Fluorescence and atomic force microscopy imaging of wall teichoic acids

in *Lactobacillus plantarum.* ACS chemical biology 6: 366–376.
12. Scheuring S, Dufrêne YF (2010) Atomic force microscopy: probing the spatial organization, interactions and elasticity of microbial cell envelopes at molecular resolution. Molecular Microbiology 75: 1327-1336.
13. Guillaume A, Kulakauskas S, Chapot-Chartier M-P, Navet B, Deghorain M, et al. (2010) Imaging the nanoscale organization of peptidoglycan in living *Lactococcus lactis* cells. Nature Communications 1: 1-8.
14. Alsteens D, Dupres V, Mc Evoy K, Wildling L, Gruber HJ, et al. (2008) Structure, cell wall elasticity and polysaccharide properties of living yeast cells, as probed by AFM. Nanotechnology 19: 384005-384014.
15. Wheeler R, Mesnage S, Boneca IG, Hobbs JK, Foster SJ (2011) Super-resolution microscopy reveals cell wall dynamics and peptidoglycan architecture in ovococcal bacteria. Molecular Microbiology 82: 1096-1109.
16. Hayhurst EJ, Kailas L, Hobbs JK, Foster SJ (2008) Cell wall peptidoglycan architecture in *Bacillus subtilis*. Proceedings of the National Academy of Sciences 105: 14603-14608.
17. Turner RD, Ratcliffe EC, Wheeler R, Golestanian R, Hobbs JK, et al. (2010) Peptidoglycan architecture can specify division planes in *Staphylococcus aureus*. Nature Communications 1: 1-9.
18. Touhami A, Nysten B, Dufrêne Y (2003) Nanoscale Mapping of the Elasticity of Microbial Cells by Atomic Force Microscopy. Langmuir 19: 4539-4543.
19. Gaboriauda F, Parchab BS, Geeb ML, Holdenc JA, Strugnellc RA (2008) Spatially resolved force spectroscopy of bacterial surfaces using force-volume imaging. Colloids and Surfaces B: Biointerfaces 62: 206–213.
20. Francius G, Domenech O, Mingeot-Leclercq MP, Dufrene YF (2008) Direct Observation of *Staphylococcus aureus* Cell Wall Digestion by Lysostaphin. Journal of Bacteriology 190: 7904-7909.
21. Dufrene YF (2004) Using nanotechniques to explore microbial surfaces. Nat Rev Microbiol 2: 451-460.
22. Cerf A, Cau JC, Vieu C, Dague E (2009) Nanomechanical properties of dead or alive single-patterned bacteria. Langmuir 25: 5731-5736.
23. Gaboriaud F, Dufrene YF (2007) Atomic force microscopy of microbial cells: Application to nanomechanical properties, surface forces and molecular recognition forces. Colloids and Surfaces B: Biointerfaces 54: 10-19.
24. Yao X, Jericho M, Pink D, Beveridge T (1999) Thickness and elasticity of gram-negative murein sacculi measured by atomic force microscopy. Journal of Bacteriology 181: 6865–6875.
25. Adamcik J, Berquand A, Mezzenga R (2011) Single-step direct measurement of amyloid fibrils stiffness by peak force quantitative nanomechanical atomic force microscopy. Applied Physics Letters 98: 193701-193704.
26. Berquand A (2011) Quantitative Imaging of Living Biological Samples by PeakForce QNM Atomic Force Microscopy. . http://wwwbruker-axscom: Bruker Nano Surfaces Divison. pp. 1–10.
27. Berquanda A, Roduita C, Kasasa S, Holloschia A, Poncea L, et al. (2010) Atomic Force Microscopy Imaging of Living Cells. Microscopy Today 18 8-14
28. Wyke AW, Ward JB, Hayes MV, Curtis NA (1981) A role in vivo for penicillin-binding protein-4 of *Staphylococcus aureus*. Eur J Biochem 119: 389-393.
29. Kozarich JW, Strominger JL (1978) A membrane enzyme from *Staphylococcus aureus* which catalyzes transpeptidase, carboxypeptidase, and penicillinase activities. J Biol Chem 253: 1272-1278.
30. Sieradzki K, Pinho MG, Tomasz A (1999) Inactivated pbp4 in highly glycopeptide-resistant laboratory mutants of *Staphylococcus aureus*. J Biol Chem 274: 18942-18946.
31. Memmi G, Filipe SR, Pinho MG, Fu Z, Cheung A (2008) *Staphylococcus aureus* PBP4 is Essential for β-lactam Resistance in Community-Acquired Methicillin Resistant Strains. Antimicrobial agents and chemotherapy 52: 3955-3966.
32. Daniel RA, Errington J (2003) Control of cell morphogenesis in bacteria: two distinct

ways to make a rod-shaped cell. Cell 113: 767-776.
33. Atilano ML, Pereira PM, Yates J, Reed P, Veiga H, et al. (2010) Teichoic acids are temporal and spatial regulators of peptidoglycan cross-linking in *Staphylococcus aureus.* Proceedings of the National Academy of Sciences of the United States of America: 2-7.
34. Pinho MG, Errington J (2003) Dispersed mode of *Staphylococcus aureus* cell wall synthesis in the absence of the division machinery. Molecular Microbiology 50: 871-881.
35. Touhami A, Jericho MH, Beveridge TJ (2004) Atomic force microscopy of cell growth and division in *Staphylococcus aureus*. J Bacteriol 186: 3286-3295.
36. Ou LT, Marquis RE (1970) Electromechanical interactions in cell walls of gram-positive cocci. J Bacteriol 101: 92-101.
37. Gill SR, Fouts DE, Archer GL, Mongodin EF, Deboy RT, et al. (2005) Insights on evolution of virulence and resistance from the complete genome analysis of an early methicillin-resistant *Staphylococcus aureus* strain and a biofilm-producing methicillin-resistant *Staphylococcus epidermidis* strain. J Bacteriol 187: 2426-2438.
38. Baba T, Takeuchi F, Kuroda M, Yuzawa H, Aoki K, et al. (2002) Genome and virulence determinants of high virulence community-acquired MRSA. Lancet 359: 1819-1827.
39. Veiga H, Pinho MG (2009) Inactivation of the SauI type I restriction-modification system is not sufficient to generate *Staphylococcus aureus* strains capable of efficiently accepting foreign DNA. Appl Environ Microbiol 75: 3034-3038.
40. Filipe SR, Tomasz A, Ligoxygakis P (2005) Requirements of peptidoglycan structure that allow detection by the *Drosophila* Toll pathway. EMBO reports 6: 327-333.
41. Kasas S, Ikai A (1995) A method for anchoring round shaped cells for atomic force microscope imaging. Biophysical journal 68: 1678-1680.
42. Derjaguin BV, Muller VM, Toporov YP (1975) Effect of contact deformations on the adhesion of particles. Journal of Colloid and Interface Science 53: 314-326.
43. Maugis D, editor (2000) Contact, Adhesion and Rupture of Elastic Solids Springer-Verlag.
44. Pittenger B, Erina N, Su C (2010) Quantitative Mechanical Property Mapping at the Nanoscale with PeakForce QNM. In: Bruker, editor: Bruker Corporation.

Publications and Conference Contributions

Publications

- P. Loskill, H. Hähl, N. Thewes, C. T. Kreis, M. Bischoff, M. Herrmann, and K. Jacobs. 'Influence of the Subsurface Composition of a Material on the Adhesion of Staphylococci', *Langmuir* **28**, 7242–7248 (2012).

- H. Hähl, F. Evers, S. Grandthyll, M. Paulus, C. Sternemann, P. Loskill, M. Lessel, A. K. Hüsecken, T. Brenner, M. Tolan, and K. Jacobs. 'Subsurface influence on the structure of protein adsorbates revealed by in situ X-ray reflectivity', *Langmuir* **28**, 7747–7756 (2012).

- P. Loskill, H. Hähl, T. Faidt, S. Grandthyll, F. Müller, and K. Jacobs. 'Is adhesion superficial? Silicon wafers as a model system to study van der Waals interactions', *Adv. Colloid Interface Sci.* **179–182**, 107–113 (2012).

- P. Loskill, J. Puthoff, M. Wilkinson, K. Mecke, K. Jacobs, and K. Autumn. 'Macroscale adhesion of gecko setae reflects nanoscale differences in subsurface composition', *J. R. Soc. Interface* **submitted** (2012).

- P. Loskill, C. Zeitz, M. Bischoff, M. Herrmann, and K. Jacobs. 'Fluoridation of hydroxyapatite leads to a reduced adhesion of oral bacteria', *Langmuir* **submitted** (2012).

- P. Pereira, P. Loskill, P. Jung, M. Bischoff, M. Herrmann, M. Pinho, and K. Jacobs. 'Reduction of the peptidoglycan crosslinking causes a decrease in stiffness of the Staphylococcus aureus cell envelope', *PLoS one* **submitted** (2012).

Scientific Talks

- AFM - Force Spectroscopy: A new approach for the investigation of biofilms
  Feldberg Winter School, Feldberg (D) 12/2008

- AFM - Force Spectroscopy: A new approach for the investigation of biofilms
  PhD Students' Day, Saarbrücken (D) 02/2009

- AFM as a chance for studying in situ protein adsorption and bacterial adhesion
  DPG Spring-Meeting, Dresden (D) 03/2009

- Influence of substrate composition on the adhesion of bacteria—an AFM study
  Feldberg Winter School, Feldberg (D) 12/2009

- Macroscale adhesion of the gecko is influenced by differences in microscopic van der Waals potentials
  PhD Students' Day, Saarbrücken (D) 02/2011

- Influence of long-range van der Waals forces on biological adhesion: The importance of the subsurface composition
  Circle Meeting on Biological Physics, Saarbrücken (D) 04/2011

- Influence of long-range van der Waals forces on biological adhesion: The importance of the subsurface composition
  Seminar of the Graduate College 1276, Saarbrücken (D) 09/2011

- Influence of long-range van der Waals forces on biological adhesion: The importance of the subsurface composition
  Seminar Talk at the TU Kaiserslautern, Kaiserslautern (D) 11/2011

- Influence of van der Waals forces on the adhesion of bacteria and geckos
  Nanobubbles and Micropancakes, Les Houches (F) 02/2012

- Adhesion of gecko setae reflects nanoscale differences in subsurface energy
  DPG Spring-Meeting, Berlin (D) 03/2012

- Is adhesion superficial? Silicon wafers as model system to study van der Waals interactions
  Seminar Talk at the TU Chemnitz, Chemnitz (D) 04/2012

- Are thin polymer films, proteins, bacteria, and geckos superficial?
  PhD Students' Day, Saarbrücken (D) 06/2012

Poster

- Protein adsorption and bacterial adhesion explored by AFM: Interplay of local and global properties
  3rd International Workshop on Approaches to Single-Cell Analysis, Zürich (CH) 09/2008.

- Protein adsorption and bacterial adhesion explored by AFM: Interplay of local and global properties
  Atomic Force Microscopy of Biological Interfaces, Nancy (F) 10/2008

- The influence of Van-der-Waals-forces on bacterial adhesion
  Seminar of the Graduate College 1276, Saarbrücken (D) 10/2009

- Influence of subsurface composition on the adhesion of bacteria and the adsorption of proteins
  DPG Spring-Meeting, Regensburg (D) 03/2010

- AFM force spectroscopy with gecko probes and bacterial probes
  Topical workshop - Bioinspired adhesion: from geckos to new products?, Saarbrücken (D) 07/2010

- Influence of subsurface composition on the adhesion of bacteria and the adsorption of proteins
  Biofilms4, Winchester (GB) 09/2010

- Influence of long-range van der Waals forces on biological adhesion: The importance of the subsurface composition
  Gordon Research Seminar: Science of Adhesion, Lewiston (USA) 07/2011

- Influence of long-range van der Waals forces on biological adhesion: The importance of the subsurface composition
  Gordon Research Conference: Science of Adhesion, Lewiston (USA) 07/2011

- Influence of long-range van der Waals forces on biological adhesion: The importance of the subsurface composition
  BioMicroWorld2011, Torremolinos (E) 09/2011

- Influence of subsurface properties on proteins, bacteria and geckos: Is adhesion superficial?
  DPG Spring-Meeting, Berlin (D) 03/2012

- Influence of long-range van der Waals forces on biological adhesion: The importance of the subsurface composition
  Gordon Research Seminar: Biointerfaces, Les Diablerets (CH) 05/2012

- Influence of long-range van der Waals forces on biological adhesion: The importance of the subsurface composition
  Gordon Research Conference: Biointerfaces, Les Diablerets (CH) 05/2012

- Influence of subsurface properties on proteins, bacteria and geckos: Is adhesion superficial?
  Physics of the Extracellular Matrix, Bad Honnef (D) 06/2012

Selected further Conference (Poster) Contributions

- AFM as a chance for studying protein adsorption and bacterial adhesion
  DPG Spring-Meeting, Dresden (D) 03/2009

- Bacterial probes with defined contact area for force spectroscopy
  DPG Spring-Meeting, Regensburg (D) 03/2010

- Influence of subsurface composition on the adhesion of bacteria and the adsorption of proteins
  AFM BioMed Rovinj (HR) 05/2010

- Influence of subsurface composition on the adhesion of bacteria and the adsorption of proteins
  Gordon Research Conference: Biointerfaces, Les Diablerets (CH) 09/2010

- The role of van der Waals forces on the dynamic adhesion of bacteria
  BioMicroWorld2011, Torremolinos (E) 09/2011

- Measurement of adhesion forces of bacteria on controlled hydroxyapatite surfaces
  DPG Spring-Meeting, Berlin (D) 03/2012

- Subsurface influence on the structure of protein adsorbates revealed by in situ X-ray reflectivity
  DPG Spring-Meeting, Berlin (D) 03/2012

- Static and dynamic adhesion of Staphylococci on model substrates, studied by AFM
  DPG Spring-Meeting, Berlin (D) 03/2012

- Static and dynamic Adhesion of Staphylococci on model substrates, studied by AFM
  Physics of the Extracellular Matrix, Bad Honnef (D) 06/2012

Danke

... an alle, die mich während meiner Promotion in jedweder Form unterstützt haben.

Zuallererst gebührt dieser Dank Prof. Dr. Karin Jacobs, die mir die Möglichkeit gab, nach meiner Diplomarbeit auch meine Doktorarbeit in ihrer Gruppe anzufertigen. Da sie mir zum einen die Freiheit gab, jederzeit meine eigene Ideen zu realisieren und zum anderen stets einen Rat, eine Idee oder eine Anregung parat hatte, habe ich die Entscheidung, in ihrer AG zu bleiben, nie bereut. Vielen Dank für die stete und engagierte Unterstützung!

Des Weiteren bedanke ich mich bei der gesamten AG Jacobs. An erster Stelle möchte ich Judith Rech und Monika Schuck, den guten Seelen der Gruppe, meinen Dank für die Hilfe bei organisatorischen Angelegenheiten jeder Art aussprechen. Außerdem danke ich meinem Bürokollegen Dr. Hendrik Hähl für die vielen interessanten Diskussionen, Frage- sowie Nachhilfestunden zu wichtigen Themen wie Nanotypographie, Dr. Oliver Bäumchen, der immer für Tipps und Anregungen zur Verfügung stand, Ludo Marquant für die vielen außerwissenschaftlichen Diskussionen, Matthias Lessel, Nicolas Thewes, Christian Zeitz, Samuel Grandthyll und Dr. Frank Müller für die gute Zusammenarbeit bei gemeinsamen Projekten, Mischa Klos für die Hilfe bei allen IT-Problemen, Sabrina Haefner für die kooperative Kaffeeversorgung, und generell allen Mitgliedern der AG für die tolle Arbeitsatmosphäre, die Hilfsbereitschaft und die schöne Zeit! Dankbar bin ich speziell auch Nicolas Thewes, Christian Kreis, Christian Spengler und Sebastian Hümbert, deren Bachelor-, Master- oder Diplomarbeit ich betreuen durfte und von denen einige Messungen auch Eingang in diese Arbeit fanden.

Als nächstes möchte ich mich bedanken bei Prof. Dr. Mathias Herrmann für die mikrobiologische Betreuung meiner Arbeit und die Begeisterung für die interdisziplinäre Arbeit. Ein großer Dank geht auch an Dr. Markus Bischoff für die Hilfsbereitschaft bei medizinischen bzw. mikrobiologischen Fragestellungen, an Karin Hilgert für das Engagement und die Unmengen an Bakterienlieferungen, sowie an Pedro Matos Pereira aus der AG Pinho in Lissabon, von dem ich viel über mikrobiologische Arbeitsweisen gelernt habe.

Moreover, I would like to thank Prof. Dr. Kellar Autumn from the Lewis & Clark College in Portland, OR, for giving me the opportunity to spend a research period

in his laboratory! I benefited a lot from the vivid discussions and the constructive criticism. Many thanks also to Dr. Jon Puthoff, Matt Wilkinson and Andrew Schnell—the other members of the Gecko lab.

Vielen Dank auch an Prof. Dr. Ludger Santen für die vielen Diskussionen und die Anleitung bei der Entwicklung einer Biofilm-Simulation, welche im Endeffekt leider noch keinen Eingang in diese Arbeit fand. Für weitere Hilfestellungen bei theoretischen Fragestellungen danke ich auch Prof. Dr. Klaus Mecke von der Universität Erlangen-Nürnberg und Prof. Dr. Jacob Israelachvili von der University of California, Santa Barbara. Außerdem danke ich Prof. Dr. Ralf Seemann und Prof. Dr. Stefan Hüfner, die jederzeit für Ratschläge und Antworten bereitstanden.

Darüber hinaus möchte ich denjenigen danken, die dafür gesorgt haben, die Rechtschreibfehler dieser Arbeit um einiges zu minimieren. Danke Viola, Flo, Ralf, Helge, Helge und Norbert für das Korrekturlesen.

Ein sehr großer Dank gebührt meiner Familie, die mir während meiner Promotion und auch schon während meines Studiums Halt gegeben und mich in jedweder Art unterstützt hat. Ohne euch wäre ich sicher nie so weit gekommen!

Zum Schluss möchte ich diejenigen nicht vergessen, die mich immer wieder daran erinnert haben, dass es im Leben Wichtigeres als promovieren und arbeiten gibt und auf die ich immer zählen konnte! Mein Dank gilt meinen Freunden und ganz besonders Viola. Danke!

Erklärung

Hiermit versichere ich an Eides statt, dass ich die vorliegende Arbeit selbstständig und ohne Benutzung anderer als der angegebenen Hilfsmittel angefertigt habe. Die aus anderen Quellen oder indirekt übernommenen Daten und Konzepte sind unter Angabe der Quelle gekennzeichnet. Die Arbeit wurde bisher weder im In- noch im Ausland in gleicher oder ähnlicher Form in einem Verfahren zur Erlangung eines akademischen Grades vorgelegt.

Saarbrücken, den 16. August 2012

Peter Moritz Loskill